DISSERTATION

Generalized Energetic Model for Characterizing the Magnetic Hysteresis of Anisotropic Thin Films

ausgeführt zum Zwecke der Erlangung des akademischen Grades

eines Doktors der technischen Wissenschaften

unter der Leitung von

Ao. Univ. Prof. Dr. Hans HAUSER (†)
Ao. Univ. Prof. Dr. Johann NICOLICS
E366
Institut für Sensor- und Aktuatorsysteme
Abteilung für Angewandte Materialwissenschaften in der Elektronik

eingereicht an der Technischen Universität Wien
Fakultät für Elektrotechnik und Informationstechnik

von

Peter HAUMER
Matr.Nr.: 9625854
Georg-Sigl-Str. 47,
3151 St. Georgen

Wien, im August 2014

The research presented in this thesis was carried out at the Department of Applied Electronic Materials of the Institute of Sensor and Actuator Systems, Vienna University of Technology, Austria.

Reviewer 1:

Ao. Univ. Prof. Johann NICOLICS
Vienna University of Technology, Austria.

Reviewer 2:

Prof. David C. JILES
Iowa State University, USA.

Contents

Abstract **v**

Kurzfassung **vi**

Nomenclature **vii**
List of Abbreviations . . . vii
List of Constants . . . vii
List of Variables . . . vii

1 Introduction **1**
1.1 Magnetic Hysteresis Modeling . . . 1
1.1.1 Theoretical Concepts . . . 1
1.1.2 State of the Art . . . 2
1.1.3 Characteristics of Magnetic Hysteresis Models . . . 2
1.1.4 Philosophical Conclusion . . . 3
1.2 Objective of the Thesis . . . 4
1.2.1 Historical Basis . . . 4
1.2.2 Generalized Model . . . 4
1.3 Scope of the Thesis . . . 5

I Theoretical Framework **7**

2 Magnetism Overview **8**
2.1 Origin of Magnetism in a Microscopic Treatment . . . 9
2.1.1 Magnetic Moment of an Electron . . . 9
2.1.2 Magnetic Moment of an Isolated Atom . . . 12
2.1.3 Magnetic Moment of Materials . . . 15
2.1.4 Exchange Interactions . . . 16
2.2 Continuous Magnetization and Susceptibility . . . 18
2.2.1 Microscopic Description and Continuum Models . . . 18
2.2.2 Magnetization . . . 19
2.2.3 Magnetic Susceptibility and Permeability . . . 20
2.3 Classification of Magnetic Behavior . . . 22
2.3.1 Diamagnetism . . . 22
2.3.2 Paramagnetism . . . 23

2.3.3 Ferromagnetism . . . 25
2.3.4 Antiferromagnetism . . . 28
2.3.5 Ferrimagnetism . . . 29
2.3.6 Summary . . . 29

3 Magnetic Energies, Domains, and Hysteresis 30
3.1 Ferromagnetic Energy Contributions . . . 30
3.1.1 General Considerations . . . 30
3.1.2 Exchange Energy . . . 32
3.1.3 Stray Field Energy . . . 32
3.1.4 Applied Field Energy . . . 35
3.1.5 Anisotropy Energy . . . 35
3.1.6 Magnetostrictive Self-Energy . . . 38
3.1.7 Magneto-Elastic Energy with Non-Magnetic Stresses . . . 39
3.1.8 Energy Minimization . . . 39
3.2 Magnetic Domains . . . 40
3.2.1 Domain Theory . . . 40
3.2.2 Domain Walls . . . 41
3.3 Magnetization Process . . . 43
3.3.1 Descriptive Analysis of the Magnetization Process . . . 43
3.3.2 Reversible and Irreversible Magnetization Process . . . 47
3.3.3 Dissipative Losses . . . 50
3.4 Summary . . . 53

II Magnetic Modeling 55

4 State of the Art in Magnetic Hysteresis Modeling 56
4.1 Characterization of Magnetic Hysteresis Models . . . 56
4.2 Micromagnetic Modeling . . . 58
4.2.1 Model Definition . . . 58
4.2.2 Computation Techniques . . . 61
4.2.3 Applications . . . 62
4.3 Preisach Model . . . 63
4.3.1 Classical Scalar Preisach Model . . . 63
4.3.2 Model Properties and Extensions . . . 68
4.4 Jiles-Atherton Hysteresis Model . . . 70
4.4.1 Scalar Jiles-Atherton Model . . . 70
4.4.2 Implementation and Extensions . . . 73
4.5 Other Approaches in Hysteresis Modeling . . . 74
4.5.1 Stoner-Wohlfarth Model . . . 74
4.5.2 Chemical Reaction Hysteresis Model . . . 76
4.6 Summary . . . 78

5 Generalized Two-Dimensional Energetic Model 79
5.1 Generalized Formulation of the Model . . . 80

5.1.1 Elementary Magnetic Entities . . . 80
5.1.2 Aggregation of Magnetic Entities to Statistical Domain Classes . . . 82
5.1.3 Basic Distributions of Magnetic Entities within a Domain Class . . . 85
5.1.4 Total Macroscopic Magnetization . . . 89
5.2 Energetic Framework of the Model . . . 92
5.2.1 General Aspects and Historical Review . . . 92
5.2.2 Energy Contributions Originating from Local Energy Terms . . . 96
5.2.3 Energy Contributions Originating from Non-Local Energy Terms . . . 102
5.2.4 Reversible and Irreversible Work during Magnetization Process . . . 106
5.3 Calculation Procedure . . . 113
5.3.1 Model Setup . . . 113
5.3.2 Calculation of the Model Variables . . . 115
5.4 Summary . . . 119

III Simulation and Evaluation 121

6 Model Evaluation on Permalloy Thin Films 122
6.1 Production, Material Properties, and Measurement . . . 122
6.1.1 Thin Film Production by Cathodic Sputtering . . . 122
6.1.2 Basic Properties of Permalloy Thin Films . . . 124
6.1.3 Magneto-Optical Kerr Measurement . . . 129
6.2 Model Setup for Thin Films with Dominant Coherent Rotation . . . 131
6.2.1 General Model Parameters . . . 131
6.2.2 Energy Terms for Magnetization Dispersion . . . 133
6.3 Directional Dependence of Magnetization Curves Near the Hard Axis . . . 134
6.3.1 Identification of the Model Parameters . . . 134
6.3.2 Simulation Results . . . 134
6.3.3 Measurement and Model Prediction for Small Deviations from the Hard Axis Direction . . . 137
6.4 Relation to Parameters of the Sputter Process . . . 139
6.4.1 Identification of the Model Parameters . . . 139
6.4.2 Simulation Results . . . 140
6.4.3 Discussion . . . 140
6.5 Temperature Dependence of Spontaneous Magnetization . . . 143
6.5.1 Model Setup . . . 144
6.5.2 Comparison with Classical Mean Field Models . . . 145
6.5.3 Ultrathin Permalloy Films . . . 146
6.6 Summary . . . 148

7 Conclusion and Outlook 149
7.1 Conclusion . . . 149
7.1.1 Limits of the Classical Energetic Model . . . 149
7.1.2 Development of the Generalized Energetic Model . . . 149
7.1.3 Current State of the Generalized Energetic Model . . . 150

7.1.4 Limits of the Generalized Energetic Model 150
7.2 Outlook 151
7.2.1 Comprehensive Evaluation of the Model Characteristics 151
7.2.2 Improvements in Model Formulation and Calculation 151
7.2.3 Further Applications 151

Appendix **153**

A Detailed Derivations to the Generalized Energetic Model **154**
A.1 Expectation Value of Wrapped Circular Distributions 154
A.1.1 Expectation Value for 2π-Periodic Functions 155
A.1.2 Analytical Results for the Wrapped Normal Distribution 155
A.1.3 Application to Domain Class Magnetization 157
A.1.4 Application to Local Energy Contributions 158
A.2 Expectation Value of Bivariate Wrapped Circular Distributions 158
A.2.1 Expectation Value for 2π-Periodic Functions 158
A.2.2 Analytical Results for the Wrapped Normal Distribution 159
A.3 Reversible Anhysteretic Energy 162
A.3.1 Fermi Statistics and Stirling's Approximation 162
A.3.2 Reversible Anhysteretic Energy 163
A.4 Volume Change due to Domain Wall Motion 165
A.4.1 Estimation of the Transition Matrix for 2 Domain Classes 165
A.4.2 Estimation of the Transition Matrix for 3 Domain Classes 165
A.4.3 Estimation of the Transition Matrix for 4 Domain Classes 166
A.5 Probability of Reversible Domain Wall Motion 170
A.5.1 Properties of the Probability Function 170
A.5.2 Distance of Reversible Movement 170
A.5.3 Reversal Point of Domain Wall Motion 172

Bibliography **177**

List of Publications **183**
Publications in Scientific Journals 183
Contributions to Books 183
Presentations and Conference Proceedings 184

Acknowledgements **187**

Abstract

Within this work, a generalized two-dimensional energetic hysteresis model for characterizing the magnetization process of thin ferromagnetic films is presented. Based on the "Energetic Model of Ferromagnetic Hysteresis" (EM), which has been introduced by H. HAUSER in 1994, so called statistical domain classes adapted from the magnetic easy directions of the material sample are distinguished. With respect to HAUSER's formulation of the EM, two major extensions are provided in this work. As a first generalization, the orientation of the elementary magnetic dipoles within a statistical domain class is no longer restricted to the specified easy direction, but is represented by a stochastic circular distribution function that is characterized by a mean orientation and a certain variance. So local misalignments of magnetic moments due to imperfections within the material can be modeled on the one hand, and the temperature dependence of the spontaneous magnetization can be described from the first principles on the other hand. The second key extension is the fully two-dimensional formulation of the EM. Although, the original model of HAUSER is intended for a certain number of easy directions, most of the investigations are based on a one-dimensional model setup in consideration of the symmetry properties of the crystalline axes. In particular, the terms for reversible and irreversible work during the magnetization process have to be reformulated in order to allow fully two-dimensional modeling. Further, the magnetocrystalline and induced anisotropy are directly incorporated in the model by corresponding energy terms. Thereby, the two-dimensional approach allows predicting the magnetic hysteresis curves of anisotropic thin films for all directions of the applied field with a single set of parameters. Besides, the generalized model accounts for coherent magnetization rotation as well as non-coherent magnetization reversal mechanisms by using a corresponding parameterization of domain classes.

The evaluation of the presented generalized two-dimensional energetic hysteresis model is done by the example of Permalloy thin films used for anisotropic magneto-resistive (AMR) sensors. Especially for AMR sensor applications the directional properties of the magnetization curve are important, particularly the hard-axis characteristics. The model parameters are identified by a comparison of the simulated hysteresis loops to those obtained from a magneto-optical Kerr measurement setup in easy axis and hard axis direction. Then, the magnetization curves can be calculated for any arbitrary direction of the magnetic field with respect to the easy axis. Furthermore, the identified model parameters reflect several microstructural properties of the thin film, like microscopic misalignments due to inhomogeneities, for example. Amongst others, these microstructural properties are related to characteristics of the thin film production process, such as the distance between target and substrate during sputtering. Due to the fact that the magnetic hysteresis model presented within this work allows an inference from measured magnetization curves to the structural properties of the film, laborious and expensive microscopic analyses can be reduced. Hence, significantly less effort is needed to improve the technological parameters of the production process.

Kurzfassung

In der vorliegenden Arbeit wird ein zweidimensionales energiebasiertes Modell zur Beschreibung der ferromagnetischen Hysterese von dünnen Schichten präsentiert. Die Grundlage bildet das 1994 von H. HAUSER erstmals publizierte „Energetic Model of Ferromagnetic Hysteresis“ (EM), in welchem so genannte statistische Domänenklassen, basierend auf den magnetisch leichten Richtungen im Material, unterschieden werden. Darauf aufbauend, werden in dieser Arbeit zwei wesentliche Erweiterungen beschrieben. In einer ersten Verallgemeinerung wird die Ausrichtung der magnetischen Dipole in einer Domänenklasse nicht auf die leichte Richtung beschränkt, sondern mittels einer statistischen Verteilungsfunktion beschrieben. Damit können einerseits lokale Abweichungen von der parallelen Ausrichtung aufgrund von Material-Inhomogenitäten abgebildet und andererseits die Temperaturabhängigkeit der spontanen Magnetisierung direkt aus dem Modell erklärt werden. Die zweite Erweiterung besteht in einer vollständigen zweidimensionalen Formulierung des Modells. Obwohl HAUSER bereits Ansätze zur Behandlung mehrerer leichter Richtungen beschreibt, wurden die meisten Untersuchungen, unter Berücksichtigung der Symmetrie im Kristallgitter, auf Basis eines eindimensionalen Modellansatzes durchgeführt. Die zweidimensionale Erweiterung erfordert insbesondere eine Neuformulierung der Ausdrücke der im Magnetisierungsprozess geleisteten reversiblen und irreversiblen Arbeit. Zusätzlich werden die aus einer magnetokristallinen oder einer induzierten Anisotropie resultierenden Energiebeiträge direkt im Modell berücksichtigt. Damit kann der Magnetisierungsprozess in anisotropen dünnen Schichten für beliebige Richtungen des angelegten Magnetfeldes mit einem Parametersatz beschrieben werden. Darüber hinaus lassen sich kohärente Rotation der Magnetisierung und nicht-kohärente Ummagnetisierungsprozesse durch entsprechend parametrierte Domänenklassen unterscheiden.

Die Evaluierung des zweidimensionalen Hysterese-Modells erfolgt am Beispiel von dünnen Permalloy-Schichten, die für den Einsatz in anisotropen magneto-resistiven (AMR) Sensoren hergestellt werden. Insbesondere für AMR-Anwendungen ist die Richtungsabhängigkeit der Magnetisierungskurve, speziell deren Verlauf in der schweren Richtung, von entscheidender Bedeutung. Die Identifizierung des Modells erfolgt durch Abgleich der Simulationsergebnisse mit den, aus magneto-optischen Kerr-Messungen gewonnenen Hysteresekurven in den magnetisch leichten und schweren Richtungen. Alle dazwischen liegenden Kurven können dann direkt aus dem Modell berechnet werden. Ferner spiegeln einige der identifizierten Modellparameter mikrostrukturelle Eigenschaften der dünnen Schichten wider, wie etwa lokale Fehlausrichtungen aufgrund von Inhomogenitäten. Diese Eigenschaften hängen meist von den technologischen Parametern des Herstellungsprozesses, also beispielsweise vom Target-Substrat-Abstand beim Sputtern ab. Das im Rahmen dieser Arbeit vorgestellte Modell erlaubt Rückschlüsse von den gemessenen Hysteresekurven auf die strukturellen Eigenschaften der dünnen Schichten und kann so dazu beitragen, aufwendige und teuere mikroskopische Analysen zu reduzieren. Somit kann der Aufwand bei der Optimierung der technologischen Parameter des Herstellungsprozesses deutlich verringert werden.

Nomenclature

List of Abbreviations

1D ..... One-dimensional

2D ..... Two-dimensional

3D ..... Three-dimensional

AMR .... Anisotropic magneto-resistive

BHJ ..... Barkhausen jump

DWM .... Domain wall motion

EM ..... Energetic model of ferromagnetic hysteresis

MOKE ... Magneto-optical Kerr effect

Py ..... Permalloy

List of Constants

ε_0 ..... Permittivity of vacuum ($8.854 \cdot 10^{-12}$ $\mathrm{A\,s\,V^{-1}\,m^{-1}}$)

$\hbar$ ..... Planck's constant ($6.626 \cdot 10^{-34}$ $\mathrm{kg\,m^2\,s^{-1}}$)

μ_0 ..... Permeability of vacuum ($4\pi \cdot 10^{-7}$ $\mathrm{V\,s\,A^{-1}\,m^{-1}}$)

μ_B ..... Bohr's magneton ($9.274 \cdot 10^{-24}$ $\mathrm{A\,m^2}$)

e ..... Elementary electric charge ($1.602 \cdot 10^{-19}$ $\mathrm{A\,s}$)

k_B ..... Boltzmann's constant ($1.381 \cdot 10^{-23}$ $\mathrm{kg\,m^2\,s^{-2}\,K^{-1}}$)

m_e ..... Electron mass ($9.109 \cdot 10^{-31}$ kg)

List of Variables

$\vec{\nabla}$ ..... Nabla operator $\mathrm{m^{-1}}$

$\alpha_{v,x}, \alpha_{v,y}, \alpha_{v,z}$ Direction cosines of vector $\vec{v}$ in a Cartesian coordinate system

γ ..... Gyromagnetic ratio $\mathrm{m\,A^{-1}\,s^{-1}}$

$\Delta\xi_{ij}$ ..... Equivalent domain wall motion between $\mathcal{D}_i$ and $\mathcal{D}_j$ related to Δv_{ij}

$\Delta\xi_{\mathrm{Irr}}$ ..... Irreversible part of equivalent domain wall motion $\Delta\xi$

$\Delta\xi_{\mathrm{Rev}}$ .... Reversible part of equivalent domain wall motion $\Delta\xi$

λ ..... Magnetostriction constant

λ_{mf}	Molecular field constant	
λ_{s}	Isotropic magnetostriction constant	
μ	Magnetic permeability	$\mathrm{V\,s\,A^{-1}\,m^{-1}}$
μ_{ini}	Initial permeability	$\mathrm{V\,s\,A^{-1}\,m^{-1}}$
μ_{r}	Relative permeability	
ν_{NN}	Number of nearest neighbors	
ρ	Electric charge density	$\mathrm{A\,s\,m^{-2}}$
ρ_i	Correlation coefficient of magnetic entities in $\mathcal{D}_i$	
σ_i^2	Variance of magnetic entities in $\mathcal{D}_i$	$\mathrm{rad^2}$
σ_{Stress}	Mechanical stress	$\mathrm{N\,m^{-2}}$
Φ	Stochastic random variable for polar angle φ	
φ	Polar angle with respect to the x-axis	rad
$\bar{\varphi}_i$	Mean orientation of magnetic entities in $\mathcal{D}_i$	rad
χ	Magnetic susceptibility	
χ_{C}	Differential susceptibility at coercive field	
χ_{diff}	Differential susceptibility	
χ_{inc}	Incremental susceptibility	
χ_{ini}	Initial susceptibility	
χ_{irr}	Irreversible susceptibility	
χ_{rev}	Reversible susceptibility	
$\vec{\omega}_e$	Angular velocity of an electron	$\mathrm{s^{-1}}$
$\vec{\omega}_L$	Larmor angular velocity	$\mathrm{s^{-1}}$
A_{Ex}	Continuum exchange constant	$\mathrm{J\,m^{-1}}$
$\vec{B}$	Magnetic flux density (magnetic induction)	T
$\mathcal{B}_J(.)$	Brillouin function	
$\mathrm{CN}(\bar{\varphi}_i, \beta_i)$	Circular normal distribution with mean $\bar{\varphi}_i$ and concentration β_i	
$\mathrm{CU}(-\pi, \pi)$	Circular uniform distribution for interval $[-\pi, \pi]$	
c_{ij}	Factor for equivalent DWM $\Delta\xi_{ij}$ dependent on volume change Δv_{ij}	
$\mathcal{D}$	Statistical domain class	
$\vec{D}$	Electric flux density	$\mathrm{A\,s\,m^{-2}}$
$d_{\mathrm{Rev}}^{(+)}$	Maximum equivalent distance of reversible DWM in (+)-direction	
$d_{\mathrm{Rev}}^{(-)}$	Maximum equivalent distance of reversible DWM in (-)-direction	
d_{S}	Thickness of the magnetic sample	m
d_{TS}	Target-substrate distance	m
$\mathbb{E}(.)$	Statistical expectation value (operator)	

$\mathcal{E}$	Magnetic entity	
$\vec{E}$	Electric field strength	$\mathrm{V\,m^{-1}}$
$\vec{e}_x, \vec{e}_y, \vec{e}_z$	Unit vectors in cartesian coordinate system	
F_{Gibbs}	Gibbs free energy of a system	J
F_{Helm}	Helmholtz free energy of a system	J
f	Frequency	Hz
$f(.)$	Probability density function	
$f_i(\varphi)$	Probability density function of domain class $\mathcal{D}_i$	$\mathrm{rad^{-1}}$
g	Landé factor	
$\vec{H}$	Magnetic field strength	$\mathrm{A\,m^{-1}}$
H_{Aniso}	Anisotropy field	$\mathrm{A\,m^{-1}}$
H_{C}	Coercive field or (absolute) coercivity	$\mathrm{A\,m^{-1}}$
$\mathcal{H}_{\mathrm{Ex}}$	Hamiltonian for exchange energy	
$\vec{H}_{\mathrm{in}}$	Magnetic field inside the material	$\mathrm{A\,m^{-1}}$
H_{Pin}	Pinning field	$\mathrm{A\,m^{-1}}$
$\vec{H}_{\mathrm{Stray}}$	Magnetic stray field	$\mathrm{A\,m^{-1}}$
H_{sw}	Switching field	$\mathrm{A\,m^{-1}}$
$I_0(.)$	Modified Bessel function (1st kind, order 0)	
$I_1(.)$	Modified Bessel function (1st kind, order 1)	
I_{A}	Anode current	A
I_{C}	Thermionic cathode current	A
I_{F}	Field current	A
$\mathtt{J}$	Quantum number for total angular momentum of an atom	
$\vec{\mathbf{J}}$	Operator of total angular momentum of an atom	$\mathrm{kg\,m^2\,s^{-1}}$
$\vec{J}$	Electric current density	$\mathrm{A\,m^{-2}}$
J_{Ex}	Exchange constant	J
$\vec{K}$	Electric surface current density	$\mathrm{A\,m^{-1}}$
K_0, K_1, K_2	Anisotropy constants	$\mathrm{J\,m^{-3}}$
K_{Stray}	Stray field constant	$\mathrm{J\,m^{-3}}$
k_{Disp}	Model coefficient for magnetization dispersion	$\mathrm{J\,m^{-3}}$
k_{IrrDWM}	Model coefficient for irreversible losses due to domain wall motion	$\mathrm{J\,m^{-3}}$
k_{RevAnh}	Model coefficient for reversible anhysteretic energy	$\mathrm{J\,m^{-3}}$
k_{RevDWM}	Model coefficient for reversible work due to domain wall motion	$\mathrm{J\,m^{-3}}$
$k_{\mathrm{RevIrrDisp}}$	Model coefficient for rev. and irrev. work of magnetization disp.	$\mathrm{J\,m^{-3}}$
$\mathcal{L}(.)$	Langevin function	

$\mathtt{L}$	Quantum number for total orbital angular momentum of an atom	
$\vec{\mathbf{L}}$	Operator of total orbital angular momentum of an atom	$\mathrm{kg\,m^2\,s^{-1}}$
$\vec{L}$	Angular momentum	$\mathrm{kg\,m^2\,s^{-1}}$
δL	Differential work added to a system	J
$\mathtt{l}$	Angular quantum number	
$\vec{\mathbf{l}}$	Operator of electron orbital angular momentum	$\mathrm{kg\,m^2\,s^{-1}}$
l_{Bloch}	Bloch wall width	m
l_{Ex}	Exchange length	m
l_{S}	Characteristic sample length	m
l_{Wall}	Characteristic domain wall width	m
$\vec{M}$	Magnetization	$\mathrm{A\,m^{-1}}$
M_{H}	Magnetization component in field direction	$\mathrm{A\,m^{-1}}$
M_{R}	Remanent magnetization or (absolute) remanence	$\mathrm{A\,m^{-1}}$
M_{s}	Spontaneous or technical saturation magnetization	$\mathrm{A\,m^{-1}}$
$M_{\mathrm{s,th}}$	Theoretical saturation magnetization	$\mathrm{A\,m^{-1}}$
$\vec{\mathfrak{m}}$	Magnetic moment	$\mathrm{A\,m^2}$
$\vec{m}$	Reduced magnetization $\vec{M}/M_{\mathrm{s}}$	
m_{H}	Component of reduced magnetization in field direction	
$\vec{m}_i$	Reduced magnetization of domain class $\mathcal{D}_i$	
$\mathfrak{m}_J$	Abs. value of magn. moment of total angular momentum of an atom	$\mathrm{A\,m^2}$
$\mathfrak{m}_{J,z}$	Component with respect to quantization axis of $\mathfrak{m}_J$	$\mathrm{A\,m^2}$
$\vec{\mathfrak{m}}_l$	Magnetic moment due to orbital angular momentum	$\mathrm{A\,m^2}$
$\mathfrak{m}_l$	Abs. value of magn. moment of electron orbital angular momentum	$\mathrm{A\,m^2}$
$\mathtt{m}_l$	Magnetic quantum number	
$\mathfrak{m}_{l,z}$	Component with respect to quantization axis of $\mathfrak{m}_l$	$\mathrm{A\,m^2}$
$\mathfrak{m}_s$	Abs. value of magn. moment of electron spin angular momentum	$\mathrm{A\,m^2}$
$\mathtt{m}_s$	Spin quantum number (orientation of spin angular momentum)	
$\mathfrak{m}_{s,z}$	Component with respect to quantization axis of $\mathfrak{m}_s$	$\mathrm{A\,m^2}$
N	Number of particles per unit volume	$\mathrm{m^{-3}}$
$N_{\mathrm{a}}, N_{\mathrm{b}}, N_{\mathrm{c}}$	Demagnetizing factor along the principal ellipsoid axes a,b,c	
$\tilde{N}_{\mathrm{d,2D}}$	Two-dimensional demagnetizing tensor	
$\tilde{N}_{\mathrm{d}}$	Demagnetizing tensor	
$N_{\mathcal{D}}$	Number of statistical domain classes	
$\mathtt{n}$	Principal quantum number	
$n_{\mathcal{D}_i}$	Number of magnetic entities in domain class $\mathcal{D}_i$	

$n_{\mathcal{V}}$	Number of magnetic entities in volume $\mathcal{V}$	
$P(.)$	Probability (number of states) for a certain configuration	
$P_{\mathrm{Rev}}(.)$ ...	Probability for reversible domain wall motion	
p	Pressure	$\mathrm{N\,m^{-2}}$
p_{Ar}	Argon pressure	Pa
δQ	Differential heat added to a system	J
$\delta_{\mathrm{irr}}Q$	Differential heat created irreversibly inside the system	J
q	Reduced anisotropy coefficient	
q_{p}	Average number of BHJ per equivalent distance of domain wall motion	
$\vec{r}$	Position vector	m
$\mathcal{S}$	Macroscopic area section	
$\mathtt{S}$	Quantum number for total spin angular momentum of an atom	
$\vec{\mathbf{S}}$	Operator of total spin angular momentum of an atom	$\mathrm{kg\,m^2\,s^{-1}}$
S_{Int}	Internal entropy	$\mathrm{J\,K^{-1}}$
$\mathrm{d}S$	Differential increase in entropy	$\mathrm{J\,K^{-1}}$
$\mathrm{d}_{\mathrm{ext}}S$	Differential entropy added reversibly from outside of the system	$\mathrm{J\,K^{-1}}$
$\mathrm{d}_{\mathrm{irr}}S$	Differential entropy produced irreversibly inside the system	$\mathrm{J\,K^{-1}}$
$\mathtt{s}$	Quantum number of spin angular momentum	
$\vec{\mathbf{s}}$	Operator of electron spin angular momentum	$\mathrm{kg\,m^2\,s^{-1}}$
T	Absolute temperature	K
T_{C}	Curie temperature	K
T_{N}	Neel temperature	K
T_{Para}	Characteristic temperature in Curie-Weiss law	K
T_{S}	Substrate temperature	K
Δt	Time (simulation) step	s
t	Time	s
$\mathrm{d}U$	Differential increase in internal energy	J
U_{A}	Anode voltage	V
U_{S}	Substrate voltage	V
U_{T}	Target voltage	V
$\mathcal{V}$	Topological volume section (of the magnetic sample)	
V	Volume (of the magnetic sample)	$\mathrm{m^3}$
ΔV	Elementary volume	$\mathrm{m^3}$
$\partial\mathcal{V}$	Surface of volume $\mathcal{V}$	
v	Volume fraction	

$v_{0,i}$	Initial volume fraction at demagnetized state for $\mathcal{D}_i$	
Δv_i	Change of volume fraction of $\mathcal{D}_i$ during Δt	
v_i	Volume fraction of domain class $\mathcal{D}_i$	
Δv_{ij}	Change of volume fractions between $\mathcal{D}_i$ and $\mathcal{D}_j$ during Δt	
$\Delta v_{ij,\mathrm{Irr}}$	Irreversible part of change in volume fractions Δv_{ij}	
$\Delta v_{ij,\mathrm{Rev}}$	Reversible part of change in volume fractions Δv_{ij}	
$v_{\max,i}$	Maximum volume fraction (available states) for $\mathcal{D}_i$	
W	Energy	J
W_{MESelf}	Magnetostrictive self-energy	J
$\mathrm{WN}(\bar{\varphi}_i, \sigma_i^2)$	Wrapped normal distribution with mean $\bar{\varphi}_i$ and variance σ_i^2	
W_{Pin}	Pinning energy	J
W_{Stray}	Stray field energy	J
w	Energy per unit volume (averaged)	$\mathrm{J\,m^{-3}}$
$w(\vec{r})$	Energy density at position $\vec{r}$	$\mathrm{J\,m^{-3}}$
$w_{\mathrm{Aniso}}(\vec{r})$	Anisotropy energy density	$\mathrm{J\,m^{-3}}$
$w_{\mathrm{Aniso},i}$	Anisotropy energy per unit volume for $\mathcal{D}_i$	$\mathrm{J\,m^{-3}}$
w_{Bloch}	Bloch wall energy per unit surface	$\mathrm{J\,m^{-2}}$
w_{d}	Demagnetizing energy (ext. part of stray field energy) per unit volume	$\mathrm{J\,m^{-3}}$
$w_{\mathrm{Disp},i}$	Magnetization dispersion energy per unit volume for $\mathcal{D}_i$	$\mathrm{J\,m^{-3}}$
$w_{\mathrm{Ex}}(\vec{r})$	Volume exchange energy density	$\mathrm{J\,m^{-3}}$
$w_{\mathrm{Ex},i}$	Exchange energy per unit volume for $\mathcal{D}_i$	$\mathrm{J\,m^{-3}}$
$w_{\mathrm{H}}(\vec{r})$	Zeeman (applied field) energy density	$\mathrm{J\,m^{-3}}$
$w_{\mathrm{H},i}$	Zeeman (applied field) energy per unit volume for $\mathcal{D}_i$	$\mathrm{J\,m^{-3}}$
$\Delta w_{\mathrm{IrrDWM}}$	Change in irreversible losses per unit volume for domain wall motion	$\mathrm{J\,m^{-3}}$
Δw_{irr}	Irreversible losses per unit volume	$\mathrm{J\,m^{-3}}$
w_{Loc}	Total local energy contributions per unit volume	$\mathrm{J\,m^{-3}}$
$w_{\mathrm{Loc},i}$	Local energy contributions per unit volume for $\mathcal{D}_i$	$\mathrm{J\,m^{-3}}$
w_{Loss}	Losses per unit volume and hysteresis cycle	$\mathrm{J\,m^{-3}}$
w_{RevAnh}	Reversible anhysteretic energy per unit volume	$\mathrm{J\,m^{-3}}$
$\Delta w_{\mathrm{RevDWM}}$	Change in reversible work per unit volume for domain wall motion	$\mathrm{J\,m^{-3}}$
$\Delta w_{\mathrm{RevIrrDisp}}$	Change in rev. and irrev. work due to magnetization dispersion	$\mathrm{J\,m^{-3}}$
w_{Stray}	Stray field energy per unit volume	$\mathrm{J\,m^{-3}}$
$w_{\mathrm{Stress}}(\vec{r})$	Energy density related to non-magnetic stress	$\mathrm{J\,m^{-3}}$
$w_{\mathrm{Stress},i}$	Energy per unit volume related to non-magnetic stress for $\mathcal{D}_i$	$\mathrm{J\,m^{-3}}$
$w_{\mathrm{T},i}$	Energy per unit volume due to thermal excitation for $\mathcal{D}_i$	$\mathrm{J\,m^{-3}}$

Chapter 1

Introduction

1.1 Magnetic Hysteresis Modeling

A general description of the magnetization process in magnetic materials is complex in nature, because it is affected by the microstructure of the material, the shape of the sample, external forces such as magnetic field or mechanical stress, and environmental conditions, like temperature. Hence, the atomic magnetic moments are subjected to various interactions with the surrounding matter and external fields. Particularly, the concurrence of strong short-range and long-range interactions effects a collective macroscopic magnetic behavior. In other words, the magnetization process involves a manifold of phenomena from different areas and topics of physical and technical science.

1.1.1 Theoretical Concepts

Due to the variety of contributing fields of science, there exists no unique theory to explain magnetism, in general. So quantum-mechanics has nowadays been established as basis to describe magnetism at the atomic level. If the discrete nature of the atomic structure can be disregarded, the continuum theory of classical vector fields together with Maxwell's equations might be an appropriate tool to explain magnetic behavior.

In case of ordered magnetism, such as ferromagnetism, anti-ferromagnetism, and ferrimagnetism, short-range interactions between the magnetic moments and long-range dipole interactions that result in stray fields cause the formation of magnetic domains. For such systems, the framework of statistical mechanics and thermodynamics allows to represent these interactions by means of internal energies, entropy, and work. So the minimization of an appropriate thermodynamic potential, corresponding to the estimation of a macroscopic equilibrium state, should give the magnetic state of the material, in theory.

But when the configuration of the magnetic domains changes during the magnetization process, irreversible changes of states are either caused by switching from one local energy minimum to another one or the consequence of losses. Hence, the concepts of metastability and non-equilibrium thermodynamics have to be introduced in order to describe the magnetization process.

1.1.2 State of the Art

Within this scientific environment, many hysteresis models have been developed with varying degrees of success, but currently three models become established as state of the art.

Micromagnetic models are based on the minimization of Gibb's free energy of the total magnetic sample, so that all model parameters are related to the physical properties of the material. The magnetization vector is calculated for every point inside the sample by means of finite element methods.

In the context of the *Preisach model*, the magnetic material is represented by a collection of bistable units, where the shape parameters of these "Hysterons" are described via statistical distribution functions. The magnetization of the total magnetic sample is calculated as sum of the Hysteron's states within a purely mathematical framework. Hence, the relation between the Preisach distribution functions and physical material properties is not self-evident.

The *Jiles-Atherton hysteresis model* distinguishes between anhysteretic, reversible, and irreversible contributions to the total sample magnetization. Here, the magnetization contributions are formulated on a phenomenological basis, and a small set of model parameters allows easy identification based on experimental data as well as low computational effort.

1.1.3 Characteristics of Magnetic Hysteresis Models

Basically, the first step in magnetic hysteresis modeling is the identification of the model parameters based on the physical properties of the material sample and measured magnetization curves. As a general principle, the lower the number of model parameters, the less effort is necessary for identification. Especially in case where the model parameters cannot directly assigned to physical material properties, different parameter sets may result in nearly the same calculated magnetization curve.

One potential target in hysteresis modeling is to reproduce a set of experimentally measured magnetization curves with high accuracy. If the calculation procedure is fast enough, such a model can be used to the describe the magnetic behavior in the context of finite element simulations or control applications instead of using lookup tables.

A very basic characteristic of a hysteresis model is the ability to predict the magnetization process for other than the measured curves used for identification. Here, the quality of the model prediction is determined by the accuracy of the predicted hysteresis curve with respect to the measurement results on the one hand, and the variety of useful predictions when changing the external input variables (e.g. direction of the applied field, minor loops, etc.) or the environmental parameters (e.g. temperature) on the other hand. Clearly, the predictability of a model can only be assessed on measurement results, but the aim is to cover many different phenomena with just a single set of model parameters.

Another property of a hysteresis model is to relate the identified model parameters to microstructural properties of the material sample. So it might be useful to quantify the loss mechanisms for different magnetic samples, based on the measured hysteresis curves. Further, it can be helpful, if the model can provide at least a qualitative picture of the underlying magnetization process.

1.1.4 Philosophical Conclusion

From a general point of view, magnetism seems to elude a general unique scientific description. Instead, different theories and models have been developed in order to explain a certain range of magnetic phenomena.

Whenever reflecting on this topic, the following excerpt of PLANCK's discussion about causality in physics might be helpful to gain a better appreciation of the relation between theory, modeling, and reality.

Aber allein die einfache Tatsache,
daß wir wenigstens bis zu einem gewissen Grade imstande sind,
künftige Naturereignisse unseren Gedanken zu unterwerfen
und nach unserem Willen zu lenken,
müßte ein völlig unverständliches Rätsel bleiben,
wenn sie nicht zum Mindesten eine gewisse Harmonie ahnen ließe,
die zwischen der Außenwelt und dem menschlichen Geist besteht,
und es ist nur eine Frage von sekundärer Bedeutung,
bis zu welcher Tiefe man sich die Reichweite dieser Harmonie erstreckt denken will.

[Max PLANCK, „Der Kausalbegriff in der Physik“, 1941]

But just the simple fact
that we are at least partially able to
subject future natural phenomena to our thoughts
and affect them according to our will
would be a completely unknowable mystery,
if one would not be able to sense a certain harmony
existing between the outside world and the human mind,
and it is only a matter of secondary importance
up to which depth the scope of this harmony will be extended.

loose translation from
[Max PLANCK, „Der Kausalbegriff in der Physik“, 1941]

1.2 Objective of the Thesis

1.2.1 Historical Basis

In 1994, H. HAUSER introduced the "Energetic Model of Ferromagnetic Hysteresis". Although this model was initially intended for the prediction of the anisotropic magnetic curves of grain oriented FeSi steel, most of the following investigations have been performed by employing a scalar (one-dimensional) formulation of the energetic model. Even in the case of three-dimensional crystal structures, the scalar model has been set up for certain crystalline axes by taking the symmetry properties of the lattice structure into account. For the scalar model only two statistical domain classes, containing magnetic dipoles that are either oriented parallel or antiparallel to the applied field, are defined. In this case, the solution of the corresponding model equations can be derived analytically, so that the calculation time can be reduced to a minimum.

But in case of uniaxial anisotropy, the calculation of the magnetization curves requires a change of the model parameters depending on the direction of the applied field with respect to the easy anisotropy axis. Hence, if the identification of the model parameters is done for the easy axis and the hard axis, they can be interpolated for any arbitrary direction in between. In practice, this interpolation is only applicable, when the magnetization process is mainly driven by domain wall motion. But, whenever coherent magnetization rotation governs the magnetization process, the scalar model is reaching its limits.

1.2.2 Generalized Model

The first objective of this work is the extension of the scalar energetic model such that it provides a fully two-dimensional framework to describe the magnetization process in thin film materials. In this context, the generalized model must be able to deal with more than two domain classes in order to account for the various factors driving the magnetization process. For this purpose, a reformulation of the model equations is required, even though the basic structure of HAUSER's model partly supports a vectorial formulation. Particularly, the calculation procedure for the reversal of the domain wall motion has to be substantially revised. Furthermore, uniaxial anisotropy should be directly incorporated, so that coherent magnetization rotation can be reproduced by the generalized model.

Second, the idealized perfect parallel alignment of the magnetic dipoles in the statistical domain classes has to be generalized such that the temperature dependence of the spontaneous magnetization can be estimated from the first principles. In addition, misalignment of the magnetic moments due to inhomogeneities in the thin film should be describable within the model.

As third objective, the generalized energetic model should depend on small set of parameters, which can related to either physical properties of the material or phenomenological characteristics of the magnetization process.

Generally speaking, the overall objective of this thesis is to provide a hysteresis model that allows the simulation, prediction, and interpretation of the magnetization process of anisotropic thin films. In addition, the model structure should be compact and clear, but flexible enough to handle the various mechanisms leading to the macroscopic magnetic

behavior. Under these conditions, the generalized energetic model can be a valuable tool for the investigation of magnetic thin film material, starting from the production process up to specific applications.

1.3 Scope of the Thesis

Generally, this work is subdivided into three main parts and an appendix:

Starting with a *theoretical part*, the basic principles of magnetism are reviewed, beginning from the magnetic moment of an electron up to macroscopic magnetic phenomena. Furthermore, the relevant magnetic energy contributions are defined, and an overview of domain theory and the mechanisms of the magnetization process is provided. Although this theoretical part is not of scientific evidence, it ensures a common understanding of the terminology used in the description of the generalized energetic model afterwards.

As first chapter of the *modeling part*, an overview of the state of the art in magnetic hysteresis modeling is provided. Here, the basic principles and properties of established hysteresis models are summarized in order to classify the generalized energetic model in the scientific context published in corresponding literature.
The major contribution to the modeling part is dedicated to the formulation of the generalized two-dimensional "Energetic Model of Ferromagnetic Hysteresis". Starting from the definition of magnetic entities and statistical domain classes, all relevant model equations are derived from the first principles. After the formal description of the model setup, the calculation procedure is explained as minimization of energy terms.

In the *simulation and evaluation part* of this work, the generalized energetic model is applied to Permalloy thin films designed for the use in anisotropic magneto-resistive sensors. In the beginning, a brief survey of the production process, the measurement setup, and the magnetic characteristics of Permalloy thin films is presented. Then, the evaluation is done by comparing predicted magnetization curves of the model with experimental data from magneto-optical Kerr measurements. Particular attention is paid to the relation of the model parameters to microstructural properties of the thin film, which are mainly resulting from the technological parameters of the production process.

The *appendix* contains detailed derivations of the model equations, so that elaborate calculations can be excluded from the main part of the work, for the sake of readability. But if necessary, all results can be reproduced clearly.

Part I

Theoretical Framework

In the *second chapter* an outline of different descriptive levels as viewpoints for a magnetic system is presented. Starting from the atomic level the origin of magnetic moments and the underlying mechanisms are described. Magnetization, magnetic susceptibility, and permeability are introduced in the framework of a continuum model, which is based on Maxwell's equations. Subsequently, the commonly used classification of magnetic materials is sketched in a macroscopic point of view.

On the one hand this short summary should give an impression of the wide range of topics in magnetism and provide a relationship of the thesis to the context of scientific work. On the other hand it comes out that many approaches in magnetism are based on the aggregation of microscopic properties, a fact that is also reflected in the energetic model when elementary magnetic entities are grouped into statistical domain classes.

The *third chapter* deals with the description of a ferromagnetic system beyond atomic length scales. In the framework of continuous vector fields the quantum-mechanical properties of the system are expressed in terms of energy contributions. Due to long-range interaction mechanisms the formation of magnetic domains is often energetically favorable. Hence, a short survey of domain theory and the basic domain wall structures is given. For the description of macroscopic magnetic systems as a whole it is often sufficient to focus on the total sample magnetization and its dependence with respect to an applied magnetic field. Therefore, the characteristic points and properties of the magnetization curve are explained. Finally, reversible and irreversible magnetization mechanisms are distinguished for domain wall movement as well as for domain magnetization rotation.

Exactly the extensions of the classical energetic model in order to describe the anisotropic behavior in thin films are based on anisotropic energy contributions and coherent magnetization rotation mechanisms of the magnetization process. Furthermore, the integration of irreversible losses into the model has to be adapted when changing from a one-dimensional to a two-dimensional framework. For these reasons chapter 2 provides a theoretical basis on which the energetic model can be set up.

Chapter 2

Magnetism Overview

The existence of many different concepts and theories makes magnetism to appear perhaps a little bit confusing. One way to classify the variety of approaches is a distinction by the spatial dimension of point of view (Tab. 2.1). Each level contains a set of fundamental assumptions, theories and models. Nevertheless, these descriptive levels cannot be seen as independent as far as results from underlying levels build the basics for the following levels.

	Microscopic		Mesoscopic	Macroscopic
Level of description	Atomic Level	Micromagnetic Level	Domain Level	Sample Level
Length scale	$>$ Å	$>$ nm	$> \mu$m	$>$ mm
Typical techniques	Quantum mech., statistical thermodynamics	Continuum theory of classical vector fields	Domain theory	Phenomenological approach, phase theory
Explained phenomena	Origin of magnetic moment, interactions, crystal anisotropy	Internal structure of domain walls	Domain configuration	Magnetization process, magnetic hysteresis

Table 2.1: Different viewpoints in magnetism.

The *atomic level* deals with elementary magnetic moments, their interactions and their thermodynamic behavior within a certain crystal structure. Beside classical physics quantum mechanics is the fundamental basis for nearly all theoretic considerations. When disregarding the discrete nature of matter, such that a local quantity represents the spatial average over an elementary volume, one comes to the continuum theory of classical vector fields. At this *micromagnetic level* Maxwell's equations can be used to describe the magnetic structure in idealized small regions of magnetic media. In the next level of consideration one concentrates on magnetic domains that are separated by domain walls, where the internal construction of these domains and walls is not of particular interest. In many applications, it is necessary to describe the overall behavior for the whole magnetic sample in form of magnetization curves or other representative quantities. However, it seems to be clear that magnetic properties at the *sample level* cannot be determined from the atomic characteristics without using stochastic aggregation techniques.

2.1 Origin of Magnetism in a Microscopic Treatment

Within the following sections, emphasis will be placed on the basic concepts that reason elementary magnetic moments. More details can be found in corresponding literature, like [10], [21], [56], or [87].

2.1.1 Magnetic Moment of an Electron

Magnetic dipoles coupled on electrons or cores represent the basis of magnetism. Since magnetic monopoles have not been detected up to now, these fundamental dipoles can be seen as basic elements of the magnetic structure.

For *electrons* two different mechanisms are responsible for magnetism

- magnetic moment due to orbital angular momentum $\mathfrak{m}_l$, and
- magnetic moment due to spin $\mathfrak{m}_s$.

Beside electrons also the *nucleus* shows a magnetic dipole moment, which is about more than three orders of magnitude smaller than dipole moments resulting from electrons, because the mass of protons and neutrons is about 2.000 times that of an electron. But the interaction between electrons and the field of the nucleus may cause a splitting of degenerated energy levels, the so called hyperfine structure.

As shown in the following pages magnetic moments can be associated with angular momentum.

Classical Description of Orbital Magnetic Moment

Within a simple model depicted in Fig. 2.1 we consider a single electron with mass m_e and electric charge $-e$ moving in a circular orbit of radius r at an angular velocity ω_e. The angular momentum is

$$\vec{L} = \vec{r} \times (m_e \, \vec{v}_e) = m_e \vec{\omega}_e r^2 \tag{2.1}$$

and the associated electric current

$$I_e = -e \, \frac{\omega_e}{2\pi} \tag{2.2}$$

delivers a magnetic moment of

$$\mathfrak{m}_l = I_e r^2 \pi = -\frac{e}{2} \omega_e r^2 \quad . \tag{2.3}$$

The combination of angular momentum (2.1) and magnetic moment (2.3) yields the so called *magneto-mechanical parallelism*

$$\vec{\mathfrak{m}}_l = -\frac{e}{2m_e} \vec{L} \quad , \tag{2.4}$$

which is crucial for all further considerations.

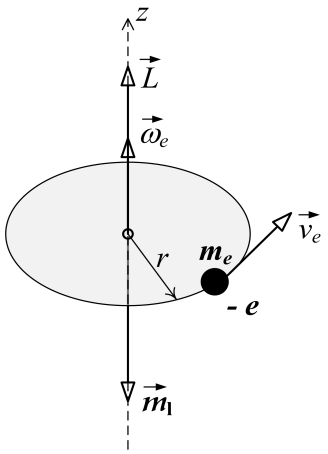

Figure 2.1: Orbital angular momentum and magnetic moment of an electron.

Quantizing the Angular Momentum

Niels Bohr postulated (about 1913) that the angular momentum L has to be an integer multiple of Planck's constant $\hbar$. This approach is often referred to as *old quantum mechanics*. Using

$$L = k\,\hbar \qquad k \in \mathbb{N} \quad , \tag{2.5}$$

the magnetic moment

$$\mathfrak{m}_l = -k\frac{e\,\hbar}{2m_e} = -k\,\mu_B \tag{2.6}$$

is a multiple of *Bohr's magneton*

$$\mu_B = \frac{e\,\hbar}{2m_e} \approx 9.27 \cdot 10^{-24}\mathrm{Am}^2 \quad . \tag{2.7}$$

So the magnetic moment of the orbital motion can change its value only by multiples of μ_B and one Bohr magneton is the smallest possible magnetic moment in this sense.

A brief survey of the historical development of quantum-mechanical theories in magnetism and related work is given in [84].

Quantum-Mechanical Description of Magnetic Moment

Bohr - van Leeuwen Theorem: In 1911 N. Bohr and in 1919 Ms. van Leeuwen showed independently that the mean value of the orbital magnetic moment $\langle\vec{\mathfrak{m}}_l\rangle$ is always zero, and therefore magnetic phenomena (dia-, paramagnetism, etc.) cannot be explained in terms of classical physics. In other words, if classical Boltzman statistics (probability for a particular state having energy U is proportional to $\mathrm{e}^{-U/(k_B T)}$) is applied to a dynamic system in thermodynamic equilibrium, this has to result in a zero susceptibility.

Spin: Beside the orbital angular momentum mentioned above, an electron provides another contribution to magnetic moment - the spin angular momentum. In principle, spin is a pure quantum-mechanical quantity without any classical analogon, nevertheless it is often interpreted as motion of the electron about its own axis. In quantum mechanics, spin is seen as intrinsic angular momentum associated with particles like electrons or neutrons. Classical spinning objects derive their angular momentum from the rotation of their constituent parts, whereas spin angular momentum is not associated with any rotating internal mass.

Orbital and spin angular momentum can be described by means of an operator of spatial rotation. So both act as angular momentum, and therefore spin causes like the classical orbital motion of the electron also a magnetic moment. Using the correspondence principle between classical and quantum mechanics, we substitute the observables[1] (the angular momentum) by the corresponding quantum-mechanical operators[2].

classic orbital angular momentum $\vec{L}$	$\longleftrightarrow$	operator of orbital angular momentum $\vec{\mathbf{l}}$
?	$\longleftrightarrow$	operator of spin angular momentum $\vec{\mathbf{s}}$

Because the operator's components do not commutate (i.e. we cannot estimate them at the same time) the norm and one component (z-component) of the operator is a useful set of observables. In this sense we get the eigenvalue problem for the orbital angular momentum operator

$$\vec{\mathbf{l}}^{\,2}\,|\,\mathtt{l},\mathtt{m}_l\rangle = \hbar^2(\mathtt{l}+1)\mathtt{l}\,|\,\mathtt{l},\mathtt{m}_l\rangle \tag{2.8a}$$

$$\mathbf{l}_z\,|\,\mathtt{l},\mathtt{m}_l\rangle = \hbar\,\mathtt{m}_l\,|\,\mathtt{l},\mathtt{m}_l\rangle \tag{2.8b}$$

and for the spin angular momentum operator

$$\vec{\mathbf{s}}^{\,2}\,|\,\mathtt{s},\mathtt{m}_s\rangle = \hbar^2(\mathtt{s}+1)\mathtt{s}\,|\,\mathtt{s},\mathtt{m}_s\rangle \tag{2.9a}$$

$$\mathbf{s}_z\,|\,\mathtt{s},\mathtt{m}_s\rangle = \hbar\,\mathtt{m}_s\,|\,\mathtt{s},\mathtt{m}_s\rangle \tag{2.9b}$$

with the eigenvalues[3] of an electron

$\mathtt{n}$	$\in \{1,2,3,\ldots\}$	principal quantum number (size and energy of the orbit)
$\mathtt{l}$	$\in \{0,1,2,\ldots,\mathtt{n}-1\}$	angular quantum number (orbital ang. m., shape of the orbit)
$\mathtt{m}_l$	$\in \{-\mathtt{l},\ldots,-1,0,1,\ldots,\mathtt{l}\}$	magnetic quantum number (orientation of orbital ang. m.)
$\mathtt{s}$	$= \frac{1}{2}$	spin angular momentum (absolute value)
$\mathtt{m}_s$	$\in \{-\frac{1}{2},\frac{1}{2}\}$	spin quantum number (orientation of spin ang. m.)

In a semi-classical point of view the angular momentum operator $\vec{\mathbf{l}}$ is plotted as a vector with length $\hbar\sqrt{(\mathtt{l}+1)\mathtt{l}}$, which z-component takes the discrete values $\hbar\,\mathtt{m}_l$, whereas x- and y-components are still undecided (see Fig. 2.2).

[1] Observables are all measurable properties of a system's state, like position, momentum, angular momentum or energy.

[2] In a quantum-mechanical system all possible states are represent by unit vectors (state vectors) residing in a complex Hilbert space (state space). Each observable is represented by a linear operator acting on this state space. Eigenstates of observables correspond to eigenvectors of the operator. The values of the observable in an eigenstate correspond to the eigenvalues associated to the eigenvector.

[3] Note, a general solution of the eigenvalue problem (2.8) gives $\mathtt{l} \in \{0, 1/2, 1, 3/2, 2, ...\}$ and therefore $\mathtt{m}_l \in \{-\mathtt{l}, -\mathtt{l}+1, ..., -1, 0, 1, ..., \mathtt{l}-1, \mathtt{l}\}$, but it can be shown that for orbital angular momentum of an electron only integer-valued eigenvalues are allowed.

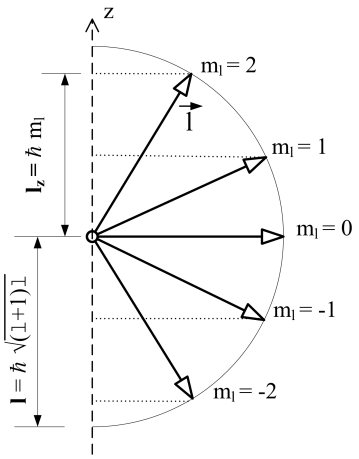

Figure 2.2: Semi-classical picture of the orbital angular momentum for l=2.

As mentioned above, we replace the classical angular momentum by the corresponding quantum-mechanical operator and get the magnetic moments of a single electron as

$$\text{orbital moment: } \vec{\mathtt{m}}_l = -g_l \frac{\mu_B}{\hbar}\vec{\mathtt{l}} \qquad \text{spin moment: } \vec{\mathtt{m}}_s = -g_s \frac{\mu_B}{\hbar}\vec{\mathtt{s}}, \tag{2.10}$$

their absolute value

$$\mathtt{m}_l = g_l \mu_B \sqrt{(\mathtt{l}+1)\mathtt{l}} \qquad \mathtt{m}_s = g_s \mu_B \sqrt{(\mathtt{s}+1)\mathtt{s}} \quad , \tag{2.11}$$

and their component in z-direction

$$\mathtt{m}_{l,z} = g_l \mu_B \mathtt{m}_l \qquad \mathtt{m}_{s,z} = g_s \mu_B \mathtt{m}_s \quad . \tag{2.12}$$

The parameter g - known as *Landé factor* or gyromagnetic ratio - is $g_l = 1$ for pure orbital moments and $g_s = 2.0023$ for spin moments. The latter is a result of the relativistic Dirac theory and may be seen as quantum-mechanical correction in view of the fact that the spin does not behave like a classical angular momentum.

2.1.2 Magnetic Moment of an Isolated Atom

In an atom or ion that consists of n electrons one has to consider $2n$ coupled magnetic moments (orbital and spin). These n electrons (each can either be in 'spin up' $\mathtt{m}_{s,i} = 1/2$ or 'spin down' $\mathtt{m}_{s,i} = -1/2$ state) reside in certain electron shells that are characterized by the quantum numbers $\mathtt{n}$ and $\mathtt{l}$. Such a state (electrons in certain shells) is referred to as *configuration*, which is usually degenerated except in full shells.

Russell Saunders Coupling and Hund's Rules: Electron systems with localized magnetic moments are described by their total angular momentum. For calculations with more than one electron we have to consider the Coulomb interaction between electrons as well as the spin-orbit coupling. For not too heavy elements the latter is smaller than the Coulomb interaction and leads to the so called *Russell Saunders coupling (L-S coupling)*.

Let us denote $\vec{\mathbf{l}}_i$ as (operator of) orbital angular momentum and $\vec{\mathbf{s}}_i$ as spin angular momentum of an individual electron $i = 1 \dots n$. Assuming that the interaction between orbital and spin angular momentum is small compared to orbital-orbital and spin-spin interaction, we obtain the total orbital angular momentum of n electrons

$$\vec{\mathbf{L}} = \sum_{i=1}^{n} \vec{\mathbf{l}}_i \quad , \tag{2.13}$$

the total spin angular momentum

$$\vec{\mathbf{S}} = \sum_{i=1}^{n} \vec{\mathbf{s}}_i \quad , \tag{2.14}$$

and the *total angular momentum*

$$\vec{\mathbf{J}} = \vec{\mathbf{L}} + \vec{\mathbf{S}} \quad . \tag{2.15}$$

The corresponding quantum numbers, which define the state of the electron system, are denoted in capital letters as $\mathtt{L}$, $\mathtt{S}$ and $\mathtt{J}$.

$$\mathtt{L} = \sum_{i=1}^{n} \mathtt{m}_{l,i} \qquad \mathtt{S} = \sum_{i=1}^{n} \mathtt{m}_{s,i} \qquad \mathtt{J} = |\mathtt{L} \pm \mathtt{S}| \tag{2.16}$$

For filled shells we get $\mathtt{L} = 0$ (orbital angular momentum adds up to zero) as well as $\mathtt{S} = 0$ (spin angular momentum adds up to zero), and that is why closed shells do not produce any permanent magnetic moment. Accordingly, these quantum numbers $\mathtt{L}$, $\mathtt{S}$ and $\mathtt{J}$ represent the whole atom and the electronic configuration of the partially filled shells, too.

The energy minimizing sequence of occupation used to determine the most stable orbital and spin configuration (multiplet structure of a certain atom) is given by the empirical *Hund's rules*:

1. The lowest energy corresponds to a state with a maximum value for the multiplicity $2\,|\mathtt{S}| + 1$. A maximization of $\mathtt{S}$ (meaning that as many electrons as possible are 'spin up') can be seen as minimization of Coulomb energy, because Pauli's exclusion principle prevents that electrons of the same spin are in the same (neighboring) state.

2. The state having the largest value of $\mathtt{L}$ (angular momentum) for a given multiplicity is the one with the lowest energy. A maximization of $\mathtt{L}$ can also be interpreted as minimization of Coulomb energy, because electrons in a shell that have the same sign of $\mathtt{m}_l$ can be imagined to rotate in the same direction and therefore reducing Coulomb repulsion.

3. In the case of a less than half filled shell the total angular momentum is given by $\mathtt{J} = |\mathtt{L} - \mathtt{S}|$, otherwise by $\mathtt{J} = |\mathtt{L} + \mathtt{S}|$.

The union of all $(2\mathtt{L} + 1)\,(2\mathtt{S} + 1)$ states for given $\mathtt{L}$ and $\mathtt{S}$ of a certain electronic configuration is denoted as *term*.

Total Magnetic Moment: In analogy to the magnetic moment of a single electron the orbital and spin magnetic moment of the electron system

$$\vec{\mathfrak{m}}_L = -g_l \frac{\mu_B}{\hbar}\vec{\mathbf{L}} \qquad \vec{\mathfrak{m}}_S = -g_s \frac{\mu_B}{\hbar}\vec{\mathbf{S}} \tag{2.17}$$

add up to the *total magnetic moment*

$$\vec{\mathfrak{m}} = \vec{\mathfrak{m}}_L + \vec{\mathfrak{m}}_S = -\frac{\mu_B}{\hbar}\left(g_l\vec{\mathbf{L}} + g_s\vec{\mathbf{S}}\right) \approx -\frac{\mu_B}{\hbar}\left(\vec{\mathbf{L}} + 2\vec{\mathbf{S}}\right) \quad . \tag{2.18}$$

Since we can only measure the component with respect to $\vec{\mathbf{J}}$ and due to spin-magnetic anomaly orbital and spin component cannot simply be added (see Fig. 2.3), we define the Landé factor

$$g_j = 1 + \frac{\mathtt{J}(\mathtt{J}+1) - \mathtt{L}(\mathtt{L}+1) + \mathtt{S}(\mathtt{S}+1)}{2\mathtt{J}(\mathtt{J}+1)} \tag{2.19}$$

and get the total magnetic moment

$$\vec{\mathfrak{m}}_J = -g_j \frac{\mu_B}{\hbar}\vec{\mathbf{J}} \tag{2.20a}$$

$$\mathfrak{m}_J = g_j \mu_B \sqrt{(\mathtt{J}+1)\mathtt{J}} \tag{2.20b}$$

$$\mathfrak{m}_{J,z} = g_j \mu_B \mathfrak{m}_J \qquad \text{with } \mathfrak{m}_J \in \{-\mathtt{J}, \ldots, -1, 0, 1, \ldots, \mathtt{J}\} \quad . \tag{2.20c}$$

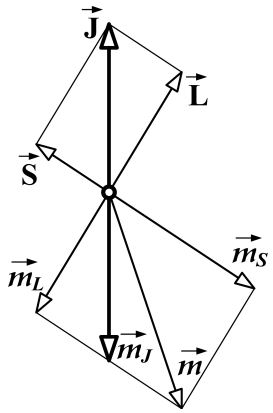

Figure 2.3: Addition of angular and magnetic moments in a semi-classical representation.

Finally, it can be summarized that the first two of Hund's rules are based on the minimization of Coulomb energy between neighboring electrons. But Hund's third rule relates to a minimization of the spin-orbit interaction, assuming that this is the next most significant energy term after Coulomb energy, a fact that is not always true, when atoms are placed in a crystal lattice, for example.

2.1.3 Magnetic Moment of Materials

Magnetic Materials

From a generic point of view a material is said to be magnetic, if it possesses permanent magnetic moment, at least in some parts of the sample volume. While most of the pure elements are magnetic in the atomic state (as an isolated atom), only a small fraction carry a permanent magnetic moment in the solid state (as molecule or crystal), because the electronic orbits, which are responsible for the magnetic properties, are influenced by the formation of a chemical bond. However, a permanent magnetic moment results from partially filled electronic shells that are deep enough (and therefore protected by shells lying further outside) to remain non-saturated even when they are in a polyatomic ensemble.

Hence, there are two series of elements that are of theoretical interest as well as practical importance[4] (antiferromagnetic elements are in *italic*):

- 3d elements - iron group of transition metals (*Cr*, *Mn*, Fe, Co, Ni)
- 4f elements - rare earths (lanthanides, e.g. *Nd*, *Sm*, Eu, Gd, Tb, Dy, Ho, Er, Tm)

The magnetic behavior of materials that consist of different elements (compounds, alloys) cannot be explained by their constituents in a simple way. For example the ferromagnetic Heusler alloy (Cu_2MnAl) is made of diamagnetic copper, antiferromagnetic manganese, and paramagnetic aluminium.

When analyzing more than a single isolated atom, one has to consider the electronic structure and the interaction mechanisms between the particles. In principle one has to deal with a many body problem that cannot be solved exactly in practice. Thus, the two approximations of *localized magnetic moments* and *itinerant (delocalized) magnetic moments* are used as simplified models in order to describe magnetic materials.

Localized Magnetic Moments

A major characteristic of such localized systems is the fact, that each individual electron is assigned to one orbital place within the atom according to *Pauli's principle*[5]. *Exchange* within the atoms (*intra-atomic* spin-orbit interaction) is the major contribution to interaction and therefore magnetic moment results from angular momentum of the electron system. In other words, the relativistic spin-orbit (Russell Saunders) coupling is much stronger than crystal field effects, so that the magnetic behavior can be estimated as in free atoms and `J` together with `L` and `S` are good quantum numbers to determine the magnetic moment. This description can be applied for free atoms, ions in chemical complexes, and rare earth elements. For the rare earth elements the partially filled 4f shell, which is responsible for magnetism, is located deep inside the atom[6], shielded by the outlying shells (5s, 5p, ...), and thus only little affected by bonding mechanisms and crystal field.

[4] The name 3d and 4f elements comes from the partially filled 3d (`n`=3, `l`=2) or 4f (`n`=4, `l`=3) shell that is responsible for magnetism.

[5] Each electron must occupy a different orbit (energy state) which is defined by the four quantum numbers `n` , `l` , m_l, and m_s.

[6] The probability at which distance from the nucleus an electron within a certain shell can be found (radial distribution function) can be calculated from the corresponding wave-functions.

Itinerant Magnetic Moments

Opposite to localized systems electrons[7] are no longer bound to discrete energy levels, they can move quasi freely in the crystal's periodic potential. The effect of the environment is represented by the electric crystal field of the neighboring atoms. In consequence of that, the quantum numbers are not able to describe the particles' behavior, so the metallic state is seen as electron gas represented by an *electronic band structure* instead of discrete momentum levels. In the simplest case one can consider the valence electrons as particles that can freely move in a constant potential[8]. Therefore, the *wave vector* $\vec{k}$ (which represents a plane wave as solution of the Schrödinger equation in a constant potential) and the *spin direction* (spin up - spin down), or equivalently the *energy* and the *density of states* are used to describe the magnetic moment of such a delocalized (itinerant) system.

The major interaction exists between neighboring atoms or ions (electrostatic interaction) by an *inter-atomic exchange* via valence electrons. Due to crystal field effects, which are much stronger than spin-orbit interaction, the spherical symmetry of the free atom is destroyed and the *orbital momentum* becomes *quenched* ($\mathtt{L} = 0$, $\mathtt{J} = \mathtt{S}$, and $g_j = 2$). In a semi-classical picture the net orbital angular momentum averages to zero due to the crystal field.

Within the framework of this itinerant electron model one is able to explain magnetism in metals, such as the 3d transition metals.

2.1.4 Exchange Interactions

In order to describe collective magnetic phenomena, one has to consider long-range interaction mechanisms between the magnetic moments of a solid. The most intuitive mechanism is the *dipolar interaction* between two magnetic dipoles. But this classical type of interaction is so weak that it just plays a role at very low temperatures. In practice, the quantum mechanical *exchange interactions*, which are of electrostatic origin, are the mechanisms of relevance.

Direct Exchange

When the exchange interaction takes place between electrons on neighboring magnetic atoms (without intermediary atoms) it is called direct exchange. Unfortunately, this direct exchange is not a dominant exchange mechanism for most of the materials, because neighboring orbitals (of the magnetic relevant shells) have only a small overlap.

Electrons are represented by fermions that are defined by antisymmetric[9] wave functions for an ensemble of two or more electrons. Since the total wave function is the product of a spatial and a spin wave function, one of them has to be symmetric and the other one antisymmetric. For *two electrons* the spin wave function can either be antisymmetric (representing the singlet state with $\mathtt{S} = 0$) or symmetric (representing the triplet state with $\mathtt{S} = 1$). The difference in energies of the singlet and the triplet state defines the *exchange*

[7] Strictly speaking *valence electrons*, because electrons of full shells do not contribute to magnetic moment.

[8] In practice the presence of the ionic atom cores tends to localize the freely moving valence electrons and leads to a periodic potential.

[9] Antisymmetric related to the pairwise exchange of particles.

constant between two electrons as $J_{\mathrm{Ex}} = 1/2\ (E_{\mathrm{Singlet}} - E_{\mathrm{Triplet}})$, and the Hamiltonian (that is related to the energy) in terms of two spins $\vec{\mathbf{s}}_1$ and $\vec{\mathbf{s}}_2$

$$\mathcal{H}_{\mathrm{Ex}} = -2\, J_{\mathrm{Ex}} \frac{1}{\hbar^2}\, \vec{\mathbf{s}}_1 \cdot \vec{\mathbf{s}}_2 \quad . \tag{2.21}$$

A generalization to a *many-body system* can only be done as approximation, such that one accounts only for interactions between the nearest neighbors that are all characterized by the same exchange constant J_{Ex}. The Hamiltonian of the so called *Heisenberg model* is then

$$\mathcal{H}_{\mathrm{Ex}} = -2\, J_{\mathrm{Ex}} \frac{1}{\hbar^2} \sum_{\langle i,j \rangle} \vec{\mathbf{s}}_i \cdot \vec{\mathbf{s}}_j \quad , \tag{2.22}$$

where $\langle i, j \rangle$ denotes the summation over all nearest neighbor spins in an ensemble of electrons.

Positive exchange constants effect parallel alignment of neighboring spins (triplet ground state), and negative exchange constants antiparallel alignment (singlet ground state). Although direct exchange is rather rarely dominant in practice, the form of the Heisenberg Hamiltonian is a good approximation for more general kinds of exchange mechanisms.

Indirect Exchange

Indirect exchange mechanisms describe concepts of a long-range magnetic order, when no direct interaction via overlapping orbitals is possible.

Superexchange: For a number of ionic solids[10] the exchange interaction between non-neighboring magnetic ions (transition metal) is mediated by a non-magnetic ion (e.g. O^{2-}). The energy of the compound can be reduced by a virtual hopping of the corresponding 3d- and p-electrons, if the 3d-spins between contiguous metal ions are aligned antiparallel.

RKKY Exchange: In rare earth elements the exchange interaction between localized magnetic electrons (4f) is mediated by conduction electrons (s or d), such that the localized moment spin-polarizes the conduction electrons and therefore couples to the neighboring localized moment. This mechanism is named after its discoverers (Ruderman, Kittel, Kasuya, and Yoshida) and leads either to parallel or to antiparallel alignment of spins[11], depending on the distance between neighboring spins and the filling of the band.

Double Exchange: If the magnetic ions can exist in more than one oxidation state (e.g. Mn^{3+} and Mn^{4+}, Fe^{2+} and Fe^{3+}) within a compound, one electron can hop between these ions. Simply spoken, this hopping that reduces energy is only possible when the spins of the magnetic ions are parallel. One example is the series $La_{1-x}Sr_xMnO_3$ (with trivalent La^{3+} and bivalent Sr^{2+}), where x determines the fraction of Mn^{3+} and Mn^{4+} ions. In this case the electron transfer from the Mn^{3+} to the Mn^{4+} ion is mediated via the oxygen ion. Another example is magnetite Fe_3O_4 that contains Fe^{2+} as well as Fe^{3+} ions.

[10] Most of the magnetic insulators comprise of magnetic transition metal ions and non-magnetic ions (such as O^{2-}, S^{2-}, Cl^-, or F^-).

[11] The localized magnetic moments produce an oscillating magnetization of the electron gas. So it depends on the distance and on the wavelength of this oscillation, whether the coupling is parallel or antiparallel.

2.2 Continuous Magnetization and Susceptibility

If one is interested in magnetic modeling, when the relevant length scale is orders larger than the inter-atomic distance, *continuum models* are used. Since the individual position of an atom is no longer of relevance, the discrete nature of the underlying characteristics is replaced by a local average over an *elementary volume* ΔV around the position vector $\vec{r}$.

2.2.1 Microscopic Description and Continuum Models

The *microscopic description* is based on a discrete set of charged particles $\mathcal{P}_i$ (charge $q_{\mathcal{P}_i}$, magnetic moment $\vec{\mathfrak{m}}_{\mathcal{P}_i}$) moving in vacuum media. The motion of these particles is represented by the microscopic current density $\vec{J}_{\text{Micro}}$ and their charge by the microscopic charge density ρ_{Micro}. Together with the microscopic electric and magnetic fields $\vec{E}_{\text{Micro}}$ and $\vec{B}_{\text{Micro}}$, which give reasons for the Lorentz force acting on the particles, the microscopic Maxwell equations can be stated as

$$\vec{\nabla} \cdot \vec{E}_{\text{Micro}} = \frac{\rho_{\text{Micro}}}{\varepsilon_0} \qquad \vec{\nabla} \times \vec{E}_{\text{Micro}} = -\frac{\partial \vec{B}_{\text{Micro}}}{\partial t} \tag{2.23a}$$

$$\vec{\nabla} \cdot \vec{B}_{\text{Micro}} = 0 \qquad \vec{\nabla} \times \vec{B}_{\text{Micro}} = \mu_0 \vec{J}_{\text{Micro}} + \mu_0 \varepsilon_0 \frac{\partial \vec{E}_{\text{Micro}}}{\partial t} \quad . \tag{2.23b}$$

Here we have the *permeability of vacuum*

$$\mu_0 = 4\,\pi\,10^{-7}\ \text{Vs/Am} \tag{2.24}$$

and the *vacuum permittivity*

$$\varepsilon_0 = 8.854\ 10^{-12}\ \text{As/Vm} \tag{2.25}$$

as universal constants.

The corresponding *continuum model* is obtained by applying the spatial average $\langle . \rangle$ over the microscopic values for the elementary volumes ΔV around the position vector $\vec{r}$ (see [83]). Thus, one get the classical electromagnetic fields as

$$\vec{E}(\vec{r}) = \left\langle \vec{E}_{\text{Micro}} \right\rangle |_{\vec{r}} \quad \text{and} \quad \vec{B}(\vec{r}) = \left\langle \vec{B}_{\text{Micro}} \right\rangle |_{\vec{r}} \quad . \tag{2.26}$$

The spatial average of the microscopic current density can be separated into three contributions

$$\left\langle \vec{J}_{\text{Micro}} \right\rangle |_{\vec{r}} = \vec{J}(\vec{r}) + \vec{J}_{\text{P}}(\vec{r}) + \vec{J}_{\text{M}}(\vec{r}) \quad , \tag{2.27}$$

where $\vec{J}$ describes the motion of free charged particles, $\vec{J}_{\text{P}}$ the motion of charged particles bound on electric dipoles, and $\vec{J}_{\text{M}}$ the motion of charged particles bound on magnetic dipoles. The spatial average of the microscopic charge density can also be separated in the free electric charge density ρ and the charge density ρ_{P} bound on electric dipoles

$$\langle \rho_{\text{Micro}} \rangle |_{\vec{r}} = \rho(\vec{r}) + \rho_{\text{P}}(\vec{r}) \quad . \tag{2.28}$$

2.2.2 Magnetization

In magnetic media the continuous *magnetization* $\vec{M}(\vec{r})$ is given by the sum of the atomic or ionic magnetic moments $\vec{\mathfrak{m}}_{\mathcal{P}_i}$ per elementary volume ΔV

$$\vec{M}(\vec{r}) = \frac{1}{\Delta V} \sum_{i \epsilon \Delta V} \vec{\mathfrak{m}}_{\mathcal{P}_i} \quad , \tag{2.29}$$

and represents the density of magnetic moment $\vec{\mathfrak{m}}_{\mathcal{V}}$ within a sample volume $\mathcal{V}$

$$\vec{\mathfrak{m}}_{\mathcal{V}} = \int\limits_{\mathcal{V}} \vec{M}(\vec{r}) \, \mathrm{d}V \quad . \tag{2.30}$$

Orbital as well as spin[12] magnetic moments can be seen as elementary magnetic (dipole) moments, which are represented by the intrinsic bound current density $\vec{J}_{\mathrm{M}}(\vec{r})$ in the framework of the continuum model. Compared to the classical free current density $\vec{J}(\vec{r})$ the intrinsic current density $\vec{J}_{\mathrm{M}}(\vec{r})$ involves no macroscopic flow of charges

$$\vec{\nabla} \cdot \vec{J}_{\mathrm{M}}(\vec{r}) = 0 \tag{2.31}$$

and can be figured as current loops at the atomic scale. Hence, the surface integral over an arbitrary cross-section $\mathcal{S}$ must vanish

$$\int\limits_{\mathcal{S}} \vec{J}_{\mathrm{M}}(\vec{r}) \cdot \overrightarrow{\mathrm{d}S} = 0 \quad , \tag{2.32}$$

which allows a reformulation as curl of another vector field $\vec{M}(\vec{r})$

$$\vec{J}_{\mathrm{M}}(\vec{r}) = \vec{\nabla} \times \vec{M}(\vec{r}) \quad . \tag{2.33}$$

Elementary current loops that cancel out inside the volume $\mathcal{V}$ may cause a bound surface current density

$$\vec{K}_{\mathrm{M}}(\vec{r}) = \vec{M}(\vec{r}) \times \vec{n}(\vec{r}) \quad , \tag{2.34}$$

where $\vec{n}(\vec{r})$ is the unit vector perpendicular to the surface. Using the generic definition of the magnetic moment $\vec{\mathfrak{m}}_{\mathcal{V}}$ resulting from the current distribution $\vec{J}_{\mathrm{M}}(\vec{r})$ inside some region $\mathcal{V}$ and the surface current distribution $\vec{K}_{\mathrm{M}}(\vec{r})$ on the corresponding surface $\partial\mathcal{V}$

$$\vec{\mathfrak{m}}_{\mathcal{V}} = \int\limits_{\mathcal{V}} \frac{\vec{r} \times \vec{J}_{\mathrm{M}}(\vec{r})}{2} \, \mathrm{d}V + \int\limits_{\partial\mathcal{V}} \frac{\vec{r} \times \vec{K}_{\mathrm{M}}(\vec{r})}{2} \, \mathrm{d}S = \int\limits_{\mathcal{V}} \vec{M}(\vec{r}) \, \mathrm{d}V \tag{2.35}$$

gives together with (2.33) and (2.34) the well known expression (2.30) for the magnetization.

[12] Although the spin magnetic moment is explained in a pure quantum-mechanical framework, the relativistic Dirac equation allows to prove that the expectation value of the spin moment can be represented by a classical dipole moment and the corresponding current density.

Applying the spatial averaging[13] to the microscopic Maxwell equations (2.23) together with (2.26)-(2.28), (2.31), (2.33), and the electric polarization $\vec{P}(\vec{r})$

$$\vec{J}_{\mathrm{P}}(\vec{r}) = \frac{\partial \vec{P}(\vec{r})}{\partial t} \qquad \vec{\nabla} \cdot \vec{J}_{\mathrm{P}}(\vec{r}) = -\frac{\partial \rho_{\mathrm{P}}(\vec{r})}{\partial t} \tag{2.36}$$

gives rise to the vector fields of the magnetic field strength $\vec{H}(\vec{r})$

$$\vec{B}(\vec{r}) = \mu_0 \left(\vec{H}(\vec{r}) + \vec{M}(\vec{r}) \right) \tag{2.37}$$

and the electric flux density $\vec{D}(\vec{r})$

$$\vec{D}(\vec{r}) = \varepsilon_0 \vec{E}(\vec{r}) + \vec{P}(\vec{r}) \quad . \tag{2.38}$$

Thus, the magnetic flux density $\vec{B}$ comprises of a vector field $\vec{H}$ that is basically determined by free current $\vec{J}$ and dielectric displacement current $\frac{\partial \vec{D}}{\partial t} = \varepsilon_0 \frac{\partial \vec{E}}{\partial t} + \vec{J}_{\mathrm{P}}$

$$\vec{\nabla} \times \vec{H}(\vec{r}) = \vec{J}(\vec{r}) + \frac{\partial \vec{D}(\vec{r})}{\partial t} \quad , \tag{2.39}$$

and a vector field $\vec{M}$ that originates from the intrinsic magnetic dipoles (2.33).

According to Maxwell's law the magnetic flux density is globally divergence-free

$$\vec{\nabla} \cdot \vec{B}(\vec{r}) = 0 \qquad \text{or} \qquad \int\limits_{\partial \mathcal{V}} \vec{B}(\vec{r}) \cdot \overrightarrow{\mathrm{d}S} = 0 \tag{2.40}$$

and therefore prevents the existence of magnetic monopoles within any arbitrary region $\mathcal{V}$ (having a surface $\partial \mathcal{V}$).

Concluding, it should be shown that a continuum treatment allows the aggregation of microscopic quantum-mechanical properties of magnetism into macroscopic quantities by postulating the existence of elementary magnetic moments. So the ensemble of these elementary moments can be treated with Maxwell's equations in a pure classical framework.

2.2.3 Magnetic Susceptibility and Permeability

In this section a survey about the various aspects of magnetic susceptibility is presented. One of the first comprehensive treatment of electric and magnetic susceptibilities has been provided by Van Vleck [83] in 1932.

For homogeneous materials there is a functional dependence $\vec{M}(\vec{H})$ or $\vec{B}(\vec{H})$ that describes the reaction of the magnetization or induction on an applied field $\vec{H}$. Physicists often denote this dependence as *response function*

$$\vec{M} = \chi(\vec{H}) \quad , \tag{2.41}$$

[13] Formally, the spatial averaging is done by means of quantum-mechanics. But the relation between atomic properties and continuous ones is quite intricate.

where the magnetic system (e.g. a crystal consisting of several thousands of atoms or ions) is modeled as black box. The function $\chi(.)$ is called (*general*) *magnetic susceptibility*[14], which degenerates in case of linear, homogeneous, isotropic, non-hysteretic media to a scalar value

$$\vec{M} = \chi \, \vec{H} \quad . \tag{2.42}$$

Because material properties cover a wide range of physical phenomena, there is a big variety of definitions for magnetic susceptibility:

- Anisotropic material: In case of linear or linearized homogeneous anisotropic media one can use a *susceptibility tensor* in order to describe the response of the material.
- Nonlinear material: For small changes in field around an operating point $(H_0; M_0)$ the *differential susceptibility* is defined as

$$\chi_{\text{diff}} = \left. \frac{\mathrm{d}M}{\mathrm{d}H} \right|_{H_0} \quad . \tag{2.43}$$

- Hysteretic material: If there are non-reversible processes present, it makes sense to define several characteristic susceptibilities, which will be explained in the following chapter.
- Time dependent phenomena: Most of the magnetization processes are time dependent, so one has to distinguish between *static* and *dynamic susceptibility* particularly when dealing with high frequencies or transient behavior.
- The concept of susceptibility is based on the magnetization as field-induced magnetic moment per unit volume. In practice it might be reasonable to consider magnetic moment per mass unit or per mole. Thus, *mass* or *molar magnetic susceptibility* can be used instead of the dimensionless volume based susceptibility. The conversion is defined via mass density or molar volume (volume occupied by one mole).

The *magnetic permeability* μ is defined via the functional dependence

$$\vec{B} = \mu(\vec{H}) \quad . \tag{2.44}$$

In case of linear, homogeneous, isotropic, non-hysteretic media there is a scalar dependence

$$\vec{B} = \mu \, \vec{H} = \mu_0 \, \mu_{\mathrm{r}} \, \vec{H} \quad , \tag{2.45}$$

where the dimensionless *relative permeability* μ_{r} is related to the magnetic susceptibility via (2.37) and (2.42) as

$$\mu_{\mathrm{r}} = 1 + \chi \quad . \tag{2.46}$$

In analogy to the various definitions of the magnetic susceptibility given above, there exist corresponding concepts for the magnetic permeability, too.

The response of a magnetic material on an applied magnetic field can be classified in terms of field- and temperature-dependence, which is the issue of the following section.

[14] In quantum theory one can also define a generalized susceptibility as response function, based on the wave-vector and the frequency of the applied field.

2.3 Classification of Magnetic Behavior

2.3.1 Diamagnetism

In general, diamagnetism is characterized by a field induced magnetization in substances of non-magnetic atoms. The resulting susceptibility is very small, negative, and nearly temperature independent as sketched in Fig. 2.4. For atoms or molecules with full electron shells the *Larmor model* is used to describe diamagnetism, whereas in metals (free electron gas) one has also to consider the *Landau diamagnetism*.

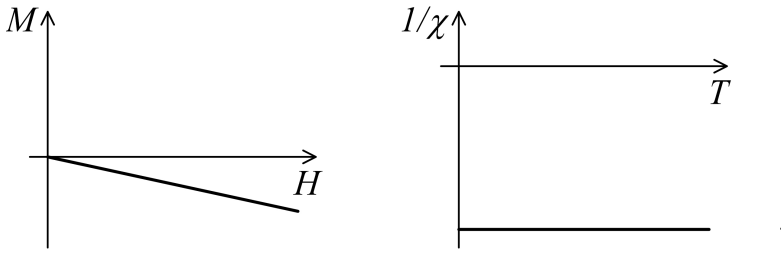

Figure 2.4: Characteristics of a typical diamagnet: magnetization curve (a), and inverse susceptibility (b).

Larmor (Langevin[15]) Diamagnetism

Within a *semi-classical treatment* electrons are assumed to move around the nucleus with angular velocity $\vec{\omega}_e$ in the absence of any magnetic field. Larmor's theorem states that the orbital motion of an electron in an external magnetic field $\vec{H}$ is the same as without the field (no-field solution) plus an additional rotation with the angular velocity $\vec{\omega}_L$

$$\vec{\omega}_e(\vec{H}) \approx \vec{\omega}_e(\vec{H} = \vec{0}) + \vec{\omega}_L(\vec{H}) \quad . \tag{2.47}$$

The resulting *Larmor angular velocity* $\vec{\omega}_L$ is obtained from the introduction of the Lorentz force[16] into the electron system as

$$\vec{\omega}_L(\vec{H}) = \frac{e}{2m_e}\mu_0\,\vec{H} \tag{2.48}$$

and assumed to be much lower than the motion of the electron in the central field $\omega_L \ll \omega_e$. Thus, the superposition of the angular velocities with no field and with an applied field

[15] The diamagnetic susceptibility was first calculated by LANGEVIN by means of classical electrodynamics using Lenz's rule. Another approach, which leads to identical results, is done by employing Larmor's theorem. So Langevin as well as Larmor diamagnetism are terms that describe the same phenomena.

[16] Assume that in a classical system without an external magnetic field, the angular velocity of the electron is determined from the equilibrium of the Coulomb force (between electron and nucleus) and the centrifugal force due to rotation. If there is an additional Lorentz force resulting from an external field, the angular velocity has to change in order to fulfill the equilibrium condition.

as Larmor's theorem states, is only valid for weak fields. However, because the additional Larmor angular velocity is parallel to $\vec{H}$ for every electron of the atomic system, there is a net magnetic moment antiparallel to the originating field, leading to a negative diamagnetic susceptibility.

In a pure *quantum mechanical treatment* one starts with the definition of a Hamiltonian operator, which represents the kinetic energy, the Zeeman (field) energy, and the Coulomb (potential) energy of the electron system with an applied field. Assuming that the solution (eigenvalues and eigenstates) of the problem without field is known, one adds the field-dependent energy terms to the original Hamiltonian as (first-order) perturbation. Finally, one ends up in a perturbed Hamilton operator that is the sum of the unperturbed operator (no-field solution), a paramagnetic part (reducing total energy), and a diamagnetic part (increasing total energy).

Diamagnetic susceptibilities are small in size (in the order of -10^{-6} to -10^{-5}) and can only be observed if the other magnetic contributions vanish. Thus, typical diamagnets are solid inert gases and ionic crystals, having full electron shells.

Landau Diamagnetism

Additionally to the Larmor diamagnetism of full electronic orbitals, there is another diamagnetic contribution from the free valence electrons in metals. Without an applied field the free electron states are uniformly distributed in the k-space (of wave vectors), whereas in the presence of a magnetic field only certain energies (k-vectors) - the so called *Landau levels* - are allowed. This field induced breaking up of states into discrete levels leads to a (field dependent) difference in total energy and therefore to a magnetic susceptibility that depends on the density of states at the fermi energy. Landau diamagnetism is entirely based on the orbital motion of the electrons.

2.3.2 Paramagnetism

In principle, paramagnetic behavior is observed, when atoms or ions carry permanent magnetic moment, and the interaction between these magnetic moments is negligible. So, in the absence of a magnetic field the atomic magnetic moments are randomly distributed, whereas they become oriented with an increasing applied field. Hence, the paramagnetic susceptibility is positive.

Langevin Paramagnetism

In a *classical picture* the atomic magnetic moments $\vec{\mathfrak{m}}$ can take any arbitrary direction in space. The competition between the magnetic field energy -$\mu_0\,\vec{\mathfrak{m}}\cdot\vec{H}$ and the thermal agitation $k_\mathrm{B}T$ is expressed via classical Boltzman statistics, where k_B is the Boltzman factor and T denotes the temperature. The magnetization M in direction of the applied field can be estimated by the average (expectation value) of the component of magnetic moments in field

direction multiplied with the number of magnetic particles per unit volume N as

$$M = N \frac{\int_0^\pi \mathfrak{m}\,\cos(\varphi)\,\exp\left(-\frac{-\mu_0\, m\, H\,\cos(\varphi)}{k_\mathrm{B}T}\right)\,2\pi\sin(\varphi)\,\mathrm{d}\varphi}{\int_0^\pi \exp\left(-\frac{-\mu_0\, m\, H\,\cos(\varphi)}{k_\mathrm{B}T}\right)\,2\pi\sin(\varphi)\,\mathrm{d}\varphi} = N\,\mathfrak{m}\,\mathcal{L}\left(\frac{\mu_0\,\mathfrak{m}\,H}{k_\mathrm{B}T}\right) \quad , \tag{2.49}$$

where $\mathcal{L}(x) = \coth(x) - 1/x$ is the Langevin function and φ is the angle between $\vec{\mathfrak{m}}$ and $\vec{H}$. In the weak field limit one can use the first term of the series expansion of $\mathcal{L}(x)$ in order to get an expression for the susceptibility

$$\chi = \frac{N\,\mu_0\,\mathfrak{m}^2}{3\,k_\mathrm{B}T} \quad , \tag{2.50}$$

which supports the experimentally determined *Curie law* (discovered by P.Curie)

$$\chi \propto \frac{1}{T} \quad . \tag{2.51}$$

In the view of *quantum mechanics* the magnetic moment and its component along the magnetic field are quantized according to (2.20c). Accounting for the discrete nature of the problem, one obtains the magnetization in field direction as

$$M = N \frac{\sum_{\mathfrak{m}_J=-\mathtt{J}}^{\mathtt{J}} g_j\mu_B\mathfrak{m}_J\,\exp\left(-\frac{-\mu_0\, g_j\mu_B\mathfrak{m}_J\, H}{k_\mathrm{B}T}\right)}{\sum_{\mathfrak{m}_J=-\mathtt{J}}^{\mathtt{J}} \exp\left(-\frac{-\mu_0\, g_j\mu_B\mathfrak{m}_J\, H}{k_\mathrm{B}T}\right)} = N\; g_j\,\mu_B\,\mathtt{J}\,\mathcal{B}_J\left(\frac{\mu_0\, g_j\,\mu_B\,\mathtt{J}\,H}{k_\mathrm{B}T}\right) \quad , \tag{2.52}$$

with the Brillouin function $\mathcal{B}_J(x)$. Again, the series expansion of $\mathcal{B}_J(x)$ gives an approximation for the paramagnetic susceptibility in the weak field limit

$$\chi = \frac{N\,\mu_0\,\mathfrak{m}_J^2}{3\,k_\mathrm{B}T} \quad , \tag{2.53}$$

where $\mathfrak{m}_J$ defined in (2.20b) is referred to as *effective magnetic moment* $\mathfrak{m}_\mathrm{eff}$.

Depending on the quantum number $\mathtt{J}$ we have two limiting cases:

- Spin magnetic moments ($\mathtt{J} = 1/2$; $g_j = 2$; $\mathcal{B}_{1/2}(x) = \tanh(x)$)

$$M = N\;\mu_B\,\tanh\left(\frac{\mu_0\,\mu_B\,H}{k_\mathrm{B}T}\right) \tag{2.54}$$

- Classical magnetic moments ($\mathtt{J} \to \infty$; $\mathcal{B}_\infty(x) = \mathcal{L}(x)$)

$$M = N\,\mathfrak{m}\,\mathcal{L}\left(\frac{\mu_0\,\mathfrak{m}\,H}{k_\mathrm{B}T}\right) \tag{2.55}$$

Paramagnetic susceptibilities are about one order larger than diamagnetic ones and range between 10^{-5} to 10^{-3}.

Pauli Paramagnetism

In the free electron gas the magnetic moment is proportional to the number of unpaired spins (i.e. the difference of spin-up and spin-down electrons). In the presence of a magnetic field the spin-up[17] electrons are energetically favored, whereas the spin-down electrons are narrowed. Hence, the corresponding energy bands are shifted by an energy that is proportional to the magnetic field, meaning that spin-down electrons in the Fermi surface[18] switch to spin-up state. The resulting magnetization increases linearly on the magnetic field, leading to the paramagnetic *Pauli susceptibility*, which is nearly temperature independent. For non interacting electrons one has to choose Fermi statistics to describe the energy boundary for occupied and non-occupied states at finite temperatures.

In contrast to the Langevin paramagnetism (of insulators), where at least one electron per atom or ion contributes to the paramagnetic behavior, in metals only the electrons near the Fermi surface are of importance[19]. Consequently, the Pauli susceptibility is small compared to the paramagnetic susceptibility for localized magnetic moments.

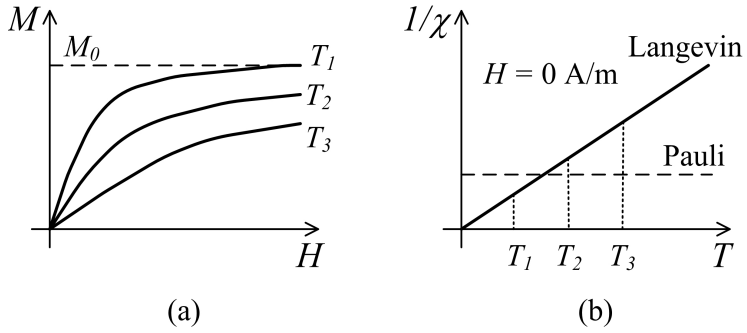

Figure 2.5: Characteristics of a typical paramagnet for different temperatures $T_1 < T_2 < T_3$: magnetization curve (a), and inverse susceptibility (b).

2.3.3 Ferromagnetism

In contrast to diamagnetic and paramagnetic materials, ferromagnetica have a spontaneous magnetization without an applied field[20], which is founded in the long-range exchange interaction acting between the atomic magnetic moments. In the ferromagnetic case this exchange interaction leads to a parallel alignment as long as thermal agitation is comparably small. Hence, the spontaneous magnetization decreases to zero at the so called *Curie temperature* T_C. For temperatures above T_C the material becomes paramagnetic, and the

[17] Consider the spin-up electrons as those ones that magnetic moments point parallel to the field.

[18] The Fermi surface separates filled states (allowed solutions from Schrödinger equation) from non-filled states in the phase space of wave vectors ($\vec{k}$-space).

[19] For the free electron gas that consists of fermions only electrons on the Fermi sphere can be excited, which causes a proportionality to the density of states at the Fermi energy for those phenomena.

[20] In many cases this spontaneous magnetization can be found in several regions of the ferromagnetic sample, which are called magnetic domains.

corresponding paramagnetic susceptibility is in a first-order approximation given by the *Curie-Weiss law* (see Fig. 2.6(b))

$$\chi \propto \frac{1}{T - T_{\mathrm{Para}}} \quad , \tag{2.56}$$

where $T_{\mathrm{Para}} \approx T_{\mathrm{C}}$. By the way, in this paramagnetic state just the long-range interaction has broken down, but magnetic moments still exist.

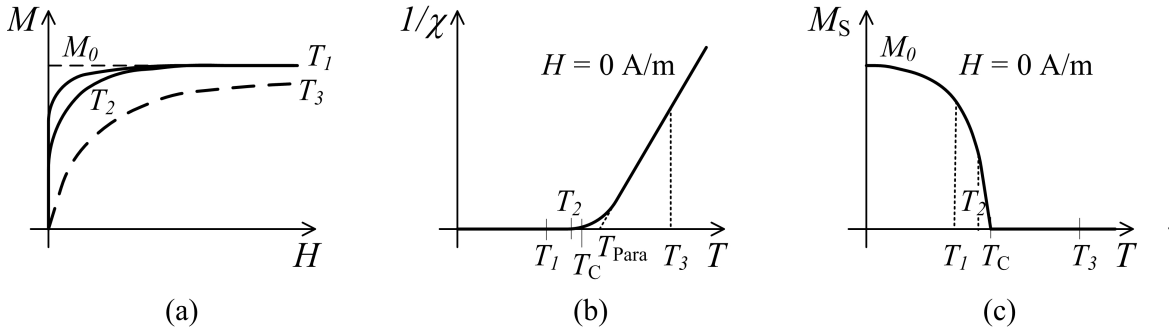

Figure 2.6: Characteristics of a typical ferromagnet for temperatures $T_1 < T_2 < T_{\mathrm{C}} < T_3$: magnetization curve (a), inverse susceptibility (b), and spontaneous magnetization (c).

Over the years a couple of physical theories have been established in order to explain ferromagnetic behavior and the spontaneous magnetization in particular. For a detailed description see [62].

Mean-Field Models

First, there are models that can be grouped into a *mean-field approach*, where it is postulated that a magnetic moment is influenced by a field resulting from the average over all the neighbors' moments. Such mean-field models are able to explain phase transitions between ferromagnetic and paramagnetic behavior qualitatively. But naturally they give an inappropriate description of the magnetic behavior in the critical region around the Curie temperature, because local correlations and fluctuations are not incorporated, since all regions of the sample are treated identically.

- *Weiss Molecular Field Model*: In 1907 P. Weiss proposed a so called 'molecular field' of magnetic origin that a single atomic magnetic moment feels additionally to the external field. This molecular field $\vec{H}_{\mathrm{mf}} = \lambda_{\mathrm{mf}}\vec{M}$ represents the influence of all the neighbors and is therefore proportional to the magnetization $\vec{M}$ with the molecular field constant λ_{mf}. Thus, the ferromagnetic case can be treated in a similar way as the Langevin paramagnetic case, just by adding the molecular field to the applied field. Unfortunately, this fictive magnetic molecular field would be extremely high in order to get realistic Curie temperatures, because in reality the exchange interaction is entirely an electrostatic effect.

- *Landau Theory of Ferromagnetism*: The Landau theory is a generalized approach to describe phase transitions, which is based on a power series expansion of the free energy

F with respect to the order parameter M. Under assumption of an internal magnetic field H, this power series can only contain even terms[21] (due to symmetry to $\pm M$) in M and a field energy term $-\mu_0 H\, M$

$$F(T, M) = F_0(T) + a(T)\, M^2 + b\, M^4 - \mu_0 H\, M \tag{2.57}$$

with a temperature dependent coefficient $a(T)$ and a positive valued coefficient b. The minimization of the free energy with respect to the magnetization M gives

$$M^2 = \frac{\mu_0}{4b}\frac{H}{M} - \frac{a(T)}{2b} \quad , \tag{2.58}$$

where the transition from ferromagnetic to paramagnetic behavior is represented by the sign of the coefficient $a(T)$.

Quantum-Mechanical Models

With introduction of quantum mechanical theories in science, HEISENBERG (1926) represented exchange interactions between (localized) neighboring spins in terms of a Hamiltonian (2.22), which can be seen as the quantum mechanical origin of the molecular-field. The corresponding models differ in the dimensionality of the order parameter (spin momentum) and the dimensionality of the considered geometry. Within the basic *Heisenberg model* spins are treated in the framework of a 3-dimensional Hilbert (state) space, whereas the *Ising model* considers just the z component of the spin as 1-dimensional quantity (either spin-up or spin-down is allowed). The dimensionality of the geometry determines the characteristics of the models. Without further reasoning it can be stated that there exists no transition between paramagnetic and ferromagnetic phases in 1-dimensional spin chains, because there is no long range order possible for non-zero temperatures.

In a spectral point of view, the Heisenberg Hamiltonian describes collective excitations of the whole spin system. These collective excitations can also be expressed in terms of *spin-waves* or as quantized quasi-particles, called '*magnons*'.

Band Ferromagnetic Models of Itinerant Electrons

The development of the energy band model enabled the description of magnetic behavior in itinerant electron systems, whereas the previous models are based on the assumption of localized electrons.

- *Stoner Model* (1930's): In the framework of an itinerant electron system the effects of exchange are treated within a molecular field term, which causes a shift in the spin-up and spin-down energy band, like an external magnetic field in case of Pauli paramagnetism. The so called Stoner exchange integral describes the interactions instead of the molecular-field constant used in the Weiss model. However, the Stoner model does not provide a good description of ferromagnetic behavior for finite temperatures, because it is based on single particle excitations (from spin-up to spin-down band). As a consequence, the Curie temperature is reached, when magnetic moments vanish for each atom individually, which is not true for real materials.

[21] The mean-field enters as energy $-\mu_0 \vec{H}_{\mathrm{mf}}\, \vec{M}$ that results in energy terms proportional to M^2.

- *Spin Fluctuation Model*: Here, one assumes the existence of a statistical spin density, where fluctuations of this spin density are used to describe collective excitations for itinerant electron systems. The total magnetization comprises of a bulk magnetization of ordered magnetic moments (that becomes zero above T_C) and a spatial average of the thermally fluctuating magnetic moments.

2.3.4 Antiferromagnetism

As the name suggests, in antiferromagnetic materials the exchange interaction leads to antiparallel alignment of neighboring atomic magnetic moments. In many cases the antiferromagnetic structure can be considered as superposition of two equivalent sublattices having a magnetization of the same amplitude, but antiparallel orientation. Thus, the net magnetization of antiferromagnetic substances is zero in the absence of an external magnetic field. Comparable with the Curie temperature of ferromagnets, there exists also an ordering *Neel temperature* T_N for antiferromagnetic materials, where thermal agitation exceeds exchange interactions. For $T > T_N$ one can find paramagnetic behavior according the Curie-Weiss law (2.56) with a (negative) characteristic temperature $T_{Para} < 0$ that differs significantly from the ordering temperature T_N. Hence, there is a finite susceptibility for $T = T_N$. In the ordered antiferromagnetic regime ($T < T_N$) it is intricate to describe the macroscopic magnetization process as function of an external field, because exchange coupling within the sublattices and between them has to be considered as well as crystalline anisotropy[22]. Typical characteristics of antiferromagnetic material are sketched in Fig. 2.7, where the magnetic field is applied parallel $\parallel$ or perpendicular $\perp$ to the alignment of the atomic magnetic moments.

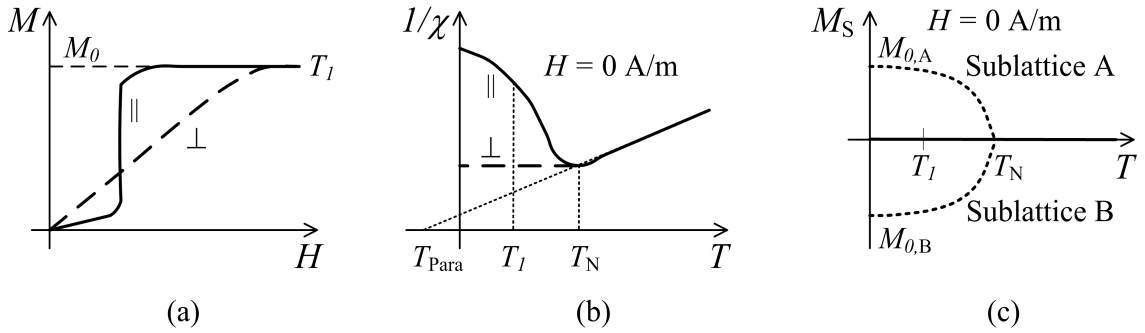

Figure 2.7: Characteristics of a typical antiferromagnet: magnetization curve (a), inverse susceptibility (b), and spontaneous magnetization (c).

Although antiferromagnetic materials are interesting from the theoretical point of view, they are relatively uncommon in practical applications. Chromium, manganese, and some oxides (MnO, CoO, FeO) show antiferromagnetic behavior.

[22] At least there are several possibilities to arrange the atoms belonging to the sublattices within a given crystal structure.

2.3.5 Ferrimagnetism

Similar to antiferromagnetism ferrimagnetic materials comprise of two sublattices, but due to different number or different type of atoms in each sublattice they are magnetically not identical. Hence, there is a net magnetic moment even in the absence of an external magnetic field. Again the *Curie temperature* T_C is the temperature, where thermal agitation exceeds exchange coupling. Above T_C the paramagnetic behavior can be described by the Curie-Weiss law (2.56) with $T_\mathrm{Para} < T_\mathrm{C}$. At the ordering temperature T_C the paramagnetic susceptibility becomes infinite and the spontaneous magnetization is zero. In the ordered regime ($T < T_\mathrm{C}$) the spontaneous magnetization can be derived from the difference of the magnetizations in the two sublattices (Fig. 2.8). Therefore, one has to account for the temperature dependence of the spontaneous magnetizations in the sublattices, which can lead to a change in sign of the net magnetization at the so called *compensation temperature* T_Comp in some cases.

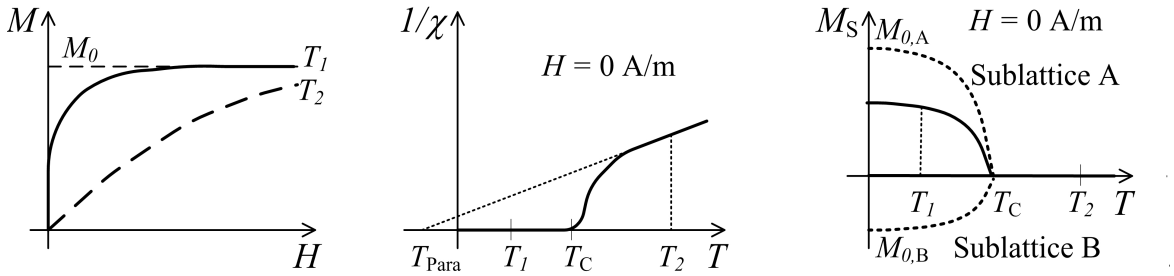

Figure 2.8: Characteristics of a typical ferrimagnet: magnetization curve (a), inverse susceptibility (b), and spontaneous magnetization (c).

Before NEEL's seminal work [66] about antiferromagnetism and ferrimagnetism in 1948, both were treated as ferromagnetic materials. There are several families of ferrimagnetic materials, among them ferrites (spinel ferrites, hexagonal ferrites, orthoferrites) and rare earth garnets. In contrast to ferromagnetic materials, most of the ferrimagnets are insulators and therefore particularly suitable for operating at high frequencies.

2.3.6 Summary

In conclusion, all these types of magnetic behavior represent a process of order, which is driven by different mechanisms leading to certain characteristic response to external magnetic fields. Clearly, the classification given in this section is not complete and does not cover the big variety of magnetic materials. Besides, there exists also other kinds of magnetic behavior, like helimagnetism, speromagnetism, superparamagnetism, or metamagnetism.

Chapter 3

Magnetic Energies, Domains, and Hysteresis

Ferromagnetism is characterized by a spontaneous magnetization as result of quantum mechanical exchange interactions. When dealing with realistic macroscopic samples one has to take structural as well as geometrical properties of the material in consideration. In length scales beyond the atomic level it is convenient to describe a magnetic system in terms of different energy contributions by means of continuous vector fields. The sum of these energy terms would at least in principle allow to calculate the space-dependent magnetization distribution.

Especially the non-local energy contributions give rise to unique magnetized regions, so called magnetic domains. Assuming the existence of such domains that are separated by domain walls, domain theory provides a framework of rules for the formation of the domains.

At the sample level one is interested in the magnetization curve that represents the total sample magnetization as response of an applied magnetic field. Finally, the magnetization process is associated with dissipation of heat, and the corresponding losses are related to the hysteretic behavior of the magnetization curve. Although the description of these macroscopic properties is mainly based on empirically found rules, they can be reasoned by micromagnetic analysis to some extent.

3.1 Ferromagnetic Energy Contributions

3.1.1 General Considerations

Basic Terms

Using terms of a Cartesian coordinate system with the unit vectors $\vec{e}_x$, $\vec{e}_y$, and $\vec{e}_z$, an arbitrary orientation $\vec{v}$ is defined by the *direction vector* $\vec{e}_v$ as

$$\vec{e}_v = \alpha_{v,x}\vec{e}_x + \alpha_{v,y}\vec{e}_y + \alpha_{v,z}\vec{e}_z \quad , \tag{3.1}$$

where $\alpha_{v,x}$, $\alpha_{v,y}$, and $\alpha_{v,z}$ are the corresponding *direction cosines* with respect to the coordinate axes.

The symbol $\mathcal{V}$ characterizes a structure in 3D space, which is bounded by the surface $\partial\mathcal{V}$ and contains a volume V measured in the dimension length^3.

The *magnetization* $\vec{M}$ is the *magnetic moment* $\vec{\mathfrak{m}}$ per unit volume. Furthermore, $\vec{m}$ represents the *reduced magnetization* as

$$\vec{m} = \frac{\vec{M}}{M_\mathrm{s}} \tag{3.2}$$

with respect to the spontaneous magnetization M_s at constant temperature[1].

If not mentioned explicitly $\vec{H}$ denotes the *external (applied) magnetic field*, whereas internal fields (inside the magnetic sample) will be identified via subscripts as $\vec{H}_\mathrm{in}$.

In order to analyze the various aspects of the magnetization process in a quantitative manner, it is useful to express them in terms of energy, which will be denoted as

W ... Energy assigned to a certain volume $\mathcal{V}$
$w(\vec{r})$ ... Energy density at an arbitrary point (position vector $\vec{r}$) in $\mathcal{V}$
w ... Energy per unit volume (averaged)

and associated via

$$W = \int_{\mathcal{V}} w(\vec{r})\,\mathrm{d}V \qquad \text{and} \qquad w = \frac{W}{V} \quad . \tag{3.3}$$

Classification of Energies

One criterion to distinguish the energies of a ferromagnetic system is the location where they take effect. *Local energy contributions* can be assigned to every point $\vec{r}$ in the continuous framework without considering the rest of the sample. Therefore they can be expressed in terms of energy densities $w(\vec{r})$. Applied field energy, anisotropy energy, and magneto-elastic interaction energy with non-magnetic stresses depend only on the magnetization $\vec{M}(\vec{r})$ at the considered point $\vec{r}$, whereas exchange energy is based on the gradient of the magnetization. *Non-local energy contributions* result as interaction of the local magnetization with the rest of the sample, such as stray field energy and magnetostrictive self-energy.

Another criterion is based on the cause of the energy terms. *Internal energy contributions* are given by the intrinsic properties of the magnetic system. Exchange energy, (magnetocrystalline) anisotropy energy, stray field energy, and magnetostrictive self-energy can be mentioned as internal energy terms. *External energy contributions* are caused by an excitation from outside of the magnetic system, like applied field energy and magneto-elastic interaction energy with external stresses.

A third criterion is related to the mechanism that is responsible for the energy. *Magnetostatic energy contributions* represent the potential energy of a magnetic system in a magnetic field, such as applied field energy and stray field energy. *Magneto-elastic energy contributions* can be grouped into magnetostrictive self-energy and magneto-elastic energy with stresses of non-magnetic origin.

[1] Whenever the temperature dependence of the spontaneous magnetization $M_\mathrm{s}(T)$ is not in the focus of interest, the magnetic system is described at a constant temperature.

3.1.2 Exchange Energy

The origin of the quantum mechanical exchange interactions has already been sketched in section 1.1.4. Although the Heisenberg Hamiltonian (1.22) is derived for direct exchange of a localized magnetic moment system, it can be used as basis for a (phenomenological) continuum approximation of exchange interactions for nearly all ferromagnetic materials.

In a continuum framework the discrete nature of the crystal lattice is ignored. Thus, the *volume*[2] *exchange energy density* of a ferromagnetic sample (having cubic symmetry) can be derived by a Taylor expansion of Heisenberg's Hamiltonian (1.22) for isotropic exchange as

$$w_{\mathrm{Ex}}(\vec{r}) = A_{\mathrm{Ex}} \left(\left(\vec{\nabla} m_x \right)^2 + \left(\vec{\nabla} m_y \right)^2 + \left(\vec{\nabla} m_z \right)^2 \right) \quad . \tag{3.4}$$

The quantum mechanical spin angular momentum operators are replaced by the continuous magnetization and the *continuum exchange constant* for cubic crystal symmetry is

$$A_{\mathrm{Ex}} = 2\, J_{\mathrm{Ex}} \mathbf{s}^2 \frac{z}{a} \quad , \tag{3.5}$$

with the nearest neighbor distance (lattice constant) a and the number of sites per crystal unit cell z (1 for simple cubic, 2 for body centered cubic, and 4 for face centered cubic). One has to take care that J_{Ex} has the dimension of energy, whereas A_{Ex} has the dimension of energy per length.

In a macroscopic point of view quantum mechanical exchange is described phenomenologically via (3.4) for nearly all kinds of ferromagnetic material.

3.1.3 Stray Field Energy

The stray field energy can be seen as potential energy of magnetic dipoles in the field created by themselves and is therefore often called dipole energy. Even though the dipole field decreases with distance proportional to r^{-3}, the number of neighboring magnetic dipoles increases, so that a long-range interaction results. In another picture the stray field energy corresponds to the work that would be necessary to arrange the magnetic system, when bringing each of the dipoles from infinity in space to the final position. The energy to build up each of the (isolated) elementary magnetic dipoles is of quantum mechanical origin and represents an intrinsic property of the magnetic system, which is not considered explicitly.

In principle, the stray field $\vec{H}_{\mathrm{Stray}}$ results from a summation over the dipole fields created by all elementary magnetic moments in their final configuration[3]. Together with an external applied field $\vec{H}$ the total magnetic field $\vec{H}_{\mathrm{in}}$ inside the material is

$$\vec{H}_{\mathrm{in}} = \vec{H} + \vec{H}_{\mathrm{Stray}} \quad . \tag{3.6}$$

Because inside the material $\vec{H}_{\mathrm{Stray}}$ is normally in opposition to the applied field, the stray field is often referred to as *demagnetizing field*, if the focus is set on the inner of the sample.

[2] There is also an interface exchange coupling for multilayer thin films that is related to the surface of the sample.

[3] But in this point of view one assumes that the distribution of magnetic dipoles (or the magnetization) in the material is a-priori known.

Since the stray field $\vec{H}_{\text{Stray}}$ emerges from magnetic dipoles (elementary current loops that current density vanishes for any macroscopic cross-section)

$$\vec{\nabla} \times \vec{H}_{\text{Stray}} = \vec{0} \tag{3.7}$$

is valid. Because of

$$\vec{B}_{\text{Stray}} = \mu_0 \left(\vec{H}_{\text{Stray}} + \vec{M} \right) \tag{3.8}$$

and

$$\vec{\nabla} \cdot \vec{B}_{\text{Stray}} = 0 \tag{3.9}$$

one ends up with

$$\vec{\nabla} \cdot \vec{H}_{\text{Stray}} = -\vec{\nabla} \cdot \vec{M} \quad . \tag{3.10}$$

Hence, the sources and sinks of the magnetization[4] can be interpreted as *magnetic charges* causing the stray field.

The summation of the potential energies for all magnetic dipoles in the sample volume $\mathcal{V}_{\text{Sample}}$ gives the stray field energy

$$W_{\text{Stray}} = -\frac{1}{2}\mu_0 \int\limits_{\mathcal{V}_{\text{Sample}}} \vec{H}_{\text{Stray}} \cdot \vec{M} \, \mathrm{d}V \quad , \tag{3.11}$$

where the factor 1/2 results, because every dipole in the sample acts as source of the stray field as well as magnetic moment within the summation of the potential energies.

Estimation of the Stray Field

General Solution: In principle, the stray field energy can be calculated by applying (3.10) and (3.11). Since (3.7) is valid, a scalar potential ϕ can be defined as

$$\vec{H}_{\text{Stray}} = -\vec{\nabla}\phi \tag{3.12}$$

that gives together with (3.10) the Poisson equation

$$\triangle\phi = \vec{\nabla} \cdot \vec{M} = -\rho_M \tag{3.13}$$

and defines the *magnetic (volume) charge density* ρ_M. Similarly, one can define a magnetic surface charge density

$$\sigma_M = \vec{M} \cdot \vec{n} \tag{3.14}$$

with the surface normal vector $\vec{n}$. By means of potential theory the scalar potential ϕ can be calculated via integration of volume and surface charge densities over the sample. The calculation of the stray field energy according to (3.11) needs again an integration over the sample volume. Because of the computational effort, stray field problems are normally calculated via finite element methods. But for some simple geometries there exists analytical solutions for the stray field energy.

[4] In simple cases, the surface of the sample or the interfaces between different regions in the sample act as sources or sinks for magnetization.

Uniformly Magnetized Ellipsoid: Here the stray field can be calculated via

$$\vec{H}_{\text{Stray}} = -\tilde{N} \cdot \vec{M} \tag{3.15}$$

with a symmetrical *demagnetizing tensor* $\tilde{N}$. The stray field energy is proportional to the volume V of the ellipsoid

$$W_{\text{Stray}} = \frac{1}{2}\mu_0 \, \vec{M}^T \cdot \tilde{N} \cdot \vec{M} \, V \tag{3.16a}$$

$$= \frac{1}{2}\mu_0 M_{\text{s}}^2 \, \vec{m}^T \cdot \tilde{N} \cdot \vec{m} \, V \quad , \tag{3.16b}$$

where

$$K_{\text{Stray}} = \frac{1}{2}\mu_0 M_{\text{s}}^2 \tag{3.17}$$

is a material parameter that characterizes energy densities associated with stray fields.

If the ellipsoid is magnetized along one of the principal axes (Fig. 3.1), the demagnetizing tensor becomes diagonal and the *demagnetizing factors* along the principal axes $(\vec{a}, \vec{b}, \vec{c})$ of the ellipsoid have to sum up to one

$$N_{\text{a}} + N_{\text{b}} + N_{\text{c}} = 1 \quad . \tag{3.18}$$

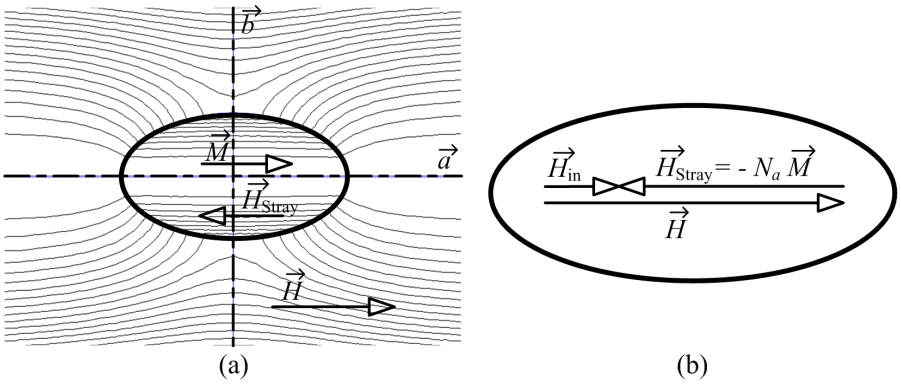

Figure 3.1: Ferromagnetic ellipsoid in homogeneous magnetic field: magnetic field lines (a) and magnetic field inside the ellipsoid (b).

Thus, one can estimate the demagnetizing factors for some special cases:

- Sphere: $N_{\text{a}} = N_{\text{b}} = N_{\text{c}} = 1/3$
- Long rod along the axis c: $N_{\text{a}} = N_{\text{b}} = 1/2 \quad N_{\text{c}} = 0$
- Thin plate in-plane a-b: $N_{\text{a}} = N_{\text{b}} = 0 \quad N_{\text{c}} = 1$

For such a thin plate (infinitely extended, normal to the plate is given by $\vec{e}_{\text{c}}$) the stray field energy can be expressed as energy density

$$\begin{aligned} w_{\text{Stray}} &= K_{\text{Stray}} \, (\vec{m} \cdot \vec{e}_{\text{c}})^2 \\ &= K_{\text{Stray}} \, \cos^2(\varphi_{mc}) \\ &= K_{\text{Stray}} - K_{\text{Stray}} \sin^2(\varphi_{mc}) \end{aligned} \tag{3.19}$$

that is formally equivalent to uniaxial (easy plane) anisotropy.

3.1.4 Applied Field Energy

The applied field energy or *Zeeman energy* represents the potential energy of the magnetic dipoles in an external applied field $\vec{H}$. The energy density is

$$w_{\mathrm{H}}(\vec{r}) = -\mu_0 M_{\mathrm{s}}\, \vec{H} \cdot \vec{m}(\vec{r}) \quad . \tag{3.20}$$

If the applied field is uniform over the sample, the Zeeman energy is proportional to the component of sample magnetization relative to the field direction.

Applied field and stray field energy together are summarized as *magnetostatic energies*.

3.1.5 Anisotropy Energy

In general, anisotropy energy accounts for a directional dependence of the magnetization.

Origin of Magnetic Anisotropy

Magnetocrystalline Anisotropy: In crystalline material the orientation of the magnetization is influenced by the symmetry of the hosting lattice and the crystallographic axes. The electronic orbitals and hence the orbital angular momentum is coupled with the crystal (electric) field of the neighboring atoms. Furthermore, the spin angular momentum interacts with the orbital angular momentum via relativistic spin-orbit coupling.

For localized magnetic moments (rare earth metals), where spin-orbit coupling dominates over crystal field effects, the magnetization direction is related to spin and orbital angular momentum. So the anisotropy energy arises from a change in the coupling of the electronic orbits with respect to the crystal lattice, leading to large anisotropies in general. For itinerant magnetic moments (transition metals) the magnetization direction is related to spin angular momentum. Because of the strong crystal field effects, the anisotropy energy arises from a change in spin-orbit coupling, which gives moderate anisotropy effects.

Induced Anisotropy: Induced anisotropy is related to structural changes in the material in comparison to the ideal bulk behavior, mostly during production or heat treatment of the material. Deviations from the ideal structure are caused either by a magnetic field or by mechanical stress. Hence, annealing with magnetic field or external stress, flow casting, or cold rolling give rise to an induced anisotropy.

Applying a magnetic field during the deposition of thin magnetic films also causes an induced anisotropy, which is often a crucial property for the application. Even the deposition of a film on a bulk substrate with different lattice constants leads to a distortion of the film lattice and via magneto-elastic coupling to anisotropy.

Furthermore, during epitaxial evaporation of a crystalline film the symmetry on the surface is broken, meaning that lattice sites which are equivalent inside the bulk crystal may differ on the surface. So for two different ions competing on one lattice site there can be a systematic preference for one of them, leading to anisotropy.

Shape Anisotropy: Strictly speaking, shape anisotropy is a consequence of magnetostatic stray fields and is often not seen as separate anisotropy term. However, it accounts for the directional dependence of the magnetization caused by the geometrical shape of the magnetic sample. For some sample geometries (spheroid with two equal axes) the term for the stray field energy takes the form of uniaxial anisotropy as given in 3.19 for example.

Formulation of Magnetic Anisotropy

Whatever mechanism may be responsible for the anisotropy, the quantitative treatment is done phenomenologically by series expansion in the direction cosines α_{mc_i} of $\vec{m}(\vec{r})$ with respect to the characteristic directions $\vec{c}_i$ given by the symmetry.

The anisotropy energy can be figured as energy surface in the 3D space, where every point on this surface refers to the anisotropy energy that results when the local magnetization is oriented in the direction of this point. The local minima of this energy surface are referred to as *easy directions*, the maxima as *hard directions* and the saddle-points as medium-hard directions. If these extrema are restricted to a finite number of distinct directions, one calls them *easy axes* or *hard axes*. But the terms easy and hard are only in conjunction with the type of energy well-defined.

Anisotropy Field: Sometimes it is convenient to express the anisotropy energy in terms of a magnetic *anisotropy field* that represents the strength of binding the magnetization to the easy direction. Hence, the (polar) angle θ between the magnetization and the considered easy axis is assumed to be small ($|\theta| \ll \pi/2$) in the domain of interest. The behavior around the minimum $\theta = 0$ is given by a Taylor approximation of the energy surface[5]

$$\begin{aligned} w_{\mathrm{Aniso}}(\theta)|_{\theta=0} &\approx w_{\mathrm{Aniso}}(0) + \frac{\theta}{1!}\left.\frac{\partial w_{\mathrm{Aniso}}(\theta)}{\partial\,\theta}\right|_{\theta=0} + \frac{\theta^2}{2!}\left.\frac{\partial^2 w_{\mathrm{Aniso}}(\theta)}{\partial\,\theta^2}\right|_{\theta=0} \\ &\approx \mathrm{const} + \frac{\theta^2}{2}\left.\frac{\partial^2 w_{\mathrm{Aniso}}(\theta)}{\partial\,\theta^2}\right|_{\theta=0} , \end{aligned} \tag{3.21}$$

which should be reproduced by a corresponding field energy, i.e.

$$\begin{aligned} w_{\mathrm{H}}(\theta)|_{\theta=0} &= -\mu_0 M_{\mathrm{s}} H_{\mathrm{Aniso}} \cos(\theta)|_{\theta=0} \\ &\approx -\mu_0 M_{\mathrm{s}} H_{\mathrm{Aniso}} \left(1 - \frac{\theta^2}{2!}\right) \\ &\approx \mathrm{const} + \frac{\theta^2}{2}\mu_0 M_{\mathrm{s}} H_{\mathrm{Aniso}} \quad . \end{aligned} \tag{3.22}$$

So the anisotropy field can be estimated by a comparison of the second-order coefficients as

$$H_{\mathrm{Aniso}} = \frac{1}{\mu_0 M_{\mathrm{s}}}\left.\frac{\partial^2 w_{\mathrm{An}}(\theta)}{\partial\,\theta^2}\right|_{\theta=0} \quad . \tag{3.23}$$

[5] Under the assumption that the energy surface has a local minimum at $\theta = 0$ the first derivative $\left.\frac{\partial w_{\mathrm{Aniso}}(\theta)}{\partial\,\theta}\right|_{\theta=0} = 0$ vanishes.

Uniaxial Anisotropy: In uniaxial systems there is just one characteristic direction in space that determines the anisotropy energy. Let $\varphi_{mc}(\vec{r})$ be the angle between the local magnetization $\vec{m}(\vec{r})$ and the characteristic axis $\vec{c}$, then

$$w_{\text{Aniso}}(\vec{r}) = K_0 + K_1 \sin^2(\varphi_{mc}(\vec{r})) + K_2 \sin^4(\varphi_{mc}(\vec{r})) + \ ... \tag{3.24}$$

is a generic expression for the anisotropy energy density. The material specific *anisotropy constants* $K_0, K_1, K_2, ...$ are temperature dependent in general. Because the uniaxial anisotropy is invariant to the reversal of $\vec{m}$ the series expansion contains only even powers of $\sin(\varphi_{mc}(\vec{r}))$. For most of the practical applications the series expansion (3.24) is truncated after the second- or fourth-order term. Then the energy minimizing easy directions depend on the sign of K_1 and the ratio K_2/K_1 as given in Tab. 3.1. Fig. 3.2 shows typical energy density surfaces for easy axis and easy plane anisotropy.

$K_1 > 0$	$K_2/K_1 > -1$	easy axis	$\varphi_{mc} = 0$
	$K_2/K_1 < -1$	easy plane	$\varphi_{mc} = \pi/2$
$K_1 < 0$	$K_2/K_1 > -1/2$	easy plane	$\varphi_{mc} = \pi/2$
	$K_2/K_1 < -1/2$	easy cone	$\varphi_{mc} = \arcsin\left(\sqrt{-K_1/2K_2}\right)$

Table 3.1: Type of easy directions for uniaxial anisotropy depending on the anisotropy constants.

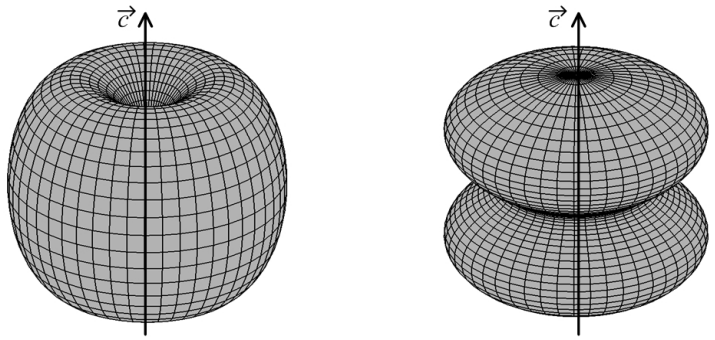

Figure 3.2: Energy density surface for uniaxial anisotropy of easy axis type (a) and easy plane type (b).

For the easy axis case the material has one easy axis along $\vec{c}$ (unit vector) and (3.23) gives with $\theta = \varphi_{mc}$ the anisotropy field

$$H_{\text{Aniso}} = \frac{2K_1}{\mu_0 M_{\text{s}}} \quad , \tag{3.25}$$

and for the easy plane case with $\theta = \varphi_{mc} - \pi/2$

$$H_{\text{Aniso}} = \frac{-2K_1 - 4K_2}{\mu_0 M_{\text{s}}} \quad . \tag{3.26}$$

The uniaxial approach is typical for hexagonal and tetragonal crystal structure, many kinds of induced anisotropy, as well as for shape anisotropy. Just the meaning and interpretation of the anisotropy constants is different.

Cubic Anisotropy: In cubic systems there are three characteristic directions, which can be assumed as c_1-, c_2-, and c_3-axis. When α_{mc_1}, α_{mc_2}, and α_{mc3} denote the direction cosines of the local magnetization with respect to the cubic axes, the anisotropy energy can be written as

$$w_{\mathrm{Aniso}}(\vec{r}) = K_0 + K_1 \left(\alpha_{mc_1}^2\alpha_{mc_2}^2 + \alpha_{mc_2}^2\alpha_{mc_3}^2 + \alpha_{mc_3}^2\alpha_{mc_1}^2\right) + K_2\,\alpha_{mc_1}^2\alpha_{mc_2}^2\alpha_{mc_3}^2 + \ldots \quad . \tag{3.27}$$

The energy minimizing easy directions yield from the anisotropy constants K_1 and K_2 according to Tab. 3.2. Fig. 3.3 depicts the energy density surfaces for the magnetocrystalline anisotropy of α-Fe (easy $\langle 100\rangle$-directions) and Ni (easy $\langle 111\rangle$-directions).

$K_1 > 0$	$K_2/K_1 > -1/9$	easy $\langle 100\rangle$-directions
	$K_2/K_1 < -1/9$	easy $\langle 111\rangle$-directions
$K_1 < 0$	$K_2/K_1 > -4/9$	easy $\langle 111\rangle$-directions
	$K_2/K_1 < -4/9$	easy $\langle 110\rangle$-directions

Table 3.2: Type of easy directions for cubic anisotropy depending on the anisotropy constants.

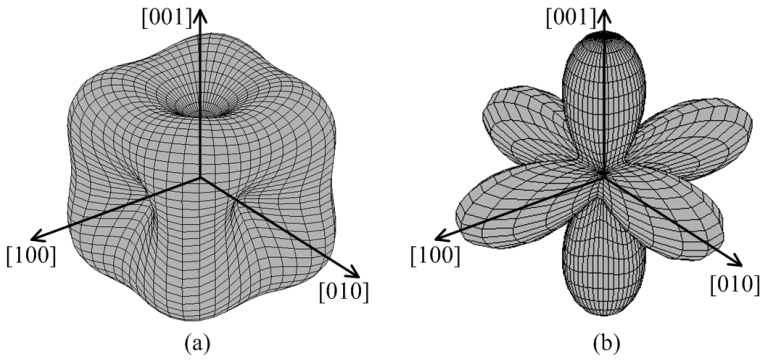

Figure 3.3: Energy density surface for cubic anisotropy having easy $\langle 100\rangle$-directions (a) and easy $\langle 111\rangle$-directions (b).

This approach is characteristic for materials with cubic crystal structure.

3.1.6 Magnetostrictive Self-Energy

In general, *magnetostriction* is characterized by a variation of interatomic distances with respect to magnetization. Any elastic deformation of a material sample can be partitioned into an *elastic strain* part and a *lattice rotation* part, where the second one is not of great significance for many applications. Because a distortion of the crystal lattice changes the

distance of neighboring magnetic atoms, there is a coupling between magnetization and elastic strain, represented by the *magneto-elastic interaction energy*. The *elastic energy* acting as counterpart for the magneto-elastic interactions is usually independent of the magnetization. The minimization of both energy terms at a fixed value of magnetization gives the tensor of free or *spontaneous magnetostrictive strain* $\tilde{\varepsilon}^0$. If magneto-elastic and elastic energies are taken to the lowest possible order with respect to the strain, one operates in the linear elastic regime, characterized by Hooke's law.

For cubic crystals the energy related to the spontaneous deformation is equivalent in structure to the first-order cubic anisotropy term. Hence, the magnetostrictive self-energy for uniformly magnetized samples can be assigned to the anisotropy constants. But in a magnetic sample with regions of different magnetization, where spontaneous deformations do not fit together (domain walls, surface regions), additional magnetostrictive self-energies emerge. The calculation of these self-energies requires usually a huge effort to solve the elastic and the magnetic problem together.

3.1.7 Magneto-Elastic Energy with Non-Magnetic Stresses

Stress of non-magnetic origin is either an applied external stress or an internal stress due to inhomogeneities (dislocations). For a given stress tensor[6] $\tilde{\sigma}_{\mathrm{Stress}}(\vec{r})$ the magneto-elastic energy density is related to the spontaneous magnetostrictive strain $\tilde{\varepsilon}^0(\vec{r})$

$$w_{\mathrm{Stress}}(\vec{r}) = -\tilde{\sigma}_{\mathrm{Stress}}(\vec{r}) \cdot \tilde{\varepsilon}^0(\vec{r}) \quad , \tag{3.28}$$

in general.

Assume a *uniaxial stress* σ_{Stress} along an axis $\vec{c}$ having an angle $\varphi_{mc}(\vec{r})$ relative to the local magnetization $\vec{m}(\vec{r})$. For (elastic) isostropic materials, and cubic crystals along the [100]- or [111]-axis the magnetization dependent part of the magneto-elastic interaction energy density can be formulated as

$$w_{\mathrm{Stress}}(\vec{r}) = \frac{3}{2}\lambda\,\sigma_{\mathrm{Stress}}\sin^2(\varphi_{mc}(\vec{r})) \quad , \tag{3.29}$$

where λ is the corresponding magnetostriction constant (isotropic $\lambda = \lambda_{\mathrm{s}}$, cubic $\lambda = \lambda_{100}$ or $\lambda = \lambda_{111}$). Because (3.29) is formally equal to uniaxial anisotropy, these special cases are often referred to as *stress anisotropy*. Depending on the sign of the applied stress and the magnetostriction constant the magnetization tends to align parallel with or perpendicular to the stress.

3.1.8 Energy Minimization

In principle, it would be possible to calculate a stationary magnetic configuration for a certain ferromagnetic sample by a minimization of the sum of energy contributions described in 3.1.2 to 3.1.7. That concept is employed in the framework of *Micromagnetism*, which is presented in section 3.2.

[6] In the following parts of this work the symbol σ is assigned to the variance of statistical distribution functions, so σ_{Stress} is used to indicate for stresses.

But even when using finite element techniques, the calculation effort is quite high so that only samples of small dimension can be treated reasonably within the micromagnetic framework. For large-scale samples one is often interested in the macroscopic magnetic behavior rather than in the internal structure of the ferromagnetic system. Thus, the following section introduces magnetic domains as higher level of abstraction.

3.2 Magnetic Domains

The following paragraphs provide a short overview about the reasoning of magnetic domains. A detailed treatment including measurement and observation techniques is given in the textbook [42].

3.2.1 Domain Theory

In the beginning of the 20$^{\text{th}}$ century P. WEISS [86] postulated the existence of magnetic domains, although there were no appropriate observation techniques available. Simply formulated, a *magnetic domain* is a closed region within the magnetic sample that is uniformly magnetized. The interface between two neighboring domains is referred to as *domain wall*.

Within the heuristic framework of *domain theory* the existence of magnetic domains separated by domain walls is presumed. In this picture, domain walls are taken as infinitesimal small, having a certain amount of wall energy per unit of wall area. Based on this postulation, different domain patterns can be analyzed by focusing on the relevant energy terms described in section 3.1 and the corresponding wall energies. So one gets a good interpretation of the macroscopic domain structure of the ferromagnetic sample.

Dependent on material and geometry of the sample there are different mechanisms that are responsible for the setup of the domain structure. In the short-scale range exchange and anisotropy effects are leading to the uniformly orientated magnetization at preferred directions. Usually, the non-local energy contributions, mainly the stray field energies determine the building of magnetic domains at large-scale ranges. A reduction of the stray field energy can be achieved, when magnetic volume and surface charges are avoided.

According to (3.16) the stray field energy of a uniformly magnetized ellipsoid is proportional to its volume, whereas the domain wall energy is just proportional to the cross section of the ellipsoid. Thus, the number of domains in such a sample increases with its size, which is a universal rule that can be generalized to other shapes, too.

Basically, one distinguishes between *primary domains* and *secondary domains* in bulk materials. The first one occupy a large portion of the sample volume in quite simple domain structures and therefore determine the macroscopic magnetization state. Secondary domains are relatively complex in structure and are mainly responsible for the reduction of stray fields and residual stress at the surface of the material or around defects.

Two neighboring magnetic domains are said to be *compatible*, if the normal component of the magnetization is equal on both sides of the domain wall. Thus, compatible domains exhibit no additional contribution to stray field or magnetostrictive self-energy.

Characteristic Domain Parameters

The *reduced anisotropy coefficient* is defined as dimensionless constant

$$q = \frac{K_{\mathrm{Aniso}}}{K_{\mathrm{Stray}}} \quad , \tag{3.30}$$

where K_{Aniso} is the most significant anisotropy constant for the material and K_{Stray} is given in (3.17). High anisotropy materials are characterized by $q \gg 1$, whereas low anisotropic ideal soft magnetic materials fulfill the relation $q \ll 1$.

The competition between exchange and stray field energy can be summarized in the so called *exchange length*

$$l_{\mathrm{Ex}} = \sqrt{\frac{A_{\mathrm{Ex}}}{K_{\mathrm{Stray}}}} \quad . \tag{3.31}$$

For small samples, with a characteristic length less than some multiples of l_{Ex} single domain behavior is favored over a multi-domain state.

A typical measure for the characteristic domain wall width is given by

$$l_{\mathrm{Wall}} = \sqrt{\frac{A_{\mathrm{Ex}}}{K_{\mathrm{Aniso}}}} \tag{3.32}$$

with the representative anisotropy constant K_{Aniso}.

3.2.2 Domain Walls

In practice, domain walls can be of complex structure, but there are two simple cases that represent the basic aspects one has to consider.

Bloch Wall

In 1932 Bloch [9] published his concept for the transition of magnetization between two domains. The idea is that magnetization changes from a certain direction gradually across a number of atomic planes until it reaches the direction of the second domain. Assuming that the total rotation in magnetization is shared equally among the atomic planes and that exchange and anisotropy energy are the dominating parts of the wall energy, one obtains [54]

$$l_{\mathrm{Bloch}} = \pi\, l_{\mathrm{Wall}} \tag{3.33}$$

for the *wall width*[7]. The *wall energy per unit surface* is for uniaxial anisotropy

$$w_{\mathrm{Bloch}} = 4\sqrt{A_{\mathrm{Ex}} K_{\mathrm{Aniso}}} \tag{3.34}$$

[7] Because the direction of the local magnetic moments change gradually between two domains, there exist no sharp boundaries for the corresponding domain wall. Thus, the definition of the wall width is not unique, in general. The most commonly used definition for the Bloch wall width is related to the slope of the magnetization angle in the middle of the wall, leading to (3.33).

and for cubic anisotropy (domain magnetization in [100]-direction)

$$w_{\mathrm{Bloch}} = 2\sqrt{A_{\mathrm{Ex}} K_{\mathrm{Aniso}}} \quad . \tag{3.35}$$

If at least one dimension of the rotation planes becomes small, stray field energy from magnetic poles on the surface has also to be considered. For example, in thin films the wall width decreases and the wall energy increases with decreasing film thickness. Hence, Bloch walls are energetically unfavorable in thin magnetic films.

Néel Wall

An approach, where the magnetization changes its direction in the plane of a magnetic thin film has been formulated by NEEL 1955 [67]. In Néel walls magnetic volume charges inside the film appear instead of the surface charges that would result from Bloch walls.

In *bulk* soft-magnetic materials ($K_{\mathrm{Aniso}} < K_{\mathrm{Stray}}$) the wall width of a Néel wall is mainly determined by stray fields and proportional to the exchange length l_{Ex}.

In *thin films* Néel walls have no sharp boundaries with respect to the adjacent domains, and one has to distinguish between the kernel region and the tail region. Within the narrow kernel region the main part of magnetization rotation occurs around a direction perpendicular to the domain magnetization. Hence, the behavior in this kernel region is governed by stray field (favors a narrower kernel) and anisotropy energy which is counter-balanced by the exchange energy, so that the kernel width is proportional to $\sqrt{A_{\mathrm{Ex}}/(K_{\mathrm{Aniso}} + K_{\mathrm{Stray}})}$ [42]. In the tail regions magnetization change is driven by a competition between the stray field energy (favors wider tails) and the anisotropy energy leading to tail widths that are multiples of the kernel width and proportional to $K_{\mathrm{Stray}}/K_{\mathrm{Aniso}}$.

Because of the long-range interaction of the stray fields in the tails of two neighboring Néel walls, irreversible state transitions in the magnetization process can result, especially when the domain between these walls becomes small.

Other Types of Domain Walls

In principle, Bloch as well as Néel walls represent simplified models for the transitional behavior of magnetization between two neighboring domains. In thin films the Bloch wall energy decreases with thickness, whereas the Néel wall energy increases. Theoretically, there exists a film thickness where Bloch and Néel walls are energetically equivalent, which is about 50 nm for Permalloy (see [73]). Particularly in this range of thickness several other types of domain wall structures occur in practice.

One example are *cross-tie walls* that consists of a periodic arrangement of Néel wall segments with Bloch lines as sub-structure in between. So a part of the 180° wall energy can be saved by replacing it with several energetically favorable 90° wall structures resulting in a reduction of the total wall energy.

In asymmetric domain walls, the change in magnetization is different inside the film compared to the region near to the surface. This asymmetry in the wall structure allows a reduction of the stray field.

Various domain wall structures are described and illustrated in detail in [42].

3.3 Magnetization Process

3.3.1 Descriptive Analysis of the Magnetization Process

From a generic point of view, the magnetization process describes the change in sample magnetization $\vec{M}$ as a reaction of the material to an external magnetic field $\vec{H}$. In general, a *magnetization curve* represents the component of sample magnetization in direction of the applied field M_H dependent on H. In order to shorten the notation, we write just M instead of M_H.

At constant temperature the sample magnetization can either change by changing the relative volume fractions of the domains (domain *wall motion*) or by changing the direction of domain magnetization (domain magnetization *rotation*). Each of these processes can be *reversible* or *irreversible* [46].

Demagnetized State

A ferromagnetic sample is called *demagnetized*, if it has no residual magnetization at zero field, yielding in the necessary macroscopic condition

$$\vec{M}\Big|_{\vec{H}=\vec{0}} = \vec{0} \quad . \tag{3.36}$$

Practically, there are two procedures how to demagnetize a ferromagnetic sample:

- The method of *thermal demagnetization* consists in heating the magnetic sample up to the Curie temperature and cooling it down at zero external field. This procedure requires that all parts of the sample (including coating, substrate, etc.) are thermally stable during the heating.
- Usually, an alternating magnetic field with decreasing amplitude is applied to the sample, which is referred to as *AC field demagnetization*. At the beginning of the demagnetizing procedure, the alternating field amplitude has to be significantly larger than the coercivity H_C.

Although one attempts to erase the magnetic history of the material sample in order to find a magnetic ground state with minimum total energy during the demagnetizing procedure, the resulting domain patterns can be ambiguous. Especially in magnetic films the domain structure in the resulting demagnetized state is not always reproducible and depends on the axis of the applied ac field, in general. In very thin films, where domain wall pinning is big in comparison with the domain energies, it is extremely difficult to identify unique demagnetized states. In short, even if the macroscopic condition (3.36) for a demagnetized state is fulfilled, the microscopic configurations need not necessarily be unique or reproducible.

Initial Magnetization Curve

The initial magnetization curve describes the magnetic behavior, when the magnetization process starts from the demagnetized state.

A characteristic material parameter is the *initial susceptibility*

$$\chi_{\mathrm{ini}} = \left.\frac{\mathrm{d}M}{\mathrm{d}H}\right|_{H=0,M=0} \tag{3.37}$$

as the slope of the initial magnetization curve in the origin. The corresponding initial permeability is related via (2.46)

$$\mu_{\mathrm{ini}} = \mu_0 \left(1 + \chi_{\mathrm{ini}}\right) \quad . \tag{3.38}$$

In domain theory μ_{ini} is a measure for the strength of intrinsic restoring forces for small movements of domain walls. As a structure sensitive property of the material, the initial permeability can significantly change as a result of small change in composition or metallurgical treatment.

Rayleigh Law: For weak fields the permeability can be expressed as

$$\mu = \mu_{\mathrm{ini}} + \nu H \quad , \tag{3.39}$$

which leads to an approximation of the magnetization curve around the demagnetized state (Fig. 3.4(a))

$$M = \chi_{\mathrm{ini}} H + \frac{\nu}{\mu_0} H^2 \quad . \tag{3.40}$$

This expression is named after its investigator as *Rayleigh law* with the Rayleigh constant ν. It is often used to extrapolate the initial permeability from measurements.

Saturation

When all magnetic dipoles are perfectly aligned the magnetization has its maximum value, known as *theoretical saturation magnetization* $M_{\mathrm{s,th}}$. There is no further increase in magnetization possible, so

$$\chi|_{M_{\mathrm{s,th}}} = 0 \quad \text{and} \quad \mu|_{M_{\mathrm{s,th}}} = \mu_0 \quad . \tag{3.41}$$

But as presented in section 1.3.3 the spontaneous magnetization depends on temperature, meaning that thermal agitation works against the perfect alignment at finite temperatures. So it would effort extremely high magnetic fields to reach the theoretical saturation. Therefore, one defines the *technical saturation magnetization* M_{s} as magnetization that is reached, when all domains of a ferromagnetic sample are merged to a single domain and the resulting magnetization (as averaged dipole moment) points in the direction of the field H.

Law of Approach to Saturation: The magnetization curve near saturation can be approximated by the *law of approach to saturation* (Fig. 3.4(b)) as

$$\left.\frac{M}{M_{\mathrm{s}}}\right|_{M_{\mathrm{s}}} = 1 - a\frac{1}{H} - b\frac{1}{H^2} + kH \quad . \tag{3.42}$$

The coefficient a accounts for non-magnetic inclusions, secondary domains around defects, and inhomogeneities, where the local magnetization differs from place to place. The quadratic coefficient b comes from the magnetocrystalline forces that act as counterpart of the applied field. Dependent on the type of anisotropy, b can be derived as function from the anisotropy constants. The last term kH describes the *forced magnetization*, which leads to a further increase of M above the technical saturation magnetization.

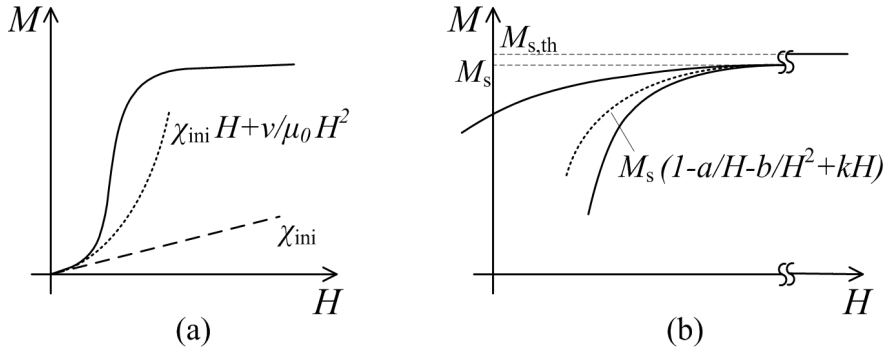

Figure 3.4: Initial magnetization curve and approximation by Rayleigh law (a), law of approach to saturation, theoretical $M_{\mathrm{s,th}}$ and technical saturation magnetization M_{s} (b).

Anhysteretic Magnetization Curve

Comparable to the ac demagnetizing procedure with a field amplitude $\hat{H}(t)$ decreasing to zero, a similar process can be done by the superposition of a constant dc field H_0 as $H(t) = H_0 + \hat{H}(t)\sin(\omega t)$. This ends up in a point (H_0, M_0) that represents a state of minimum energy for a certain field H_0. For different bias fields H_0 one yields the so called ideal or *anhysteretic magnetization curve*.

The anhysteretic magnetization curve is usually interpreted as result if there were no hindrances to domain wall motion and magnetization rotation that prevent the domain configuration from reaching the state of minimal energy. Hence, it describes an ideal completely reversible magnetization process independent of the magnetic history.

Remanence and Coercivity

When a ferromagnetic material is magnetized up to a point (H_0, M_0) and the field is reduced to zero, the *remanent magnetization* $M_{\mathrm{R}}(H_0, M_0)$ remains. Because the value of the remanent magnetization depends on the history of the magnetization process, especially on H_0, the (absolute) *remanence* M_{R} is defined as remaining magnetization for $H = 0$ after the material has been magnetized to (technical) saturation M_{s}. As such the remanence M_{R} is used to characterize the magnetic material.

The *coercive field* $H_{\mathrm{C}}(H_0, M_0)$ is defined as magnetic field that is necessary to reach a stable zero magnetization[8] state from an arbitrary magnetized state (H_0, M_0). Again, the

[8] It is important to distinguish between the (intrinsic) coercive field $H|_{M=0}$ for zero magnetization and $H|_{B=0}$ for zero magnetic flux density.

(absolute) *coercivity* H_C is the field, which is needed to reach zero magnetization from saturation according to Fig. 3.5(a).

For a stable point of coercivity the differential susceptibility

$$\chi_\mathrm{C} = \left.\frac{\mathrm{d}M}{\mathrm{d}H}\right|_{(H_\mathrm{C},0)} < \infty \tag{3.43}$$

has to be finite. Otherwise the magnetization reversal is the result of a switching process and the intersection of the vertical magnetization curve with the field axis is referred to as *switching field* H_Sw (Fig. 3.5(b)). Such global magnetization switching occurs mainly due to strong anisotropy energies, when the magnetization jumps from one local energy minimum to another one.

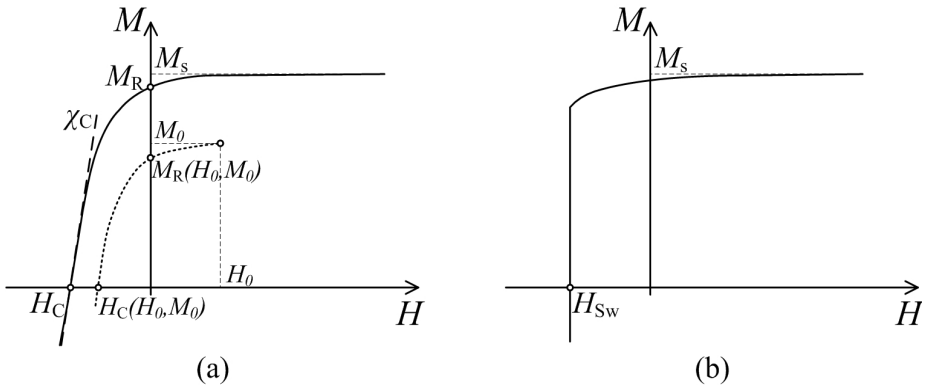

Figure 3.5: Remanent magnetization $M_\mathrm{R}(H_0, M_0)$, (absolute) remanence M_R, coercive field $H_\mathrm{C}(H_0, M_0)$, and (absolute) coercivity H_C (a) versus switching field H_Sw (b).

In general, coercivity determines the area of the hysteresis loop and is therefore related to the amount of irreversible work involved in the magnetization process. Just as the initial susceptibility, the coercivity is a structure sensitive material parameter that can change significantly on small changes in composition or production process.

Minor Hysteresis Loops

Generally, minor loops result by applying a small alternating field ΔH starting from a magnetized state[9] (H_0, M_0). When the alternating field returns to zero, i.e. $\Delta H = H_0$ the resulting loops are called *recoil loops*. Depending on the material the minor loops can either be closed or not, as depicted in Fig. 3.6. If they are closed, all the magnetic history from the minor loops is erased when the state (H_0, M_0) is reached again and the magnetic system exhibits the property of *return point memory*.

The ratio

$$\chi_\mathrm{inc} = \left.\frac{\Delta M}{\Delta H}\right|_{(H_0,M_0)} \tag{3.44}$$

[9]In a narrow sense, minor loops are seen as hysteresis loops that are symmetrical with respect to the origin, but not magnetized up to saturation. If the hysteresis loops are not symmetrical to the demagnetized state they are called biased minor loops.

is referred to as *incremental susceptibility* χ_{inc}. For the limit of small ΔH the *reversible susceptibility* χ_{rev} yields as

$$\chi_{\mathrm{rev}} = \lim_{\Delta H \to 0} \left. \frac{\Delta M}{\Delta H} \right|_{(H_0, M_0)} \quad , \tag{3.45}$$

and the difference between differential and reversible susceptibility is defined as *irreversible susceptibility*

$$\chi_{\mathrm{irr}} = \chi_{\mathrm{diff}} - \chi_{\mathrm{rev}} \quad . \tag{3.46}$$

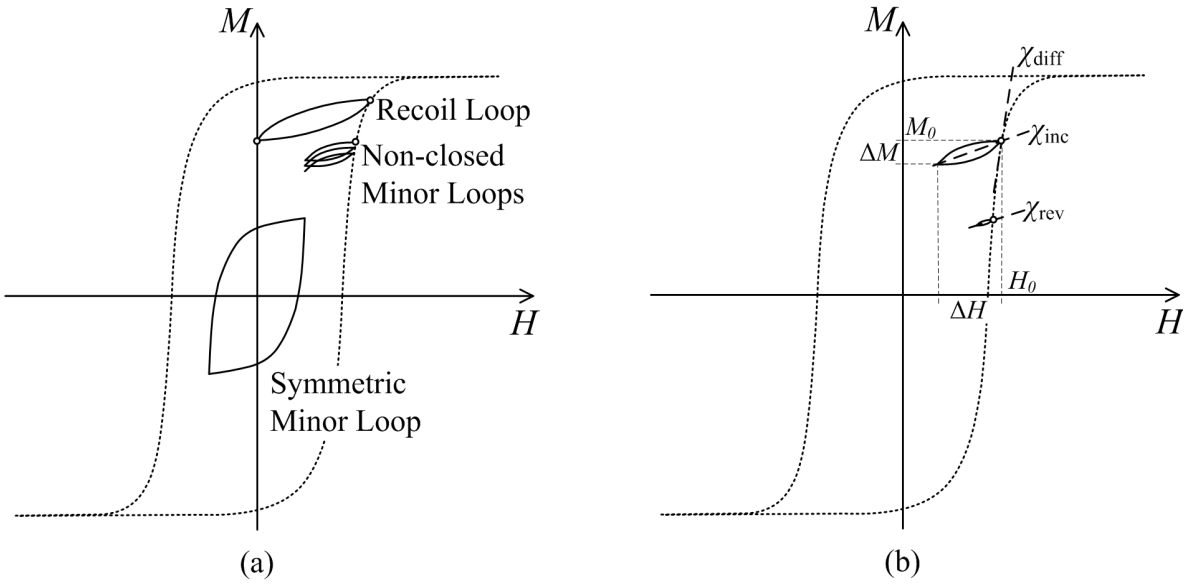

Figure 3.6: Different types of minor loops (a), differential, incremental, and reversible susceptibility (b).

3.3.2 Reversible and Irreversible Magnetization Process

In ferromagnetic materials the magnetization process is intrinsically tied to irreversibility that results in the dissipation of energy. Within this section the (uniform) applied field H is treated as external control variable and the component of magnetization with respect to this field M $(=M_H)$ is considered as state variable for the magnetic system.

When the magnetic field changes from $H_0 \rightarrow H_1$ the transition from state (H_0, M_0) to (H_1, M_1) is called *reversible*, if the inverse field change $H_1 \rightarrow H_0$ ends up in the original state (H_0, M_0), otherwise it is called *irreversible*. Irreversible processes are mainly related to a switching from one local energy minimum to another one.

Domain Wall Motion

In practice, the domain wall displacement is strongly influenced by inhomogeneities inside the material.

At the micromagnetic level several types of inhomogeneities can be distinguished [54]

- Point defects on the atomic level (interstitial sites, vacancies, or impurity atoms)
- Dislocations in the crystal lattice
- Planar defects, like stacking faults, phase-, or grain-boundaries

All these forms of microstructural disorder lead to local changes in anisotropy, exchange or internal stresses. In a macroscopic point of view, the interaction of the domain wall with any kind of material inhomogeneity is referred to as *pinning*. This simplification allows the treatment of domain wall motion independent of the structure of adjacent domains and the internal of the wall.

A basic model to explain the domain wall movement in a non-perfect magnetic system goes back to NEEL [63]. Within this model a single rigid domain wall of infinitesimal thickness and cross-section A is moving with just one degree of freedom along a coordinate x in a material that contains pinning sites (Fig. 3.7(a)). For simplicity, assume that the domain wall separates two domains with anti-parallel magnetization $\pm M_\mathrm{s}$ (180° wall), and the applied field H is oriented in the direction of the domain magnetization. Hence, the total free energy can be written as sum of the applied field energy (3.20), the remaining energy terms $W(x)$ from section 3.1, and an additional pinning energy $W_\mathrm{Pin}(x)$

$$W_\mathrm{Tot}(x) = -\mu_0 M_\mathrm{s} H 2xA + W(x) + W_\mathrm{Pin}(x) \quad . \tag{3.47}$$

In the context of the pinning model, the pinning energy $W_\mathrm{Pin}(x)$ is oscillating with respect to the wall position x. Each local minimum of $W_\mathrm{Tot}(x)$ represents a stable equilibrium, yielding in the condition

$$-2\mu_0 M_\mathrm{s} H A + \frac{\mathrm{d}W}{\mathrm{d}x} + \frac{\mathrm{d}W_\mathrm{Pin}}{\mathrm{d}x} = 0 \quad \text{or} \quad H = \frac{1}{2\mu_0 M_\mathrm{s} A}\left(\frac{\mathrm{d}W}{\mathrm{d}x} + \frac{\mathrm{d}W_\mathrm{Pin}}{\mathrm{d}x}\right) \quad . \tag{3.48}$$

The derivative of the energy terms with respect to x can be interpreted as a force acting on the domain wall. Equivalently to the pinning energy (per unit area of the wall), one can define a *pinning field* as

$$H_\mathrm{Pin} = \frac{1}{2\mu_0 M_\mathrm{s}} \frac{\mathrm{d}\left(W_\mathrm{Pin} \,/\, A\right)}{\mathrm{d}x} \quad . \tag{3.49}$$

Usually the domain wall interacts with a considerable number of pinning sites, so that the pinning energy or the pinning field is described by means of statistics.

As depicted in Fig. 3.7(b) the domain wall moves reversible from a starting position x_0 to x_1 and performs an irreversible discontinuous jump from x_1 to x_2. These discontinuities in the magnetization process (Fig. 3.7(c)) have been detected by BARKHAUSEN in 1919 [5] and are therefore referred to as *Barkhausen jumps*.

However, in real materials the domain wall movement is more complicated than in the presented model, but the fact that the displacement of the wall is partly reversible and partly irreversible due to Barkhausen jumps is still valid.

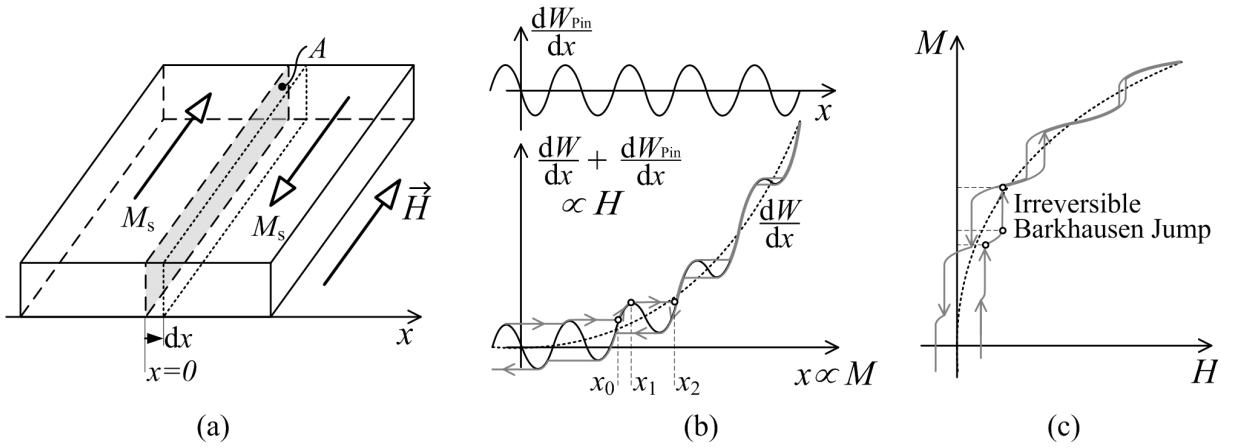

Figure 3.7: Simplified model of a moving domain wall in a material containing pinning sites (a), oscillating pinning energy and wall movement (b), resulting magnetization process (c).

Magnetization Rotation

Here one considers the case, when the magnetic moments rotate coherently in a domain of constant volume, as in single domain particles for example. Assume that the material's behavior is governed by uniaxial anisotropy (3.24) and the applied field H is oriented at an angle φ_{H} with respect to the easy axis. So, the free energy density depends on the angle φ of magnetization relative to the easy axis

$$w_{\mathrm{Tot}}(\varphi) = -\mu_0 M_{\mathrm{s}} H \cos(\varphi - \varphi_{\mathrm{H}}) + K_0 + K_1 \sin^2(\varphi) \quad . \tag{3.50}$$

Fig. 3.8(b) shows the contour of the resulting energy density (3.50) for different values of H. Qualitatively, one can see that the magnetization rotates reversibly up to a certain angle and jumps irreversibly to the new minimum of energy.

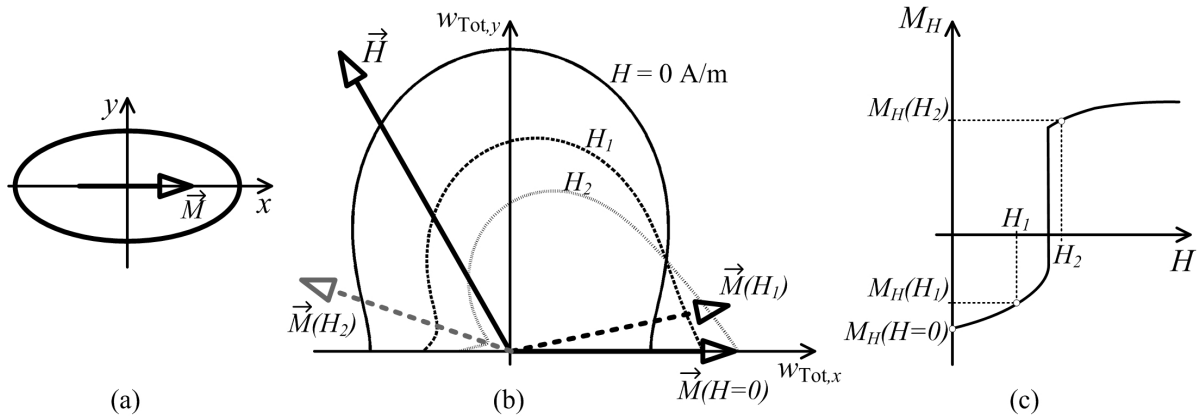

Figure 3.8: Single domain particle with uniaxial anisotropy ($K_0, K_1 > 0$) (a), energy surface $w_{\mathrm{Tot}}(\varphi)$ at increasing magnetic field $0 < H_1 < H_2$ (b), component of magnetization in field direction M_H (c).

3.3.3 Dissipative Losses

Frequency Dependent Loss Contributions

Hysteresis losses occur even in a quasi-static regime and are related to discontinuities in the magnetization process. For harmonic excitation, in each period a full hysteresis cycle is passed, so that hysteresis losses are strictly proportional to the frequency f.

Dependent on the electrical conductivity of the material there are *classical eddy current losses* that can be derived from Maxwell's equations. The induced eddy current is proportional to the frequency, leading to a f^2 dependence of the eddy current losses.

When a domain wall is moving with a certain velocity, the magnetization in the vicinity of the moving wall changes. In conducting bulk material eddy currents are induced such that they generate a magnetic field opposite to the applied field causing the wall displacement. Thus, the average wall velocity is reduced (wall damping), and the corresponding losses are called *excess eddy current losses*. In general, the domain wall velocity depends on the domain configuration, especially on the number of domains (walls). Besides eddy current damping, domain wall motion can be damped by intrinsic effects that are also relevant in insulators, but complex in their nature.

In Fig. 3.9 the losses per hysteresis cycle (dissipated power P_{Loss}) and per unit volume

$$w_{\mathrm{Loss}} = \frac{P_{\mathrm{Loss}}}{f\,V} \tag{3.51}$$

are plotted against frequency f for a typical bulk material sample of volume V.

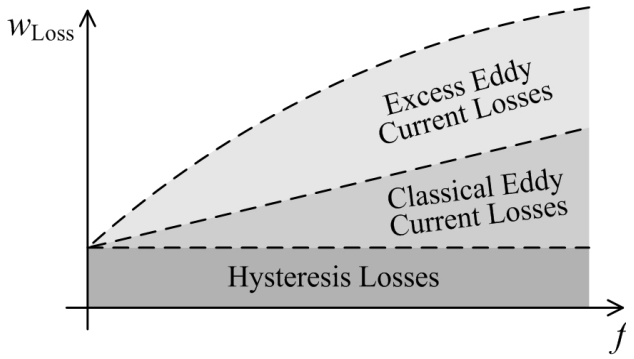

Figure 3.9: Characteristic frequency dependence of various loss contributions.

Static Hysteresis Losses

In a thermodynamical treatment the irreversible Barkhausen jumps due to pinning can be related to losses. Therefore we assume a simple magnetic system by excluding local relaxation phenomena and diffusion processes as well as all kinds of spatial inhomogeneities. So the magnetic system can be described as whole, having a constant temperature, a homogeneous distribution of losses, and a uniform entropy distribution.

According to the first law of thermodynamics an increase in internal energy $\mathrm{d}U$ is either due to heat δQ added to the system or due to work δL supplied to the system[10]

$$\mathrm{d}U = \delta Q + \delta L \tag{3.52}$$

for transitions between two equilibrium states. If we consider a magnetic system with uniform applied field H and a magnetization component M in direction of the field, the work supplied to the system is given as the sum of volume work (expansion or compression) and magnetic work

$$\delta L = -p\mathrm{d}V + V\mu_0 H\,\mathrm{d}M \quad . \tag{3.53}$$

The second law of thermodynamics states that the heat δQ added to the system is always smaller or equal than the increase of (total) entropy $\mathrm{d}S$

$$\delta Q \leq T\,\mathrm{d}S \quad , \tag{3.54}$$

where equality is valid for reversible state transitions. In case of irreversible processes, the total change in entropy $\mathrm{d}S$ can be separated in the entropy added reversibly from outside the system $\mathrm{d}_{\mathrm{ext}}S$ and the entropy produced inside the system $\mathrm{d}_{\mathrm{irr}}S$ due to irreversible mechanisms

$$\mathrm{d}S = \mathrm{d}_{\mathrm{ext}}S + \mathrm{d}_{\mathrm{irr}}S \quad . \tag{3.55}$$

Hence, the second law of thermodynamics can be reformulated as

$$\begin{aligned} \delta Q &= T\,\mathrm{d}_{\mathrm{ext}}S \\ &= T\,\mathrm{d}S - T\mathrm{d}_{\mathrm{irr}}S \\ &= T\,\mathrm{d}S - \delta_{\mathrm{irr}}Q \quad , \end{aligned} \tag{3.56}$$

where the amount of heat created by the system due to irreversible processes is always positive $\delta_{\mathrm{irr}}Q \geq 0$.

The change in *Helmholtz free energy*

$$\mathrm{d}F_{\mathrm{Helm}} = \mathrm{d}U - T\,\mathrm{d}S \tag{3.57}$$

characterizes the amount of work obtainable from a closed system at constant temperature T. If we further assume constant pressure p and constant magnetic field H, the change in *Gibbs free energy*

$$\mathrm{d}F_{\mathrm{Gibbs}} = \mathrm{d}F_{\mathrm{Helm}} - \delta L \tag{3.58a}$$

$$= \mathrm{d}U - T\,\mathrm{d}S + p\mathrm{d}V - V\mu_0 H\,\mathrm{d}M \tag{3.58b}$$

gives the amount of work that can be obtained from the magnetic system. For reversible transitions between two equilibrium states[11] $\mathrm{d}F_{\mathrm{Gibbs}} = 0$, otherwise $\mathrm{d}F_{\mathrm{Gibbs}} < 0$. As a matter of principle, for reversible state transitions the magnetic work added to the system can either

[10] The operator δ accounts for inexact differentials, since heat and work do not represent a state of the magnetic system. The integral over such inexact differentials is path-dependent, in general.

[11] Correctly speaking, the classical Gibbs free energy $F_{\mathrm{Gibbs}}(H,T)$ assumes an equilibrium state of M for given H and T, whereas in magnetic systems $F_{\mathrm{Gibbs}}(M;H,T)$ characterizes the free energy at a non-equilibrium state for given M, H, and T.

increase the internal energy or decrease the entropy (which is equivalent to an increase of order)

$$\delta L = \mathrm{d}U - T\,\mathrm{d}S \quad . \tag{3.59}$$

For irreversible state transitions a part of the supplied work is transformed into heat

$$\delta L = \mathrm{d}U - T\,\mathrm{d}S + \delta_{\mathrm{irr}}Q \quad , \tag{3.60}$$

yielding in

$$-\mathrm{d}F_{\mathrm{Gibbs}} = \delta_{\mathrm{irr}}Q \quad . \tag{3.61}$$

However, in magnetic systems Gibbs free energy is given by the sum of the energy contributions of section 3.1 and the reversible part of the pinning energy $W_{\mathrm{Pin,rev}}$ as

$$F_{\mathrm{Gibbs}} = W_{\mathrm{Ex}} + W_{\mathrm{Stray}} + W_{\mathrm{H}} + W_{\mathrm{Aniso}} + W_{\mathrm{MEself}} + W_{\mathrm{Stress}} + W_{\mathrm{Pin,rev}} \quad . \tag{3.62}$$

When magnetostriction, magneto-elastic interactions, and thermal expansion of the material is disregarded, a constant sample volume V can be assumed. Then magnetic work is the only one supplied to the system, i.e.

$$\delta L = -\mathrm{d}W_{\mathrm{H}} = V\mu_0 H\,\mathrm{d}M \tag{3.63}$$

and the remaining energy terms give the Helmholtz free energy

$$F_{\mathrm{Helm}} = W_{\mathrm{Ex}} + W_{\mathrm{Stray}} + W_{\mathrm{Aniso}} + W_{\mathrm{Pin,rev}} \quad . \tag{3.64}$$

By combining (3.58a), (3.61), and (3.63) an incremental change in state of this simplified magnetic system can be expressed as

$$\delta L = V\mu_0 H\,\mathrm{d}M = \mathrm{d}F_{\mathrm{Helm}} + \delta_{\mathrm{irr}}Q \quad . \tag{3.65}$$

For a transition from state $\mathcal{S}_1$ to $\mathcal{S}_2$

$$V\mu_0 \int_{\mathcal{S}_1}^{\mathcal{S}_2} H\,\mathrm{d}M_{\mathrm{H}} = \Delta F_{\mathrm{Helm}} + \int_{\mathcal{S}_1}^{\mathcal{S}_2} \delta_{\mathrm{irr}}Q \tag{3.66}$$

the supplied magnetic work is partly stored in the Helmholtz free energy and irreversibly transformed into heat. For a complete hysteresis cycle with identical start and end state the Helmholtz free energy does not change, and (3.66) yields to

$$\mu_0 \oint H\,\mathrm{d}M = \frac{1}{V} \oint \delta_{\mathrm{irr}}Q \quad . \tag{3.67}$$

The fact that the area of the hysteresis loop is proportional to the irreversible losses per cycle has been first observed by E. Warburg [85] in 1881 and is therefore known as *Warburg's law*.

For an adiabatic magnetic system (without exchange of heat with the environment) the change in temperature is a measure for the entropy contained in the system. Based on this fact several measurements of the distribution of losses over a hysteresis cycle have been published in [6], [17], and [79], for example. The change in temperature can be separated into a reversible part (due to the magneto-caloric effect) and an irreversible part. The latter is sketched in Fig. 3.10, where the temperature T_{irr} is representative for the *irreversible losses* Δw_{irr} per unit volume for a transition between two states $\mathcal{S}_1$ and $\mathcal{S}_2$

$$\Delta w_{\mathrm{irr}} = \frac{1}{V} \int_{\mathcal{S}_1}^{\mathcal{S}_2} \delta_{\mathrm{irr}} Q \;\geq 0 \quad . \tag{3.68}$$

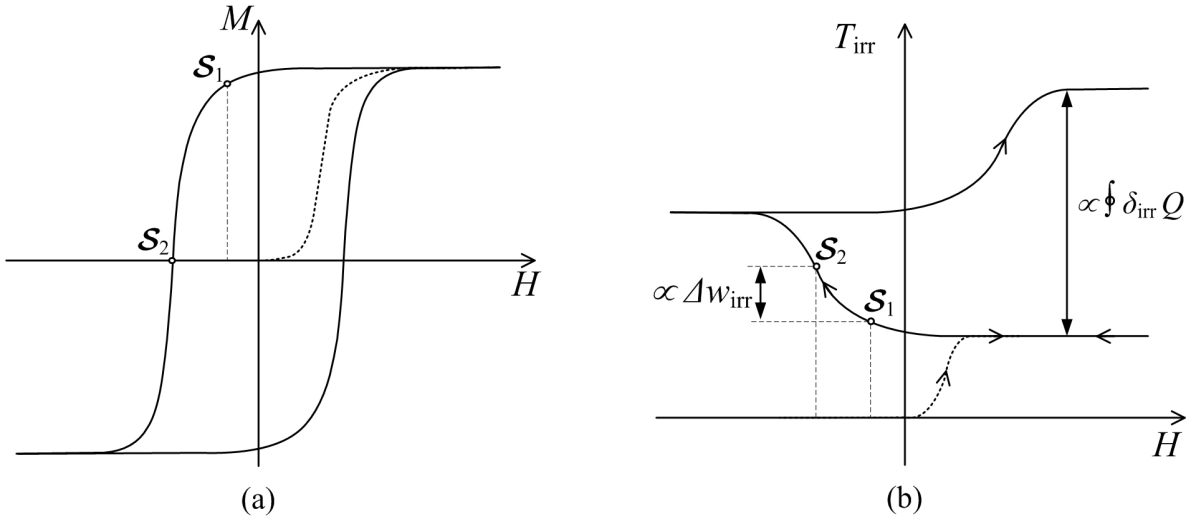

Figure 3.10: Characteristic results of irreversible heat measurements over a hysteresis cycle (a), represented by temperature increase T_{irr} in an adiabatic system (b).

3.4 Summary

Beyond atomic length scales a ferromagnetic system can be described in terms of continuous vector fields. The intrinsic quantum-mechanical properties as well as the interactions with external field or stress are captured by different energy contributions.

When the detailed spatial arrangement of the magnetic moments is not of primary interest, the ferromagnetic system can be characterized as ensemble of magnetic domains, which are reasoned by long-range interaction mechanisms.

Focusing on the total sample magnetization and its dependence to an applied magnetic field, the magnetization process can be described in terms of magnetization curves. A change in sample magnetization can either be due to domain wall motion or due to magnetization rotation, where each of this two mechanisms are partly reversible and partly irreversible. Especially the irreversible processes that create losses inside the material are substantial for hysteresis modeling.

Part II

Magnetic Modeling

Within the *fourth chapter* the state of the art in magnetic hysteresis modeling is summarized. In addition to a brief survey on the basic principles, the major characteristics of the models published in scientific literature are described in chronological order. The models presented in this chapter are based on either physical, mathematical or phenomenological principles, so the properties of ferromagnetic hysteresis are derived from different point of views. Some of these models have been developed based on a scalar approach and extended to vector models in the course of time. Exactly this vector generalization of scalar models can be checked against the two-dimensional extension of the Energetic Model that is also a part of this thesis.

Furthermore, the effort to identify the model parameters and the expenditure for calculation have to be related to ability of predicting the magnetization curves with a sufficient accuracy. This synopsis of well established hysteresis models is of vital importance for the comparison of the generalized Energetic Model with the current state of the art.

The *fifth chapter* represents the fundamental core of this thesis, since it describes the generalized two-dimensional "Energetic Model of Ferromagnetic Hysteresis". Starting from the definition of magnetic entities as basic elements of magnetic moment, the aggregation of these magnetic entities to statistical domain classes provides the topological framework of the model. In a two-dimensional setup, the orientation of the magnetic entities' magnetization in such a domain class is characterized by a statistical distribution function of the polar angle. Hence, local energy contributions that are based on energy densities can be assigned to the domain classes via statistical expectation value in a quite natural way. In contrast, non-local energy terms as well as reversible and irreversible work due to domain wall motion are treated phenomenologically. Whenever applicable, the concepts are substantiated by physical interpretations and corresponding literature.

After a comprehensive presentation of the generalized Energetic Model, the calculation process is summarized. In general, the minimization of a total energy term subject to several constraints determines the model variables and thus allows the simulation of the magnetization curves. In order to reduce the numerical calculation effort, the setup has to be chosen adequate to the problem to be modeled.

Chapter 4

State of the Art in Magnetic Hysteresis Modeling

In ferromagnetic materials the description of the macroscopic magnetization process is still quite complex in nature, because it is influenced by microstructural properties of the material as well as by sample geometry, and environmental conditions, like temperature or stress. Due to the fact that the response of a hysteretic system depends on the history of states, there is need for a more sophisticated mathematical formalism than just a simple functional dependence between magnetic field and magnetization. Within the different contexts of scientific approaches and technological requirements several magnetic hysteresis models have been established in the course of the 20^{th} century. The following sections provide an overview of the most significant hysteresis models in chronological order.

4.1 Characterization of Magnetic Hysteresis Models

Even though the fact that some hysteresis models are developed, extended, and evaluated in a broad range, there exists no general unified theory of ferromagnetic hysteresis so far. However, magnetic hysteresis modeling comprises several topics of science:

- **Physical Aspects:** Starting point is the fact that magnetic material behavior originates at the atomic level and is described by means of quantum mechanics. Nevertheless, the classical approach, where magnetic materials are treated as continuous media is often an appropriate choice, which makes calculations easier without loosing accuracy. Intrinsic material properties and influences from the environment (like magnetic field or heat) are expressed in terms of energy. Finally, every magnetic behavior is determined by a competition of different energy contributions.

- **Phenomenological Aspects:** In this case one starts at the macroscopic level by studying various kinds of hysteresis phenomena. Directional dependencies, behavior in the low and high field regimes, accommodation of minor loops, or Barkhausen jumps are only a few examples representing the wide area of magnetic hysteresis phenomena. Based on this macroscopic properties one tries to find an appropriate "microscopic picture" (like domain walls moving in an energy landscape) in accordance with the physical background, which is able to explain the considered hysteresis phenomena.

- **Mathematical Aspects:** There also exist mathematical techniques to describe hysteresis behavior independent of any physical or phenomenological background. Elementary hysteresis operators are mentioned to give an example. If one starts from a pure mathematical description in order to model magnetic hysteresis, the abstract elements of the approach have to be related to a physical meaningful reality.
- **Stochastic Aspects:** Since the "source of magnetism" is located at the atomic level and magnetic hysteresis analysis is done on a macroscopic level, statistical techniques can be considered as adequate tool in order to summarize microscopic effects into a globally describable formalism. Hysteresis phenomena are always accompanied by a process of order, antagonizing thermal disorder. Like in the classical theory of ideal (perfect) gases, similar concepts can also be applied to model ferromagnetic behavior. Last but not least, whenever terms of averaging are used in magnetic models, this refers to statistics.

Scalar and Vector Hysteresis Models

Most of the presented hysteresis models are based on a scalar approach, so that one is able to identify the basic mechanisms of the model and study its fundamental properties. In principle, these scalar models can be applied to describe hysteresis phenomena for many technical applications, especially when one is interested in the magnetic behavior along a certain characteristic direction. In order to capture the full directionality of the magnetic relations, it becomes necessary to extend the scalar models to vector formulations.

Identification of Model Parameters

Especially in the case when models contain many parameters that are hardly to relate to physical and technological properties of the material, the identification procedure can prevent from practical usage. So there is always a trade-off between the ability of a model to describe a given hysteresis behavior with high accuracy and the effort to identify the model parameters, based on the underlying physics.

Length Scale of the Problem

In the beginning of chapter 1 it is stated that the theoretical framework to describe magnetic behavior is related to the length scale (number of involved atoms) of the considered problem. Consequently, the same argument can be applied to magnetic hysteresis models. So microscopic models are designed to explain the internal structure of domains (and walls), whereas macroscopic models are focused on the various features of the magnetization process as a whole.

In the following pages some of the most significant hysteresis models are described succinctly. Thus, the basic assumption and properties are pointed out at the expense of the further development, which can be found in detail in corresponding literature. Among other literature the text books [1], [8], [61], and [78] provide a survey of magnetic hysteresis modeling under various points of view.

4.2 Micromagnetic Modeling

In the 1930's LANDAU and LIFSHITZ [57] proposed first quantitative approaches for micromagnetic modeling with a study on the magnetic domain wall structure. Subsequently in the early 1940's W. F. BROWN [12] developed the fundamental steps to set up a theory he called *Micromagnetism*. Within this theory details of magnetic microstructures, neglected in the classical domain theory, are considered, whereas the discrete atomic nature of matter is ignored. Consequently, the magnetization can be regarded as continuous vector function of space.

In short, micromagnetism is the concept of finding a stationary or dynamic spatial distribution of magnetization inside a ferromagnetic body so as to minimize the total free Gibb's energy assigned to this body. The competition between different energy contributions expected in the material determines its magnetic behavior.

4.2.1 Model Definition

As mentioned above, the aim of micromagnetism is to find a magnetization distribution

$$\vec{M}(\vec{r}) = M_\mathrm{s}\,\vec{m}(\vec{r}) \qquad |\vec{m}(\vec{r})| = \vec{m}^2(\vec{r}) = 1 \quad \forall\,\vec{r} \in \mathcal{V} \tag{4.1}$$

in a ferromagnetic sample, occupying a volume region $\mathcal{V}$. The unit magnetization vector function $\vec{m}(\vec{r})$ is derived by a minimization of the (Gibb's) *total free energy* dedicated to the sample volume $\mathcal{V}$ when an external field $\vec{H}$ is applied. Assuming a rigid crystal (to neglect magnetostriction) maintained at a uniform temperature below the Curie point, the total energy functional can be written as

$$W_\mathrm{Tot}(\vec{m}(\vec{r}); \vec{H}) = \int\limits_{\mathcal{V}} \Big(w_\mathrm{H}(\vec{m}, \vec{H}) + w_\mathrm{Stray}(\vec{m}) + w_\mathrm{Ex}(\vec{m}) + w_\mathrm{Aniso}(\vec{m}) \Big)\ \mathrm{d}V \quad , \tag{4.2}$$

where w_i represent the different energy contributions described in section 2.1. Here the magnetization vector $\vec{m}(\vec{r})$ is considered as the only independent variable, and the optimization problem can be formulated as

$$W_\mathrm{Tot}(\vec{m}(\vec{r}); \vec{H}) \underset{\vec{m}(\vec{r})}{\longrightarrow} \mathrm{MIN} \quad . \tag{4.3}$$

To complete the optimization problem one has to add the magnetostatic equations (2.7) and (2.10)

$$\vec{\nabla} \cdot \vec{H}_\mathrm{Stray} = -\vec{\nabla} \cdot (M_\mathrm{s}\,\vec{m}(\vec{r})) \quad \text{with} \quad \vec{\nabla} \times \vec{H}_\mathrm{Stray} = \vec{0} \quad , \tag{4.4}$$

which describe the dependence of the (demagnetizing) stray field on magnetization.

As can be seen, the independent variable of the optimization problem is not just a number, but is a vector field defined over the entire body volume. For this reason we have to use variational calculus to derive a set of partial differential equations, which have to be solved numerically, in general. This means if $\vec{m}(\vec{r})$ is varied in each sample point $\vec{r}$ by a small quantity $\delta\vec{m}$, the corresponding variation of the total energy δW_Tot has to be zero and the second-order variation $\delta^2 W_\mathrm{Tot}$ is positive in a local minimum.

Boundary Conditions

At the surface $\partial\mathcal{V}$ of the considered body one has to introduce boundary conditions yielding from the variational procedure. In absence of surface anisotropy the boundary conditions reduce to the simple form ($\vec{n}$ is the surface normal)

$$\left(\vec{n}\cdot\vec{\nabla}\right)\vec{m}(\vec{r})=0 \qquad \forall\,\vec{r}\in\partial\mathcal{V} \quad . \tag{4.5}$$

The normal derivatives of all magnetization components must be zero at the surface.

Stationary Solution - Brown's Equation

The solution of the variational problem (4.3) is expressed in terms of a so called *effective field* $\vec{H}_{\text{eff}}$ given by the negative functional derivative[1] of the total free energy

$$\vec{H}_{\text{eff}}(\vec{m}(\vec{r}))=-\frac{1}{\mu_0 M_s}\frac{\delta W_{\text{Tot}}(\vec{m}(\vec{r});\vec{H})}{\delta\vec{m}(\vec{r})} \quad . \tag{4.6}$$

For the system to be in a stationary equilibrium the stability condition, known as *Brown's equation*

$$\vec{m}(\vec{r})\times\vec{H}_{\text{eff}}(\vec{m}(\vec{r}))=\vec{0} \qquad \forall\,\vec{r}\in\mathcal{V} \tag{4.7}$$

has to be fulfilled at each point inside the sample.

As simple interpretation it can be stated that the torque exerted on any magnetization vector by the effective field must vanish in a stationary equilibrium. So the effective field has to be directed along the magnetization vector at every point in the magnetic body.

Dynamic Solution

For further investigations the magnetization is considered as a function of space and time

$$\vec{M}(\vec{r},t)=M_{\text{s}}\,\vec{m}(\vec{r},t) \quad , \tag{4.8}$$

but to simplify the notation the arguments are suppressed, so $\vec{m}$ is written instead of $\vec{m}(\vec{r},t)$, for example.

If the magnetic system is not in an equilibrium state as described above, the magnetization vector performs a precession motion under the action of a torque exerted by $\vec{H}_{\text{eff}}$ acting on $\vec{M}$. The corresponding equation of motion is

$$\frac{\partial\vec{m}}{\partial t}=-\gamma\left(\vec{m}\times\vec{H}_{\text{eff}}\right) \quad , \tag{4.9}$$

[1] Note, that the variational derivative of a functional $G(y(x))=\int g(y(x),y'(x),x)\,\mathrm{d}x$ is defined as $\frac{\delta G}{\delta y}=\frac{\partial g}{\partial y}-\frac{\mathrm{d}}{\mathrm{d}x}\frac{\partial g}{\partial y'}$ (i.e. it is related to the derivative of the integrand $g(.)$), when dealing with units.

where γ is the *gyromagnetic ratio* depending on the Landé factor g, mass m_e, and electric charge -e of an electron (see section 1.1.1)

$$\gamma = \mu_0 \, g \, \frac{e}{2m_e} \quad . \tag{4.10}$$

But in realistic cases this free gyromagnetic precession (with frequency $\vec{\omega} = \gamma \vec{H}_{\text{eff}}$, i.e. $\approx$ 28 MHz/mT for free electron spin) is restricted by dissipative processes (losses). The assumption of such dissipation allows the magnetization to turn towards the effective field into a stationary equilibrium. In their pioneering work LANDAU and LIFSHITZ [57] proposed the introduction of a phenomenological damping term and reformulated the equation of motion (4.9) as

$$\frac{\partial \vec{m}}{\partial t} = -\frac{\gamma}{1+\alpha^2}\left(\vec{m} \times \vec{H}_{\text{eff}}\right) - \frac{\alpha\gamma}{1+\alpha^2}\left(\vec{m} \times \left(\vec{m} \times \vec{H}_{\text{eff}}\right)\right) \tag{4.11}$$

referred to as *Landau-Lifshitz equation* with the damping parameter[2] α. The second term signifies a damping force acting on the precession magnetization in a direction towards the effective field (Fig. 4.1).

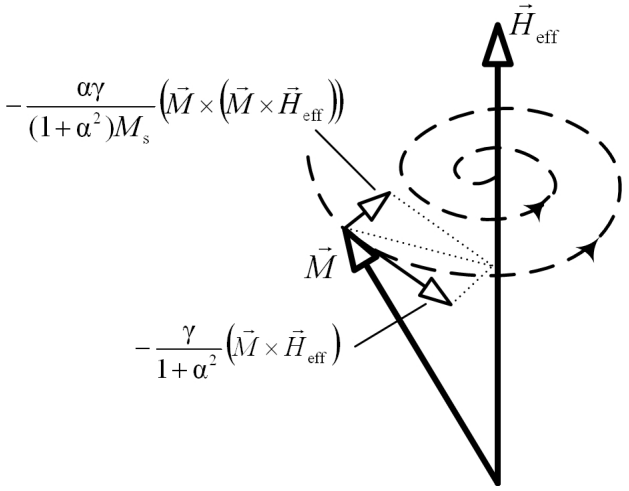

Figure 4.1: Magnetization precession with damping.

If we imagine that the damping acts on the resultant motion of the magnetization $\partial\vec{m} \,/\, \partial t$ instead of the pure precession motion $-\gamma\left(\vec{m} \times \vec{H}_{\text{eff}}\right)$, we get an equivalent formulation of (4.11)

$$\frac{\partial \vec{m}}{\partial t} = -\gamma\left(\vec{m} \times \vec{H}_{\text{eff}}\right) + \alpha\left(\vec{m} \times \frac{\partial \vec{m}}{\partial t}\right) \quad , \tag{4.12}$$

[2]Strictly speaking, this is the "Gilbert damping parameter", because it is explicitely adressed to the damping term of Gilbert's equation. To avoid confusion by introducing a lot of parameters, it is also used in the Landau-Lifshitz equation. To allow a coincident transformation between (4.11) and (4.12) the term $(1+\alpha^2)$ is obtained in the denominator of (4.11).

which was first derived by GILBERT [28] in 1955, and is known as *Gilbert equation*. The damping parameter α is used to fit experimental data to the model. Under various conditions (like magnetization state) α may take different values, for numerical convenience [22] it is chosen from the interval $[0.1, 1]$.

4.2.2 Computation Techniques

In the case of static considerations the spatial distribution of the magnetization vector is obtained from Brown's equation (4.7), whereas in the case of dynamics either Landau-Lifshitz equation (4.11) or Gilbert's equation (4.12) can be used. But these micromagnetic equations can not be solved analytically, in general. Depending on the scale of the magnetic problem different numerical techniques are applied. By means of high-performance computer technology it has become possible to solve micromagnetic problems numerically without having to make oversimplifying assumptions or to superimpose a priori arbitrary functions on the nature of the magnetic system.

Finite Difference Method

For numerical computations the magnetic sample is divided in small cubic elements of volume $\Delta V = \Delta x\, \Delta y\, \Delta z$ in which the magnetization is assumed to be constant in its norm but varying in its direction. So the continuum is replaced by a discrete number of lattice points each located in the center of the computational cell i at $\vec{r} = \vec{r}_i$. Within this discretization process partial derivatives were approximated by finite difference quotients

$$\vec{m}(\vec{r}_i + \Delta x\, \vec{e}_x,\, t) = \vec{m}(\vec{r}_i, t) + \Delta x \left.\frac{\partial \vec{m}(\vec{r}, t)}{\partial x}\right|_{\vec{r}=\vec{r}_i} + \ \ldots \quad , \tag{4.13}$$

and the partial differential equation changes to a system of algebraic equations. Therefore, one is able to express the effective field (4.6) depending on the magnetization in the lattice sites. Among other problems a difficulty arises from the discretization of the demagnetizing field, which has been successfully captured by different approaches, described in [1] or [22], for example. In order to get the dynamic magnetization behavior one has to perform a time integration of the Landau-Lifshitz (4.11) or the Gilbert (4.12) equation for each computational cell. This is done by a discretization in time into a regular lattice of time points.

Finite Element Method

Since the finite element technique is an appropriate tool for solving partial differential equations, it becomes essentially as a minimization technique for variational problems. Starting point of micromagnetic finite element calculations is a discretization of the total free energy (4.2). In a so called triangulation process the whole solution domain is divided into a collection of many finite elements (usually triangles in 2D or tetrahedra in 3D). Within these elements the magnetization $\vec{m}(\vec{r})$ is interpolated by piecewise polynomials with respect

to the magnetization values $\vec{m}_i = \vec{m}(\vec{r}_i)$ at the nodal points $i \in \mathcal{N}$, where $\mathcal{N}$ is the set of all nodal points within the considered finite element mesh. So one can write

$$\vec{m}(\vec{r}) = \sum_{i \in \mathcal{N}} \varphi_i(\vec{r})\, \vec{m}_i \quad , \tag{4.14}$$

using a so called shape function $\varphi_i(\vec{r})$ satisfying the condition

$$\varphi_i(\vec{r}_j) = \delta_{ij} = \begin{cases} 1 & \text{for } i = j \\ 0 & \text{for } i \neq j \end{cases} \quad . \tag{4.15}$$

Thus, if the continuous magnetization is approximated by piecewise polynomial functions, the energy functional reduces to an energy function with the nodal magnetization values $\vec{m}_i$ as unknowns.

$$W_{\mathrm{Tot}}(\vec{m}(\vec{r}); \vec{H}) = W_{\mathrm{Tot}}(\vec{m}_i; \vec{H}) \tag{4.16}$$

The minimization of this energy function with respect to unknown nodal magnetizations $\vec{m}_i$ subject to $|\vec{m}_i| = 1$ can be done by a well established gradient method. Thus one defines a volume V_i ("box") around mesh-node i in order to approximate the effective field in this point as

$$\vec{H}_{\mathrm{eff},i} = -\frac{1}{\mu_0 M_{\mathrm{s}}} \left. \frac{\delta W_{\mathrm{Tot}}(\vec{m}(\vec{r}); \vec{H})}{\delta \vec{m}} \right|_{\vec{r}_i} \approx -\frac{1}{V_i} \frac{1}{\mu_0 M_{\mathrm{s}}} \frac{\partial W_{\mathrm{Tot}}(\vec{m}_i; \vec{H})}{\partial \vec{m}_i} \quad . \tag{4.17}$$

This is often referred to as box method [27].

A problem within this context is the treatment of the demagnetizing field, because it depends on the magnetization distribution over the entire sample and not locally (like exchange or anisotropy) on the magnetization. Further details is can be found in the literature to the related topics.

4.2.3 Applications

The investigation of nanoshaped magnetic elements for *high-density magnetic storage media* has reached a length scale, where the concepts of micromagnetism lead to reasonable calculation effort. Therefore, modeling patterned magnetic elements used in magnetic random access memories (MRAM) is a central objective in micromagnetism. Besides other aspects, a well defined switching characteristic and switching speed behavior is of interest [88].

As a further application the investigation of microstructure of *high energy density permanent magnets* (e.g. Nd-Fe-B magnets) can be mentioned. Especially the influence of different exchange mechanisms at the grain or subgrain level can be obtained from finite element simulations [22].

Generally, new spatially fine resolving measurement techniques enforce micromagnetic modeling in order to describe the dynamic behavior or thermal stability of *small magnetic particles in the nanometer regime.*

4.3 Preisach Model

The framework for Preisach modeling has its genesis in 1935 by the idea of FERENC PREISACH [72] to describe hysteresis in ferromagnetic systems as a superposition of elementary bistable units, called "Hysterons". Following this approach, the magnetization process can be interpreted as a sequence of Barkhausen jumps. During the 1970's an abstract reformulation of this model has been derived by KRASNOSELSKII and POKROVSKII [53], where they encapsulated the ideas of Preisach's original model into a mathematical framework using well established operator techniques. MAYERGOYZ summarized these methodologies in his book [61] and provided mathematical clarity to the hysteresis theory. Up to now a large number of literature concerning the Preisach model has been published with investigations focused either on physical interpretation, mathematical analysis, or on extensions to a rich variety of applications.

4.3.1 Classical Scalar Preisach Model

Assuming that the magnetic field is applied along a fixed direction, one concentrates only on the component of magnetization with respect to this field direction. In principle the setup of the Preisach model originates from elementary *Preisach units*, also called "*Hysterons*".

Elementary Hysterons

The unit volume of the system is imaginarily split into many small abstract regions, which are characterized by a square-looped hysteresis behavior, as shown in Fig. 4.2. Within the Preisach model the switching fields H_{up} and H_{down} or alternatively the local coercive field H_{c} and the interaction field H_{i} are treated as random variables, whereas the hysteron's magnetic moment $+\hat{\mathfrak{m}}$ or $-\hat{\mathfrak{m}}$ is assumed to be constant, in general. This characterization in terms of random variables, especially the offset in presence of an interaction field $H_{\mathrm{i}} \neq 0$ should express the fact that each hysteron does not feel only the external magnetic field H, but also an interaction due to adjacent Preisach units. As consequence of the assumption of bistable Preisach units, each such unit can either be in the state $S^{(+)} : \mathfrak{m} = +\hat{\mathfrak{m}}$ or in the state $S^{(-)} : \mathfrak{m} = -\hat{\mathfrak{m}}$.

Alternative Hypothesis for the Existence of Preisach Units: BERTOTTI [8] used the term Preisach unit to refer to an entity, which is characterized by an energy profile, as depicted in Fig. 4.3. Depending on the characteristic fields H_{i} and H_{c}, $F_{\mathrm{Helm}}(\mathfrak{m})$ is the *free energy profile* of the Preisach unit and $F_{\mathrm{Gibbs}}(\mathfrak{m}, H) = F_{\mathrm{Helm}}(\mathfrak{m}) - \mu_0 H\,\mathfrak{m}$ is the *Gibb's energy* under the assumption that the Preisach unit is coupled linearly to the applied field H.

Within this point of view the magnetization process is interpreted as a sequence of Barkhausen instabilities and does not necessarily require the introduction of individual elementary hysteresis loops. However, within this picture the variables H_{i} and H_{c} relate to stored versus dissipated energy terms. Assuming the Preisach unit is in the state $S^{(-)}$, an increasing field causes a Barkhausen jump (at the switching field $H = H_{\mathrm{up}}$), and the magnetic system leaves the metastable state in order to reach the state $S^{(+)}$ of lower energy.

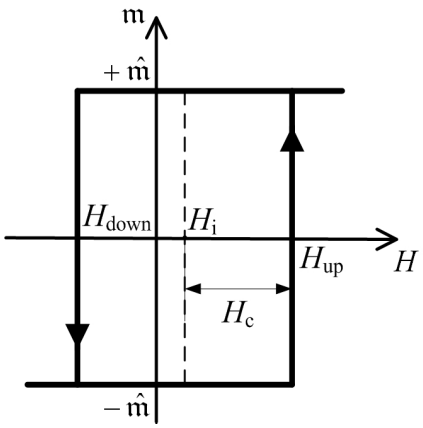

Figure 4.2: An elementary hysteron in the classical Preisach model.

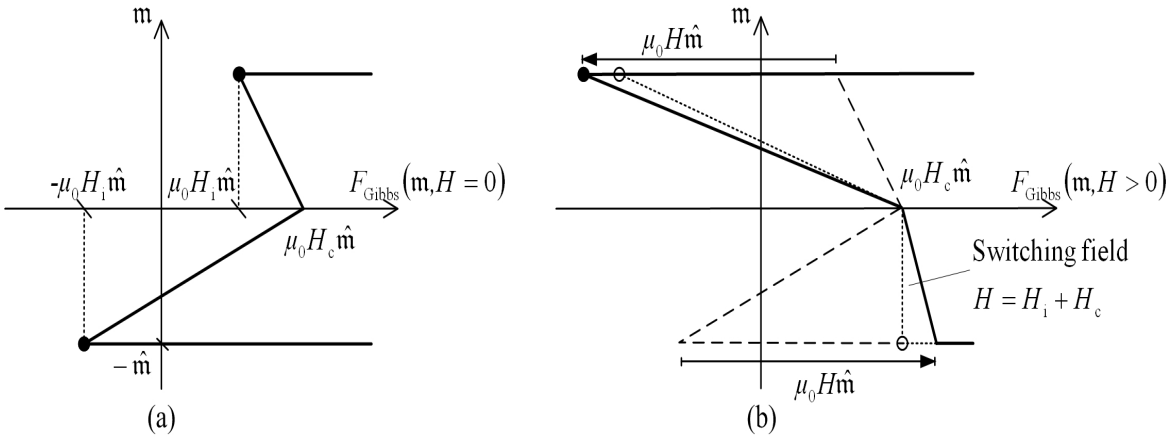

Figure 4.3: Free energy profile of a hysteron for $H = 0$ with two metastable states (a), and for $H > H_{\mathrm{up}} = H_{\mathrm{i}} + H_{\mathrm{c}}$ exhibiting one stable state (b).

Thereby the free energy changes by $\Delta F_{\mathrm{Helm}} = 2\mu_0 H_{\mathrm{i}}\,\hat{\mathfrak{m}}$ on the one hand, and the Gibb's energy decreases by $\Delta F_{\mathrm{Gibbs}} = 2\mu_0 H_{\mathrm{c}}\,\hat{\mathfrak{m}}$ on the other hand. The latter amount of energy is dissipated as heat.

Mathematical Description of the Hysteron: In a mathematical framework the hysteron's behavior is defined by a *Preisach kernel* or *Preisach relay* $\mathfrak{m}_{\mathrm{P}}(H,\xi)$, where $\xi \in \{-1,1\}$ denotes the state of the hysteron. The initial condition of this relay is given by

$$\left[\mathfrak{m}_{\mathrm{P}}(H,\xi)\right](0) = \begin{cases} -\hat{\mathfrak{m}} & \text{if} \quad H(0) \le H_{\mathrm{down}} \\ \xi\,\hat{\mathfrak{m}} & \text{if} \quad H_{\mathrm{down}} < H(0) < H_{\mathrm{up}} \\ +\hat{\mathfrak{m}} & \text{if} \quad H(0) \ge H_{\mathrm{up}} \end{cases} \tag{4.18}$$

and the dependence of the kernel on time t is defined as

$$\left[\mathfrak{m}_{\mathrm{P}}(H,\xi)\right](t) = \begin{cases} \left[\mathfrak{m}_{\mathrm{P}}(H,\xi)\right](0) & \text{if} \quad \tau(t) = \{\} \\ -\hat{\mathfrak{m}} & \text{if} \quad H(\max\{\tau(t)\}) = H_{\mathrm{down}} \\ +\hat{\mathfrak{m}} & \text{if} \quad H(\max\{\tau(t)\}) = H_{\mathrm{up}} \end{cases}, \tag{4.19}$$

where $\tau(t)$ is the set of time points at which the thresholds (switching fields) are reached

$$\tau(t) = \{t_s \in (0,t] \mid H(t_s) = H_{\text{down}} \vee H(t_s) = H_{\text{up}}\} \quad . \tag{4.20}$$

This is by no means the only formulation of an appropriate kernel, there exists a variety of modifications of the classical Preisach kernel[3] with the intention to accommodate certain material properties. The Krasnoselskii-Pokrovskii kernel [53] can be mentioned as a well known example.

Preisach Plane

In order to get a graphical representation of the Preisach units, each hysteron is associated with a point in the so called Preisach plane describing the loop behavior in its width as well as in its shift along the field axis. Depending on the pair of characteristic field values one is able to specify a Preisach plane either by H_{up}-H_{down}-axes or by H_{i}-H_{c}-axes, shown in Fig. 4.4. Nevertheless, the restrictions $H_{\text{up}} \geq H_{\text{down}}$ or $H_{\text{c}} \geq 0$ have to be fulfilled. Each hysteron can therefore be identified as a certain point of coordinates in the Preisach plane.

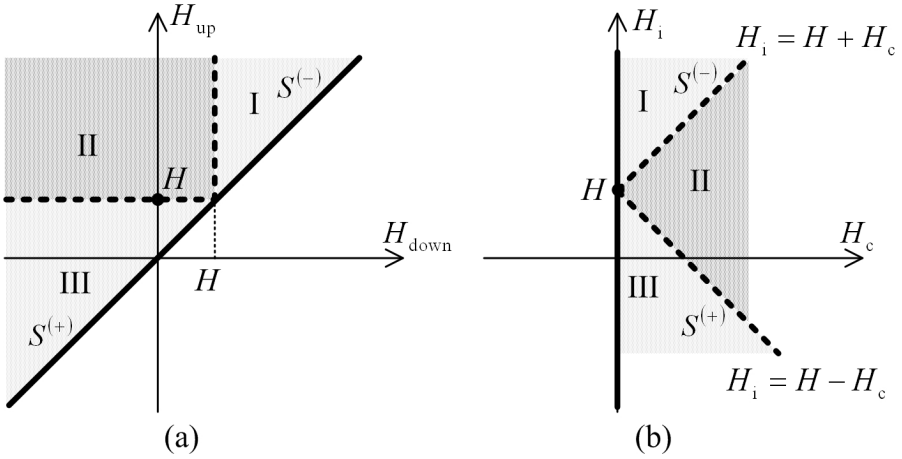

Figure 4.4: Preisach plane in terms of switching fields H_{up}-H_{down} (a) and H_i-H_c (b).

In the presence of a constant external field H the Preisach plane can be subdivided into three regions:

I $H \leq H_{\text{down}} = H_{\text{i}} - H_{\text{c}}$: Each Preisach unit in this region is certainly in the locally stable state $S^{(-)}$.

II $H_{\text{i}} - H_{\text{c}} = H_{\text{down}} \leq H \leq H_{\text{up}} = H_{\text{i}} + H_{\text{c}}$: Depending on the history both states $S^{(-)}$ and $S^{(+)}$ are locally stable.

III $H \geq H_{\text{up}} = H_{\text{i}} + H_{\text{c}}$: Each Preisach unit in this region is certainly in the locally stable state $S^{(+)}$.

[3] In practice, the modification of the kernel is bound up with a modification of the hysteresis behavior of the Preisach units.

A magnetic system as a whole is represented by a collection of hysterons, which are randomly distributed in the Preisach plane, switching under the action of an applied field. If the system reaches any metastable state for a certain field H as result of the field history, the Preisach plane is partitioned in only one $S^{(+)}$ region and one $S^{(-)}$ region, separated by a *boundary line* $L^{(\pm)}(H_c)$ as depicted in Fig. 4.5. In principle, this boundary line is a chain of linear segments of alternating slope, depending on the sequence of field reversals in the history[4]. By applying an oscillating field with varying amplitude one can imagine that the resulting boundary line takes the form of a fine sawtooth. Thus, from a generic point of view the boundary line $L^{(\pm)}(H_c)$ is approximated by a continuous function with a slope in the interval $-1 \leq \frac{\mathrm{d}L^{(\pm)}(H_c)}{\mathrm{d}H_c} \leq 1$.

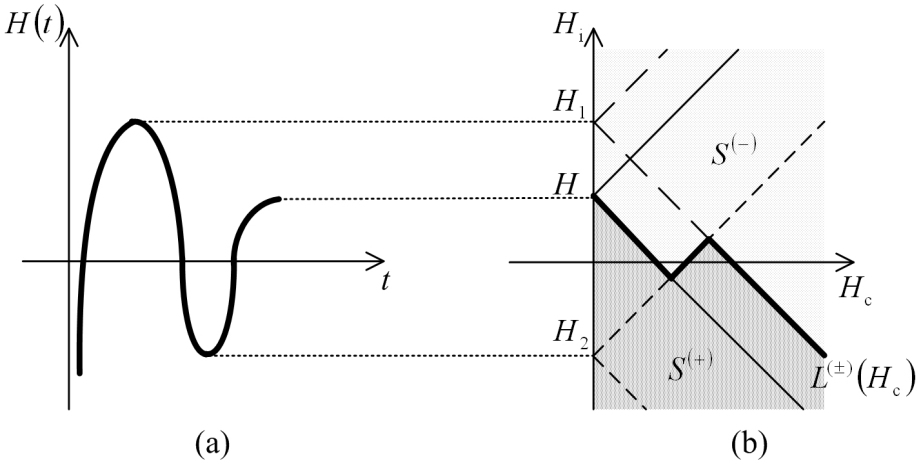

Figure 4.5: Boundary line (b) generated by the field history $H(t)$ (a).

Preisach Distribution

Assuming that the ferromagnetic sample consists of N Preisach units, the average magnetization M of the entire system is estimated as the sum of the contributions from each individual hysteron. Further we define the density function $p(H_\mathrm{c}, H_\mathrm{i})$ of the *Preisach distribution* so that

$$N \; p(H_\mathrm{c}, H_\mathrm{i}) \, \mathrm{d}H_\mathrm{i} \, \mathrm{d}H_\mathrm{c}$$

is the number of Preisach units in the small range $[(H_\mathrm{c}, H_\mathrm{i}), (H_\mathrm{c} + \mathrm{d}H_\mathrm{c}, \; H_\mathrm{i} + \mathrm{d}H_\mathrm{i})]$ of the Preisach plane and

$$\int_0^\infty \int_{-\infty}^\infty p(H_\mathrm{c}, H_\mathrm{i}) \, \mathrm{d}H_\mathrm{i} \, \mathrm{d}H_\mathrm{c} = 1 \tag{4.21}$$

[4]It is remarkable that the shape of the boundary line does not depend on the exact time behavior of the field and is therefore characteristic for the rate-independency of the Preisach model.

is fulfilled as general property of a probability density function. The magnetization of the system results as

$$M = M_{\mathrm{s}} \left[\int_0^{\infty} \int_{-\infty}^{L^{(\pm)}(H_{\mathrm{c}})} p(H_{\mathrm{c}}, H_{\mathrm{i}}) \, \mathrm{d}H_{\mathrm{i}} \, \mathrm{d}H_{\mathrm{c}} - \int_0^{\infty} \int_{L^{(\pm)}(H_{\mathrm{c}})}^{\infty} p(H_{\mathrm{c}}, H_{\mathrm{i}}) \, \mathrm{d}H_{\mathrm{i}} \, \mathrm{d}H_{\mathrm{c}} \right] \quad . \tag{4.22}$$

This equation shows that the state of the system is characterized by the boundary line $L^{(\pm)}(H_{\mathrm{c}})$, whereas all microstructural and magnetic hysteresis features are condensed in the Preisach distribution $p(H_{\mathrm{c}}, H_{\mathrm{i}})$.

Using the Preisach kernel defined in (4.19) we get a similar formulation for the magnetization (V is the sample volume)

$$M(t) = \frac{1}{V} \int_0^{\infty} \int_{-\infty}^{\infty} \left[\mathfrak{m}_{\mathrm{P}}(H, \xi) \right](t) \, p(H_{\mathrm{c}}, H_{\mathrm{i}}) \, \mathrm{d}H_{\mathrm{i}} \, \mathrm{d}H_{\mathrm{c}} \quad , \tag{4.23}$$

which already incorporates the time dependence.

Symmetry: If $\{-H(t), -M(t)\}$ is also an admissible history for the given input-output history $\{H(t), M(t)\}$, as it is observed for most of the conventional ferromagnetic materials, then the Preisach distribution has to be an even function of H_i

$$p(H_{\mathrm{c}}, H_{\mathrm{i}}) = p(H_{\mathrm{c}}, -H_{\mathrm{i}}) \quad . \tag{4.24}$$

In consideration of this symmetry the magnetization (4.22) becomes

$$M = 2M_s \int_0^{\infty} \int_{-\infty}^{L^{(\pm)}(H_{\mathrm{c}})} p(H_{\mathrm{c}}, H_{\mathrm{i}}) \, \mathrm{d}H_{\mathrm{i}} \, \mathrm{d}H_{\mathrm{c}} \quad . \tag{4.25}$$

Specific Choices for the Preisach Distribution: Setting up a Preisach model in terms of a general density function $p(H_{\mathrm{c}}, H_{\mathrm{i}})$ has the advantage of high flexibility and accuracy on the one hand, but the disadvantage in the requirement of a huge number of parameters, none of which are directly connected to physical properties, on the other hand. So one needs a sufficiently large set of experimental data to identify the density function. Furthermore, it can happen that these parameters change due to different environmental conditions (like temperature), a fact which enforces a re-identification.

However, in most of the applications one is choosing an *a-priori density function* (i.e. presuming material properties) in order to get a reduced set of parameters. Applying the central limit theorem, Della Torre [78] derived that a Gaussian (normal) distribution is the appropriate one for the interaction field H_{i}, with the mean interaction field $\bar{H}_{\mathrm{i}} = 0$. Taking the positivity of H_{c} into account, one obtains either a log-normal or again a normal distribution (with sufficient positive mean value $\bar{H}_{\mathrm{c}}$) for the local coercive field H_{c}.

4.3.2 Model Properties and Extensions

The classical Preisach model has some important properties, which lead to several extensions of this approach, if magnetic materials do not behave in the sense of these properties. In the following paragraphs the nature of the extensions developed to overrule the intrinsic properties of the classical Preisach model are briefly summarized.

Deletion (Wiping-out) Property Versus Non-closure of Minor Loops

Whenever the external field $H(t)$ achieves a local minimum (maximum), all boundary lines $L^{(\pm)}(H_\mathrm{c})$ resulted from minima (maxima) greater (smaller) than this are deleted.

As a consequence the deletion property ensures that every biased minor loop has to be closed. So if we return to the starting point, where the minor loop was initiated, all history concerning this minor loop is erased. The system is in the same state as it has been before.

But in some cases accommodation phenomena or the after-effect result in a non-closure behavior of the minor loops. Modifying the hysteron to permit outputs different from the constant values $\pm\hat{\mathfrak{m}}$ enables the model to describe such accommodation effects. Further details can be found in [61] or [78], for example.

Congruency Property Versus Magnetization-dependent Minor Loops

All minor loops generated from fields in the range between H_min and H_max have the same shape, i.e. they are congruent, regardless of the bias magnetization at which the loop was initiated.

Unfortunately, most of ferromagnetic materials exhibit magnetization-dependent minor loops, far away from congruency. One approach to circumvent the congruency problem is to generalize the Preisach distribution so as to make it field-dependent $p(H_\mathrm{c}, H_\mathrm{i}, H)$ [61]. Alternatively, there is also a magnetization-dependent Preisach distribution $p(H_\mathrm{c}, H_\mathrm{i}, M)$ possible, which is motivated by the mean field theory in a way that the mean of the interaction field of randomly orientated hysterons is proportional to the magnetization M [8].

Reversible Contributions

The classical Preisach model describes the system behavior as superposition of many bistable Preisach units with piecewise constant contributions. Thus, if ascending and descending hysteresis branches merge at a certain field H^*, the common M-H curve has zero slope

$$\frac{\mathrm{d}M(H)}{\mathrm{d}H} = 0 \quad \forall \ |H| > |H^*| \quad , \tag{4.26}$$

in contrast to the reversible M-H behavior of many ferromagnetic materials, where the slope approaches to zero only as the field H goes to infinity

$$\lim_{H \to \pm\infty} \frac{\mathrm{d}M(H)}{\mathrm{d}H} = 0 \quad . \tag{4.27}$$

Therefore, it was proposed to use generalized hysterons comprised of a reversible and an irreversible component [78] , as it is shown in Fig. 4.6, for example.

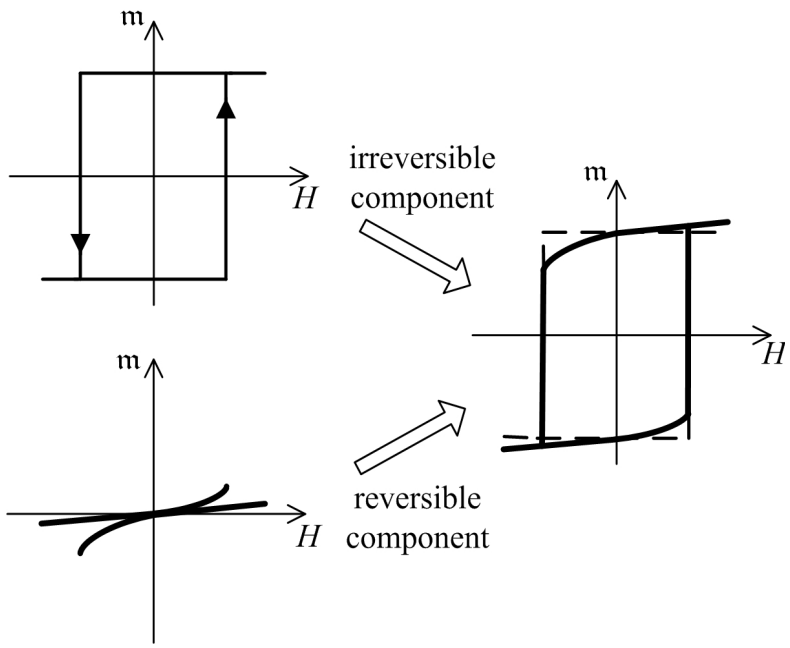

Figure 4.6: Extended hysteron comprised of a reversible and an irreversible component.

Representation Theorem

MAYERGOYZ [61] formulated the equivalence between the classical Preisach model and the deletion and congruency property within the so called representation theorem:

The hysteresis of any system can be described by the classical Preisach model if and only if it obeys deletion and congruency property. Both properties constitute necessary and sufficient conditions for a hysteresis non-linearity to be represented by the classical Preisach model.

Correspondence between Preisach and Jiles-Atherton Hysteresis Model

It has been shown [71] that the formulation of Preisach and Jiles-Atherton (described in the next section) models can be brought to an (partial) agreement for a special choice of the Preisach distribution. This unified model provides quite satisfying results in the medium and high field regime, but there remain still discrepancies of the observed and modelled ferromagnetic behavior at low magnetization and around the demagnetized state.

The relationship between the model parameters has been identified by DUPRE [18] in the form of implicit relations that describe the impacts of a parameter variation in one model on the other model. The results were compared with measurements of quasi-static hysteresis loops of silicon iron alloys.

4.4 Jiles-Atherton Hysteresis Model

In the 1980's D.C. JILES and D.L. ATHERTON proposed a basic version of their hysteresis model [48], [49], which uses a macroscopic energy balance in order to describe magnetization curves and hysteresis loops. This means that the energy supplied to a magnetic body by a change in applied field can either change the magnetostatic energy, or dissipate as hysteresis loss. Due to the advantages of a small number of physical parameters and reasonable computational effort, the Jiles-Atherton model makes a substantial contribution to hysteresis modeling techniques.

In the course of time the original scalar Jiles-Atherton model has been adapted according to different requirements with numerous extensions and generalizations published in subsequent literature.

4.4.1 Scalar Jiles-Atherton Model

In the original formulation of this model [49] the *total magnetization* is assumed as the sum of a reversible and an irreversible contribution

$$M(H) = M_{\mathrm{rev}}(H) + M_{\mathrm{irr}}(H) \quad . \tag{4.28}$$

Ferromagnetic regimes are characterized by interactions between magnetic moments. Hence, an *effective field* H_{e} is defined by adding an interaction field $H_{\mathrm{i}} = \alpha M$ to the external applied field H, written as

$$H_{\mathrm{e}} = H + \alpha M \quad , \tag{4.29}$$

following the ideas of Weiss' mean field approach [86]. The parameter α quantifies the amount of domain or particle interaction and has to be obtained from measurements for a given system.

Anhysteretic Magnetization $M_{\mathbf{an}}$

Neglecting dissipative processes the nonlinear H-M relation describes the anhysteretic magnetization curve, which can be calculated through consideration of the material's thermodynamic properties. Having regard to classical Boltzmann statistics the anhysteretic magnetization in the 3D formulation[5] is given by the Langevin function $\mathcal{L}(.)$ as

$$M_{\mathrm{an}}(H_{\mathrm{e}}) = M_{\mathrm{s}}\, \mathcal{L}\left(\frac{H_{\mathrm{e}}}{a}\right) \quad , \tag{4.30}$$

where the temperature dependent parameter a follows from the classical thermodynamic derivation as $a = N\, k_{\mathrm{B}} T \,/\, (\mu_0 M_{\mathrm{s}})$. Due to the fact that the (pseudo) domain density N is unknown, a is treated as model parameter determining the shape of the anhysteretic magnetization curve.

[5] Depending on the dimensionality of the problem, there are also other anhysteretic functions in use.

Irreversible Magnetization M_{irr}

Dislocations and other defects affect the motion of domain walls through magneto-elastic coupling, and magnetic inclusions reduce the magnetostatic energy (due to impurities) when intersected by a domain wall. From a general point of view all these phenomena are summarized in the concept of pinning sites without any further distinction of the underlying mechanisms. In consideration of this magnetic domain wall pinning on defect sites, a frictional force opposing the movement of domain walls leads to dissipative losses. Jiles and Atherton presumed randomly distributed pinning sites, all of which having the same (average) pinning energy density $\langle w_{\mathrm{Pin}} \rangle$ depending on the domain wall angle ϕ

$$\langle w_{\mathrm{Pin}} \rangle = \langle w_{\pi} \rangle \, \frac{1 - \cos(\phi)}{2} \tag{4.31}$$

with the maximum value $\langle w_{\pi} \rangle$ in the case of 180° domain walls. For a moving domain wall (sketched in Fig. 4.7) of area A and an average pinning site density $\langle n \rangle$, the energy dissipated against pinning is

$$\mathrm{d}W_{\mathrm{Pin}} = \langle n \rangle \, \langle w_{\mathrm{Pin}} \rangle \, A \, \mathrm{d}x \quad , \tag{4.32}$$

if the wall is moving over an incremental distance $\mathrm{d}x$. Associated with this wall displacement a net change in irreversible magnetization appears as

$$\mathrm{d}M_{\mathrm{irr}} = M_{\mathrm{s}} \, (1 - \cos(\phi)) \, A \, \mathrm{d}x \quad , \tag{4.33}$$

which allows one to express the pinning energy in terms of magnetization change

$$\mathrm{d}W_{\mathrm{Pin}} = \frac{\langle n \rangle \, \langle w_{\pi} \rangle}{2 M_{\mathrm{s}}} \, \mathrm{d}M_{\mathrm{irr}} = \mu_0 \, k \, \mathrm{d}M_{\mathrm{irr}} \quad , \tag{4.34}$$

where the pinning parameter k quantifies the energy dissipation due to pinning and unpinning of domain walls.

Equating the supplied work[6] during a change in effective field from $H_{\mathrm{e}1}$ to $H_{\mathrm{e}2}$ with the sum of the magnetostatic energy and the losses due to pinning as

$$\mu_0 \int_{H_{\mathrm{e}1}}^{H_{\mathrm{e}2}} M_{\mathrm{an}}(H_{\mathrm{e}}) \, \mathrm{d}H_e = \mu_0 \int_{H_{\mathrm{e}1}}^{H_{\mathrm{e}2}} M_{\mathrm{irr}}(H_{\mathrm{e}}) \, \mathrm{d}H_{\mathrm{e}} + \mu_0 \, k \int_{H_{\mathrm{e}1}}^{H_{\mathrm{e}2}} \frac{\mathrm{d}M_{\mathrm{irr}}(H_{\mathrm{e}})}{\mathrm{d}H_{\mathrm{e}}} \, \mathrm{d}H_{\mathrm{e}} \tag{4.35}$$

yields in the local relation

$$\frac{\mathrm{d}M_{\mathrm{irr}}(H_{\mathrm{e}})}{\mathrm{d}H_{\mathrm{e}}} = \frac{M_{\mathrm{an}}(H_{\mathrm{e}}) - M_{\mathrm{irr}}(H_{\mathrm{e}})}{\delta \, k} \quad . \tag{4.36}$$

The parameter δ =sign(dH) ensures that the energy to break pinning sites always opposes changes in magnetization. In consideration of (4.29) one gets the differential equation for the irreversible contribution

$$\frac{\mathrm{d}M_{\mathrm{irr}}(H)}{\mathrm{d}H} = \frac{M_{\mathrm{an}}(H) - M_{\mathrm{irr}}(H)}{\delta \, k - \alpha \, (M_{\mathrm{an}}(H) - M_{\mathrm{irr}}(H))} \tag{4.37}$$

to total magnetization with respect to the external applied field H.

[6] Therefore one has to postulate that the work over part of the hysteresis loop can be expressed as $L = -\int_{H_{\mathrm{e}1}}^{H_{\mathrm{e}2}} M \, \mathrm{d}H_{\mathrm{e}}$, derived in [43], for example.

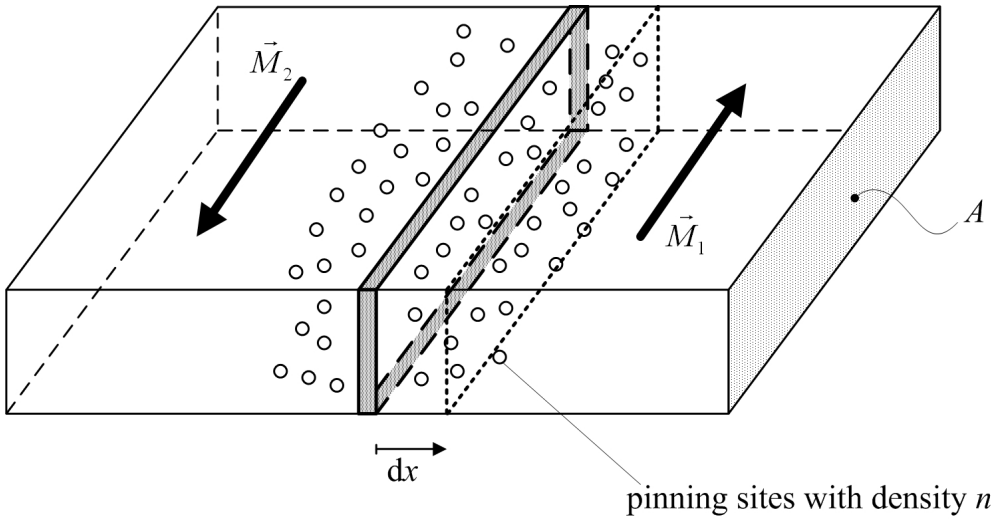

Figure 4.7: Energy dissipation of a moving 180° domain wall due to pinning effects.

Reversible Magnetization $M_{\mathbf{rev}}$

To introduce reversible processes in the model, Jiles and Atherton assumed a reversible magnetization to be proportional to the difference between the anhysteretic magnetization contribution and the irreversible one.

$$M_{\mathrm{rev}}(H) = c\,(M_{\mathrm{an}}(H) - M_{\mathrm{irr}}(H)) \tag{4.38}$$

The reversibility coefficient c quantifies the degree of reversible mechanisms like domain wall bending in comparison with the energy necessary to break the pinning sites.

Total Magnetization M

As mentioned in the beginning of this section (4.28), the total magnetization as the sum of an irreversible and a reversible contribution, defined by (4.37) and (4.38) leads to the differential equation

$$\frac{\mathrm{d}M(H)}{\mathrm{d}H} = \hat{\delta}\frac{M_{\mathrm{an}}(H) - M_{\mathrm{irr}}(H)}{\delta\, k - \alpha\,(M_{\mathrm{an}}(H) - M_{\mathrm{irr}}(H))} + c\left(\frac{\mathrm{d}M_{\mathrm{an}}(H)}{\mathrm{d}H} - \frac{\mathrm{d}M_{\mathrm{irr}}(H)}{\mathrm{d}H}\right) \quad . \tag{4.39}$$

The parameter $\hat{\delta}$ enforces the property that a domain wall exhibits reversible displacements immediately following the field reversal until the anhysteretic curve is achieved and is therefore defined as

$$\hat{\delta} = \begin{cases} 1 & \text{if} \quad (\mathrm{d}H < 0) \wedge (M > M_{\mathrm{an}}) \\ 1 & \text{if} \quad (\mathrm{d}H > 0) \wedge (M < M_{\mathrm{an}}) \\ 0 & \text{otherwise} \end{cases} \quad . \tag{4.40}$$

4.4.2 Implementation and Extensions

The full Jiles-Atherton model quantifying the magnetization M in terms of the applied field H can be summarized in the following algorithm:

(4.6) $H_\mathrm{e} = H + \alpha M$

(4.30) $M_\mathrm{an}(H_\mathrm{e}) = M_\mathrm{s}\, \mathcal{L}\left(\frac{H_\mathrm{e}}{a}\right)$

(4.37) $M_\mathrm{irr}(H) : \frac{\mathrm{d}M_\mathrm{irr}(H)}{\mathrm{d}H} = \frac{M_\mathrm{an}(H) - M_\mathrm{irr}(H)}{\delta\, k - \alpha(M_\mathrm{an}(H) - M_\mathrm{irr}(H))}$

(4.38) $M_\mathrm{rev}(H) = c\,(M_\mathrm{an}(H) - M_\mathrm{irr}(H))$

(4.28) $M(H) = M_\mathrm{rev}(H) + M_\mathrm{irr}(H)$

Typically the initial values (H_0, M_0) are chosen as the demagnetized state $(0, 0)$, saturation, or remanence points. The five model parameters $(M_\mathrm{s}, \alpha, a, k, c)$ have to be determined from experimental data. Details regarding this identification procedure have been developed in [50] or [58], for example.

A second approach is to combine all model equations to a single ordinary differential equation[7]

$$\frac{\mathrm{d}M(H)}{\mathrm{d}H} = \mathcal{G}(M(H), H) \tag{4.41}$$

with the initial condition

$$M(H_0) = M_0 \quad . \tag{4.42}$$

A detailed formulation of $\mathcal{G}(M(H), H)$ is shown in [76], which is particularly advantageous in the case of control applications.

Extensions to the Scalar Jiles-Atherton Model

In principle the Jiles-Atherton model is not able to guarantee *closure of biased minor loops*, because the irreversible magnetization M_irr is always driven towards the anhysteretic M_an. So Jiles [47] enforced this closure by using a-priori knowledge of the turning points.

For applications where the applied field is parallel to the magnetization, the scalar models can be used with sufficient precision. But whenever the vector relationship between field and magnetization is needed for several predictions of directional dependence, one has to derive a *vector generalization* of the original Jiles-Atherton model, as performed by Bergqvist [7], for example.

[7] More precisely, this hysteresis model is of the so called Duhem type [82] with a relation between magnetization and field in the form of $\frac{\mathrm{d}M(H)}{\mathrm{d}H} = \mathcal{G}(M(H), H, \frac{\mathrm{d}H}{|\mathrm{d}H|})$.

4.5 Other Approaches in Hysteresis Modeling

4.5.1 Stoner-Wohlfarth Model

In 1948 E.C. STONER and E.P. WOHLFARTH [77] proposed a simple model to analyze the magnetic behavior of materials consisting of small particles.

Ellipsoidal Particles: STONER and WOHLFARTH assumed ellipsoidal shaped particles with a uniform magnetization. The magnetocrystalline (uniaxial) easy axis is aligned with the long axis of the ellipsoid and the magnitude of the magnetization is assumed to be constant (equal to the saturation magnetization M_s) and parallel aligned even during rotation. In this case one speaks of *coherent magnetization rotation* as the dominating reversal mechanism. Within the following considerations we take only a planar problem into account, in which φ_M denotes the angle between the magnetization and the easy axis, as shown in Fig. 4.8.

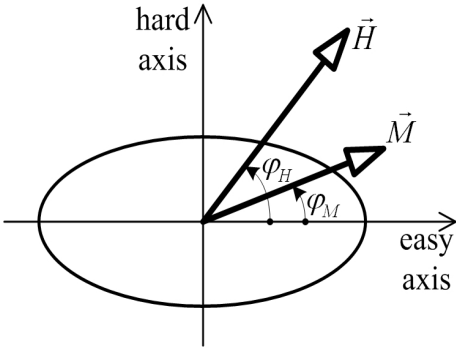

Figure 4.8: Ellipsoidal uniaxial Stoner-Wohlfarth particle with applied field $\vec{H}$.

Energy Considerations: For ellipsoidal single domain particles the exchange energy does not affect the calculations, and the demagnetizing (stray field) energy[8] can be treated as "shape anisotropy" in a generalized anisotropy energy function, which can be written as

$$w_\mathrm{Aniso}(\varphi_M) = K_0 + K_1 \sin^2(\varphi_M) \tag{4.43}$$

in the simplest case. In the view of this planar model an external field $\vec{H}$ is applied with an angle φ_H to the easy axis. Let $\vec{e}_\parallel$ be the direction parallel to the easy axis and $\vec{e}_\perp$ the orthogonal one, then we get the components of the applied field with respect to these directions as

$$H_\parallel = \vec{H} \cdot \vec{e}_\parallel = H\cos(\varphi_H) \quad \text{and} \quad H_\perp = \vec{H} \cdot \vec{e}_\perp = H\sin(\varphi_H) \quad . \tag{4.44}$$

[8] Maxwell derived for a uniformly magnetized general ellipsoid that the demagnetizing field is uniform, too. Hence, in the case of coincident easy axes, uniaxial magnetocrystalline anisotropy and demagnetizing field have same spatial variations and can therefore be combined into a single energy term.

So the total energy density assigned to the so called "Stoner-Wohlfarth particle" can be expressed as a function of the magnetization direction φ_M

$$w_{\mathrm{Tot}}(\varphi_M) = -\mu_0 M_{\mathrm{s}} \left(H_{\parallel} \cos(\varphi_M) + H_{\perp} \sin(\varphi_M) \right) + K_0 + K_1 \sin^2(\varphi_M) \quad . \tag{4.45}$$

In a static stable equilibrium of minimum energy density

$$\frac{\partial w_{\mathrm{Tot}}(\varphi_M)}{\partial \varphi_M} = 0 \quad \text{and} \quad \frac{\partial^2 w_{\mathrm{Tot}}(\varphi_M)}{\partial \varphi_M^2} > 0 \tag{4.46}$$

must be fulfilled. The corresponding stability limit is obviously given by

$$\frac{\partial^2 w_{\mathrm{Tot}}(\varphi_M)}{\partial \varphi_M^2} = 0 \quad , \tag{4.47}$$

which results in the case of the energy function (4.45) to

$$h_{\parallel}^* = -\cos^3(\varphi_M) \quad \text{and} \quad h_{\perp}^* = \sin^3(\varphi_M) \quad . \tag{4.48}$$

Here h denotes the reduced field $h = H\,\mu_0 M_{\mathrm{s}} \,/\, K_1$. The graphical representation of the switching curve (4.48) is depicted in Fig. 4.9 and is known as *Stoner-Wohlfarth astroid*. Within the astroid only reversible coherent magnetization rotation is possible, whereas outside the astroid irreversible switching occurs.

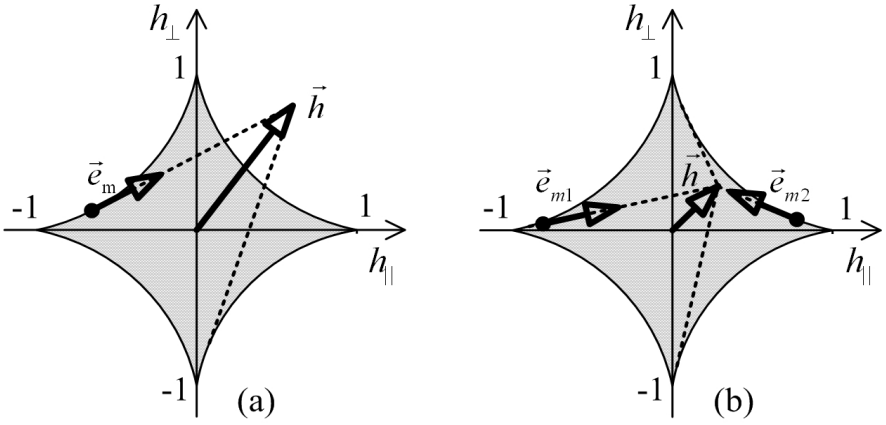

Figure 4.9: Stoner-Wohlfarth astroid with Slonczewski's construction of the equilibrium magnetization direction in the case of one (a) and two stable solutions (b).

Equilibrium Magnetization Orientation: SLONCZEWSKI [75] derived a method which can be used to determine the equilibrium magnetization directions for any applied field. Therefore, the vector of reduced field $\vec{h} = h_{\parallel}\vec{e}_{\parallel} + h_{\perp}\vec{e}_{\perp}$ has to be drawn in the astroid plane. Then, the tangents from the endpoint of the field vector to the astroid line represent the equilibrium magnetization direction.

If the field vector lies inside the astroid, four tangents can be found, where the two stable solutions are those with the smaller angle relative to the easy axis. Which of the both stable solutions is obtained, depends on the history of magnetization.

In the other case, where the field vector lies outside the astroid one obtains exactly one stable solution for the magnetization direction. The second tangent is the direction of the energy maximum.

Stoner-Wohlfarth Calculations: The method explained above can be used to determine hysteresis loops of an isolated particle for arbitrary field directions. STONER and WOHLFARTH [77] calculated the hysteresis loop for an ensemble of such particles with uniaxial anisotropy but with easy axis orientated randomly in space.

4.5.2 Chemical Reaction Hysteresis Model

By comparing electronic transformation of a material's behavior to a chemical reaction A. NOURDINE et al. [68] developed a static hysteresis model in the year 2000.

Chemical Reaction as Pendant to Spin Behavior: At the thermodynamic balance the atoms or molecules in a chemical solution react so that the potential energy becomes minimized. The *activity* $[X]$ of a component X is defined to be proportional to chemical concentration. Assuming that $1/K$ is the constant of a chemical acid-base reaction, for example

$$\text{base} + \text{proton} \longrightarrow \text{acid} \quad ,$$

the thermodynamic balance is reached, if

$$K = \frac{[\text{base}]\,[\text{proton}]}{[\text{acid}]} \tag{4.49}$$

is met. Let $\{X\}$ denote the *quantity* of X, then the corresponding equation of quantity conservation is

$$\{\text{base}\}_{\text{introduced}} = \{\text{acid}\}_{\text{formed}} + \{\text{base}\}_{\text{remaining}} \quad . \tag{4.50}$$

Magnetic Model: In order to hold the formulation as simple as possible, it is assumed that the domain structure of the magnetic material is dominated by 180° Bloch walls with magnetization directions parallel and antiparallel to a prespecified easy axis (see Fig. 4.10).

In analogy to the explained chemical process it is assumed that the magnetic sample consists of positive spins s^+ and negative spins s^-. The "activities" assigned to these spins can be interpreted as relative magnetization of the entire s^+ or s^- contributions, respectively:

$$\left[s^+\right] = \frac{M^+}{M_\mathrm{s}} = m^+ \qquad \left[s^-\right] = \frac{M^-}{M_\mathrm{s}} = m^- \quad . \tag{4.51}$$

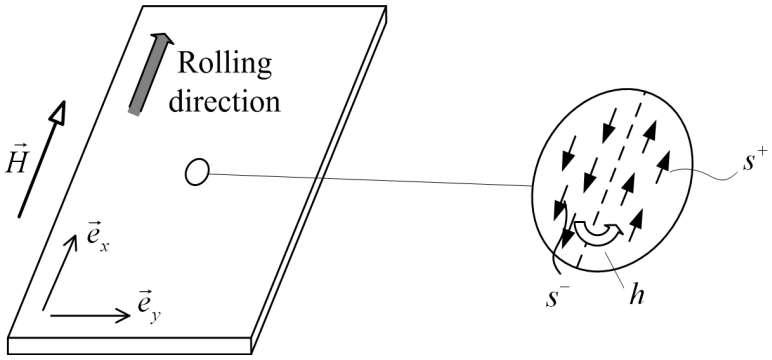

Figure 4.10: Domain wall movement as chemical reaction.

If an increasing external field H is applied in direction of the positive oriented spins, a part h of this external field is needed for the "reaction", formulated as

$$s^- + h \longrightarrow s^+ \quad . \tag{4.52}$$

Furthermore, it is assumed that the "activity" of h varies exponentially with the model parameter β as

$$[h] = \exp(\beta h) \quad , \tag{4.53}$$

yielding in a thermodynamic balance according to (4.49)

$$K = \frac{[s^-]\,[h]}{[s^+]} = \frac{m^-}{m^+} \exp(\beta h) \quad . \tag{4.54}$$

Using another temperature dependent model parameter h_T (with the dimension of magnetic field), the quantities of the magnetic fields are defined via exponential functions as

$$\{h\} = \exp\left(\frac{h}{h_T}\right) \qquad \{H\} = \exp\left(\frac{H}{h_T}\right) \tag{4.55}$$

and the conservation equation (4.50) in terms of magnetic fields is

$$\exp\left(\frac{h}{h_T}\right) = \exp\left(\frac{H}{h_T}\right) + b \quad , \tag{4.56}$$

where b depends on the history of the applied field H. At the field reversal points b is adapted so as to get a continuous hysteresis curve.

One obtains the resulting *magnetization due to spin moment reversal* (domain wall motion) first as

$$M_{\mathrm{spr}} = M_{\mathrm{s}} \left(m^+ - m^-\right) \quad , \tag{4.57}$$

and via the coercive field H_c (which is characterized by $m^+ = m^-$) in consideration of (4.54) one can write

$$K = \exp(\beta H_c) \quad . \tag{4.58}$$

Finally, one estimates $M_{\mathrm{spr}}(H)$ in the case of increasing external fields as

$$M_{\mathrm{spr}}(H) = M_{\mathrm{s}} \tanh\left(\frac{\beta\, h_T}{2} \ln\left(\exp\left(\frac{H}{h_T}\right) + b\right) - \frac{\beta\, H_c}{2}\right) \quad . \tag{4.59}$$

In order to get the total magnetization one has to add a magnetization contribution due to *magnetic moment rotation* $M_{\mathrm{rot}}(H)$, which is specified in detail in [68]

$$M(H) = M_{\mathrm{spr}}(H) + M_{\mathrm{rot}}(H) \quad . \tag{4.60}$$

Thermodynamic Interpretation: Inspired from the thermodynamical calculations for ideal gases, the internal energy, the chemical potential, and the thermodynamic balance of magnetic material is derived in [68] and leads to the same results as mentioned above.

Applications and Extensions: This chemical reaction hysteresis model has been applied to *grain oriented SiFe sheets* in rolling direction as well as in the transverse direction [69]. In the latter case NOURDINE extended the basic version of the model so that one "molecule" (group of corresponding spin moments) with different properties is assigned to each of the magnetocrystalline easy axes.

In [70] the chemical reaction model has been evaluated on *cube textured NiFe sheets*, which also delivers satisfying predictions of the material's magnetic behavior.

Concluding, the advantage of this unusual kind of magnetic modeling is a small set of model parameters, which makes identification process easier and the analytical expression of the magnetization curve allows easy implementation in several algorithms. Unfortunately, this model provides low flexibility and can therefore only be applied to materials with "conventional" magnetization behavior.

4.6 Summary

The fact that all particular aspects of hysteresis cannot be comprehended within one model is reflected by the number of state of the art models. Even though each of the presented models is based on a different scientific framework, all of them have the common objective to explain magnetic hysteresis phenomena. Thus, it depends on the problem to be solved which approach is considered as the most appropriate one. In conclusion, one may approve a magnetic hysteresis model, if it is able to describe several phenomena of ferromagnetic hysteresis with a small but flexible set of parameters. Furthermore, it should be derived in a consistent mathematical or stochastic framework, and its concepts as well as its parameters should allow a physically correct interpretation.

Chapter 5

Generalized Two-Dimensional Energetic Model

This chapter specifies the generalized two-dimensional "Energetic Model of Ferromagnetic Hysteresis", which should be referred to as "Energetic Model" (EM) in further discussion. Whenever a clear differentiation between the existing model formulation and the extensions discussed within this thesis are essential, the denotation of "Classical EM" and "Generalized EM" will be used.

Classical Energetic Model: The original approach developed and published by H. HAUSER [34] in 1994 is based on energy considerations and statistic domain behavior. Inspired by previous work of D.C. JILES and D.L. ATHERTON [49] reversible and irreversible contributions to total energy density are included. During the following years, the research on this model has been progressing, see e.g. [3, 23–26, 29, 35–39] to get an overview.

Most of these investigations have been done by employing a scalar formulation of the EM, because the solution of the corresponding model equations can be done analytically. But even in the case of three-dimensional crystal structures the EM has been set up for certain crystalline axes in consideration of symmetry properties. The original EM from 1994 and the following investigations based on that formulation will be referred to as *Classical Energetic Model* in order to distinguish from the generalized formulation.

Generalized Energetic Model: In order to describe the anisotropic magnetic behavior of thin film material a fully two-dimensional (2D) framework of the EM is required. For this reason, a generalization of the Classical Energetic Model is presented within the following sections. It is exactly this extension of the EM that builds the fundamental core of the thesis.

5.1 Generalized Formulation of the Model

From a generic point of view the Energetic Model may be categorized as mesoscopic magnetic model. On the one hand, it describes local microscopic energy terms, such as anisotropy or applied field energy, and macroscopic phenomenological aspects are applied to complete the model, on the other hand. In this context, the magnetic sample is considered as collection of *elementary magnetic entities*, which can be grouped into several *statistical domain classes*. These statistical domain classes can be seen as a topological generalization of real magnetic domains observed by common techniques.

5.1.1 Elementary Magnetic Entities

Since beginning of the investigation of magnetic materials there is evidence to regard magnetic matter as collection of elementary magnetic entities. In 1820 AMPERE proposed the hypothesis that magnetism is caused by circulating electrical currents on a molecular level. Nowadays the origin of magnetism is treated within the framework of quantum-mechanics. However, there are several arguments motivating the assumption of magnetic entities:

- *Magnetic saturation* is achieved, if all entities are oriented in the same direction.
- *Interaction* between these magnetic entities is used to describe "strong" magnetism, like ferromagnetism.
- Due to the inability in separating magnetic monopoles there is evidence to suggest dipole characterized magnetic entities containing an intrinsic magnetic moment.

Within the scope of this work a *magnetic entity* $\mathcal{E}$ is considered as basic element of magnetic moment of a magnetic sample $\mathcal{V}$, as depicted in Fig. 5.1. In this point of view, the concrete physical nature of these entities depends on the problem to be modeled. So atomic magnetic moments resulting from orbital and spin motion of electrons, magnetic inclusions in a non-magnetic matrix, or crystallites in poly-crystalline materials may act as magnetic entities.

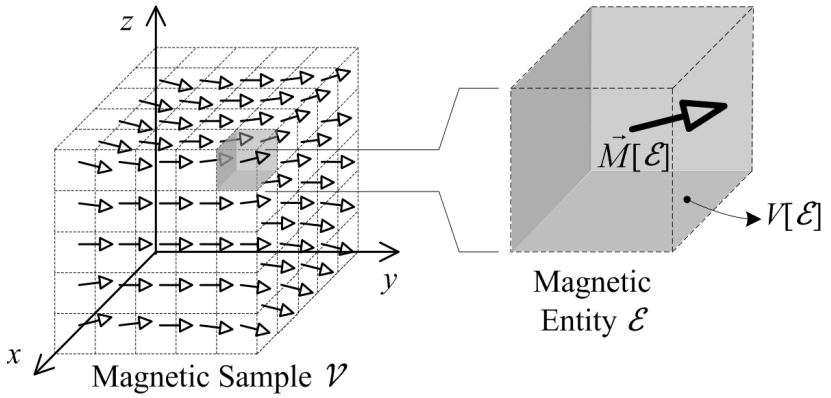

Figure 5.1: Magnetic entity as basic element of magnetic moment.

By all means, one is able to assign several properties to each magnetic entity (Fig. 5.2):
-) position is space (given by a position vector) $\vec{r}[\mathcal{E}]$,
-) volume fraction $V[\mathcal{E}]$, and
-) magnetic moment $\vec{\mathfrak{m}}[\mathcal{E}]$ or magnetization $\vec{M}[\mathcal{E}]$ respectively.

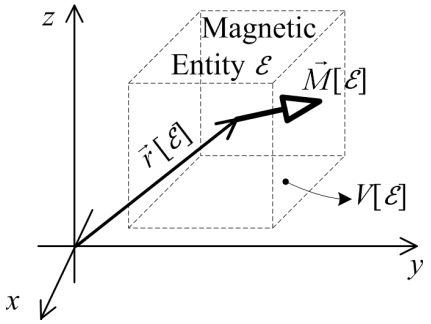

Figure 5.2: General properties of a magnetic entity.

Properties of Magnetic Entities in the Context of the EM

Let us consider a representative ferromagnetic sample of total volume V consisting of $n_{\mathcal{V}}$ elementary *magnetic entities* $\mathcal{E}_k$ that are assumed to be all of the same, constant volume

$$V[\mathcal{E}_k] = \frac{V}{n_{\mathcal{V}}} \qquad \forall\, k = 1...n_{\mathcal{V}} \quad , \tag{5.1}$$

resulting in a volume fraction with respect to the total sample volume V

$$v[\mathcal{E}_k] = \frac{V[\mathcal{E}_k]}{V} = \frac{1}{n_{\mathcal{V}}} \qquad \forall\, k = 1...n_{\mathcal{V}} \quad . \tag{5.2}$$

In the framework of the EM magnetic entities are handled by means of statistics, so the information about the position in space of a single entity $\vec{r}[\mathcal{E}_k]$ gets lost. From a topological point of view, each magnetic entity $\mathcal{E}_k$ is considered as an element of the total set of entities $\mathcal{V}$ within the sample

$$\mathcal{E}_k \in \mathcal{V} \qquad \forall\, k = 1...n_{\mathcal{V}} \quad . \tag{5.3}$$

Each entity's magnetization has the same amplitude according to the spontaneous magnetization M_s, but a different direction $\vec{m}[\mathcal{E}_k]$ in space

$$\vec{M}[\mathcal{E}_k] = M_\mathrm{s}\, \vec{m}[\mathcal{E}_k] \qquad \forall\, k = 1...n_{\mathcal{V}} \quad . \tag{5.4}$$

Ignoring special cases where M_s varies inside the material, $\vec{m}[\mathcal{E}_k]$ can be regarded as vector field of magnetization direction with $\vec{m}^2[\mathcal{E}_k] = 1$.

5.1.2 Aggregation of Magnetic Entities to Statistical Domain Classes

Generally, it is extremely intricate to describe the behavior of individual magnetic entities in a ferromagnetic body. So if one is interested in effects taking place on a coarse scale compared to the size of the magnetic entities, it necessitates a more simplified treatment. According to requirements different types of aggregation are used. Before going into detail the following terms related to this topic should be distinguished.

Magnetic Domains, Statistical Domains, and Statistical Domain Classes

As described in section 3.2, a *magnetic domain* can be explained as a connected set (region) of aligned magnetic entities within a ferromagnetic material, which act together in a coordinated manner.

FASCHING [20] extended this classical domain formulation by the proposition of *statistical domains*, which he defined as fictive volume-invariant region of uniform (directed) magnetization. In principle, these statistical domains are comparable with the magnetic entities mentioned above, so that the total sample volume is split up into n statistical domains equal in size. All n_i statistical domains having identical magnetization direction $\vec{e}_i$ (corresponding to the material's easy axes) are combined to the so-called i-th *magnetic phase* of the sample. The phrase "statistical" refers to FASCHING's probabilistic approach, which will be discussed in more detail in section 5.2.1.
In contrast to (real) magnetic domains magnetic phases need not build a connected region in space. Instead, the latter can be spread over different regions within the sample, only their total fraction is of importance. Inspired by the FASCHING's concept of magnetic phases, the classical formulation of the EM is also based on statistical domains.

But in real materials a perfect alignment of the magnetic moments within a domain is rarely the case. To be more authentic and more flexible in modeling, so called domain classes are defined. Generally speaking, a *domain class* is a topological collection of elementary magnetic entities that share a common set of well-defined properties or characteristics. Due to the fact that the properties of individual entities are aggregated via statistical techniques, the term *statistical domain class* is used. The magnetic entities assigned to such a (statistical) domain class are oriented according to a common statistical distribution function.

Statistical Domain Classes in the EM

Within a ferromagnetic sample the total set of magnetic entities $\mathcal{V}$ is subdivided into a finite number $N_{\mathcal{D}}$ of subsets $\mathcal{D}_i$, called *statistical domain classes*

$$\mathcal{D}_i \subseteq \mathcal{V} \quad \text{with} \quad \bigcup_{i=1}^{N_{\mathcal{D}}} \mathcal{D}_i = \mathcal{V} \quad \text{and} \quad \mathcal{D}_i \cap \mathcal{D}_j = \emptyset \text{ for } i \neq j \quad . \tag{5.5}$$

Pursuant to the domain classes one can define a set of indices $k^{(i)}$

$$k^{(i)} = \{k \in \{1, \ldots, n_{\mathcal{V}}\} \,|\mathcal{E}_k \in \mathcal{D}_i\} \quad \text{or} \quad \bigcup_{k \in k^{(i)}} \mathcal{E}_k = \mathcal{D}_i \quad , \tag{5.6}$$

which assign magnetic entities to the domain classes. In order to shorten the notation we write $\mathcal{E}^{(i)}$ for a representative[1] entity of domain class $\mathcal{D}_i$.

Assuming a substantial number of magnetic entities per domain class, we describe the entities' *directional behavior* in terms of probability density functions. In the context of a spherical coordinate system with the azimuth φ and the elevation θ the distribution of magnetization directions in domain class $\mathcal{D}_i$ is modeled via a bivariate probability density function $f_i(\varphi, \theta)$ for general 3D problems. Thus, $f_i(\varphi, \theta)\,\mathrm{d}\varphi\,\mathrm{d}\theta$ is the probability to find a magnetic entity in the i-th domain class with magnetization orientation in the range $[(\varphi, \theta); (\varphi + \mathrm{d}\varphi, \theta + \mathrm{d}\theta)]$.

For thin film material and in-plane magnetization[2] it is sufficient to deal with a 2D formulation of the model, where the magnetization direction is described by the polar angle φ relative to the x-axis. Therefore, one can use univariate probability density functions $f_i(\varphi)$ to define the directional distribution in domain class $\mathcal{D}_i$. In the following we restrict our discussions to these two-dimensional problems, but most of the results can be generalized to the 3D case without elementary changes.

As depicted in Fig. 5.3, the direction of magnetization in the domain class $\mathcal{D}_i$ is represented by the stochastic (continuous) random variable Φ_i, which is dedicated to a circular probability density function $\Phi_i \sim f_i(\varphi)$. Consequently, the angle φ is bounded to the interval $(-\pi; \pi]$ to ensure unique directions, and the circular probability density functions have to fulfill the standardization condition

$$\int_{-\pi}^{\pi} f_i(\varphi)\,\mathrm{d}\varphi = 1 \quad . \tag{5.7}$$

Finally, the *directional distribution* $f(\varphi)$ *of all magnetic entities* within the ferromagnetic sample is a weighted sum of the domain class contributions

$$f(\varphi) = \sum_{i=1}^{N_{\mathcal{D}}} v_i\, f_i(\varphi) \quad , \tag{5.8}$$

where the weights v_i are corresponding to the volume fractions of the domain classes

$$v_i = v(\mathcal{D}_i) = v\Big(\bigcup_{k \in k^{(i)}} \mathcal{E}_k\Big) = \sum_{k \in k^{(i)}} v(\mathcal{E}_k) = \frac{n_{\mathcal{D}_i}}{n_{\mathcal{V}}} \quad . \tag{5.9}$$

$n_{\mathcal{D}_i}$ denotes the number of magnetic entities belonging to domain class $\mathcal{D}_i$. Hence the boundary conditions result as

$$\sum_{i=1}^{N_{\mathcal{D}}} v_i = 1 \qquad \text{and} \qquad \sum_{i=1}^{N_{\mathcal{D}}} n_{\mathcal{D}_i} = n_{\mathcal{V}} \quad . \tag{5.10}$$

[1] Since the magnetic entities are assumed to be indistinguishable, it makes sense to focus on "representative" entities.

[2] Particularly this applies to thin Permalloy films, which are investigated in the following part of this work.

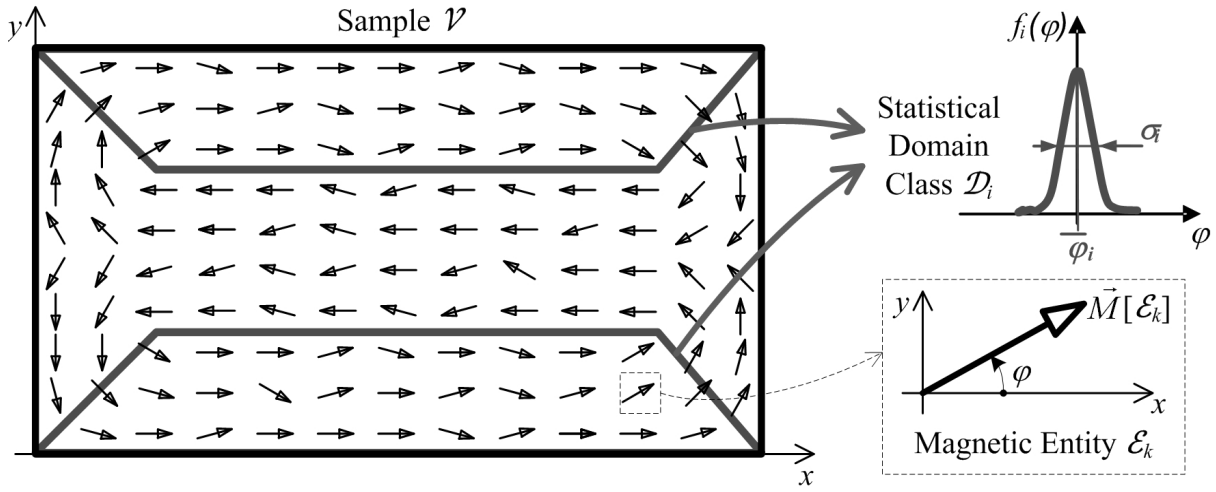

Figure 5.3: Concept of statistical domain classes in the EM.

Conclusion

Magnetic entities are defined as basic elements of magnetic moment in a ferromagnetic sample. In principle, all magnetic entities are assumed to have the same absolute value of the spontaneous magnetization, but they have different orientation in space. Since this thesis deals with the characterization of the magnetization process in thin film materials with in-plane anisotropy, a two-dimensional model setup is required. Within this 2D framework, the orientation of the magnetic entities' magnetization is represented by the polar angle φ with respect to an arbitrary chosen x-axis.

In the framework of the EM, interactions between magnetic entities are considered by grouping them into statistical domain classes. The precise position of the magnetic entities is not of relevance in the context of the EM. Instead, only probabilities for the orientation of the entities' magnetic moments are given. Hence, a statistical domain class $\mathcal{D}_i$ is defined by its volume fraction v_i and the probability distribution for the orientation of its magnetic entities $f_i(\varphi)$.

As a next step, an adequate probability distribution has to be chosen in order to describe the alignment of the magnetic entities in the domain class.

5.1.3 Basic Distributions of Magnetic Entities within a Domain Class

According to the results of domain observation techniques and micromagnetic calculations one is able to deduce basic distributions of the magnetic entities in certain predefined domain classes. For this purpose we define Φ_i as *stochastic random variable* for the angle of magnetic moments with respect to the x-axis. The corresponding probability density functions $f_i(\varphi)$ are shown in Fig. 5.4 and described in the following paragraphs.

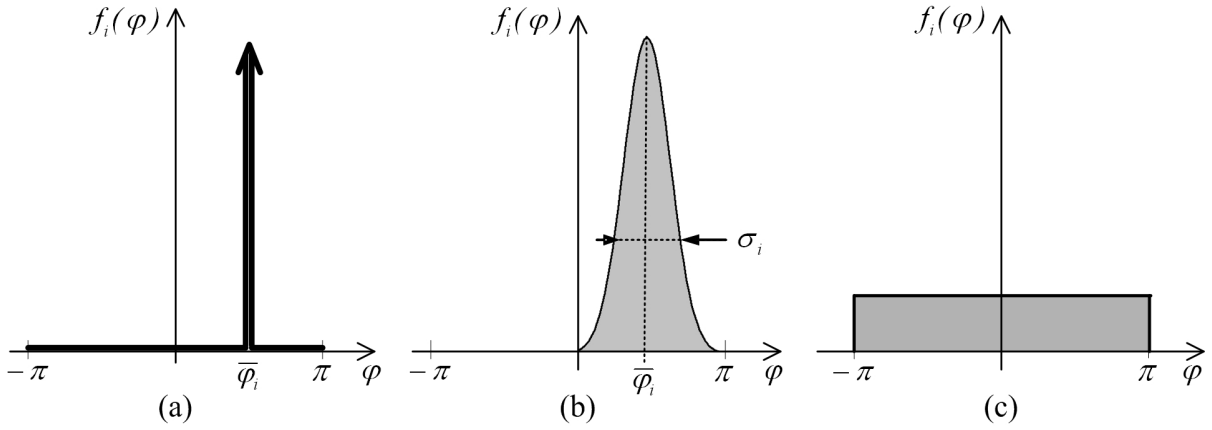

Figure 5.4: Probability density function $f_i(\varphi)$ for perfect alignment (a), wrapped normal distribution $\mathrm{WN}(\bar{\varphi}_i, \sigma_i^2)$ (b), and circular uniform distribution $\mathrm{CU}(-\pi, \pi)$ (c).

Perfect Alignment

In an idealized case all magnetic entities of domain class $\mathcal{D}_i$ point in a unique direction, so that the probability distribution degenerates to determinism. For the considered 2D problems all the magnetic moments belonging to the i-th domain class have an angle

$$\Phi_i = \bar{\varphi}_i \tag{5.11}$$

with respect to the x-axis.

This corresponds to the classical formulation of the EM.

Circular Uniform Distribution

Contrary to this unique orientation one may consider a totally random directional distribution of entities' magnetic moments, resulting in a *circular uniform distribution* $\mathrm{CU}(-\pi, \pi)$ of magnetic moments

$$\Phi_i \sim \mathrm{CU}(-\pi, \pi) \quad \text{or} \quad f_i(\varphi) = \frac{1}{2\pi} \quad \text{for } -\pi < \varphi \leq \pi \quad . \tag{5.12}$$

Paramagnetic materials in demagnetized state or vortex domains would be practical examples for this case.

Wrapped Normal Distribution

For most of the ferromagnetic materials the magnetic entities within a domain class $\mathcal{D}_i$ are aligned according to a main direction $\bar{\varphi}_i$. But due to boundaries, inhomogeneities, and thermal agitation some entities' magnetic moments deviate from this common direction. A simple way to model this behavior is the general assumption of a *wrapped normal distribution* $\mathrm{WN}(\bar{\varphi}_i, \sigma_i^2)$ for the random angle Φ_i

$$\Phi_i \sim \mathrm{WN}(\bar{\varphi}_i, \sigma_i^2) \quad \text{or} \quad f_i(\varphi) = \sum_{k \in \mathbb{Z}} f_i^{\phi}(\phi = \varphi + 2\pi k) \quad , \tag{5.13}$$

by wrapping the linear normal distribution

$$f_i^{\phi}(\phi) = \frac{1}{\sqrt{2\pi}\sigma_i} \exp\left(-\frac{1}{2} \frac{(\phi - \bar{\varphi}_i)^2}{\sigma_i^2} \right) \tag{5.14}$$

around the circle, as shown in Fig. 5.5. Within this context $\bar{\varphi}_i \in (-\pi; \pi]$ denotes the mean direction and $\sigma_i \geq 0$ the standard deviation for the angular distribution of magnetic entities in domain class $\mathcal{D}_i$.

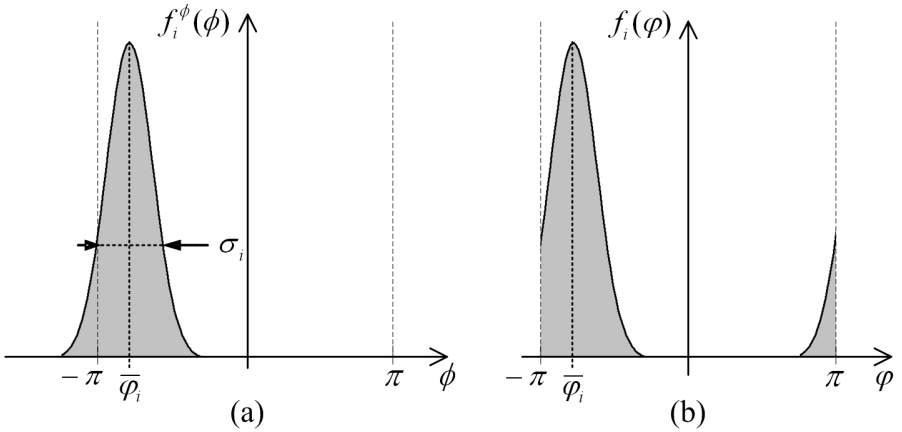

Figure 5.5: Densitiy functions of linear normal distribution (a), and wrapped normal distribution (b).

In consideration of the limiting values for the variance σ_i^2 one obtains convergence to

- perfect alignment as $\Phi_i = \bar{\varphi}_i$ for $\sigma_i^2 \to 0$, or
- a circular uniform distribution $\Phi_i \sim \mathrm{CU}(-\pi, \pi)$ by approximating $\sigma_i^2 \to \infty$.

In principle, the *circular normal (von Mises) distribution* $\mathrm{CN}(\bar{\varphi}_i, \beta_i)$

$$\Phi_i \sim \mathrm{CN}(\bar{\varphi}_i, \beta_i) \quad \text{or} \quad f_i(\varphi) = \frac{1}{2\pi\, I_0\left(\beta_i\right)} \exp\left(\beta_i \cos\left(\varphi - \bar{\varphi}_i\right)\right) \quad , \tag{5.15}$$

with β_i as measure of concentration and the modified Bessel function (of 1st kind, order 0)

$$I_0(\beta_i) = \frac{1}{2\pi} \int_{-\pi}^{\pi} \exp(\beta_i \cos(\varphi)) \, \mathrm{d}\varphi \tag{5.16}$$

as normalization constant, would also provide an applicable description for the angular distribution of the magnetic entities. Although the circular normal and the wrapped normal distribution are quite similar in shape, the latter leads to an algebraic formulation.

Interpretation of the Variance

As mentioned before, the variance σ_i^2 describes the degree of order within a domain class $\mathcal{D}_i$. It is influenced by ordering forces (like magnetic fields, or interactions leading to exchange energy) on the one hand, and disordering factors (such as thermal excitations, or material inhomogeneities) on the other hand.

In the following paragraphs an empirical approach is used to determine an expression for the variance.

First, we have to assume that the main orientation $\bar{\varphi}_i$ of the considered domain class $\mathcal{D}_i$ is a-priori known, as the result of a macroscopic analysis, for example. Thus, the "mesoscopic order", which is represented by σ_i^2 is always regarded with respect to this main orientation $\bar{\varphi}_i$. So the *ordering energy term* of a representative magnetic entity $\mathcal{E}^{(i)}$ in domain class $\mathcal{D}_i$ can be assumed[3] as

$$W_{\mathrm{Order}}[\mathcal{E}^{(i)}] = -W_{\mathrm{Order},i} \cos(\varphi - \bar{\varphi}_i) \quad , \tag{5.17}$$

where the continuous valued angle φ characterizes the state of $\mathcal{E}^{(i)}$. In contrast to the ordering forces the *disordering energy term* does not depend on the state of the magnetic entity

$$W_{\mathrm{Disorder}}[\mathcal{E}^{(i)}] = W_{\mathrm{Disorder},i} \quad , \tag{5.18}$$

like any kind of inhomogeneities within the domain class.

Accordingly, the classical *Boltzmann weight* can be written as

$$\exp\left(-\frac{W_{\mathrm{Order}}[\mathcal{E}^{(i)}]}{W_{\mathrm{Disorder}}[\mathcal{E}^{(i)}]}\right) = \exp\left(\frac{W_{\mathrm{Order},i}}{W_{\mathrm{Disorder},i}} \cos(\varphi - \bar{\varphi}_i)\right) \tag{5.19a}$$

$$= \exp(\beta_i \cos(\varphi - \bar{\varphi}_i)) \quad , \tag{5.19b}$$

where β_i characterizes the ratio between ordering and disordering energies within the domain class. Now the probability (density) to find a magnetic entity oriented in angular interval $[\varphi; \varphi + \mathrm{d}\varphi]$ yields by standardization of (5.19)

$$f_{\mathrm{Boltzm}}(\varphi)\,\mathrm{d}\varphi = \frac{\exp(\beta_i \cos(\varphi - \bar{\varphi}_i)) \, \mathrm{d}\varphi}{\int_{-\pi}^{\pi} \exp(\beta_i \cos(\varphi\prime - \bar{\varphi}_i)) \, \mathrm{d}\varphi\prime} \qquad \text{for } \varphi \in (-\pi; \pi] \quad . \tag{5.20}$$

[3]Imagine a kind of exchange energy between the magnetic moment of entity $\mathcal{E}^{(i)}$ and a "mean field" caused by the remaining entities within the domain.

Empirical analysis (Fig. 5.6) show that this Boltzmann distribution is compared to the normal distribution quite similar in shape. Without further reasoning one can find a relation between β_i and the variance σ_i^2 of the normal distribution given by

$$\sigma_i^2 = \ln\left(1+\frac{2}{\beta_i}\right)\frac{2}{1+3\exp\left(-\frac{2}{\beta_i}\right)} \quad . \tag{5.21}$$

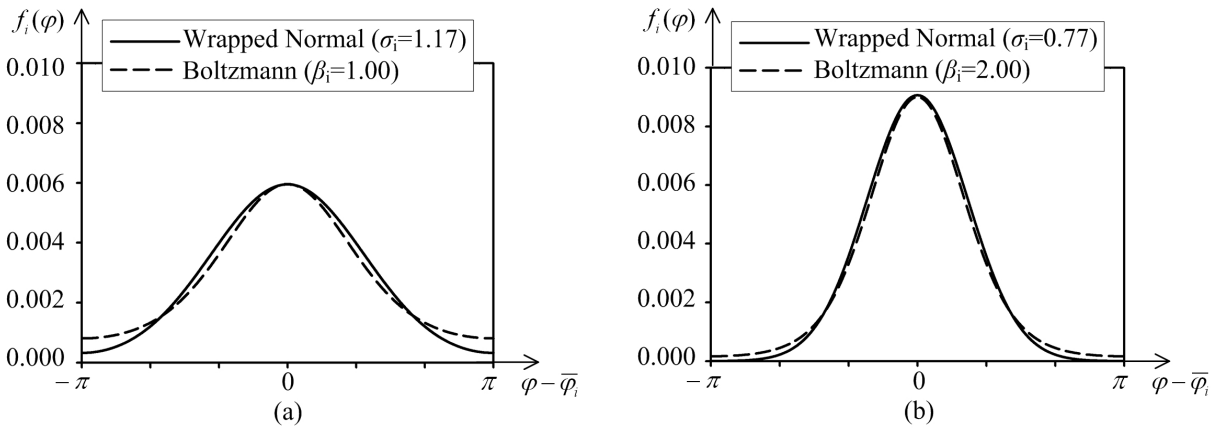

Figure 5.6: Comparison of probability density functions for wrapped normal and Boltzmann distribution for $\beta_i = 1$ (a), and $\beta_i = 2$ (b).

If we assume a *high degree of alignment* of the magnetic moments within the domain class, which is characterized by a small variation from the main direction $\bar{\varphi}_i$, the cosine dependence of the energy contributions can be approximated by the first terms of the series expansion

$$\cos\left(\varphi-\bar{\varphi}_i\right) \approx 1-\frac{\left(\varphi-\bar{\varphi}_i\right)^2}{2} \quad \text{for } \varphi-\bar{\varphi}_i \ll 1 \quad .$$

Hence, the Boltzmann probability density (5.20) approximates the normal distribution

$$f_{\text{Boltzm}}(\varphi) \propto \exp\left(-\beta_i\frac{\left(\varphi-\bar{\varphi}_i\right)^2}{2}\right)$$

and the variance can be directly assigned as

$$\sigma_i^2 = \frac{1}{\beta_i} = \frac{W_{\text{Disorder},i}}{W_{\text{Order},i}} \quad . \tag{5.22}$$

The same result can also be obtained by a series expansion of (5.21) at the point $\beta_i \to \infty$

$$\sigma_i^2 \approx \frac{1}{2}\left(\frac{2}{\beta_i}\right)+\frac{1}{8}\left(\frac{2}{\beta_i}\right)^2+\frac{7}{96}\left(\frac{2}{\beta_i}\right)^3+\ldots \quad . \tag{5.23}$$

However, depending on the problem and the microstructural properties of the material, if it is possible to find algebraic expressions for the ordering and disordering energies, the variances σ_i^2 can be estimated endogenously in the EM dependent on field, temperature, or other quantities of interest. Alternatively, the variances can be treated as exogenous model parameters.

Conclusion

By applying a certain probability density function, the angular distribution of the magnetization of the magnetic entities within a domain class can be quantified in terms of numerical parameters. In case of the normal distribution we are able to describe the magnetic behavior within a domain class by only two parameters. The mean orientation $\bar{\varphi}_i$ can be obtained by macroscopic (energetic) considerations. In contrast, the variance σ_i^2 represents a kind of mesoscopic order within the domain class. In the limiting cases $\sigma_i^2 = 0$ and $\sigma_i^2 \to \infty$ one is able to model total alignment on the one hand, and random distribution of magnetic entities' magnetization on the other hand. But, in general, this mesoscopic order is determined as a consequence of concurrent ordering (exchange interactions) and disordering (thermal agitation, material inhomogeneities) energy terms.

5.1.4 Total Macroscopic Magnetization

On assumption (5.4) that each magnetic entity $\mathcal{E}_k$ is magnetized with the spontaneous magnetization M_s, one obtains the components with respect to the x-axis and y-axis

$$M_x[\mathcal{E}_k] = \vec{M}[\mathcal{E}_k] \cdot \vec{e}_x = M_\mathrm{s} \cos\left(\varphi[\mathcal{E}_k]\right) \quad , \tag{5.24}$$

$$M_y[\mathcal{E}_k] = \vec{M}[\mathcal{E}_k] \cdot \vec{e}_y = M_\mathrm{s} \sin\left(\varphi[\mathcal{E}_k]\right) \quad . \tag{5.25}$$

Hence, the respective magnetization components of the entire sample $\mathcal{V}$ result as

$$M_x[\mathcal{V}] = \sum_{k=1}^{n_\mathcal{V}} M_x[\mathcal{E}_k] = M_\mathrm{s} \sum_{k=1}^{n_\mathcal{V}} \cos\left(\varphi[\mathcal{E}_k]\right) \quad , \tag{5.26}$$

$$M_y[\mathcal{V}] = \sum_{k=1}^{n_\mathcal{V}} M_y[\mathcal{E}_k] = M_\mathrm{s} \sum_{k=1}^{n_\mathcal{V}} \sin\left(\varphi[\mathcal{E}_k]\right) \quad . \tag{5.27}$$

The magnetization angle $\varphi[\mathcal{E}_k]$ of the magnetic entities is represented by the random variable $\Phi \sim f(\varphi)$, which is distributed according to the probability density function (5.8). So the expectation value for the magnetization components can be estimated via

$$\begin{aligned} M_x &= \mathbb{E}\left(M_x[\mathcal{V}]\right) \qquad (5.28)\\ &= \mathbb{E}\left(M_\mathrm{s} \cos\left(\Phi\right)\right) \\ &= \int_{-\pi}^{\pi} M_\mathrm{s} \cos\left(\varphi\right)\ f(\varphi)\,\mathrm{d}\varphi \\ &= M_\mathrm{s} \sum_{i=1}^{N_\mathcal{D}} v_i \int_{-\pi}^{\pi} \cos\left(\varphi\right)\ f_i(\varphi)\,\mathrm{d}\varphi \\ &= M_\mathrm{s} \sum_{i=1}^{N_\mathcal{D}} v_i\, m_{i,x} \quad , \qquad (5.29) \end{aligned}$$

where $m_{i,x}$ is the expected (averaged) magnetization component of domain class $\mathcal{D}_i$ with respect to the x-axis. In analogy to (5.29) the corresponding y-component can be derived

$$M_y = M_\mathrm{s} \sum_{i=1}^{N_\mathcal{D}} v_i\, m_{i,y} \quad , \tag{5.30}$$

with

$$m_{i,y} = \int_{-\pi}^{\pi} \sin(\varphi)\ f_i(\varphi)\,\mathrm{d}\varphi \quad . \tag{5.31}$$

In the case of a wrapped normal distribution $f_i(\varphi) \sim \mathrm{WN}(\bar{\varphi}_i, \sigma_i^2)$ it can be shown (appendix A.1) that

$$m_{i,x} = \exp\left(-\frac{\sigma_i^2}{2}\right)\cos(\bar{\varphi}_i) \quad \text{and} \quad m_{i,y} = \exp\left(-\frac{\sigma_i^2}{2}\right)\sin(\bar{\varphi}_i) \tag{5.32}$$

is valid. Table 5.1 summarizes the results for the basic distributions of domain class magnetization, and Fig. 5.7 illustrates the calculation procedure.

	σ_i^2	$\lvert\vec{m}_i\rvert$	$\arg(\vec{m}_i)$	$m_{i,x}$	$m_{i,y}$
aligned	0	1	$\bar{\varphi}_i$	$\cos(\bar{\varphi}_i)$	$\sin(\bar{\varphi}_i)$
$\mathrm{CU}(-\pi,\pi)$	∞	0	undef.	0	0
$\mathrm{WN}(\bar{\varphi}_i,\sigma_i^2)$	$\in(0;\infty)$	$\exp\left(-\frac{\sigma_i^2}{2}\right)$	$\bar{\varphi}_i$	$\exp\left(-\frac{\sigma_i^2}{2}\right)\cos(\bar{\varphi}_i)$	$\exp\left(-\frac{\sigma_i^2}{2}\right)\sin(\bar{\varphi}_i)$

Table 5.1: Domain class magnetization for different directional distributions of magnetic entities.

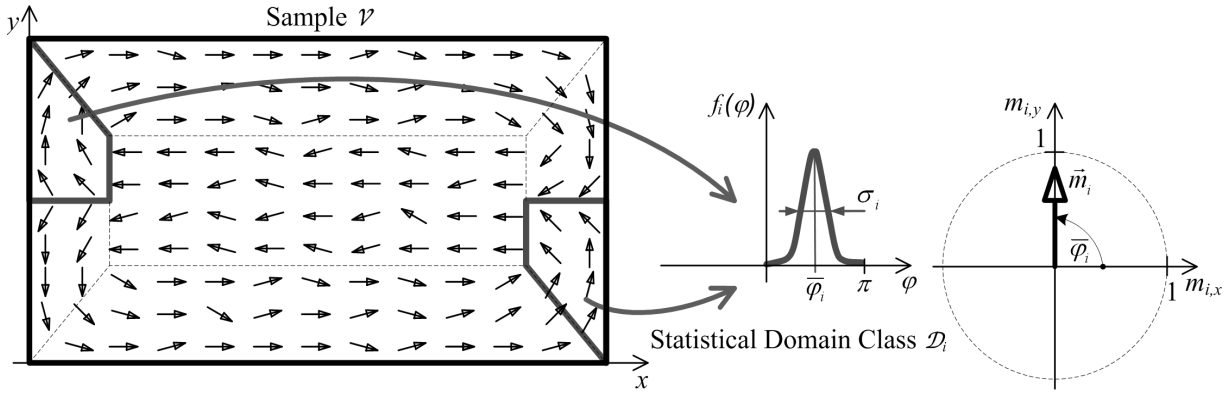

Figure 5.7: Example for estimating the average magnetization for a certain statistical domain class $\mathcal{D}_i$.

Finally, the total magnetization of the entire sample is (Fig. 5.8)

$$\left|\vec{M}\right| = M_\mathrm{s}\sqrt{\left(\sum_{i=1}^{N_\mathcal{D}} v_i\, m_{i,x}\right)^2 + \left(\sum_{i=1}^{N_\mathcal{D}} v_i\, m_{i,y}\right)^2} \tag{5.33}$$

and

$$\arg\left(\vec{M}\right) = \arctan\left(\frac{\sum_{i=1}^{N_\mathcal{D}} v_i\, m_{i,y}}{\sum_{i=1}^{N_\mathcal{D}} v_i\, m_{i,x}}\right) \quad . \tag{5.34}$$

Magnetization in the Direction of the Applied Field

In general, one is interested in the component M_H of magnetization in the direction φ_H of the applied field $\vec{H}$, which is analogously given by

$$M_\mathrm{H} = M_\mathrm{s} \sum_{i=1}^{N_\mathcal{D}} v_i \, m_{i,\mathrm{H}} \quad , \tag{5.35}$$

with

$$m_{i,\mathrm{H}} = \int_{-\pi}^{\pi} \cos\left(\varphi - \varphi_\mathrm{H}\right) \, f_i(\varphi) \, \mathrm{d}\varphi = \exp\left(-\frac{\sigma_i^2}{2}\right) \cos\left(\bar{\varphi}_i - \varphi_\mathrm{H}\right) \quad . \tag{5.36}$$

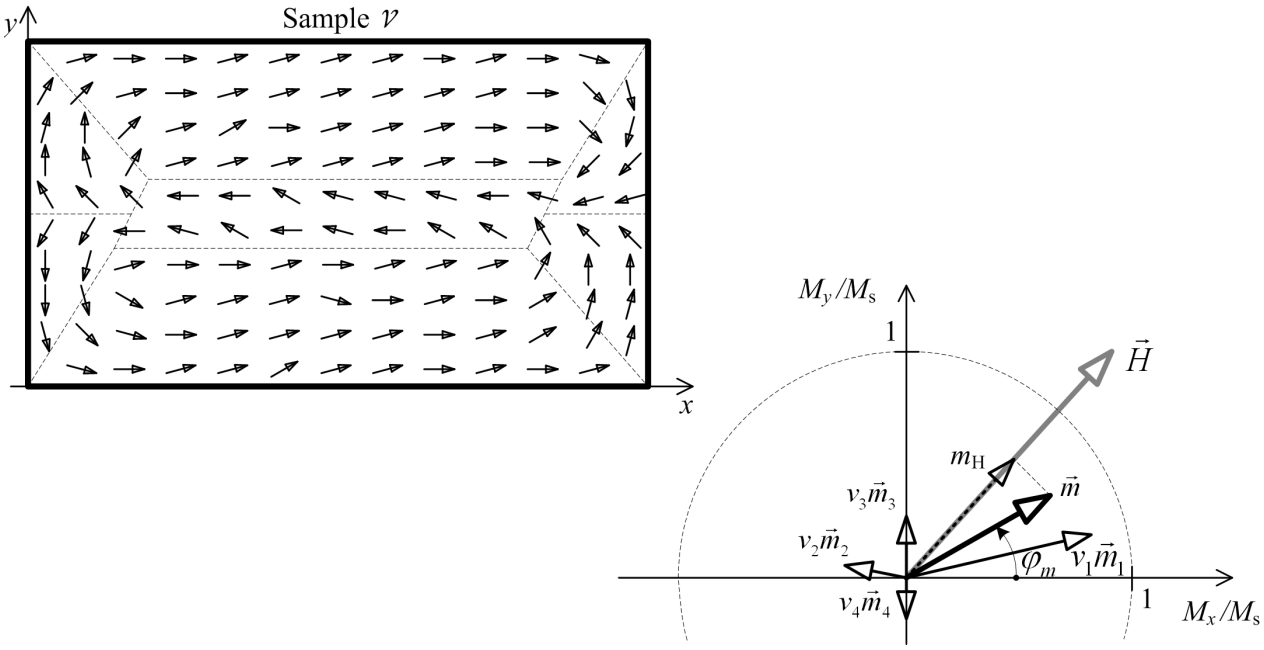

Figure 5.8: Total sample magnetization as weighted sum of domain class magnetization.

Conclusion

The relative magnetization $\vec{m}_i$ of an individual domain class $\mathcal{D}_i$ depends on the parameters $\bar{\varphi}_i$ and σ_i^2 of the corresponding probability distribution. Then, the total sample magnetization $\vec{m}$ results as the volume weighted (v_i) sum of the domain class magnetization vectors $\vec{m}_i$.

So the very basic objective of the generalized EM is to determine the volume fractions v_i and directions $\bar{\varphi}_i$ in order to calculate the magnetization curve $M_\mathrm{H}(\vec{H})$ with respect to the applied field $\vec{H}$. Therefore, a macroscopic energetic framework is needed, which is described in the following section.

5.2 Energetic Framework of the Model

5.2.1 General Aspects and Historical Review

Heisenberg's Fundamental Work (1931)

In his paper [40] HEISENBERG presented a description of magnetostriction in ferromagnetic single crystals with cubic crystal structure. At that time WEISS' theory of ferromagnetism provided a particularly suitable description for the magnetization process near saturation, especially for the temperature dependence of magnetization. But for magnetic fields below saturation magnetic interaction terms have to be considered. In a two-dimensional context HEISENBERG used the total free energy

$$\begin{aligned} F &= \text{WeissCorrection}(M) + \text{AnisotropyEnergy}(M_y^2) + \\ &\quad + \text{FieldEnergy}(\vec{M}, \vec{H}) + \text{DemagnetizingEnergy}(M^2) \end{aligned}$$

to estimate the magnetization $\vec{M} = \binom{M_x}{M_y}$ by minimization of this expression. Thereby "WeissCorrection" is a function, which is nearly constant below saturation and increases significantly when magnetization approaches saturation. Stating that n_1 regions are magnetized along the x-axis (which is the [100]-direction, for example), n_3 regions anti-parallel, and n_2 regions are magnetized along the remaining four crystal axes, the probability for a certain distribution (n_1, n_2, n_3) is defined as

$$P(n_1, n_2, n_3) = \frac{(n_1 + n_2 + n_3)!}{n_1!\, n_2!\, n_3!} \left(\frac{1}{6}\right)^{n_1} \left(\frac{4}{6}\right)^{n_2} \left(\frac{1}{6}\right)^{n_3} \quad .$$

Solving the optimization problem

$$\max_{n_1,n_2,n_3} \{P(n_1, n_2, n_3)\} \qquad \text{s.t.} \quad n_1 + n_2 + n_3 = n \quad \text{and} \quad n_1 - n_3 = n\frac{M}{M_\text{s}}$$

delivers the size of the three regions for a given magnetization M. The total change in length with respect to the x-axis due to magnetostriction consists of a longitudinal part (determined by n_1 and n_3) and a transversal part (n_2).

Finally, it is mentioned that the expansion of a preferred region n_i increases free energy as a consequence of an entropy reduction.

Survey of Brown's Approach (1937)

Based on HEISENBERG's statistical domain theory BROWN [11] presented a derivation of formulas to estimate magnetostriction behavior of both, single crystal and polycrystalline materials. Provided that the magnetization curve at zero stress is known, he calculated the magnetization for any arbitrary stress. However, the focus should be set to BROWN's theoretical approach:

He regarded a ferromagnetic sample as a collection of equally sized domains (comparable to magnetic entities in the EM) with a certain number n_φ^τ of domains per unit volume (with magnetization in direction[4] φ). According to the nature of anisotropy, he divided the

[4] There is only a specified number of discrete directions allowed within a class τ. Thus, it makes sense to count the number of domains having a certain magnetization direction.

domains into classes τ. So a single crystal consists of only one class, whereas polycrystalline materials contain several classes, distinguished by the direction of the magnetocrystalline easy axis.

Furthermore, BROWN assumed that any thermodynamic potential V (per unit volume) contributes of ...

... a component V^0 independent of magnetization direction,
... a part V^I as contribution from individual domains, and
... a part V^{II} due to interaction between different domains.

Under the assumption that these domains (magnetic entities) are macroscopically indistinguishable the statistical weight

$$P(n_\varphi^\tau) = \frac{\prod\limits_{\tau=1}^{N}\left[\left(\sum\limits_{\varphi} n_\varphi^\tau\right)!\right]}{\prod\limits_{\tau=1}^{N}\prod\limits_{\varphi}\left[n_\varphi^\tau!\right]}$$

is characterizing a certain macroscopic state. If V^I as well as V^{II} were known in their functional form, one would have to solve the optimization problem

$$\min_{n_\varphi^\tau}\left\{V^I(n_\varphi^\tau) + V^{II}(n_\varphi^\tau)\right\} \qquad \text{s.t.} \quad \sum_{\varphi} n_\varphi^\tau = n^\tau$$

in order to get the macroscopic distribution of number of domains n_φ^τ. Under the absence of concrete knowledge of the interaction term's functional form, the safest way of predicting n_φ^τ is the maximization of the statistical weight

$$\max_{n_\varphi^\tau}\left\{P(n_\varphi^\tau)\right\} \qquad \text{s.t.} \quad \sum_{\varphi} n_\varphi^\tau = n^\tau \quad \text{and} \quad V^I(n_\varphi^\tau) = V^I_{\text{const}}$$

for a pre-specified value of the localized component V^I_{const}.

Phase Theory - Neel, Lawton, and Stewart (1944)

The basic aim of phase theory is the description of a reversible, vectorial magnetization curve, which should approximate the "ideal" anhysteretic magnetization curve. According to the seminal work of NEEL [64] a certain phase i includes all domains, where the magnetic moments are parallel aligned to a specified direction $\vec{m}_i$. Such a phase is strongly bounded to the magnetocrystalline easy axes and occupies a volume fraction v_i. On principle, there are some premises to apply the concept of phase theory:

- Interface energies between domains are neglected, which is valid in sufficiently *extended samples.*
- Internal local stray fields are not considered explicitly (only in the form of global demagnetizing fields[5]), a fact that is conformable met in *soft magnetic materials.*

[5] Assuming that the arrangement of domains is such that there are no magnetic poles on their boundaries ($\vec{\nabla} \cdot \vec{J} = 0$). Therefore, the only demagnetizing field results from the discontinuities at the surface of the sample.

- External as well as demagnetizing fields are supposed to be uniform, like in approximately *ellipsoidal sample geometries.*
- Optimal phase volumes can be reached without hindrances, so coercivity and *irreversible processes are ignored.*

So the total energy comprises the following terms

$$E = \text{AnisotropyEnergy}(v_i, \vec{m}_i) + \text{FieldEnergy}(v_i, \vec{m}_i, \vec{H}_{\text{in}}) + \text{DemagnetizingEnergy}(\vec{m})$$

and a minimization with respect to the volume fractions v_i and directions $\vec{m}_i$ delivers the average magnetization $\vec{m} = \sum_i v_i \vec{m}_i$ as vector. The optimization problem can be solved in two steps: First, the magnetization directions $\vec{m}_i$ are determined depending on the internal field $\vec{H}_{\text{in}}$. For cubic crystal symmetry phase theory distinguishes four magnetization modes:

Mode I: zero internal field; all 6 phases coexist.

Mode II: non-zero internal field; 3 phases are energetically equivalent.

Mode III: non-zero internal field; 2 phases coexist.

Mode IV: non-zero internal field; only 1 phase has minimum (potential) energy.

Second, the phase volumes v_i appear in a configuration that the resulting demagnetizing field $\vec{H}_{\text{d}} = M_{\text{s}}\, \vec{m} \cdot \tilde{N}_{\text{d}}$ ($\tilde{N}_{\text{d}}$ is the demagnetizing tensor) gives in superposition with the external field $\vec{H}$ the internal field $\vec{H}_{\text{in}} = \vec{H} - \vec{H}_{\text{d}}$ required for the corresponding magnetization mode.

Finally, phase theory provides good results for materials with nearly undisturbed crystal structure and dominating[6] anisotropy energies (preferring magnetization rotation processes).

Fasching's Model (1964)

In his original work [20] FASCHING demonstrated his model of statistical domains considering cubic materials as example. Thus, he defined six phase volumina corresponding to the crystalline easy axes, each containing n_i statistical domains (per unit volume). Using $v_i = \frac{n_i}{n}$ ($n = \sum_{i=1}^{6} n_i$) the probability for the existence of a certain phase configuration is derived from NEWTON's probability formula (conforms to a multinomial distribution) by the help of Stirling approximation as

$$P(v_1, \ldots, v_6) = c \left(\prod_{i=1}^{6} \frac{p_i^{v_i} \mathrm{e}^{v_i}}{v_i^{v_i}} \right)^a \quad ,$$

where c and a are constant model parameters and the weights p_i are designed to favor certain crystalline directions. Denoting α_{iH} as direction cosines of phase magnetization with respect to the field $\vec{H}$, the total magnetization (in field direction) is

$$m(v_i, \alpha_{iH}) = \sum_{i=1}^{6} v_i\, \alpha_{iH} \quad .$$

[6] So that neglected energy terms are rather small in comparison and can be ignored.

FASCHING's crucial idea is to assume that the field strength ΔH, which is necessary in order to move the magnetic system from state $\left(v_i^{(1)}\right)$ to state $\left(v_i^{(2)}\right)$ is proportional to the reciprocal probabilities for these states

$$\Delta H \propto \frac{1}{P(v_i^{(2)})} - \frac{1}{P(v_i^{(1)})} \quad .$$

Let the state $\left(v_i^{(1)}\right)$ be the demagnetized state, where the phase distribution is $v_i^{(1)} = p_i$, then the field H to reach the state $v_i^{(2)} = v_i$ is given by

$$H(v_i) = h\left(\frac{1}{P(v_i)} - 1\right)$$

with the constant model parameter h.

Solving the optimization problem

$$\max_{v_1,\ldots,v_6} \{P(v_1,\ldots,v_6)\} \qquad \text{s.t.} \quad \sum_{i=1}^{6} v_i = 1 \quad \text{and} \quad m(v_i, \alpha_{iH}) = m$$

by means of Lagrange technique one gets

$$v_i = v_i(\beta, \alpha_{iH}) \qquad m = m(\beta, \alpha_{iH}) \qquad H = H(\beta, \alpha_{iH})$$

with the Lagrange factor β. The minimization of the total energy

$$E = \text{AnisotropyEnergy}(v_i, \alpha_{ix}, \alpha_{iy}, \alpha_{iz}) + \text{FieldEnergy}(v_i, \alpha_{iH}, H)$$

$$\min_{\alpha_{ix},\alpha_{iy},\alpha_{iz}} \{E\} \qquad \text{s.t.} \quad 1 = \alpha_{ix}^2 + \alpha_{iy}^2 + \alpha_{iz}^2$$

with respect to the direction cosines $\alpha_{ix}, \alpha_{iy}, \alpha_{iz}$ to the coordinate axes results in expressions for the magnetization directions

$$\alpha_{iH} = \alpha_{iH}(H, v_i) \quad .$$

In order to simulate the (anhysteretic) magnetization curve, FASCHING used an iterative algorithm:

1. Choose a value for the Lagrange factor β and start with $\alpha_{iH} = \alpha_{iH}(H = 0, v_i = p_i)$
2. From maximization of probability we get $v_i = v_i(\beta, \alpha_{iH})$, $m = m(\beta, \alpha_{iH})$, and $H = H(\beta, \alpha_{iH})$
3. From energy minimization correct the directions $\alpha_{iH} = \alpha_{iH}(H, v_i)$
4. Repeat steps 2 and 3 until convergence of α_{iH}
5. The resulting tuple $(H(\beta, \alpha_{iH}), m(\beta, \alpha_{iH}))$ is a point of the magnetization curve
6. Start at step 1 with a different value of β

Although this model was evaluated on a variety of corn-oriented single crystal materials with a proven record of success, a treatment of hysteretic magnetic behavior is not intended.

5.2.2 Energy Contributions Originating from Local Energy Terms

Aggregation of Energy Densities to Domain Classes

Local energy contributions, such as the applied field energy, are expressed in terms of *energy densities* $w(\vec{r})$ depending on the local vector of magnetization $\vec{m}(\vec{r})$ only. In our two-dimensional framework, where the absolute value $|\vec{m}(\vec{r})| = 1$ and the direction is given by $\arg(\vec{m}(\vec{r})) = \varphi(\vec{r})$ one is able to write the energy density as $w(\varphi(\vec{r}))$. Thus, the local energy densities can be assigned to each of the magnetic entities $\mathcal{E}_k$ via

$$w(\varphi(\vec{r})) \longleftrightarrow w(\varphi(\mathcal{E}_k)) \quad . \tag{5.37}$$

Imagine, the total sample volume V is split into $N_\mathcal{D}$ volume regions V_i according to the statistical domain classes $\mathcal{D}_i$, then the *energy per unit volume*

$$\begin{aligned} w &= \frac{1}{V} \int\limits_{\mathcal{V}} w(\vec{r}) \, \mathrm{d}V \\ &= \sum_{i=1}^{N_\mathcal{D}} \frac{V_i}{V} \frac{1}{V_i} \int\limits_{\mathcal{V}_i} w(\vec{r}) \, \mathrm{d}V \\ &= \sum_{i=1}^{N_\mathcal{D}} v_i \, w_i \end{aligned} \tag{5.38}$$

results as weighted sum over the energy contributions w_i from the domain classes. Using the fact that the magnetization angle φ within a domain class $\mathcal{D}_i$ is represented by a stochastic random variable Φ_i following a probability density function $f_i(\varphi)$, the energy contribution w_i for domain class $\mathcal{D}_i$ can be derived via statistical expectation value (Fig. 5.9)

$$\begin{aligned} w_i &= \frac{1}{V_i} \int\limits_{\mathcal{V}_i} w(\varphi(\vec{r})) \, \mathrm{d}V \\ &= \mathbb{E}\left[w(\Phi_i)\right] \\ &= \int\limits_{-\pi}^{\pi} w(\varphi) \, f_i(\varphi) \, \mathrm{d}\varphi \quad . \end{aligned} \tag{5.39}$$

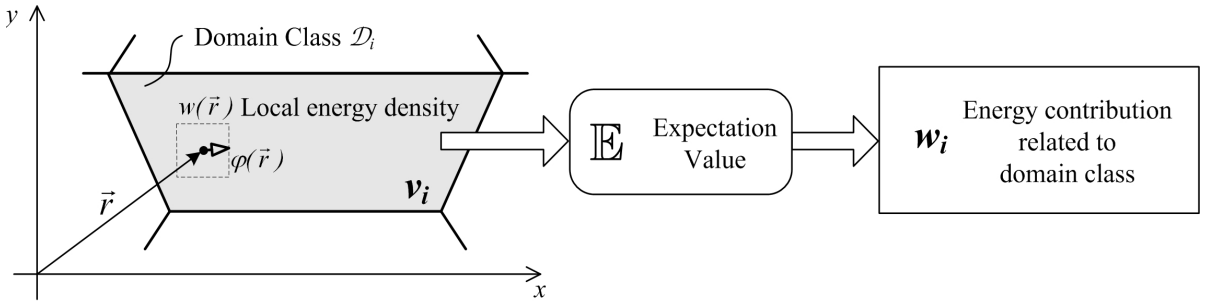

Figure 5.9: Aggregation of local energy densities $w(\varphi(\vec{r}))$ to energy per unit volume w_i via statistical expectation value for a domain class $\mathcal{D}_i$.

In this work, the wrapped normal distribution $\Phi_i \sim \mathrm{WN}(\bar{\varphi}_i, \sigma_i^2)$ as defined by (5.13) is used to calculate the local energy contributions as follows.

Applied Field Energy

For a uniform applied field $\vec{H}$ the Zeeman energy density is according to 3.1.4

$$\begin{aligned} w_{\mathrm{H}}(\varphi(\vec{r})) &= -\mu_0 M_{\mathrm{s}}\, \vec{m}(\vec{r}) \cdot \vec{H} \\ &= -\mu_0 M_{\mathrm{s}}\, H\, \cos(\varphi(\vec{r}) - \varphi_{\mathrm{H}}) \quad , \end{aligned} \tag{5.40}$$

where φ_{H} is the angle of the field $\vec{H}$ with respect to the x-axis (see Fig. 5.10). Applying (5.39) yields

$$w_{\mathrm{H},i} = -\mu_0 M_{\mathrm{s}}\, H\, \cos(\bar{\varphi}_i - \varphi_{\mathrm{H}})\, \exp(-\frac{\sigma_i^2}{2}) \tag{5.41}$$

for the applied field energy of domain class $\mathcal{D}_i$. For a detailed derivation please refer appendix A.1.

In the special case where all magnetic entities within one domain class have the same direction $\bar{\varphi}_i$ the probability distribution degenerates to determinism ($\sigma_i^2 = 0$) and (5.41) simplifies to

$$w_{\mathrm{H},i} = -\mu_0 M_{\mathrm{s}}\, H\, \cos(\bar{\varphi}_i - \varphi_{\mathrm{H}}) \quad . \tag{5.42}$$

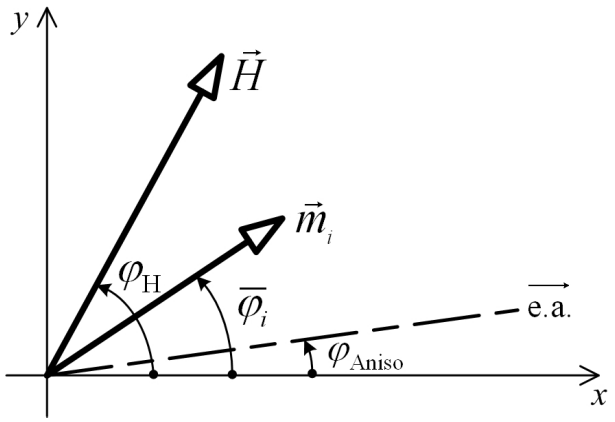

Figure 5.10: Angles for applied field energy and anisotropy energy.

Anisotropy Energy

Due to the fact that the EM will be applied to materials with *uniaxial anisotropy*, other types of anisotropy are not discussed within this work. So we approximate the uniaxial anisotropy energy density (3.1.5) as

$$w_{\mathrm{Aniso}}(\varphi(\vec{r})) = K_1 \sin^2(\varphi(\vec{r}) - \varphi_{\mathrm{Aniso}}) \quad , \tag{5.43}$$

with a temperature dependent anisotropy constant K_1 and the angle φ_{Aniso} between the anisotropy easy axis $\overrightarrow{e.a.}$ and the x-axis (see Fig. 5.10). Again the domain class specific

energy contribution can be derived using (5.39)

$$w_{\mathrm{Aniso},i} = K_1 \sin^2(\bar{\varphi}_i - \varphi_{\mathrm{Aniso}}) \exp(-2\sigma_i^2) + \frac{K_1}{2}\left(1 - \exp(-2\sigma_i^2)\right) \tag{5.44}$$

and simplifies for $\sigma_i^2 = 0$ to

$$w_{\mathrm{Aniso},i} = K_1 \sin^2(\bar{\varphi}_i - \varphi_{\mathrm{Aniso}}) \quad . \tag{5.45}$$

Magneto-Elastic Energy with Non-Magnetic Stresses

This energy term results either from external stress or from internal stress of non-magnetic origin (due to temperature inhomogeneities, dislocations, etc.). Only the special case for isotropic material and *uniaxial stress* σ_{Stress} along the axis $\vec{a}$ (angle $\varphi_{\mathrm{Stress}}$ with respect to the x-axis) should be mentioned in the framework of this section. As shown in 3.1.7, the magneto-elastic coupling energy density can be written as

$$\begin{aligned} w_{\mathrm{Stress}}(\varphi(\vec{r})) &= -\frac{3}{2}\lambda_{\mathrm{s}}\sigma_{\mathrm{Stress}}\left((\vec{m}(\vec{r})\cdot\vec{a})^2 - \frac{1}{3}\right) \\ &= -\frac{3}{2}\lambda_{\mathrm{s}}\sigma_{\mathrm{Stress}}\left(\cos^2(\varphi(\vec{r}) - \varphi_{\mathrm{Stress}}) - \frac{1}{3}\right) \\ &= \frac{3}{2}\lambda_{\mathrm{s}}\sigma_{\mathrm{Stress}}\sin^2(\varphi(\vec{r}) - \varphi_{\mathrm{Stress}}) + \mathrm{const.} \end{aligned} \tag{5.46}$$

with the isotropic magnetostriction constant λ_{s}. Because (5.46) has the same functional form as (5.43), the domain specific magneto-elastic energy $w_{\mathrm{Stress},i}$ is given by (5.44) when replacing K_1 by $\frac{3}{2}\lambda_{\mathrm{s}}\sigma_{\mathrm{Stress}}$

$$w_{\mathrm{Stress},i} = \frac{3}{2}\lambda_{\mathrm{s}}\sigma_{\mathrm{Stress}}\sin^2(\bar{\varphi}_i - \varphi_{\mathrm{Stress}})\exp(-2\sigma_i^2) + \frac{3}{4}\lambda_{\mathrm{s}}\sigma_{\mathrm{Stress}}\left(1 - \exp(-2\sigma_i^2)\right) \quad . \tag{5.47}$$

Thermal Excitations - Internal Entropy

Basically, thermal excitations degrade the alignment of the magnetic entities and thus lead to a reduced order within a domain class. In our statistical framework, the grade of order is expressed by the *internal entropy* that is represented by the differential entropy of the circular density function

$$\begin{aligned} S_{\mathrm{Int}} &= -k_{\mathrm{B}}\,\mathbb{E}\left[\ln\left(f_i(\varphi)\right)\right] \\ &= -k_{\mathrm{B}}\int_{-\pi}^{\pi} f_i(\varphi)\,\ln\left(f_i(\varphi)\right)\,\mathrm{d}\varphi \quad . \end{aligned} \tag{5.48}$$

The corresponding domain class specific energy contribution is

$$w_{\mathrm{T},i} = -\eta\, T\, S_{\mathrm{Int}} \quad , \tag{5.49}$$

with $\eta = n_{\mathcal{V}}/V$ as the *number of magnetic entities per unit volume*, the Boltzmann constant k_{B}, and the absolute temperature T.

As depicted in Fig. 5.11, the energy $w_{\mathrm{T},i}$ that is necessary to overcome the thermal excitations increases significantly as the domain class magnetization $|\vec{m}_i|$ $=\exp\left(-\sigma_i^2/2\right)$ approximates to the value of 1.

For the wrapped normal distribution $\mathrm{WN}(\bar{\varphi}_i, \sigma_i^2)$ the following approximation for the internal entropy

$$S_{\mathrm{Int}}(\sigma_i^2) \approx k_{\mathrm{B}} \left(\ln(2\pi) - \tfrac{1}{2} \ln \left(\exp(2) + \frac{2\pi}{\exp(1)} \frac{1}{\sigma_i^2} \right) \exp\left(-\sigma_i^2\right) \right) \tag{5.50}$$

can be derived from numerical calculations. Since the entropy represents the grade of order in a domain class, it increases with the variance σ_i^2 of the angular distribution. In the limiting case of of small variances the differential entropy becomes $k_{\mathrm{B}} 1/2 \ln(2\pi\sigma_i^2 \exp(1))$ appropriate to the normal distribution, and in the high variance regime the differential entropy converges to $k_{\mathrm{B}} \ln(2\pi)$ appropriate to the circular uniform distribution.

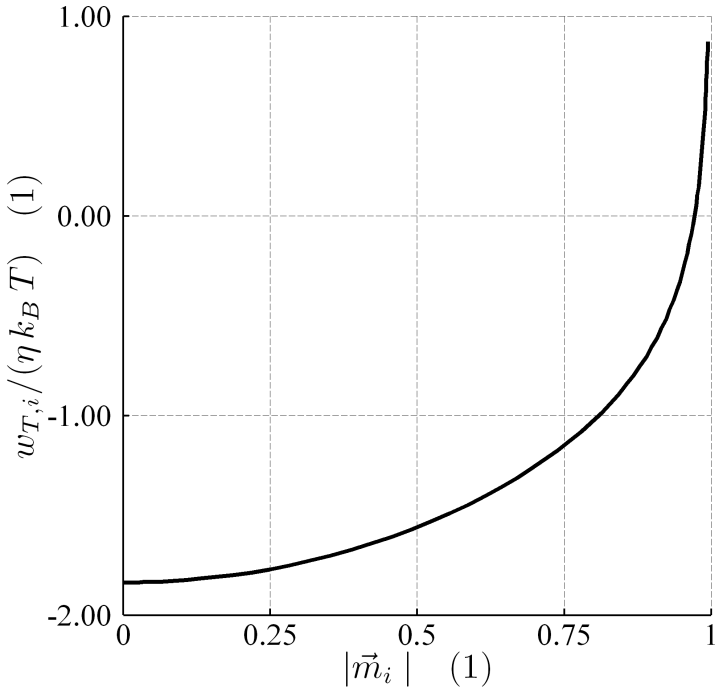

Figure 5.11: Energy term related to thermal excitations (internal entropy) depending on the domain class magnetization $|\vec{m}_i|$.

For the circular normal distribution $\mathrm{CN}(\bar{\varphi}_i, \beta_i)$ the differential entropy is given by

$$S_{\mathrm{Int}}(\beta_i) = k_{\mathrm{B}} \left(\ln(2\pi\, I_0(\beta_i)) - \beta_i \frac{I_1(\beta_i)}{I_0(\beta_i)} \right) \tag{5.51}$$

with the modified Bessel functions

$$I_0(\beta_i) = \frac{1}{2\pi} \int_{-\pi}^{\pi} \exp(\beta_i \cos(\varphi))\ \mathrm{d}\varphi$$

$$I_1(\beta_i) = \frac{1}{2\pi} \int_{-\pi}^{\pi} \cos(\varphi)\, \exp(\beta_i \cos(\varphi))\ \mathrm{d}\varphi \quad .$$

Exchange Energy within a Domain Class

From a macroscopic point of view, the competition between exchange energy and stray field energy is mainly responsible for the formation of magnetic domains, represented by the statistical domain classes in the context of the EM. Within the domain classes, the exchange energy counterbalances disordering energy terms, originating from thermal excitations or material inhomogeneities.

In a simple case, we consider a magnetic entity aligned at an angle φ with respect to the x-axis. Assuming that this entity $\vec{m}_{\mathcal{E}}$ interacts with a (fictive) neighboring entity, which is represented by the direction of the mean magnetic moment $\vec{m}_i$ of the remaining entities in the domain class, the exchange energy is given by $J_{\mathrm{Ex}}\vec{m}_{\mathcal{E}} \cdot \vec{m}_i = J_{\mathrm{Ex}} \left|\vec{m}_{\mathcal{E}}\right| \, \left|\vec{m}_i\right| \cos\left(\varphi - \bar{\varphi}_i\right)$.

In contrast to the local energy contributions mentioned before, the exchange energy does not depend just on the magnetic moment of a single entity. Moreover, it describes the interaction between neighboring magnetic entities. Hence, we have to include correlation effects between neighboring magnetic entities in the generalized EM. If $\vec{m}_{i1}$ and $\vec{m}_{i2}$ are the directions of the magnetic moment for two neighboring magnetic entities $\mathcal{E}_1$ and $\mathcal{E}_2$ of domain class $\mathcal{D}_i$, the respective angles Φ_{i1} and Φ_{i2} (as random variables) can be represented by a *bivariate wrapped normal distribution*

$$(\Phi_{i1}, \Phi_{i2}) \sim \mathrm{WN}_2(\bar{\varphi}_i, \sigma_i^2, \rho_i) \quad \text{or} \quad f_i(\varphi_1, \varphi_2) = \sum_{k,l \in \mathbb{Z}} f_i^{\phi}(\phi_1 = \varphi_1 + 2\pi k, \phi_2 = \varphi_2 + 2\pi l) \quad , \tag{5.52}$$

which is based on the linear bivariate normal distribution

$$\begin{aligned} f_i^{\phi}(\phi_1, \phi_2) \;=\; & \frac{1}{2\pi\sigma_i^2\sqrt{1-\rho_i^2}} \cdot \\ & \cdot \exp\left(-\frac{1}{2\left(1-\rho_i^2\right)}\left(\frac{\left(\phi_1-\bar{\varphi}_i\right)^2}{\sigma_i^2} + \frac{\left(\phi_2-\bar{\varphi}_i\right)^2}{\sigma_i^2} - \frac{2\rho_i\left(\phi_1-\bar{\varphi}_i\right)\left(\phi_2-\bar{\varphi}_i\right)}{\sigma_i^2}\right)\right) \end{aligned} \tag{5.53}$$

with the correlation coefficient $\rho_i \in [-1, 1]$.

The exchange energy within a domain class is given by the summation of $J_{\mathrm{Ex}}\vec{m}_{i1} \cdot \vec{m}_{i2} = J_{\mathrm{Ex}} \cos\left(\varphi_{i1} - \varphi_{i2}\right)$ over all neighboring entities, in principle. In our statistical treatment, this can be written as

$$w_{\mathrm{Ex},i} = -\eta\nu_{\mathrm{NN}} J_{\mathrm{Ex}} \, \mathbb{E}\left[\cos\left(\Phi_{i1} - \Phi_{i2}\right)\right] \tag{5.54a}$$

$$= -\eta\nu_{\mathrm{NN}} J_{\mathrm{Ex}} \, \exp(-\sigma_i^2(1-\rho_i)) \quad , \tag{5.54b}$$

where $\eta = n_{\mathcal{V}}/V$ is the number of magnetic entities per unit volume and ν_{NN} is the number of nearest neighbors. Thus, decreasing variance σ_i^2 as well as increasing correlation ρ_i decrease the exchange energy term. For a detailed derivation of the expectation value, the reader is referred to appendix A.2. The correlation coefficient ρ_i is treated as model parameter. Fig. 5.12 illustrates the alignment of magnetic entities inside a domain class for different values of ρ_i, leading to identical variance σ_i^2.

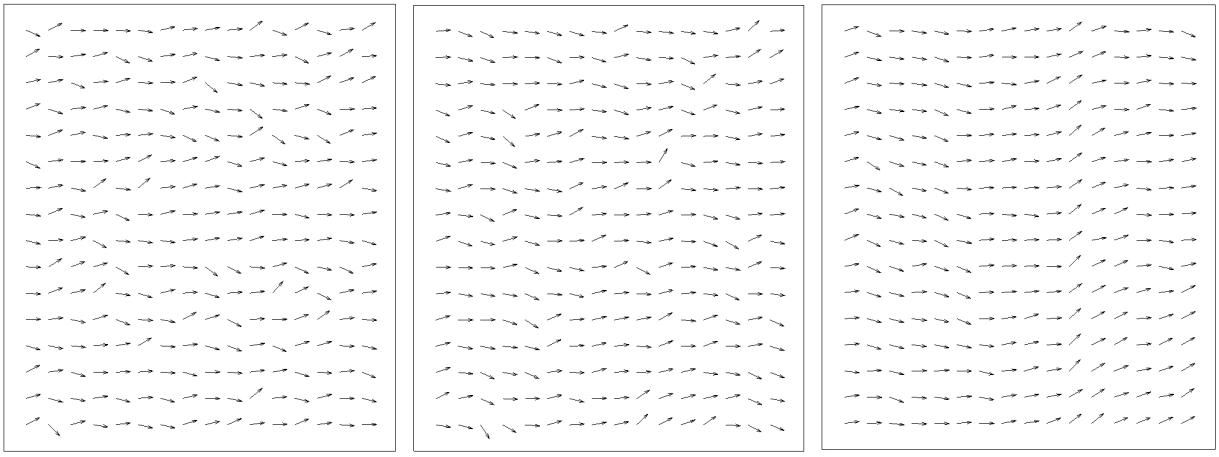

Figure 5.12: Alignment of magnetic entities depending on correlation $\rho_i = 0.03$ (a), $\rho_i = 0.35$ (b), $\rho_i = 0.71$ (c), at constant mean direction $\bar{\varphi}_i \approx 0$ and standard deviation $\sigma_i = 0.25$.

Total Local Energy

Finally, all local energy contributions considered within the model can be added up for every domain class $\mathcal{D}_i$ separately as

$$w_{\mathrm{Loc},i}(\bar{\varphi}_i, \sigma_i^2) = w_{\mathrm{H},i}(\bar{\varphi}_i, \sigma_i^2) + w_{\mathrm{Aniso},i}(\bar{\varphi}_i, \sigma_i^2) + w_{\mathrm{Stress},i}(\bar{\varphi}_i, \sigma_i^2) + w_{\mathrm{T},i}(\sigma_i^2) + w_{\mathrm{Ex},i}(\sigma_i^2) \quad . \tag{5.55}$$

For the sample $\mathcal{V}$ the total local energy (per unit volume) is the volume weighted sum

$$w_{\mathrm{Loc}} = \sum_{i=1}^{N_{\mathcal{D}}} v_i \, w_{\mathrm{Loc},i}(\bar{\varphi}_i, \sigma_i^2) \quad . \tag{5.56}$$

Conclusion

So far, only energy terms are formulated, which can be directly derived from the local value of magnetization $\vec{m}(\vec{r})$. The energy (per unit volume) of a domain class can be calculated by the statistical expectation value in the presented stochastic framework, corresponding to the summation (integration) over all points of the respective volumina in a geometric point of view.

Together with the arrangement of magnetic entities in statistical domain classes, these local energy terms of physical nature describe static short-range interactions of the magnetic moments mutually, with the crystal lattice, and with external forces (such as applied field or applied stress). But in macroscopic material samples, the domain configuration is also driven by non-local energy terms that reflect long range interaction mechanisms, such as stray fields. Furthermore, even in a quasi-static regime, the change of the domain configuration during the magnetization process leads to irreversible losses. Both issues are discussed in the following sections.

5.2.3 Energy Contributions Originating from Non-Local Energy Terms

Besides the local energy contributions, macroscopic magnetization behavior is driven by non-local mechanism that play a fundamental role for the development of magnetic domains. All above domain wall energy, stray field energy, and magnetostrictive energy due to internal interactions between regions magnetized along different axes determine the topology of domain structure. Within the EM the reasoning for specific domain configurations is treated by *phenomenological energy terms*.

All the non-local energy contributions together characterize the large-scale behavior of the magnetic system. Microscopic properties are described by a directional distribution of magnetic entities within several domain classes. The macroscopically indistinguishable magnetic entities together constitute a particular macroscopic state, which is represented by the relative size of the domain classes.

Stray Field Energy

In the framework of the EM, only the external (global) part of the stray field energy that results from the sample geometry is stated explicitly. By means of the (external) two-dimensional demagnetizing tensor $\tilde{N}_{\mathrm{d,2D}}$, the demagnetizing energy (per unit volume) is

$$w_{\mathrm{d}} = \frac{1}{2}\mu_0 M_{\mathrm{s}}^2 \ \vec{m} \cdot \tilde{N}_{\mathrm{d,2D}} \cdot \vec{m} \tag{5.57}$$

for a given total magnetization $\vec{m}$ of the sample. Regarding the components with respect to the x-axis and y-axis, the demagnetizing energy can also expressed as

$$w_{\mathrm{d}} = \frac{1}{2}\mu_0 M_{\mathrm{s}}^2 \ \left(m_x^2 N_{xx} + 2 m_x m_y N_{xy} + m_y^2 N_{yy}\right) \quad , \tag{5.58}$$

provided that

$$\tilde{N}_{\mathrm{d,2D}} = \begin{pmatrix} N_{xx} & N_{xy} \\ N_{xy} & N_{yy} \end{pmatrix} \quad . \tag{5.59}$$

The internal (local) contributions to the stray field energy, resulting from magnetic poles inside the sample (grain boundaries or inhomogeneities), are treated by phenomenological energy terms.

Demagnetized State as Point of Origin

A necessary condition for a *demagnetized state* described in section 3.3.1 proves that macroscopic magnetization is zero when the applied field is zero

$$\vec{m}|_{\vec{H}=\vec{0}} = \vec{0} \quad . \tag{5.60}$$

Unfortunately, in most of the cases there is no unique demagnetized state for a given ferromagnetic sample (see [74] for a rectangular Permalloy thin film element). In fact, the resulting domain configuration may depend on the demagnetizing procedure. But, if we are not interested in microscopic configurations, the volume fractions $v_{0,i}$ will represent the demagnetized state sufficiently accurate.

Levels of Demagnetized States: In 1995 ZHANG and ATHERTON [90] published a paper, where they assumed that a specific demagnetized state can be described as a linear combination of so called "basic demagnetized states". Such a *basic demagnetized state* is proposed as spatial distribution of magnetic dipole moments, having the simplest directional symmetric configuration that gives zero magnetization. More precisely, they used probability density functions of rectangular or cosine shape for their description. The level k of a basic demagnetized state is defined through the angular period $2\pi/k$ of the square wave or cosine function.

This concept is quite similar to the assumption of domain classes with distributed magnetic entities in the EM and therefore worth mentioning. But ZHANG and ATHERTHON provided just a formal framework for their description. There is no statement how to estimate the levels of the basic states and the weighting for their linear combination. They only indicated that an AC-demagnetization procedure with N turning points restricts the basic states to a maximum level of $4N + 1$.

Demagnetized State in the EM: In the framework of the EM the demagnetized state resulting from a thermal demagnetization procedure is considered as magnetic "ground state". The resulting domain structure is mainly caused by anisotropy, wall energy, and stray field energy.

Micromagnetic models - summarized in Section 4.2 - incorporate all these different energy terms together with the geometrical configuration of the sample in order to calculate the spatial magnetization distribution in the demagnetized state. But as mentioned above, there may exist more than one state of vanishing total magnetization, representing a local minimum of total energy.

However, within the EM these competing energy contributions are not considered explicitly. Instead, the resulting distribution of domain classes is defined by an *a-priori assumption of initial volume fractions* $v_{0,i}$ for the domain classes $\mathcal{D}_i$.

$$v_{0,i} = v_i|_{\text{Demagnetized State}}$$

Contrary to the volume fractions, the mean directions $\bar{\varphi}_{0,i}$ and variances $\sigma^2_{0,i}$ in the demagnetized state are estimated by minimization of the local energy terms. For predetermined volume fractions this minimization can be done for each domain class separately

$$\bar{\varphi}_{0,i}, \sigma^2_{0,i}: \quad w_{\text{Loc0},i} = \min_{\bar{\varphi}_i, \sigma_i^2} \left\{ w_{\text{Loc},i}(\bar{\varphi}_i, \sigma_i^2) \right\} \quad \text{s.t. } \vec{H} = \vec{0} \text{ and } \vec{\sigma}_{\text{Stress}} = \vec{0} \quad . \tag{5.61}$$

In case where uniaxial anisotropy (anisotropy axis $\vec{c}_i$ having an angle $\varphi_{\text{Aniso},i}$ with respect to the x-axis) is the only source of directional dependent local energy one obtains

$$\bar{\varphi}_{0,i} = \varphi_{\text{Aniso},i} \quad \text{or} \quad \bar{\varphi}_{0,i} = \varphi_{\text{Aniso},i} \pm \pi \quad . \tag{5.62}$$

According to the zero total magnetization condition (5.60) the expectation value for the sample magnetization must be zero

$$\vec{0} = \sum_{i=1}^{N_{\mathcal{D}}} v_{0,i}\, \vec{m}_i \quad . \tag{5.63}$$

Anhysteretic Magnetization Curve

As summarized in section 5.2.1, the macroscopic interaction between different domains (domain classes) can be described by the assignment of statistical probabilities for certain domain configurations. While HEISENBERG and BROWN proposed to maximize the probability in order to predict the domain configuration, FASCHING introduced a (virtual) magnetic field that is inverse proportional to the probability of the domain configuration.

In the context of the EM, the sample $\mathcal{V}$ has been subdivided into a certain number of domain classes $\mathcal{D}_i$ that are characterized by their average local energy $w_{\mathrm{Loc},i}$. On the basis of Fermi statistics, the number of possibilities to assign $n_{\mathcal{D}_i}$ indistinguishable magnetic entities to domain class $\mathcal{D}_i$ (with a fictive number of available states $a_{\mathcal{D}_i}$) is

$$P = \prod_{i=1}^{N_\mathcal{D}} \binom{a_{\mathcal{D}_i}}{n_{\mathcal{D}_i}} = \prod_{i=1}^{N_\mathcal{D}} \frac{a_{\mathcal{D}_i}!}{n_{\mathcal{D}_i}!\,(a_{\mathcal{D}_i} - n_{\mathcal{D}_i})!} \quad \text{for } 0 \le n_{\mathcal{D}_i} \le a_{\mathcal{D}_i} \le n_\mathcal{V} \quad . \tag{5.64}$$

Assuming that the number of magnetic entities is large enough to use Stirling's approximation

$$n! \approx \frac{n^n}{\mathrm{e}^n} \tag{5.65}$$

together with the the volume fractions

$$v_i = \frac{n_{\mathcal{D}_i}}{n_\mathcal{V}} \quad \text{and} \quad v_{\max,i} = \frac{a_{\mathcal{D}_i}}{n_\mathcal{V}} \tag{5.66}$$

allows to rewrite the probability function as

$$P(v) = \left[\prod_{i=1}^{N_\mathcal{D}} \frac{v_{\max,i}^{v_{\max,i}}}{v_i^{v_i}\,(v_{\max,i} - v_i)^{v_{\max,i} - v_i}} \right]^{n_\mathcal{V}} \quad \text{for } 0 \le v_i \le v_{\max,i} \le 1 \quad . \tag{5.67}$$

Here, the number of available states $a_{\mathcal{D}_i}$ or the corresponding maximum volume fraction $v_{\max,i}$ for domain class $\mathcal{D}_i$ is treated as model parameter. For example, if $\mathcal{D}_i$ represents closure domains, the maximum volume fraction can be limited to a value smaller than 1.

For the anhysteretic magnetization process at temperature T the free energy per unit volume is stated as

$$w_{\mathrm{Loc}} + w_{\mathrm{d}} - \frac{1}{V} T\, S \quad ,$$

where the entropy S is estimated from Boltzmann's formula $S = k_\mathrm{B} \ln(P)$. Hence, the free energy (per unit volume) becomes

$$w_{\mathrm{Loc}} + w_{\mathrm{d}} - \frac{1}{V} k_\mathrm{B} T\, \ln(P) \quad . \tag{5.68}$$

In general, the equilibrium state can be calculated by minimizing the free energy (or maximizing the entropy alternatively)

$$\min_v \left\{ w_{\mathrm{Loc}} + w_{\mathrm{d}} - \frac{1}{V} k_\mathrm{B} T\, \ln(P(v)) \right\} \tag{5.69}$$

subject to

$$\sum_{i=1}^{N_\mathcal{D}} v_i = 1 \quad .$$

Reversible Anhysteretic Energy

As shown above, the anhysteretic magnetization process can be described by means of statistics. Due to the fact that the corresponding energy term describes the reversible nature of the anhysteretic magnetization process, it is referred to as *reversible anhysteretic energy*. In the context of the generalized EM, a phenomenological reversible anhysteretic energy is defined according to (5.68) as

$$w_{\mathrm{RevAnh}} = -k_{\mathrm{RevAnh}} \frac{1}{n_{\mathcal{V}}} \ln(P) + \sum_{i=1}^{N_{\mathcal{D}}} v_i \, w_{\mathrm{RevAnh0},i} \quad , \tag{5.70}$$

where k_{RevAnh} is treated as model parameter. The second term in (5.70) ensures that the minimization of the free energy (5.69) gives the volume fractions $v_{0,i}$ for the demagnetized state.

Applying Fermi statistics together with Stirling's approximation, the reversible anhysteretic energy becomes

$$w_{\mathrm{RevAnh}} = -k_{\mathrm{RevAnh}} \sum_{i=1}^{N_{\mathcal{D}}} \ln \left(\frac{v_{\max,i}^{v_{\max,i}}}{v_i^{v_i} \, (v_{\max,i} - v_i)^{v_{\max,i} - v_i}} \right) + \sum_{i=1}^{N_{\mathcal{D}}} v_i \, w_{\mathrm{RevAnh0},i} \quad , \tag{5.71}$$

with

$$w_{\mathrm{RevAnh0},i} = k_{\mathrm{RevAnh}} \ln \left(\frac{v_{\max,i}}{v_{0,i}} - 1 \right) - (w_{\mathrm{Loc0},i} - w_{\mathrm{Loc0}}) \quad . \tag{5.72}$$

A detailed derivation is given in appendix A.3.

Conclusion

The reversible anhysteretic energy phenomenologically accounts for the fact that macroscopic magnetic order, when a single domain class is preferred related to the remaining ones, needs energy. This process of magnetic order is intrinsically bounded to a magnetic material sample. So, in [55] it is shown that anhysteretic magnetization curves for various frequencies can be standardized to a single curve by applying a simple transformation.

In the present work, the classical Fermi statistics is used to represent the anhysteretic magnetization process with respect to the statistical domain classes and their local energy contributions. Due to the fact that this energy term is entirely phenomenological, also other statistics may be applied, depending on the problem to be modeled.

By now, the generalized EM provides a two-dimensional framework to describe nonhysteretic (nondissipative) magnetization curves, by minimizing the sum of local, demagnetizing, and reversible anhysteretic energy terms. Within the next step, expressions for reversible and irreversible work have to be incorporated.

5.2.4 Reversible and Irreversible Work during Magnetization Process

Since the reversible and irreversible issues of *magnetization rotation* are covered by the local energy contributions in the domain classes, this section is focused on *domain wall motion.*

Modeling of Domain Wall Motion

For the following considerations, the *quasi-continuous static magnetization process* is described at discrete time steps

$$t, t + \Delta t, t + 2\Delta t, ... \quad ,$$

so that the rate of change $\Delta X/\Delta t$ for all relevant physical quantities X (e.g. applied magnetic field) is sufficiently small to neglect dynamic loss mechanisms (e.g. due to eddy currents). The term *quasi-continuous* refers to a scale range that allows averaging over small, but highly dynamic intrinsic effects, such as Barkhausen jumps or thermal fluctuations. Hence, in the scale of Barkhausen jumps the magnetization curve is considered as continuous, whereas irreversible jumps due to coherent magnetization rotation are still regarded.

In the framework of the EM domain wall motion can only be estimated in terms of change in volume fractions of the magnetic domain classes. Magnetic entities that change from domain class $\mathcal{D}_i$ to $\mathcal{D}_j$ during a time step Δt

$$\mathcal{E}^{(i)} \mapsto \mathcal{E}^{(j)} \quad \text{for} \quad t \mapsto t + \Delta t$$

cause a change in the corresponding volume fractions by Δv_{ij}

$$\begin{aligned} v_i(t + \Delta t) &= v_i(t) - \sum_{j=1}^{N_\mathcal{D}} \Delta v_{ij} \\ v_j(t + \Delta t) &= v_j(t) + \sum_{j=1}^{N_\mathcal{D}} \Delta v_{ij} \quad . \end{aligned} \tag{5.73}$$

More generally, during a time step Δt the volume fraction of domain class $\mathcal{D}_i$ is changing by Δv_i as

$$v_i(t + \Delta t) = v_i(t) + \Delta v_i \qquad \forall\, i = 1...N_\mathcal{D} \quad , \tag{5.74}$$

with contributions from all other domain classes $\mathcal{D}_j$

$$\Delta v_j = \sum_{i=1}^{N_\mathcal{D}} \Delta v_{ij} \quad , \tag{5.75}$$

where the sum of all volume changes Δv_i has to be zero

$$\sum_{i=1}^{N_\mathcal{D}} \Delta v_i = 0 \quad . \tag{5.76}$$

For the sake of completeness, it should be mentioned that

$$\Delta v_{ji} = -\Delta v_{ij} \quad \text{and} \quad \Delta v_{ii} = 0 \quad . \tag{5.77}$$

Furthermore, for given changes in volume fractions $\Delta v_1, \Delta v_2, ..., \Delta v_N$ the sum of absolute values is constant

$$\sum_{i=1}^{N_\mathcal{D}} \sum_{j=1}^{N_\mathcal{D}} |\Delta v_{ij}| = \sum_{i=1}^{N_\mathcal{D}} |\Delta v_i| = const \quad .$$

In the EM, the transition matrix

$$\begin{array}{c} \\ \\ \text{from} \\ \text{domain class} \end{array} \begin{array}{c} \overbrace{\qquad\qquad\qquad\qquad\qquad\qquad}^{\text{to domain class}} \\ \begin{array}{cc} & \begin{array}{cccccc} \mathcal{D}_1 & \cdots & \mathcal{D}_i & \mathcal{D}_j & \cdots & \mathcal{D}_N \end{array} \\ \begin{array}{c} \mathcal{D}_1 \\ \vdots \\ \mathcal{D}_i \\ \mathcal{D}_j \\ \vdots \\ \mathcal{D}_N \end{array} & \left(\begin{array}{cccccc} 0 & \cdots & \Delta v_{1i} & \Delta v_{1j} & \cdots & \Delta v_{1N_\mathcal{D}} \\ \vdots & & \vdots & \vdots & & \vdots \\ -\Delta v_{1i} & \cdots & 0 & \Delta v_{ij} & \cdots & \Delta v_{iN_\mathcal{D}} \\ -\Delta v_{1j} & \cdots & -\Delta v_{ij} & 0 & \cdots & \Delta v_{jN_\mathcal{D}} \\ \vdots & & \vdots & \vdots & & \vdots \\ -\Delta v_{1N_\mathcal{D}} & \cdots & -\Delta v_{iN_\mathcal{D}} & -\Delta v_{jN_\mathcal{D}} & \cdots & 0 \end{array} \right) \end{array} \end{array} \tag{5.78}$$

represents the change in domain class volume fractions within a time step Δt.

If minimum volume changes within a time step are postulated, for an increasing domain class volume $\Delta v_j > 0$ only positive contributions from other domain classes are allowed

$$\begin{aligned} \Delta v_j \;&>\; 0 \quad \Rightarrow \quad \Delta v_{ij} \geq 0 \qquad \forall\, i = 1...N_\mathcal{D} \\ \Delta v_j \;&<\; 0 \quad \Rightarrow \quad \Delta v_{ij} \leq 0 \qquad \forall\, i = 1...N_\mathcal{D} \quad . \end{aligned} \tag{5.79}$$

The procedure of estimating the transition matrix Δv_{ij} from the given volume changes Δv_i is described in appendix A.4.

Distance of Domain Wall Movement: Within the 2D framework a ferromagnetic sample of thickness d_S and sample volume V is considered, where the magnetization is oriented in-plane, in general. The characteristic length l_S of the sample is defined as

$$l_\mathrm{S} = \sqrt{\frac{V}{d_\mathrm{S}}} \gg d_\mathrm{S} \quad . \tag{5.80}$$

As sketched in Fig. 5.13, the equivalent distance $\Delta\xi_{ij}$ of wall movement (relative to the characteristic sample length l_S) for a domain wall between domain class $\mathcal{D}_i$ to $\mathcal{D}_j$ is assumed to be proportional to the relative volume change Δv_{ij}

$$\Delta\xi_{ij} = c_{ij}\, \Delta v_{ij} \quad . \tag{5.81}$$

The model-parameter c_{ij} accounts for the geometry of the sample as well as for the number of domain walls. If $n_{\mathrm{DW},ij}$ is the number of domain walls of typical length $l_{\mathrm{DW},ij}$, the constant

c_{ij} results as

$$c_{ij} = \frac{l_{\mathrm{S}}}{n_{\mathrm{DW},ij}\, l_{\mathrm{DW},ij}} \quad , \tag{5.82}$$

where l_{S} is the characteristic sample length, according to (5.80).

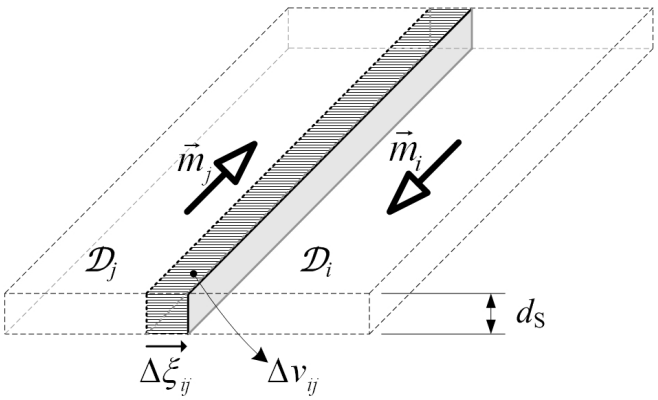

Figure 5.13: Equivalent distance of a representative moving domain wall between domain classes $\mathcal{D}_i$ and $\mathcal{D}_j$.

Probability of Reversible Domain Wall Motion

Domain wall motion over an incremental distance $\mathrm{d}\Delta\xi$ can be reversible on the one part (due to bowing or bending) and irreversible on the other part, as illustrated in Fig. 5.14. Let $P_{\mathrm{Rev}}(\Delta\xi)$ be the probability for a reversible domain wall motion as

$$\begin{aligned} \mathrm{d}\Delta\xi_{\mathrm{Rev}} &= P_{\mathrm{Rev}}(\Delta\xi)\,\mathrm{d}\Delta\xi \\ \mathrm{d}\Delta\xi_{\mathrm{Irr}} &= (1 - P_{\mathrm{Rev}}(\Delta\xi))\;\mathrm{d}\Delta\xi \quad , \end{aligned} \tag{5.83}$$

assuming that $\Delta\xi$ is the distance from the last (domain wall) reversal point.

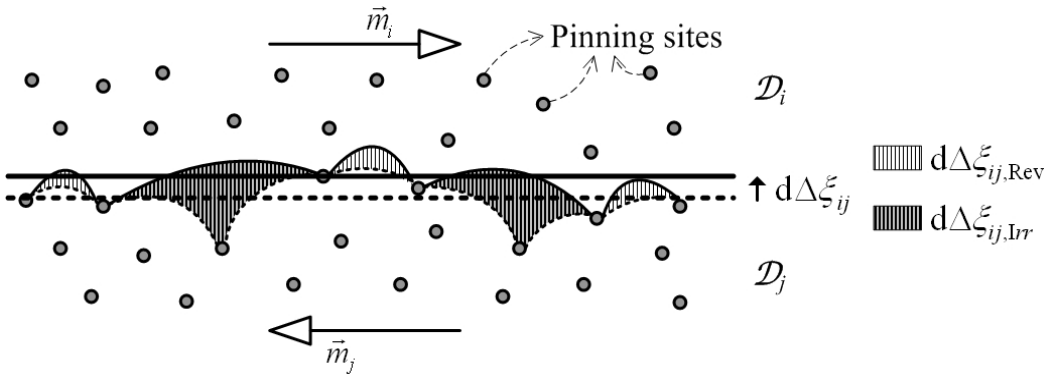

Figure 5.14: Simplified model of reversible and irreversible part of domain wall motion.

Poisson Process for Demagnetized State: In the framework of the EM, domain wall motion is based on a stochastic *Poisson process*, counting the number of Barkhausen jumps within a certain distance of domain wall motion. The parameter q_p is the average number of Barkhausen jumps per distance of domain wall motion, or $1/q_\mathrm{p}$ is the average distance between two consecutive pinning sites (Barkhausen jumps). Starting from the demagnetized state, where all domain walls are assumed to be in an equilibrium position, the probability that there is no Barkhausen jump for a wall motion of distance $\Delta\xi$ is exponentially distributed as

$$P_\mathrm{Rev}(\Delta\xi) = P_\mathrm{Poisson}(X=0,\Delta\xi) = \exp(-q_\mathrm{p}\,|\Delta\xi|) \quad . \tag{5.84}$$

So, when the notional rigid wall (within the view of the EM) is moving from the demagnetized state ξ_0 to a position $\xi_1 = \xi_0 + \Delta\xi$, a fraction of $P_\mathrm{Rev}(\Delta\xi)$ of the virtual wall segments are moving reversibly, whereas $1 - P_\mathrm{Rev}(\Delta\xi)$ perform irreversible Barkhausen jumps. Further, the area under the probability curve is corresponding to the average reversible distance of wall motion

$$\Delta\xi_\mathrm{Rev} = \int_0^{\Delta\xi} P_\mathrm{Rev}(x)\,\mathrm{d}x \tag{5.85}$$

$$\Delta\xi_\mathrm{Irr} = \Delta\xi - \Delta\xi_\mathrm{Rev} \quad . \tag{5.86}$$

Within the Poisson model, the maximum reversible distance of wall motion is limited by

$$d_\mathrm{Rev} = \Delta\xi_\mathrm{Rev,Max} = \int_0^{\infty} P_\mathrm{Rev}(x)\,\mathrm{d}x = \frac{1}{q_\mathrm{p}} \quad . \tag{5.87}$$

Reversal of Domain Wall Motion: For the domain wall motion process, a distribution function $P^{(+)}_\mathrm{Rev}(\Delta\xi)$ for movement in positive direction $\Delta\xi > 0$, and $P^{(-)}_\mathrm{Rev}(\Delta\xi)$ in negative direction $\Delta\xi < 0$ have to be considered. If the motion changes from positive to negative direction or vice versa, a so called *reversal point of domain wall motion* has been reached, and the corresponding probability distribution functions must be recalculated.

When the wall motion is reaching a reversal point (coming from positive direction) at distance $\Delta\xi_\mathrm{R}$, $P_\mathrm{R} = P^{(+)}_\mathrm{Rev}(\Delta\xi_\mathrm{R})$ wall segments are still in reversible motion (bowing, bending, etc.) and will be referred to *NJ (Not Jumped) segments*. After a wall motion reversal, these NJ segments can move back to their equilibrium position fully reversible $\Delta\xi^{(+)}_\mathrm{Rev,NJ}$ and then move reversible in the opposite direction up to the maximum distance $d^{(-)}_\mathrm{Rev,NJ}$ as

$$d^{(-)}_\mathrm{Rev,NJ,New} = \underbrace{\Delta\xi_\mathrm{R}\cdot P_\mathrm{R}}_{\Delta\xi^{(+)}_\mathrm{Rev,NJ}} + \underbrace{\int_0^{\infty} \min\left(P_\mathrm{R}, P^{(-)}_\mathrm{Rev}(x)\right)\,\mathrm{d}x}_{d^{(-)}_\mathrm{Rev,NJ}} \quad . \tag{5.88}$$

The remaining wall segments $1 - P^{(+)}_\mathrm{Rev}(\Delta\xi_\mathrm{R})$ have already performed one or more Barkhausen jumps during their motion to the reversal distance $\Delta\xi$, and are therefore referred to as *J (Jumped) segments*. After a wall motion reversal, these J segments can move back

reversible the distance $d^{(+)}_{\mathrm{Rev,J}}$ they had moved reversibly up to the reversal point and then move in the opposite direction up to the maximum distance $d^{(-)}_{\mathrm{Rev,J}}$ as

$$d^{(-)}_{\mathrm{Rev,J,New}} = \underbrace{\int_0^\infty \max\left(0, P^{(+)}_{\mathrm{Rev}}(x) - P_{\mathrm{R}}\right)\,\mathrm{d}x}_{d^{(+)}_{\mathrm{Rev,J}}} + \underbrace{\int_0^\infty \max\left(0, P^{(-)}_{\mathrm{Rev}}(x) - P_{\mathrm{R}})\right)\,\mathrm{d}x}_{d^{(-)}_{\mathrm{Rev,J}}} \quad . \tag{5.89}$$

However, the total maximum distance in the new direction of movement is

$$d^{(-)}_{\mathrm{Rev,New}} = d^{(-)}_{\mathrm{Rev,NJ,New}} + d^{(-)}_{\mathrm{Rev,J,New}} \leq \frac{2}{q_{\mathrm{p}}} \quad . \tag{5.90}$$

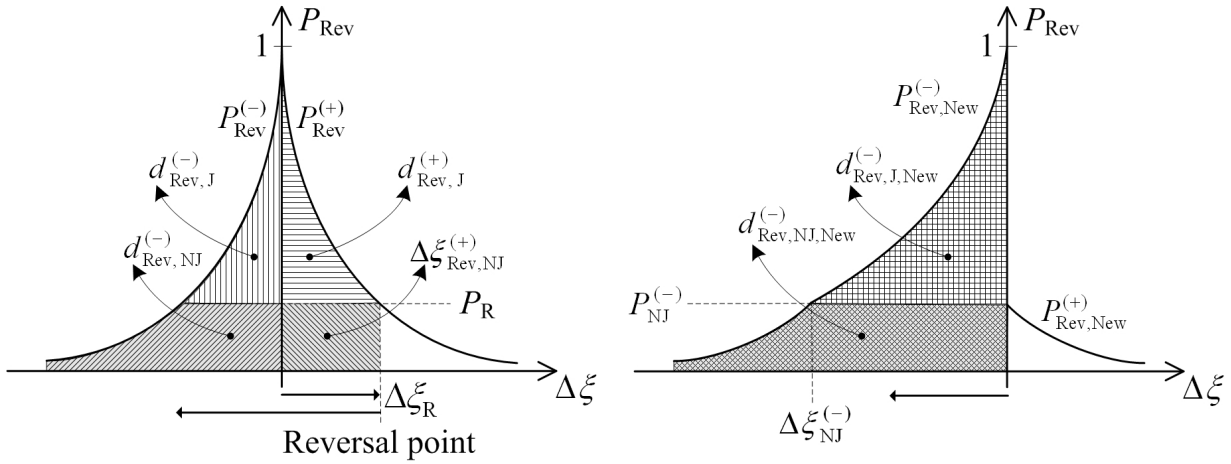

Figure 5.15: Modification of the probability for reversible domain wall motion at a reversal point.

In order to distinguish the characteristics of J and NJ segments, the reversible probability distribution has to be extended

$$P_{\mathrm{Rev}}(\Delta\xi) = \begin{cases} 1 & \text{for } \Delta\xi = 0 \\ \exp\left(-\frac{q_{\mathrm{p}}}{\kappa_{\mathrm{J}}}(|\Delta\xi| - x_{\mathrm{J}})\right) & \text{for } 0 < |\Delta\xi| \leq |\Delta\xi_{\mathrm{NJ}}| \\ \exp\left(-\frac{q_{\mathrm{p}}}{\kappa_{\mathrm{NJ}}}(|\Delta\xi| - x_{\mathrm{NJ}})\right) & \text{for } |\Delta\xi| > |\Delta\xi_{\mathrm{NJ}}| \end{cases} \quad . \tag{5.91}$$

The reversal factors

$$0 < \kappa_{\mathrm{J}}, \kappa_{\mathrm{NJ}} \leq 2 \tag{5.92}$$

are determined by the maximum reversible distances $d_{\mathrm{Rev,J}}$ and $d_{\mathrm{Rev,NJ}}$. The offset values x_{J} and x_{NJ} are dedicated to shift the probability curves, in order to guarantee continuity at $|\Delta\xi| = |\Delta\xi_{\mathrm{NJ}}|$

$$P_{\mathrm{NJ}} = P_{\mathrm{Rev}}(\Delta\xi_{\mathrm{NJ}}) = \exp\left(-\frac{q_{\mathrm{p}}}{\kappa_{\mathrm{J}}}(|\Delta\xi_{\mathrm{NJ}}| - x_{\mathrm{J}})\right) = \exp\left(-\frac{q_{\mathrm{p}}}{\kappa_{\mathrm{NJ}}}(|\Delta\xi| - x_{\mathrm{NJ}})\right) \quad . \tag{5.93}$$

Summing up, the probability for a reversible domain wall motion is described by two generalized exponential distributions according to (5.91) with the parameters

$$P^{(+)}_{\mathrm{Rev}}(\Delta\xi) \;:\quad \kappa^{(+)}_{\mathrm{J}}, x^{(+)}_{\mathrm{J}}, \kappa^{(+)}_{\mathrm{NJ}}, x^{(+)}_{\mathrm{NJ}}, \Delta\xi^{(+)}_{\mathrm{NJ}} \tag{5.94a}$$

$$P^{(-)}_{\mathrm{Rev}}(\Delta\xi) \;:\quad \kappa^{(-)}_{\mathrm{J}}, x^{(-)}_{\mathrm{J}}, \kappa^{(-)}_{\mathrm{NJ}}, x^{(-)}_{\mathrm{NJ}}, \Delta\xi^{(-)}_{\mathrm{NJ}} \quad . \tag{5.94b}$$

Starting at the demagnetized state

$$\begin{aligned} \kappa^{(+)}_{\mathrm{J}} &= \kappa^{(-)}_{\mathrm{J}} = 2.0 \qquad x^{(+)}_{\mathrm{J}} = x^{(-)}_{\mathrm{J}} = 0.0 \\ \kappa^{(+)}_{\mathrm{NJ}} &= \kappa^{(-)}_{\mathrm{NJ}} = 1.0 \qquad x^{(+)}_{\mathrm{NJ}} = x^{(-)}_{\mathrm{NJ}} = 0.0 \qquad \Delta\xi^{(+)}_{\mathrm{NJ}} = \Delta\xi^{(-)}_{\mathrm{NJ}} = 0.0 \quad , \end{aligned} \tag{5.95}$$

the parameters have to be updated at each reversal point of domain wall motion. More details on the calculation of the parameters is provided in appendix A.5.

Work Contributions due to Domain Wall Motion

Based on NEEL's work [65], the motion of a flexible domain wall in the presence of pinning sites is represented by an *equivalent rigid domain wall*, where the distance $\Delta\xi_{ij}$ of motion corresponds to the average distance of the flexible wall. Within this context, a domain wall is conceptually divided into many small sections, that can either move reversible or perform an irreversible Barkhausen jump.

The distinction between reversible and irreversible parts of the magnetization process is evident, and thus also treated within the Jiles-Atherton (4.4) hysteresis model, extensions of the Preisach model (4.3.2), as well as in literature, such as [14] or [4], for example.

Reversible Work: Starting from the demagnetized state or a reversal point, the domain wall can move reversibly by bowing or bending. Also a part of domain wall creation or annihilation is reversible in nature.

Assuming that $\Delta t^{(\mathrm{R})}$ are all simulation steps since the last reversal point (R),

$$\Delta v^{(\mathrm{R})}_{ij,\mathrm{Rev}} = \sum_{\Delta t^{(\mathrm{R})}} \Delta v_{ij,\mathrm{Rev}}(c_{ij}\,\Delta v_{ij}) \tag{5.96}$$

gives the reversible change in volume fraction since the last reversal point.

The reversible work increases disproportionate to the corresponding volume change since the last reversal point. For example, the reversible work due to domain processes since the last reversal point can be approximated as

$$\Delta w^{(\mathrm{R})}_{\mathrm{RevDWM}} = k_{\mathrm{RevDWM}} \sum_{i=1}^{N_{\mathcal{D}}} \sum_{j=1}^{N_{\mathcal{D}}} \frac{\left(1 + \left(\frac{\Delta v^{(\mathrm{R})}_{ij,\mathrm{Rev}}}{\Delta v_{\mathrm{REV}}}\right)^2\right)^{\frac{1}{2}} - 1}{\left(1 + \left(\frac{1}{\Delta v_{\mathrm{REV}}}\right)^2\right)^{\frac{1}{2}} - 1} \tfrac{1}{2}\left(1 - \cos(\bar{\varphi}_i - \bar{\varphi}_j)\right) \quad , \tag{5.97}$$

where k_{RevDWM} and Δv_{REV} are model parameters and the term $\frac{1}{2}\left(1 - \cos(\bar{\varphi}_i - \bar{\varphi}_j)\right)$ accounts for the difference in the orientation of the domain class magnetization. As sketched in Fig. 5.16, the term for the reversible work is based on the elongation of the flexible domain wall (surface) due to bowing.

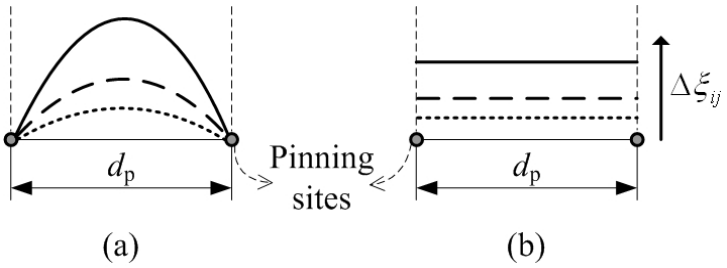

Figure 5.16: Simplified picture of a reversibly bowing domain wall (a) and the corresponding equivalent rigid wall (b) between two pinning sites.

Irreversible Losses: In general, domain wall motion is accompanied by local eddy currents and interactions with the crystal lattice (due to spin-orbit coupling), which both result in irreversible losses. Because the local eddy current losses induced by domain wall movement decrease with the film thickness (comparable to classical eddy current losses), the interactions with the crystal lattice become a dominant loss contribution in thin film material.

In a quasi-static treatment, irreversible domain wall losses arise during a Barkhausen jump, where a part of the wall moves with a finite velocity from one pinning site to the next one. Within a simplified picture, the fast local change of the magnetic moment interacts with the atoms near the pinning site via spin-orbit coupling mechanisms that causes local lattice oscillations and hence emission of phonons.

The irreversible part $\Delta v_{ij,\mathrm{Irr}}$ of the domain wall motion Δv_{ij} in the generalized EM is modeled as

$$\Delta v_{ij,\mathrm{Irr}} = \Delta v_{ij} - \Delta v_{ij,\mathrm{Rev}}(c_{ij}\,\Delta v_{ij}) \quad . \tag{5.98}$$

For a simulation step $t \mapsto t+\Delta t$, the increase in irreversible work due to domain wall motion (DWM) is proportional to the irreversibly changed volume fraction $\Delta v_{ij,\mathrm{Irr}}$

$$\Delta w_{\mathrm{IrrDWM}}|_{t\mapsto t+\Delta t} = k_{\mathrm{IrrDWM}} \sum_{i=1}^{N_\mathcal{D}} \sum_{j=1}^{N_\mathcal{D}} |\Delta v_{ij,\mathrm{Irr}}| \; \tfrac{1}{2}\left(1-\cos(\bar{\varphi}_i - \bar{\varphi}_j)\right) \quad , \tag{5.99}$$

where k_{IrrDWM} is a model parameter (loss coefficient) and the term $\frac{1}{2}\left(1-\cos(\bar{\varphi}_i - \bar{\varphi}_j)\right)$ accounts for the difference in the orientation of the domain class magnetization. For a 180° wall between domain class $\mathcal{D}_i$ and $\mathcal{D}_j$, an irreversible change in volumes $\Delta v_{ij,\mathrm{Irr}}$ generates losses of $k_{\mathrm{IrrDWM}}\,|\Delta v_{ij,\mathrm{Irr}}|$.

Conclusion

Although, the work due to reversible and irreversible domain wall processes have been derived based on the picture of a moving flexible domain wall, it should be kept in mind that the results are of phenomenological nature. The corresponding equations reproduce the macroscopic magnetization process to a greater or lesser extent, depending on the material. But nevertheless, the relation to the domain wall motion can be helpful for the interpretation of the identified model parameters.

5.3 Calculation Procedure

In the previous sections, the concept of statistical domain classes and the involved energy terms have been defined for the generalized EM. Based on this framework, the practical model setup and calculation procedure is summarized.

The basic objective of the generalized EM is to calculate the sample magnetization $\vec{M}$ or the component in field direction M_{H} dependent on an applied field $\vec{H}$ (or an external stress $\vec{\sigma}_{\mathrm{Stress}}$) within a two-dimensional framework. Currently, the generalized EM is formulated for a quasi-static magnetization process, in case of dynamic hysteresis, the model has to be extended in order to account for magnetization lag and additional losses.

5.3.1 Model Setup

As a primary requirement, the *number of statistical domain classes* $N_{\mathcal{D}}$ to be modeled has to be defined. In the majority of cases, this is an even number, because every domain class has a counterpart with an antiparallel orientation of the magnetization in the demagnetized ground state. But the more domain classes are defined, the higher is the number of model variables, and the longer is the calculation time. Generally speaking, it is recommended to start with a small set of domain classes and, if necessary, add further ones in order to refine the results or consider additional issues.

Model Variables

Every statistical domain class $\mathcal{D}_i$ is described by the following model variables:

- Volume fraction v_i of $\mathcal{D}_i$
  - The volume fractions are calculated by a minimization of all local and non-local energy terms together. A detailed description of the optimization problem is provided in the following subsection.
- Mean orientation $\bar{\varphi}_i$ of magnetic entities within $\mathcal{D}_i$
  - The mean orientation of the magnetic entities results from a minimization of the local energy terms, calculated for each domain class individually.
  - It is also possible to predefine the mean orientation exogenously for some domain classes. This can be helpful, when modeling closure domains or spike domains around inclusions or cavities, for example. The share of such domain classes in total sample magnetization is then controlled via the volume fractions, i.e. the size of the closure domains.
- Variance σ_i^2 of the orientation of the magnetic entities within $\mathcal{D}_i$
  - The variance of the orientation of the magnetic entities can be a result from a minimization of local energy terms, calculated for each domain class individually.
  - If one is interested in modeling the temperature behavior of the magnetic material, then the variance will be determined by the competition between thermal agitation and exchange energy.

  - When the variance is intended to represent disalignment around inhomogeneities, an additional local energy term (counterbalanced by the magnetic field energy) can be included or the variance can be provided exogenously to the EM.

Model Parameters

Basically, the following model parameters have to be defined, if the corresponding energy terms are included in the model setup:

- Structural model parameters
  - Number of statistical domain classes $N_{\mathcal{D}}$
  - Domain classes with fixed (non-calculated) mean orientation $\bar{\varphi}_i$
  - Domain classes with fixed (non-calculated) angular variances σ_i^2
- Geometrical parameters
  - Sample (thin film) thickness d_{S}
  - Characteristic sample length l_{S}
  - Two-dimensional demagnetization tensor $\tilde{N}_{\mathrm{d,2D}}$
- Physical model parameters for local energy terms
  - Saturation magnetization $\mu_0 M_{\mathrm{s}}$
  - Uniaxial anisotropy constant K_1 and angle of easy axis φ_{Aniso} with respect to x-axis
  - Isotropic magnetostriction constant λ_{s}
  - Number of magnetic entities per unit volume $\eta = n_{\mathcal{V}}/V$
  - Number of nearest neighbors ν_{NN}
  - Exchange constant J_{Ex}
- Phenomenological parameters for non-local energy terms
  - Initial volume fractions in the demagnetized state $v_{0,i}$
  - Maximum volume fractions $v_{\mathrm{max},i}$
  - Coefficient for reversible anhysteretic energy k_{RevAnh}
  - Domain wall motion factor c_{ij}
  - Average number of Barkhausen jumps per distance of domain wall motion q_{p}
  - Coefficient for work due to reversible domain wall motion k_{RevDWM}
  - Parameter for reversible domain wall motion Δv_{REV}
  - Coefficient for losses due to irreversible domain wall motion k_{IrrDWM}

Contrary to other hysteresis models, the generalized EM is flexible in its structure. But therefore some a-priori knowledge of the material sample and a basic idea of the relevant mechanisms that govern the magnetization process are necessary.

5.3.2 Calculation of the Model Variables

Energy Terms

In the current formulation of the generalized EM the following energy terms or work terms are included:

- Local energy $w_{\mathrm{Loc}}(v_i, \bar{\varphi}_i, \sigma_i^2 | \vec{H}, \vec{\sigma}_{\mathrm{Stress}}, T)$ according to (5.55) and (5.56)
  - Applied field energy $w_{\mathrm{H},i}(\bar{\varphi}_i, \sigma_i^2 | \vec{H})$ (5.41)
  - Anisotropy energy $w_{\mathrm{Aniso},i}(\bar{\varphi}_i, \sigma_i^2)$ (5.44)
  - Magneto-elastic energy with non-magnetic stress $w_{\mathrm{Stress},i}(\bar{\varphi}_i, \sigma_i^2 | \vec{\sigma}_{\mathrm{Stress}})$ (5.46)
  - Thermal excitations - internal entropy $w_{\mathrm{T},i}(\sigma_i^2 | T)$ (5.49) and (5.50)
  - Exchange energy within a domain class $w_{\mathrm{Ex},i}(\sigma_i^2)$ (5.54b)
- Non-local energy
  - Demagnetizing energy $w_{\mathrm{d}}(v_i | \bar{\varphi}_i, \sigma_i^2)$ (5.58)
  - Reversible anhysteretic energy $w_{\mathrm{RevAnh}}(v_i)$ (5.70)
- Reversible and irreversible work
  - Reversible work due to domain wall motion $\Delta w^{(\mathrm{R})}_{\mathrm{RevDWM}}(\Delta v^{(\mathrm{R})}_{ij,\mathrm{Rev}})$ (5.97)
  - Irreversible losses due to domain wall motion $\Delta w_{\mathrm{IrrDWM}}(\Delta v_{ij,\mathrm{Irr}})$ (5.99)

Calculation of the Mean Orientation and the Variance of Magnetic Entities

In general, the mean orientation $\bar{\varphi}_i$ and the variance σ_i^2 of the magnetic entities can be calculated for each domain class $\mathcal{D}_i$ individually by minimization of the local energy terms. As shown in Fig. 5.17, for a given applied field $\vec{H}$, applied stress $\vec{\sigma}_{\mathrm{Stress}}$, and temperature T the minimization of the local energy $w_{\mathrm{Loc},i}$ of domain class $\mathcal{D}_i$ yields

$$\bar{\varphi}_i, \sigma_i^2 : \quad \min_{\bar{\varphi}_i, \sigma_i^2} \left\{ w_{\mathrm{Loc},i}(\bar{\varphi}_i, \sigma_i^2) \right\} \quad \text{s.t.} \quad \bar{\varphi}_i \in (-\pi, \pi] \text{ and } \sigma_i^2 \geq 0 \quad . \tag{5.100}$$

As stated in 3.3.2, the mean orientation $\bar{\varphi}_i$ might perform an irreversible jump due to coherent rotation of domain class magnetization when changing the applied field $\vec{H}$. As a consequence, the optimizer must be able to handle such jumps.

Due to the fact that the domain class magnetization $|\vec{m}_i|$ is proportional to $\exp(-\sigma_i^2/2)$ (see Tab. 5.1), it makes sense to optimize the variance in a logarithmic scale and limit it by $\sigma_i^2 < (2\pi \text{ rad})^2$ for $2.7\,10^{-9} \leq |\vec{m}_i| \leq 1.0$.

Calculation of the Volume Fractions of the Statistical Domain Classes

First of all, the path-dependency of magnetic hysteresis is represented by reversible and irreversible work due to domain wall motion. So the history of the magnetization process is stored at any reversal point (R) of domain wall motion as the probability function $P^{(\mathrm{R})}_{\mathrm{Rev}}(.)$ for reversible domain wall motion.

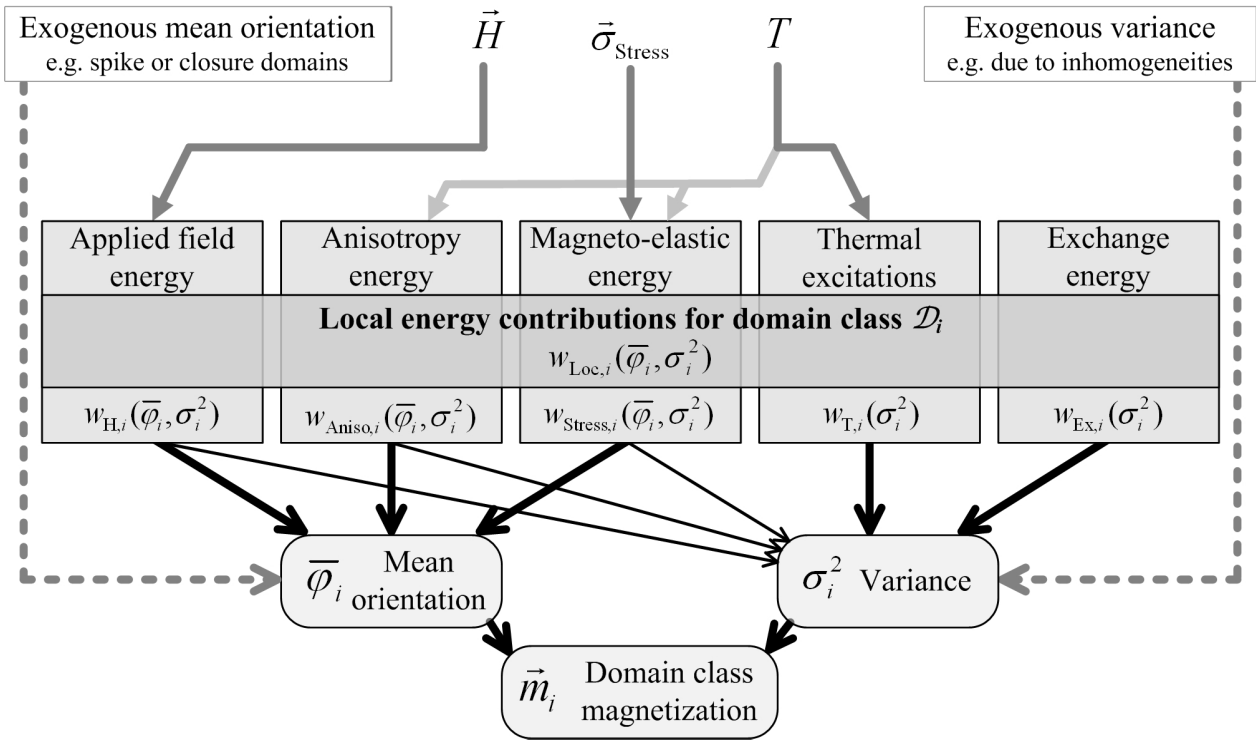

Figure 5.17: Calculation of the mean orientation $\bar{\varphi}_i$ and the variance σ_i^2 of the directional distribution of magnetic entities in a domain class $\mathcal{D}_i$ by minimizing the local energy terms.

Demagnetized State as Starting Point of Calculation: In the demagnetized state most of the local energy terms are zero, the mean orientation $\bar{\varphi}_i$ and the variance σ_i^2 of the magnetic entities are calculated by minimizing the remaining local energy terms according to (5.61).

The configuration of domain classes (i.e. the volume fractions v_i) in the demagnetized state is given as model parameter by an a-priori assumption of the initial volume fractions $v_{0,i}$.

Further, the demagnetized state is defined as the first reversal point for all domain wall motion processes. The parameters of the probability function $P_{\text{Rev}}^{(\text{R})}(.)$ for reversible domain wall motion are chosen according to (5.95).

Energy Minimization: In principle, the volume fractions v_i are determined by a minimization of the total energy as

$$v_i \quad : \quad \min_{v_i} \left\{ w_{\text{Loc}} + w_{\text{d}} + w_{\text{RevAnh}} + \Delta w_{\text{RevDWM}}^{(\text{R})} + \Delta w_{\text{IrrDWM}} \right\} \tag{5.101}$$

$$\text{s.t.} \quad : \quad v_i \in [0, v_{\max,i}] \qquad \text{and} \qquad \sum_{i=1}^{N_{\mathcal{D}}} v_i = 1 \quad ,$$

for given mean orientation $\bar{\varphi}_i$ and the variance σ_i^2 of the magnetic entities. Hence, for a model with $N_{\mathcal{D}}$ statistical domain classes, an optimization problem with $N_{\mathcal{D}} - 1$ independent variables result.

The general EM calculation procedure for a certain iterative step is sketched in Fig. 5.18.

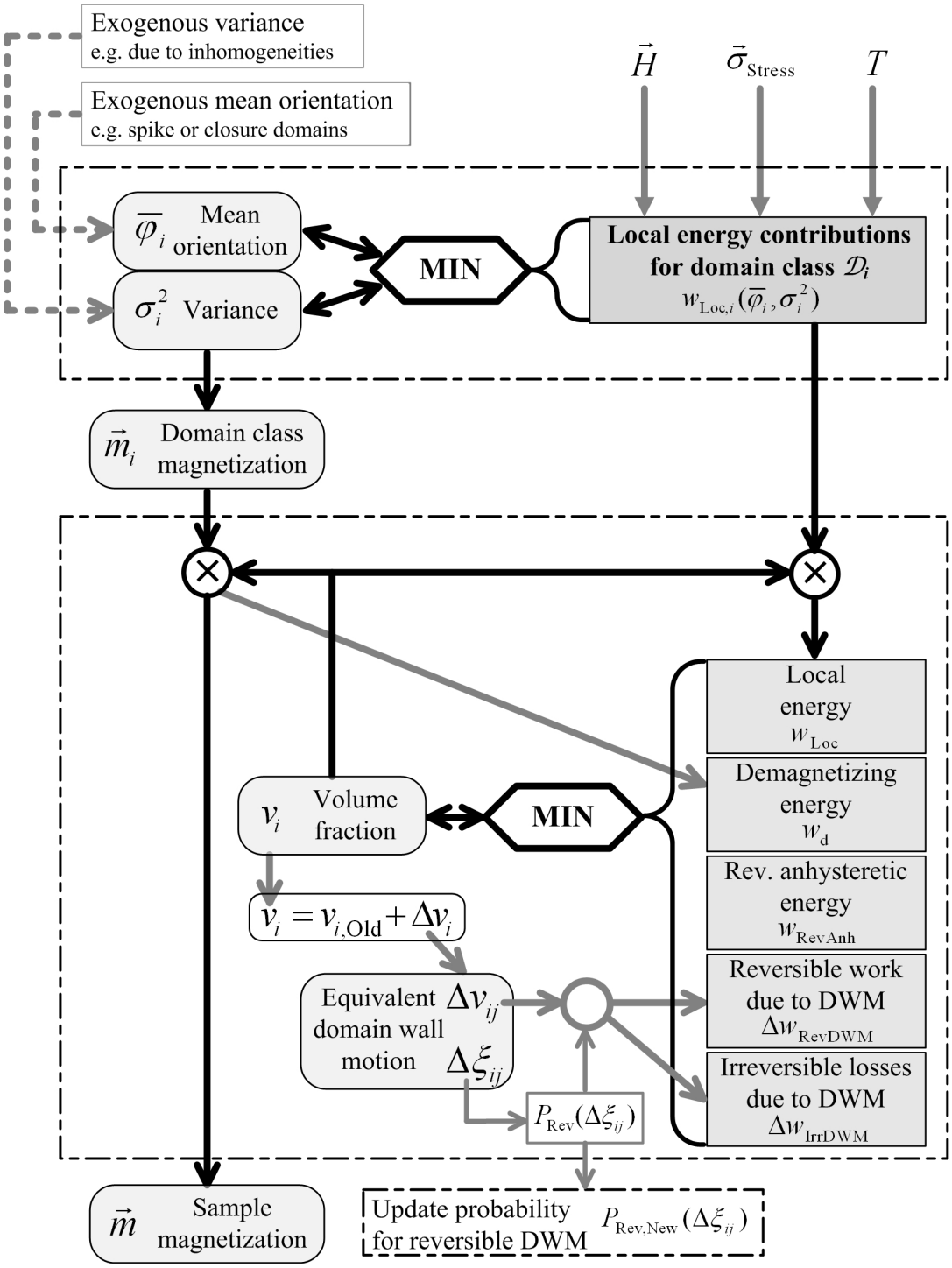

Figure 5.18: Schematic overview of a single EM calculation step.

Local Minima on the Energy Surface and Appropriate Solver

Due to the different nature of the energy terms involved, the resulting energy surface (total energy dependent in the volume space $\{v_1, v_2, ..., v_{N_\mathcal{D}}\}$) consists of many local minima, which is typical for magnetic hysteresis problems. Even in the quasi-static regime, the magnetic system is usually in a state corresponding to a local minimum of free energy. This is an important fact, because the magnetic system, being in a defined state, cannot reach the state of global energy minimum (in a finite time span), if there is an energy barrier in between. This has to considered, when calculating the volume fractions. So, the solver must not calculate the global energy minimum of (5.101). Assuming that for an applied field $\vec{H}$ the domain class configuration $\{v_1, ..., v_{N_\mathcal{D}}\}$ has been determined in simulation step t

$$\left[\begin{array}{c} \vec{H} \\ \{v_1, ..., v_{N_\mathcal{D}}\} \end{array} \right]_t \mapsto \left[\begin{array}{c} \vec{H} + \overrightarrow{\Delta H} \\ \{v_1 + \Delta v_1, ..., v_{N_\mathcal{D}} + \Delta v_{N_\mathcal{D}}\} \end{array} \right]_{t+\Delta t} , \tag{5.102}$$

then for a change in the applied field of $\overrightarrow{\Delta H}$, the new metastable domain class configuration $\{v_1 + \Delta v_1, ..., v_{N_\mathcal{D}} + \Delta v_{N_\mathcal{D}}\}$ has to be searched starting from the old configuration by following the path of minimum energy. Most of the standard solver are not able to perform this path-search along local minima, so an appropriate search algorithm has been developed in order to capture this problem.

5.4 Summary

In this chapter a generalized two-dimensional energetic model of ferromagnetic hysteresis is presented. Elementary magnetic entities that act as basis source of magnetic moment are aggregated to statistical domain classes, where their directional orientation is described by a statistical distribution function. Using a wrapped normal distribution, the magnetization and the local energy terms for a domain class can be formulated as an algebraic expression. The parameters of this wrapped normal distribution (mean orientation and variance) are calculated by minimizing the sum of the local energy terms for each domain class individually.

In order to describe the non-dissipative macroscopic magnetization process, a reversible anhysteretic energy term has been introduced. It accounts for the fact that (magnetic) order decreases entropy and thus reduces the free energy. So, it comprises all physical energy terms, which are not considered explicitly in the model. Starting point of modeling is the demagnetized state, as the magnetic "ground state", where the configuration of domain classes is defined as model parameter.

Dissipative processes that give rise to the hysteretic behavior are considered by reversible and irreversible work due to domain wall motion. Because of the statistical treatment, the exact information of domain wall motion can only be roughly approximated based on the volume change of the statistical domain classes. A probability function for reversible domain wall motion is adapted in every reversal point. Based on this probability, reversible and irreversible work are calculated. However, even if the process of a moving flexible domain wall seems to be an appropriate picture for the expressions of reversible and irreversible work, these terms phenomenologically summarize all reversible and irreversible mechanisms caused by a change of domain class configuration during the macroscopic magnetization process.

The presented generalized energetic model is not restricted to the energy terms described within this work. Depending on the problem to be modeled some energy terms can be omitted and new energy terms introduced. Similarly, the expression for the reversible anhysteretic energy can be calculated based on another statistic. But this flexibility requires at least a qualitative a-priori knowledge of the underlying mechanisms that govern the magnetization process of the material to be modeled.

Part III

Simulation and Evaluation

In the *sixth chapter* the evaluation of the generalized Energetic Model on the example of Permalloy thin film material is presented. After a brief survey of the magnetic properties and the production process of the Permalloy thin films used for anisotropic magneto-resistive sensors, the magneto-optical Kerr measurement setup is explained.

The major part in this chapter is dedicated to a comparison of measurement data and simulation results based on magnetization curves. In a first step, the hysteresis loops for an arbitrary direction of the applied field with respect to the easy anisotropy axis are evaluated based on one sample. Second, the relation between model parameters and microstructural properties of the thin film is presented by comparing samples that differ in the technological parameters of the production process. Third, the ability of the generalized Energetic model to predict the temperature behavior from the first principles by the competition of thermal excitations and exchange mechanisms is evaluated on the example of thin and ultra thin film material based on measurement data from literature.

Chapter 6

Model Evaluation on Permalloy Thin Films

After the theoretical introduction of the generalized Energetic Model in chapter 5, the model is used to describe the magnetization curves of Permalloy thin films of 50 nm thickness. The thin film samples presented within this work have been produced and investigated at Vienna University of Technology by graduate students, and the results have been published in the diploma theses of [2], [45], [52], and [81]. These films are the basis for anisotropic magneto-resistive (AMR) sensors and therefore designed that the magnetization process in mainly driven by coherent magnetization rotation.

Within the first section, some basic information about the thin film material characteristics, the sputter process and the magneto-optical Kerr measurement is provided. Based on the material properties, the setup of the generalized EM for thin films with coherent magnetization rotation is defined. In a first analysis, it is investigated how the magnetization curves changes, when the measurement is performed several degrees deviating from the hard axis direction. Second, the influence of technological process parameters on the hard axis magnetization curves is exemplarily demonstrated such that the model configuration together with the model parameters allow to qualify the microstructure of the thin film. Finally, the temperature dependence of the spontaneous magnetization is described by the generalized EM and compared to measurement data of ultrathin Permalloy films taken from literature.

6.1 Production, Material Properties, and Measurement

6.1.1 Thin Film Production by Cathodic Sputtering

Vacuum evaporation, electrodeposition, and cathodic sputtering are the most common techniques for preparing magnetic thin films. Since the thin film samples used as reference for the evaluation of the generalized EM have been produced by cathodic sputtering, this deposition technique is introduced within the following paragraphs.

Basic Principle of the Triode Sputtering System

The triode sputtering system used for the thin film production is sketched in Fig. 6.1, where the arrangement of the main components can be seen.

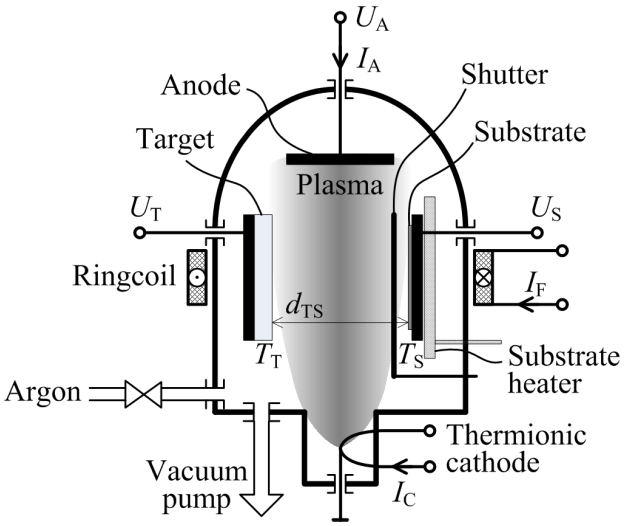

Figure 6.1: Principle and main components of a triode sputter system.

Beginning at the thermionic cathode, a water-cooled tungsten filament is heated up by a DC current, so that the thermal energy allows the electrons to leave the metallic bond. Thus, the number of emitted electrons depends on the filament temperature and is controlled by the cathode current I_C.

If there is a voltage applied between this thermionic cathode and the anode on the opposite site of the vacuum chamber, the corresponding electric field effects a force on the free electrons and accelerates them towards the positive charged electrode.

After evacuation (10^{-5} - 10^{-6} Pa via turbomolecular pump), the sputter chamber is filled with an inert gas, such as Argon, up to a certain pressure p_{Ar}, so that the electrons from the thermionic cathode ionize the Ar atoms by bouncing out an electron of the outer electron shell of the Ar atom. Hence, an Ar plasma with positive charged Ar ions is generated between cathode and anode. The plasma can be focused (in order to increase the plasma density) between target and substrate by a magnetic field of the surrounding ring coil.

Because the Permalloy target is on a negative electrostatic potential, the Ar ions accelerate towards this target. When hitting the surface of the target, the kinetic energy of the Ar ions is partly transferred to inelastic effects (such as emission of photons, X-rays or secondary electrons) and partly used to knock out particles from the target material. These sputtered Permalloy particles condense on the substrate opposite (in a distance d_{TS} between target and substrate) and forming the thin film. So, after exceeding a certain energy threshold, the sputtering yield (= number of sputtered atoms per incident Ar ion) increases with the energy of the Ar ions that is controlled by the target voltage U_T. The target temperature T_T can be increased by so called blind-sputtering before opening the shutter and starting the actual sputter process.

In general, the substrate is also on a small negative electrostatic potential (substrate voltage U_S), so that Ar ions are accelerated towards the substrate, but with a small amount of kinetic

energy, which is just enough to avoid gas inclusions and impurities on the thin film surface. The substrate temperature T_S can be controlled by a heater. For the samples investigated within this work, passivated silicon (Si-SiO_2) is used as substrate material. The magnetic field of the ring coil effects a preferred magnetic orientation of the sputtered Permalloy particles, leading to an induced anisotropy of the thin film.

Technological Process Parameters

Beside the materials for the target and the substrate, the technological parameters given in Tab. 6.1 influence the properties of the produced thin films.

Parameter	Symbol	Typical values
Target-substrate distance	d_{TS}	35 - 60 mm
Anode current	I_A	3 - 4 A
Thermionic cathode current	I_C	40 - 50 A
Field current	I_F	3 - 10 A
Argon pressure	p_{Ar}	1 - 10 Pa
Substrate temperature	T_S	40 - 300 °C
Anode voltage	U_A	40 - 60 V
Substrate voltage	U_S	-60 - 0 V
Target voltage	U_T	-(900 - 800) V

Table 6.1: Typical parameters of the sputtering process.

6.1.2 Basic Properties of Permalloy Thin Films

Before describing the characteristics of Permalloy thin films, some key facts about the bulk material are summarized.

Properties of Permalloy Bulk Material

Iron-Nickel Alloys: The *phase diagram* of the binary iron-nickel alloy system has been investigated for several decades up to present [13]. Particularly, the low temperature phases are difficult to identify, because of the slow diffusion process between Fe and Ni a stable equilibrium state is hard to reach for temperatures below 300°C. For temperatures below 200°C, it has been estimated [89] that it would last some 100 millions of years to reach the equilibrium.

However, the most important ferromagnetic materials can be found in the range of high Ni-content. Besides the bcc (A2) solid solutions of α-Fe at low temperatures and δ-Fe at high temperatures, the γ-(Fe,Ni) solution with fcc (A1) structure dominates the phase diagram according to Fig. 6.2. For a Ni-content around 75%, an fcc ($L1_2$) ordered $FeNi_3$ superstructure (of $AuCu_3$ type) is formed, where the Fe-atoms are located in the corners and the Ni-atoms are placed in the face center of the unit cube.

Depending on temperature and Ni-content, the *lattice constant* ranges between 2.86 - 2.88 Å for the α-phase and 3.52 - 3.60 Å for the γ-phase.

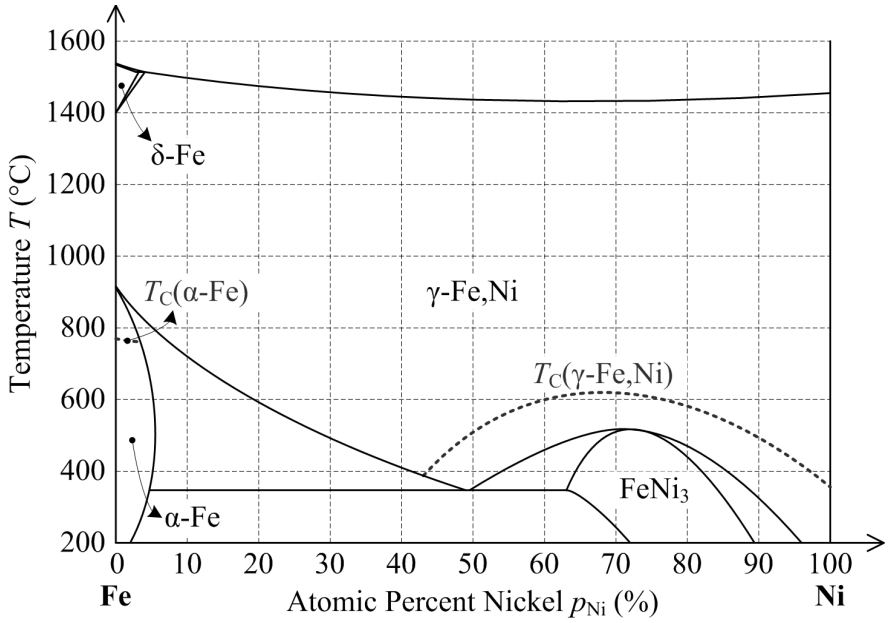

Figure 6.2: Phase diagram for the binary iron-nickel alloy system (from [59]).

Origin of the Name Permalloy: At the beginning of the 20th century, GUSTAV W. ELMEN discovered that heat-treated FeNi alloys with a dominant Ni content have excellent magnetic properties related to other soft-magnetic materials known at that time. In 1923, ELMEN and ARNOLD introduced [19] the name "Permalloy" for alloys of approximately 80% nickel and 20% iron. Since they worked as engineers at the *Western Electrical Company* (a part of the *Bell Company*), Permalloy became a trademark and has been commercially used in transformers and relays for telephone applications.

Sometimes, the name "Permalloy" (Py) is loosely applied to iron-nickel alloys (e.g. $Fe_{35}Ni_{65}$ is termed as 65 Permalloy) in a broader sense, whereas it is usually related to iron-nickel alloys with approximately 80% nickel content in the classical meaning.

The Permalloy Problem: Usually it is expected that magnetic properties of soft-magnetic alloys become improved after slow cooling or annealing. But in case of Permalloy, slow cooling and annealing at low temperatures decreases the permeability significantly. Just quenching from high temperatures gives the desired high permeability. This discrepancy is addressed as "Permalloy problem" and has been intensively investigated from 1930 up to 1960. The main result [51] is, that the magnetic properties of Permalloy are closely related to the crystal structure. When quenching from high temperatures ($> 600°C$), the disordered state with random occupation of the lattice sites by Fe and Ni atoms retains, whereas a slow cooling process leads to the formation of the ordered $FeNi_3$ superstructure. The local directional ordering of the superstructure causes an induced magnetic anisotropy that lowers the permeability of the material drastically. CHIKAZUMI [15] explained the induced anisotropy during annealing by ordering of Fe-Fe, Ni-Ni, and Fe-Ni atom pairs that depends on the difference of bond lenght[1] and the pseudo-dipole interaction between the pairs.

[1]Based on the different bond lengths, the configuration of atom-pairs during annealing is chosen such that the magnetoelastic energy becomes small.

General Data of Bulk Permalloy: In Tab. 6.2 typical values for some material parameters of bulk Permalloy ($Fe_{19}Ni_{81}$) are compared to the values of pure iron and nickel.

Parameter	**Symbol**	**Fe**	**$Fe_{19}Ni_{81}$**	**Ni**	**Unit**
Crystal structure		A2 bcc	A1 fcc $L1_2$ fcc	A1 fcc	
Lattice constant	a	2.866	3.524	3.524	Å
Mass density	ρ	7874	8715	8908	kg/m^3
Curie temperature	T_C	1044	843	628	K
Max. magnetic moment	$\mathfrak{m}_{J,z}$	2.22	1.02	0.62	μ_B/atom
Orbital moment	$\mathfrak{m}_{L,z}$	0.08		0.06	μ_B/atom
Spin moment	$\mathfrak{m}_{S,z}$	2.14		0.56	μ_B/atom
Saturation polarization (0 K)	$\mu_0 M_{s,0}$	2.15	1.04	0.61	T
Exchange integral	J_{Ex}	$1.50{\cdot}10^{-19}$	$1.60{\cdot}10^{-19}$	$1.62{\cdot}10^{-19}$	J
Exchange constant	A_{Ex}	$2.1{\cdot}10^{-11}$	$1.3{\cdot}10^{-11}$	$0.8{\cdot}10^{-11}$	J/m
Anisotropy constant	K_1	48000	1000	-5000	J/m^3
	K_2	-10000		-2000	J/m^3
Magnetostriction constant	λ_s	$-7{\cdot}10^{-6}$	$2{\cdot}10^{-6}$	$-35{\cdot}10^{-6}$	
	λ_{100}	$15{\cdot}10^{-6}$		$-51{\cdot}10^{-6}$	
	λ_{111}	$-21{\cdot}10^{-6}$		$-24{\cdot}10^{-6}$	

Table 6.2: Typical material parameters for bulk Permalloy in comparison to iron and nickel (from [16]).

Domain Theory of Permalloy Thin Films

The theory of magnetic domains in (polycrystalline) thin films is presented in the book of Hubert and Schaefer [42] in excellent detail, so that in the following paragraphs only the main issues are summarized.

Definition of a Thin Film: In general, a magnetic material is termed as *film*, if the thickness is below or at least comparable to the Bloch wall width. For Permalloy, the characteristic domain wall width is according to (3.32)

$$l_{\mathrm{Wall}} = \sqrt{\frac{A_{\mathrm{Ex}}}{K_{\mathrm{Aniso}}}} = \sqrt{\frac{1.3 \cdot 10^{-11}\mathrm{J/m}}{100\ \mathrm{J/m^3}}} = 360\ \mathrm{nm} \tag{6.1}$$

and the Bloch wall width (3.33) is

$$l_{\mathrm{Bloch}} = \pi\, l_{\mathrm{Wall}} = 1100\ \mathrm{nm} \quad . \tag{6.2}$$

Magnetic films with a thickness below the transition between Néel and Bloch wall

$$l_{\mathrm{NeelBloch}} \approx 20\, l_{\mathrm{Ex}} = 20\sqrt{\frac{A_{\mathrm{Ex}}}{K_{\mathrm{Stray}}}} = 20\sqrt{\frac{1.3 \cdot 10^{-11}\mathrm{J/m}}{4.0 \cdot 10^{5}\ \mathrm{J/m^3}}} = 114\ \mathrm{nm} \tag{6.3}$$

with the stray field energy coefficient (3.17)

$$K_{\mathrm{Stray}} = \tfrac{1}{2}\mu_0 M_{\mathrm{s}}^2 = \frac{1}{2\mu_0}(1\ \mathrm{T})^2 \approx 4.0 \cdot 10^5\ \mathrm{J/m^3} \tag{6.4}$$

are called *thin films*.

Domain Walls: Further, the analysis is limited to thin films with uniaxial *in-plane anisotropy*, so that the domain magnetization is aligned parallel to the surface of the film. Basically, in thin films the influence of the domain walls on the magnetization process is much stronger than in bulk material. In order to avoid the stray field energy caused by the magnetic poles on the surface of the film as a consequence of the magnetic dipole rotation in a Bloch wall, *Néel walls* are preferred with decreasing thickness.

In general, the preferred type of domain wall for the hard-axis magnetization process depends on the film thickness and on the applied field, as depicted in Fig. 6.3.

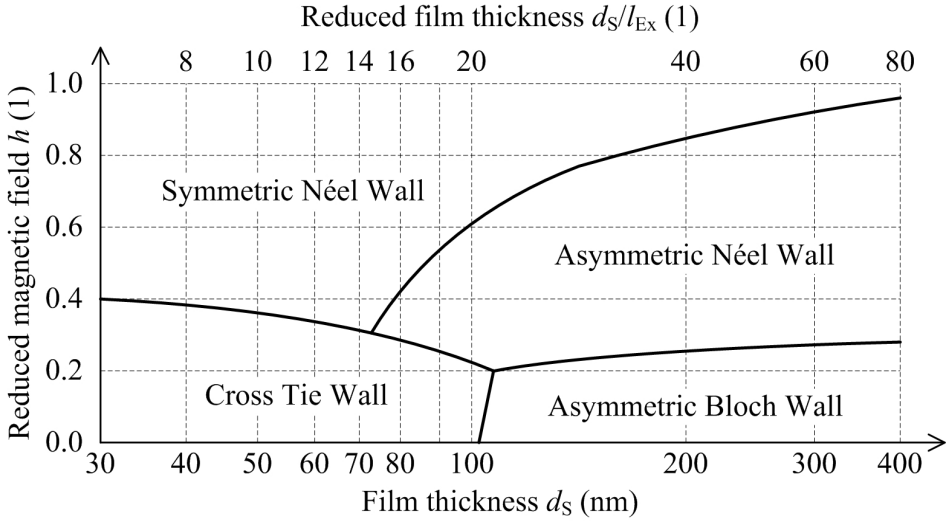

Figure 6.3: Preferred domain wall types dependent on the film thickness and the hard axis field (from [42]).

When applying a magnetic field $H_\perp$ in plane, perpendicular to the easy anisotropy axis, the magnetization of the domains rotate into the field direction according to the Stoner-Wohlfarth model. Hence, for this reduced field

$$h_\perp \ = H_\perp \frac{\mu_0 M_{\mathrm{s}}}{2K_1} \quad , \tag{6.5}$$

the domain magnetization angle according to Stoner-Wohlfarth is

$$\varphi_{\mathrm{M1,2}} = \frac{\pi}{2} \pm \arccos(h_\perp) \quad , \tag{6.6}$$

so that the domain wall angle results as

$$\varphi_{\mathrm{Wall}} = |\varphi_{\mathrm{M1}} - \varphi_{\mathrm{M2}}| = 2\arccos(h_\perp) \quad . \tag{6.7}$$

Thus, the decreasing wall angle with increasing hard axis field leads to transitions between different types of domain walls during the hard axis magnetization process.

Beside the classical (symmetric) Néel walls, so called *cross-tie walls* are formed at low applied fields. As shown in Fig. 6.4, a 180° rotation of magnetic dipoles is performed by a combination of 90° Néel walls in form of a cross. The resulting Bloch lines point into the direction perpendicular to film surface and thus lead to local magnetic poles on the thin film surface. The motion of such a cross-tie wall is impeded by pinning of the Bloch lines, particularly related to irregularities in the thin film surface or in the interface to the substrate.

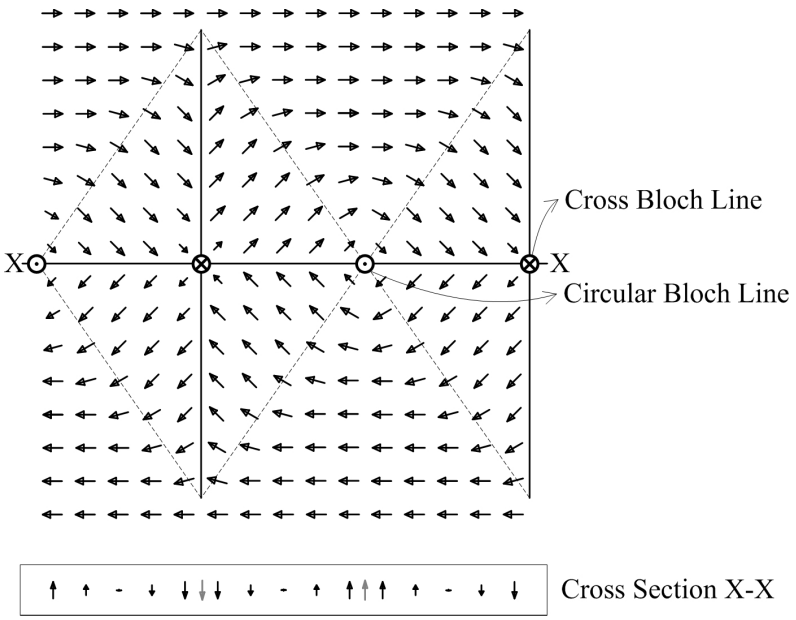

Figure 6.4: Schematic distribution of magnetic dipols for a cross-tie wall.

Magnetization Ripple and Dispersion: When describing the magnetization process of polycrystalline thin films, the (irregular) granular nature of the material has to be considered. So, the anisotropy within the grains can be statistically distributed and the interactions between individual grains have to be accounted. Further, the long-range stray field interactions due to the tails of the Néel walls and cross-tie walls cause an inter-coupling.

In low anisotropy polycrystalline thin films, a so called *ripple structure* can result, where the local magnetization is varying along a direction parallel to the total sample magnetization. This ripple phenomenon is also referred to as *magnetization dispersion* with respect to the average magnetization. Hoffmann [41] has derived the ripple structure as a consequence of anisotropy dispersion by means of variational calculus. However, even for applied magnetic fields (along the hard axis) beyond the anisotropy field this ripple structure is still present.

The long-range interaction between the domain walls can give rise to metastable *blocked domain states* that results in a remanence in the hard axis magnetization curves.

6.1.3 Magneto-Optical Kerr Measurement

For the determination of the magnetization curves of the thin film samples a magneto-optical Kerr measurement system is used. In case of magnetic thin films with in-plane anisotropy where the domain size is far beyond the film thickness, it can be assumed that the local magnetization near the surface is established throughout the whole thickness of the film. Combined with the high reflectivity of the sputtered films, magneto-optical techniques are a proper tool for measuring the magnetization curves.

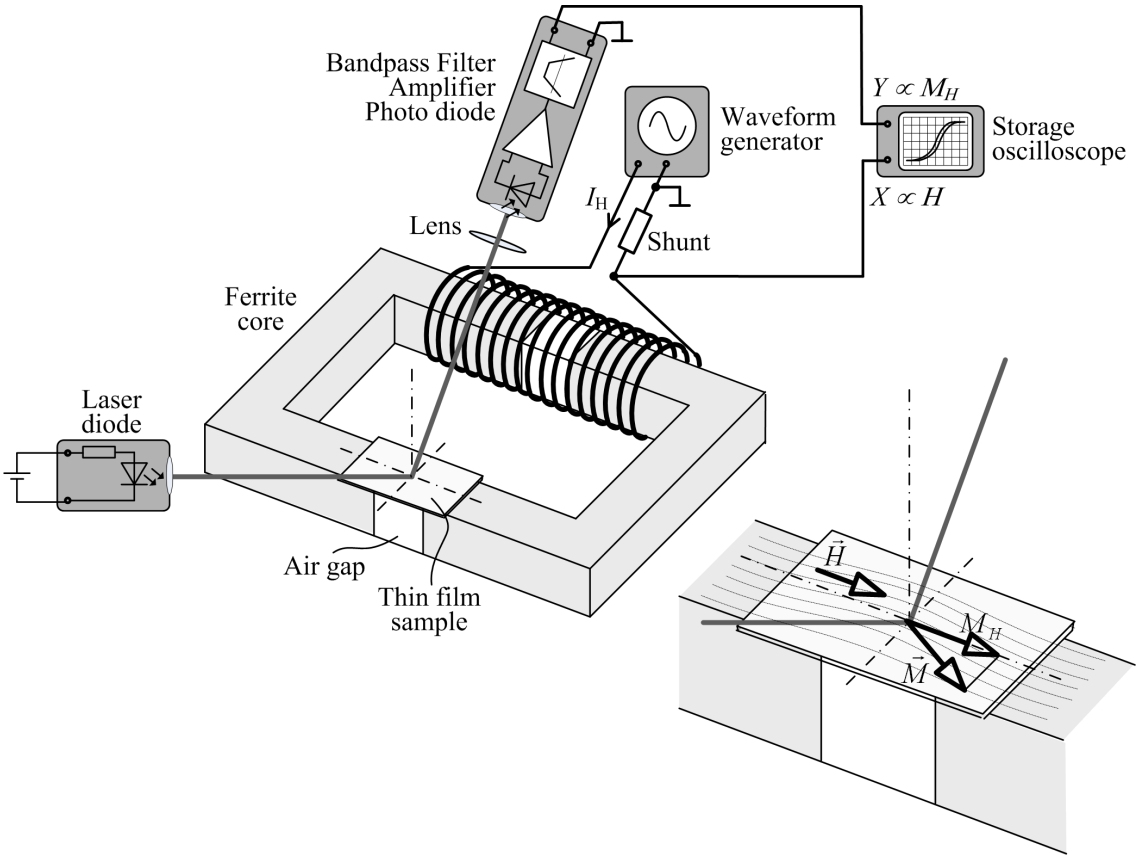

Figure 6.5: Basic principle of the magneto-optical Kerr measurement system.

Magnetic Part of the Measurement System

The magnetic field is provided by a split *ferrite core* with two air gaps of 4 mm, where one part of the core is equipped with a *coil*. The thin film sample is placed on the air gap, as sketched in Fig. 6.5, so that the stray field can be used for the characterization of the magnetization process. Due to the small thickness of the wafer (substrate and sputtered film have a thickness of about 0.4 mm in total), the homogeneity of the magnetic field in the center of the air gap is sufficient, particularly in the region of the incident laser beam. The coil is connected to an AC voltage supply, which provides a sinusoidal voltage of 200 Hz. This frequency is necessary for the operation of the bandpass filter in the optical detector.

The calibration of the applied magnetic field dependent on the current in the coil can be done by a Hall probe that is placed in the center of the air gap. For the current configuration, the scaling is 4000 A/m per ampere coil current.

Optical Part of the Measurement System

The measurement system utilizes the *magneto-optical Kerr effect* (MOKE) in order to determine the magnetization in the thin film sample. In general, the term MOKE refers to phenomena, where the magnetization at the surface of the sample causes a difference (in polarization or intensity) between incident and reflected polarized light. The *transverse Kerr effect* is sensitive to the component of magnetization that is in-plane and perpendicular to the plane of incidence. Whereas other types of MOKE (longitudinal and polar Kerr effect) cause as change in the polarization of the incident light, the transverse Kerr effect affects the reflectivity (the intensity of the reflected light compared to that of the incident light).

A standard laser-diode (of typically 800 nm wavelength) is used as light source. The emitted light is focused on the center of the thin film surface, such that the diameter of the incident laser beam in about 1 mm. The reflected light is focused again by a lens so that it is concentrated on the surface of a silicon photo diode at the detector. Because the relative change in intensity due to magnetization is rather small compared to the total intensity, the current signal of the photo diode has a big DC bias, which has to be eliminated by adequate bandpass filters[2]. After low-noise amplification and proper filtering of the photo diode signal, the detector unit provides a voltage signal (0 - 5 V) that is proportional to in-plane magnetization component perpendicular to the plane of incidence. For practical application, the whole measurement system should be covered so that the environmental light (from fluorescent lamps for example) does not interfere with the laser light to be measured.

With the presented measurement system only the relative magnetization can be provided as signal of the optical detector. For the determination of absolute magnetization values, other techniques such as vibrating sample magnetometers have to be used. Further, the measurement results have to be adjusted due to the non-linearity of the amplifier. The correction curve has been determined based on a reference sample.

Compared to the domain size of several 10 μm, a significant number of magnetic domains should be captured by the light beam focused to about 1 mm diameter, so that the measurement result can be interpreted as average magnetization of the sample. Nevertheless, there might be some local variations or inhomogeneities over the wafer's surface. Thus, the measurement should be done on three different locations on the film at least, in order to get a significant result about the magnetic properties of the thin film.

[2]In the first version of the measurement setup, a part of the light is coupled out by a semi-transparent mirror and directed to a second detector unit. The desired signal is the difference between measured signals of the directly incident light and the reflected light.

6.2 Model Setup for Thin Films with Dominant Coherent Rotation

6.2.1 General Model Parameters

As mentioned in the beginning of this chapter, the polycrystalline Permalloy films presented in the following sections are produced by DC sputtering and are intended for use in anisotropic magneto-resistive (AMR) sensor applications.

Structural Model Parameters

Transmission electron microscopic analysis [52] of the sputtered polycrystalline films yielded a *grain size* of 10 - 80 nm depending on the target material and the sputter process. Here, the grains can be associated with the magnetic entities in the EM. For a typical *domain size* of several 10 μm the statistical treatment within the context of the EM is justified.

In the best case, there would be just coherent magnetization rotation expected for the hard-axis magnetization process. But as described above, the granular structure of the polycrystalline film leads to magnetization dispersion and metastable blocking states due to the interaction of the domain walls.

Corresponding to this fact, the EM is set up with four domain classes ($N_{\mathcal{D}} = 4$) as follows:

- Coherent rotating domain classes $\mathcal{D}_1$ and $\mathcal{D}_2$:
  - Represent the ideal coherent magnetization process
  - Oriented parallel and antiparallel to the easy axis in the demagnetized state ($\bar{\varphi}_{0,1} = 0$, $\bar{\varphi}_{0,2} = \pi$)
  - Mean orientations $\bar{\varphi}_{1,2}$ are calculated by minimizing the local energy terms
  - Standard deviations are fixed to $\sigma_{1,2} = 1°$
  - The initial volume fractions $v_{0,12} = v_{0,1} = v_{0,2}$ depend on the problem to be modeled, whereas the maximum volume fractions are $v_{\max,1} = v_{\max,2} = 1.00$.
- Incoherent rotating domain classes $\mathcal{D}_3$ and $\mathcal{D}_4$:
  - Represent the parts of the thin film sample that show magnetization dispersion
  - Oriented parallel and antiparallel to the easy axis in the demagnetized state ($\bar{\varphi}_{0,3} = 0$, $\bar{\varphi}_{0,4} = \pi$)
  - Mean orientations are identical to the coherent rotating domain classes as $\bar{\varphi}_3 = \bar{\varphi}_1$ and $\bar{\varphi}_4 = \bar{\varphi}_2$
  - Standard deviations $\sigma_{3,4}$ calculated by minimizing the local energy terms
  - The initial volume fractions $v_{0,34} = v_{0,3} = v_{0,4}$ depend on the problem to be modeled, whereas the maximum volume fractions are $v_{\max,3} = v_{\max,4} = 1.00$.

Geometrical Parameters

For the magnetic hysteresis measurement, rectangular probes of 20 x 10 mm ($l_\mathrm{S} = 14$ mm) are prepared. Due to the applied magnetic field during sputtering and cooling, these samples have an induced uniaxial anisotropy with the easy axis parallel to the long edge of the probe. The presented thin films have been sputtered from a sintered Permalloy ($Fe_{19}Ni_{81}$) target and have a thickness of $d_\mathrm{S} = 50$ nm, if not stated otherwise.

Because of the huge difference between sample size (mm) and film thickness (nm), in-plane demagnetization effects due to the shape of the sample can be neglected

$$\tilde{N}_\mathrm{d,2D} \approx \begin{pmatrix} 0 & 0 \\ 0 & 0 \end{pmatrix} \quad N_{xx}, N_{yy} < 5 \cdot 10^{-6} \text{ for a 20 x 10 mm x 50 nm ellipsoid.} \tag{6.8}$$

Physical Model Parameters

The saturation magnetization is the same as in Permalloy bulk material (at room temperature)

$$M_\mathrm{s} = 800 \text{ kA/m} \qquad \mu_0 M_\mathrm{s} = 1.00 \text{ T} \quad . \tag{6.9}$$

As mentioned above, the easy axis of induced uniaxial anisotropy is aligned parallel to the long edge of the sample, which is defined as x-axis so that

$$\varphi_\mathrm{Aniso} = 0 \quad . \tag{6.10}$$

The anisotropy constant K_1 depends on the parameters of the sputter process.

Particular for the $Fe_{19}Ni_{81}$ alloy, the magnetostriction is nearly zero

$$\lambda_\mathrm{s} \approx 0 \quad , \tag{6.11}$$

so that the AMR sensor is insensitive to magneto-elastic interactions with mechanical stress.

Phenomenological Model Parameters

The coefficient for the reversible anhysteretic energy k_RevAnh is small in the range of several J/m^3 and thus allows significant deviations of the volume fractions v_i from their initial values $v_{0,12}$ or $v_{0,34}$ during the magnetization process.

In principle, the magnetization process is divided into a coherent rotating part and a incoherent rotating part, so that the boundaries between the corresponding domain classes do not necessarily represent classical domain walls. Hence, the domain wall motion factors c_{ij} are identical and can be combined with q_p, the average number of irreversible jumps per distance of wall motion as

$$c_{ij}\, q_\mathrm{p} = 80 \quad , \tag{6.12}$$

which is the average number of irreversible events per relative volume change Δv_{ij}. For the remaining parameters related to domain wall motion, the following values can be used

$$\Delta v_\mathrm{REV} = 0.002 \tag{6.13a}$$

$$k_\mathrm{RevDWM} = 2.0 \text{ J/m}^3 \tag{6.13b}$$

$$k_\mathrm{IrrDWM} = 2.0 \text{ J/m}^3 \quad . \tag{6.13c}$$

6.2.2 Energy Terms for Magnetization Dispersion

Basically, the magnetization dispersion due to domain wall interactions (e.g. magnetic ripple structure) is represented by the variances $\sigma_{3,4}^2$ of the incoherent rotating domain classes. Concerning this matter, some local energy terms have to be introduced.

Internal Entropy

Comparable to the thermal excitations, the magnetization dispersion within a domain class is represented by the internal (differential) entropy according to (5.50) as

$$w_{\mathrm{Disp},i} = -k_{\mathrm{Disp}} \sin^2(\varphi_{\mathrm{H}} - \varphi_{\mathrm{Aniso},i}) \left(\ln(2\pi) - \tfrac{1}{2} \ln \left(\exp(2) + \frac{2\pi}{\exp(1)} \frac{1}{\sigma_i^2} \right) \exp\left(-\sigma_i^2\right) \right) \quad . \tag{6.14}$$

Depending on the model parameter k_{Disp} the variance σ_i^2 can be calculated by a minimization of the (relevant) local energy contributions

$$\begin{aligned} \sigma_i^2 \quad : \quad & \min_{\sigma_i^2} \left\{ w_{\mathrm{H},i}(\bar{\varphi}_i, \sigma_i^2) + w_{\mathrm{Aniso},i}(\bar{\varphi}_i, \sigma_i^2) + w_{\mathrm{Disp},i}(\sigma_i^2) \right\} \\ & \text{s.t. given } \bar{\varphi}_i \quad . \end{aligned} \tag{6.15}$$

So the dispersion is determined by the competition between ordering field and anisotropy energy and disordering internal entropy. The term $\sin^2(\varphi_{\mathrm{H}} - \varphi_{\mathrm{Aniso}})$ accounts for the fact that magnetization dispersion is characteristic for hard-axis hysteresis curves.

Reversible and Irreversible Processes

So far, changes in domain class volume fractions (representing domain wall motion) are considered as the only source of irreversible losses. But also the change of magnetization dispersion within a domain class can be accompanied by losses, due to pinning of wall structures (e.g. Bloch lines at cross-tie walls) during the transition of different (metastable) configurations of the magnetization process.

In general, the reversible and irreversible energy contributions depend on the change of the corresponding volume fractions Δv_i

$$\Delta w_{\mathrm{RevIrrDisp}} = k_{\mathrm{RevIrrDisp}} \sum_{i=1}^{N_{\mathcal{D}}} \Delta v_i \sin^2(\varphi_{\mathrm{H}} - \varphi_{\mathrm{Aniso},i})\, d_i \left(\exp(-2\sigma_i^2) - \exp(-2\sigma_{0,i}^2) \right) \quad , \tag{6.16}$$

where

$$d_i = \operatorname{sign}\left(|m_{i,H}(t + \Delta t)| - |m_{i,H}(t)| \right) \tag{6.17}$$

accounts for the direction of the magnetization process ($d_{\mathrm{RevIrr},i} = 1$, if a state of higher domain class magnetization is reached in time step Δt). So the absolute value of change in reversible and irreversible energy contributions depends on the current value of the variance σ_i^2 compared to the variance in the demagnetized state $\sigma_{0,i}^2$.

An explicit distinction between the reversible and irreversible part is not calculated analytically, because it results from the simulated magnetization curves anyway.

6.3 Directional Dependence of Magnetization Curves Near the Hard Axis

When measuring the magnetization curves in the hard axis, it is important that the positioning of the thin film sample is exact with respect to the applied field. In this section, it is investigated how small deviations of the applied field with respect to the hard axis influence the magnetization process.

6.3.1 Identification of the Model Parameters

The following investigations are performed on a 50 nm thick sputtered Permalloy film, which is referred to as "Sample S". The measured magnetization curves for the easy axis and hard axis are shown in Fig. 6.6.

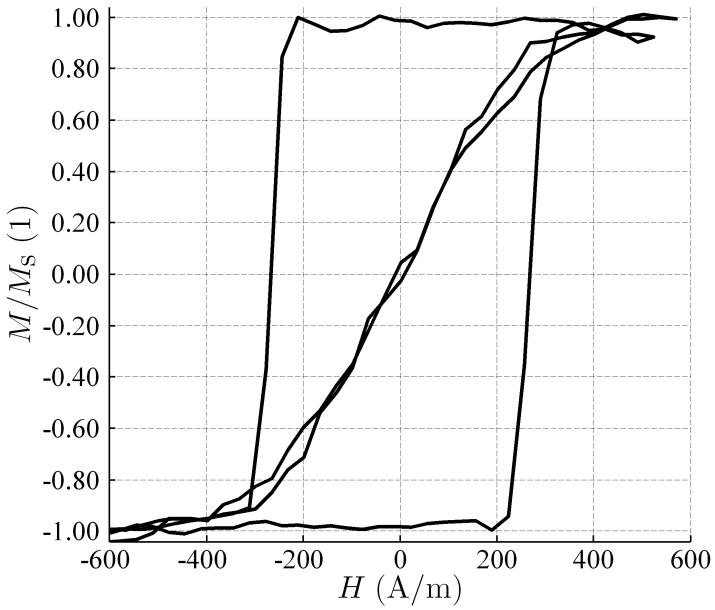

Figure 6.6: Measured easy axis and hard axis magnetization curves of sample S.

According to the measured magnetization curves, the EM parameters additional to the general parameterization described in 6.2.1 are given in Tab. 6.3.

6.3.2 Simulation Results

Magnetization Curves

In Fig. 6.7 the simulated hysteresis loops are shown. As indicated by the measured magnetization curves, the easy axis behavior corresponds to an ideal switching process according to the uniaxial anisotropy.

Parameter	Symbol	Sample S
Initial volume fractions of coherent rotation domain cl.	$v_{0,12}$	0.38
Initial volume fractions of incoherent rotation domain cl.	$v_{0,34}$	0.12
Uniaxial anisotropy constant	K_1	135 J/m^3
Coefficient for reversible anhysteretic energy	k_{RevAnh}	5.0 J/m^3
Dispersion coefficient	k_{Disp}	40 J/m^3
Coefficient for rev. and irr. dispersion change	$k_{\mathrm{RevIrrDisp}}$	58 J/m^3

Table 6.3: Identified EM parameters for thin film sample S.

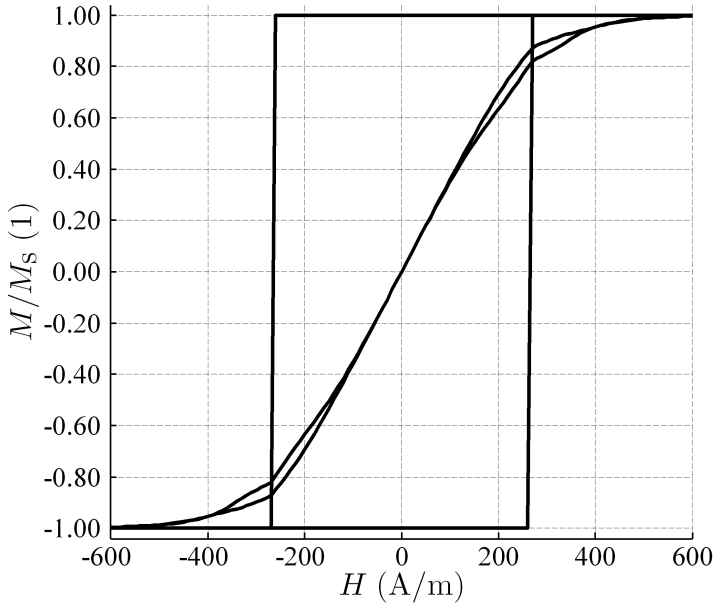

Figure 6.7: Simulated easy axis and hard axis magnetization curves of sample S.

Details for the Hard Axis Magnetization Curve

The volume fractions for the upper branch of the hard axis magnetization curve are depicted in Fig. 6.8. In Fig. 6.9 the mean angle $\bar{\varphi}_3$ and the interval of $\pm\sigma_3$ of domain class $\mathcal{D}_3$ that represents the magnetization dispersion is shown for the upper branch of the hard axis magnetization curve.

Discussion

Starting from positive saturation, the volume fractions v_3 and v_4 for the incoherent rotating domain classes increase until the anisotropy field is reached. This can be interpreted as increase in magnetization dispersion and the formation of a ripple structure. When the applied field is further decreased to zero, the fraction of coherent rotating domain classes increases, so that at zero field the initial volume fractions $v_{0,12}$ and $v_{0,34}$ are approached. When the average magnetization rotates back to easy anisotropy axis, the wall angles increase and make the ripple structure energetically unfavorable. The remaining volume

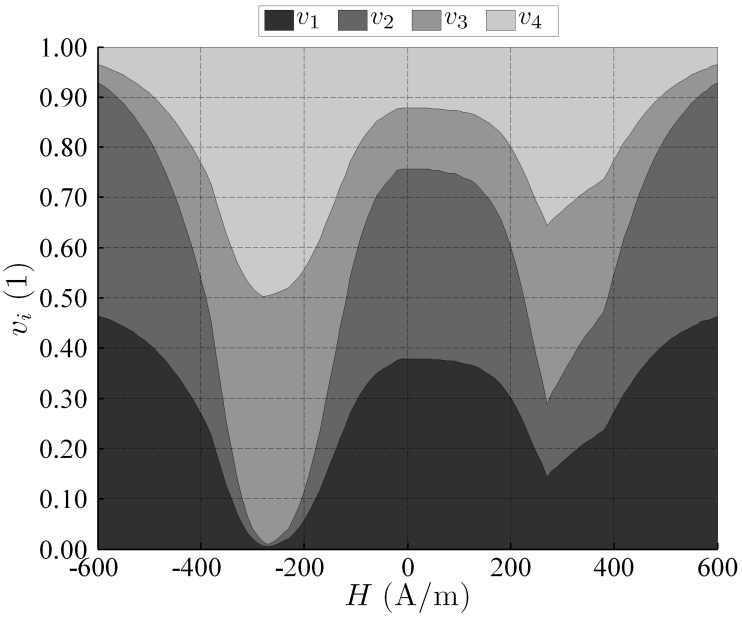

Figure 6.8: Volume fractions for the upper branch of the hard axis magnetization curve of sample S.

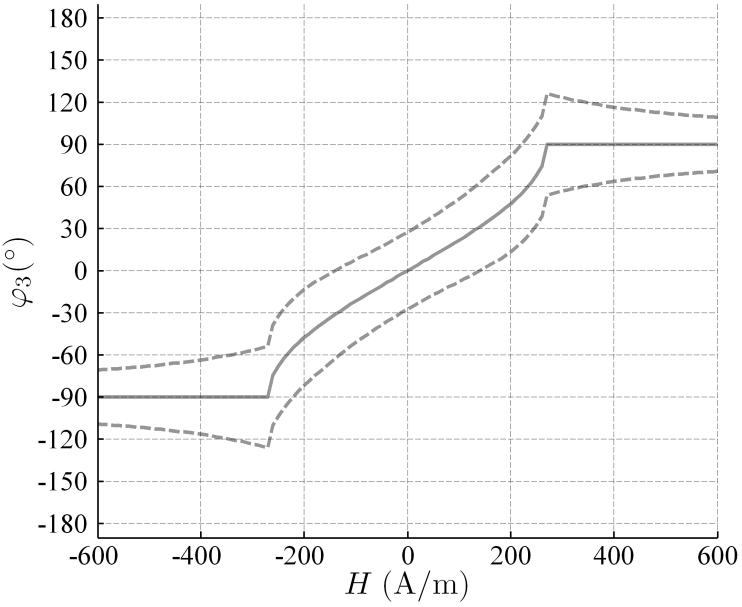

Figure 6.9: Angle $\bar{\varphi}_3$ and standard deviation $\bar{\varphi}_3 \pm \sigma_3$ (dotted line) for the upper branch of the hard axis magnetization curve of sample S.

fractions for $\mathcal{D}_3$ and $\mathcal{D}_{43}$ account for wall structures and the statistical distribution of easy anisotropy axis within the grains. In principle, the magnetization process from zero field to negative saturation is just vice versa to the described mechanisms. But quantitative the ripple structure at the anisotropy field is much more developed, when coming from zero field.

From the plot of the angular dispersion $\bar{\varphi}_3 \pm \sigma_3$ of domain class $\mathcal{D}_3$ it can be seen that the standard deviation σ_3 is about 30°. For the circular normal distribution about 68% of the magnetic entities are aligned in the interval $[\bar{\varphi}_3 - \sigma_3, \bar{\varphi}_3 + \sigma_3]$. This angular dispersion is maximal at the anisotropy field and decreases in the high field regime, because the applied field energy enforces the alignment of the remaining magnetic moments that may be pinned around inhomogeneities in the film. However, their contribution to the total magnetization is negligible for fields beyond 500 A/m.

6.3.3 Measurement and Model Prediction for Small Deviations from the Hard Axis Direction

In order to study the influence of a small misorientation of the applied field with respect to the hard axis of the thin film, the magnetization curves for field directions of 88° and 84° related to the easy axis have been measured.

Measurement

The results are depicted in Fig. 6.10.

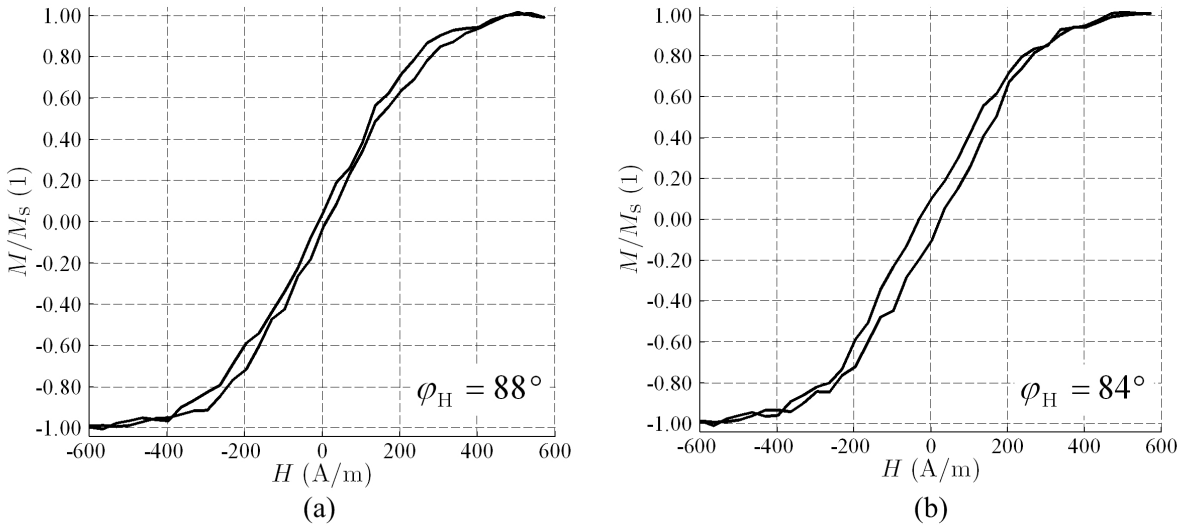

Figure 6.10: Measured magnetization curves for an applied field angle of 88° (a) and 84° (b) of sample S.

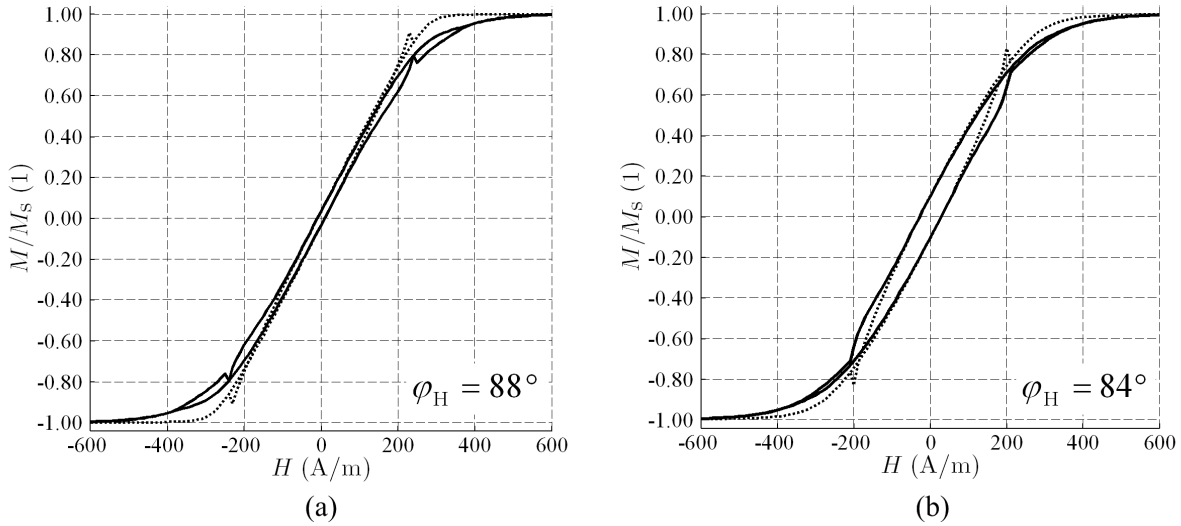

Figure 6.11: Simulated magnetization curves for an applied field angle of 88° (a) and 84° (b) of sample S (the dotted lines show the ideal rotation according to Stoner-Wohlfahrt theory).

Model Prediction

Without any changes in the parametrization of the EM, the model predicts the magnetization curves shown in Fig. 6.11. The corresponding predictions of the Stoner-Wohlfarth model assuming ideal magnetization rotation are included as dotted lines.

Discussion

Basically, there is a good agreement of the EM predictions and the measurement results within the measuring tolerances.

Particularly, it can be seen that small deviations (of some degrees) of the field axis from the hard axis cause a widening of the hysteresis loop below the anisotropy field. This widening is entirely dedicated to the coherent rotation and to misorientation of the applied field. Thus, it must not be interpreted as hard axis coercivity, which is characteristic for irreversible losses.

The influence of the magnetic ripple structure decreases, the lower the field component in hard axis direction. So for decreasing φ_H the magnetization curve approaches the ideal rotation according to Stoner-Wohlfarth theory.

6.4 Relation to Parameters of the Sputter Process

On the basis of two different thin film samples, it is investigated how the identified model parameters can be correlated to the microstructure resulting from the technological parameters of the production process.

6.4.1 Identification of the Model Parameters

For the following analysis, two Permalloy thin film samples of 50 nm thickness are considered. The production and measurement of these samples has been done by M. Janiba [45]. As shown in Tab. 6.4, the samples numbered as 219 and 246 differ in the target-substrate distance, the field current, and the target voltage.

Parameter	**Symbol**	**Sample 219**	**Sample 246**
Target-substrate distance	d_{TS}	40 mm	42 mm
Anode current	I_{A}	3.5 A	3.5 A
Thermionic cathode current	I_{C}	43 A	43 A
Field current (deposition / cooling)	I_{F}	4 A / 4 A	4 A / 2 A
Argon pressure	p_{Ar}	10 Pa	10 Pa
Substrate temperature	T_{S}	300 °C	300 °C
Substrate voltage	U_{S}	-60 V	-60 V
Target voltage	U_{T}	-900 V	-600 V

Table 6.4: Technological parameters of the sputter process for two different thin film samples.

For the magnetization curves measured by Janiba, the non-linearity of the optical detector unit (amplifier) is not considered. The measured easy axis and hard axis magnetization curves including the non-linearity correction are shown in Fig. 6.12.

Parameter	**Symbol**	**Sample 219**	**Sample 246**
Initial volume fractions of coh. rot. dom. cl.	$v_{0,12}$	0.49	0.40
Initial volume fractions of incoh. rot. dom. cl.	$v_{0,34}$	0.01	0.10
Uniaxial anisotropy constant	K_1	135 J/m^3	112 J/m^3
Coefficient for reversible anhysteretic energy	k_{RevAnh}	3.0 J/m^3	3.0 J/m^3
Dispersion coefficient	k_{Disp}	25 J/m^3	25 J/m^3
Coefficient for rev. and irr. dispersion change	$k_{\mathrm{RevIrrDisp}}$	18 J/m^3	12 J/m^3

Table 6.5: Identified EM parameters for thin film samples 219 and 246.

Basically, the EM parameter differ only in the anisotropy constant and the initial volume fractions for the different kind of domain classes.

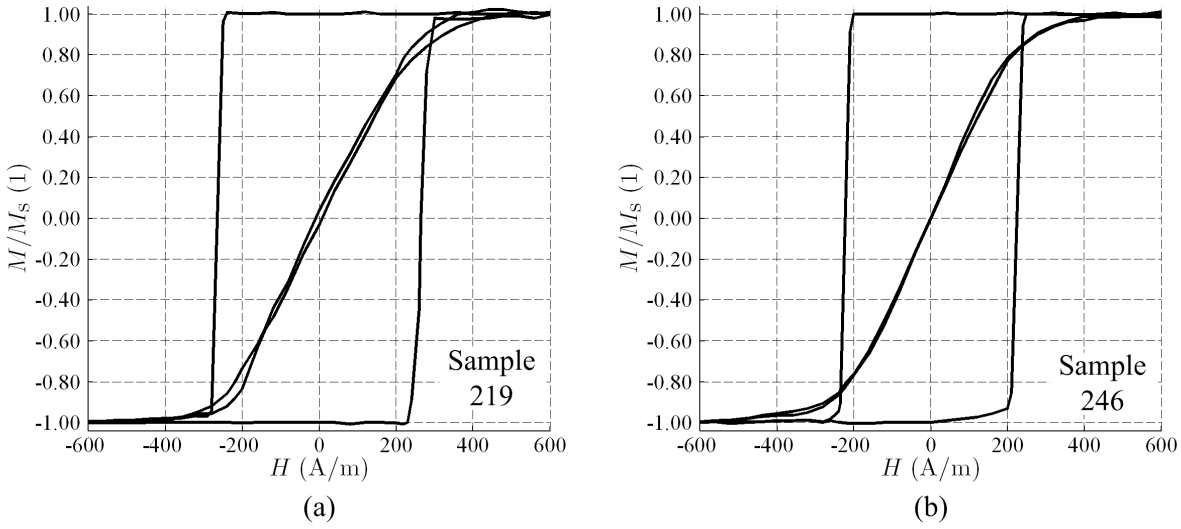

Figure 6.12: Measured easy axis and hard axis magnetization curves of sample 219 (a) and sample 246 (b).

6.4.2 Simulation Results

Magnetization Curves

In Fig. 6.13 the simulated hysteresis loops are shown. As indicated by the measured magnetization curves, the easy axis behavior corresponds to an ideal switching process according to the uniaxial anisotropy.

Details for the Hard Axis Magnetization Curve

The volume fractions for the upper branch of the hard axis magnetization curve are depicted in Fig. 6.14. In Fig. 6.15 the mean angle $\bar{\varphi}_3$ and the interval of $\pm\sigma_3$ of domain class $\mathcal{D}_3$ that represents the magnetization dispersion is shown for the upper branch of the hard axis magnetization curve.

6.4.3 Discussion

Since the simulation results are comparable to the one presented in section 6.3, the following discussion is focused on the relation between technological process parameters, identified model parameters, and the consequences on the AMR characteristics.

Change in the Field Current

As a general rule, the induced (average) anisotropy represented by K_1 is strongly correlated to the magnetic field during deposition and cooling. So the reduced field current I_F in the

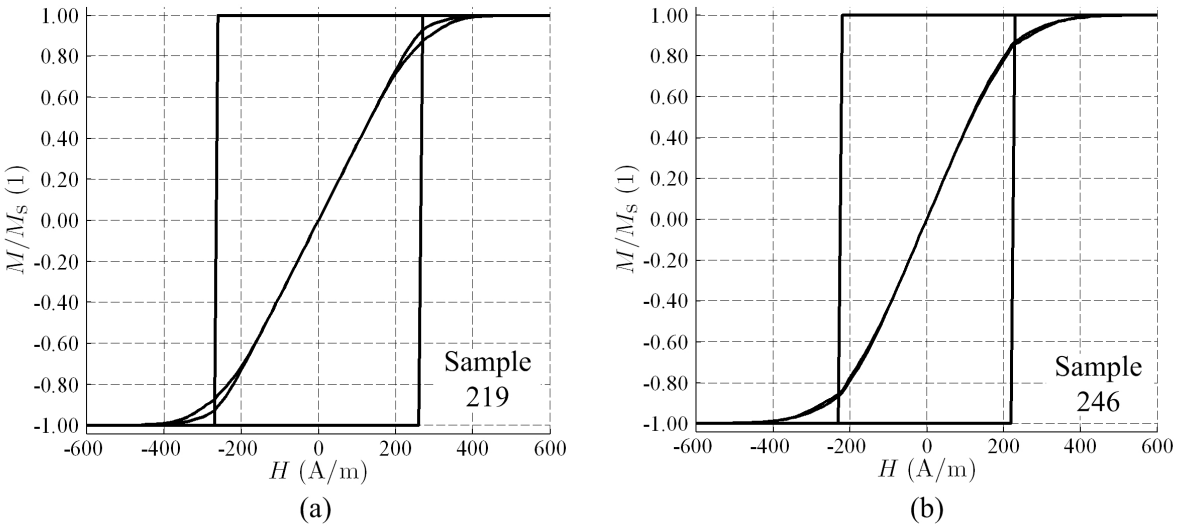

Figure 6.13: Simulated easy axis and hard axis magnetization curves of sample 219 (a) and sample 246 (b).

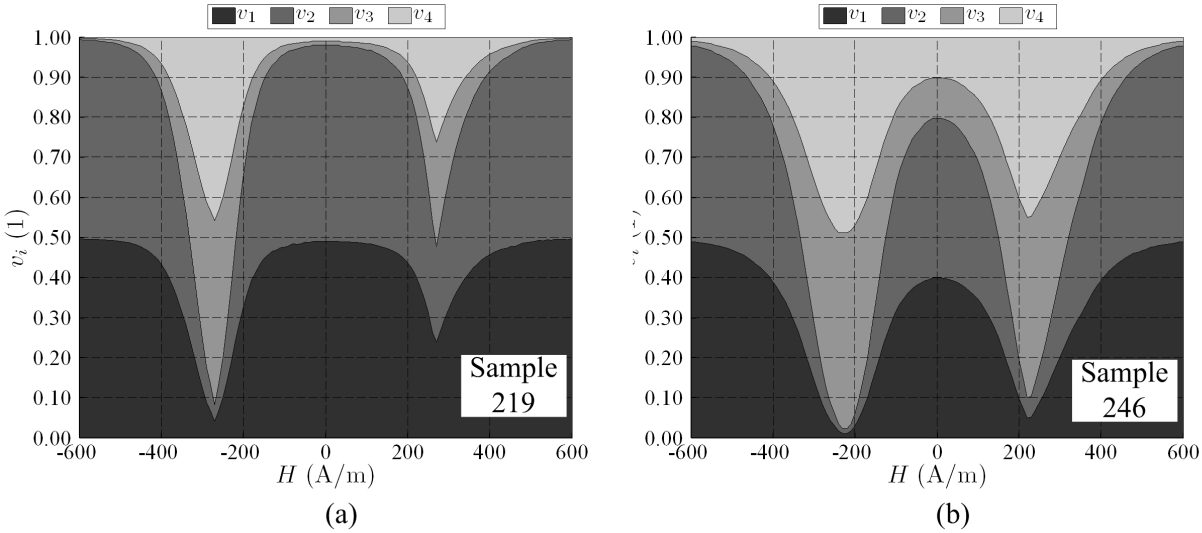

Figure 6.14: Volume fractions for the upper branch of the hard axis magnetization curve of sample 219 (a) and 246 (b).

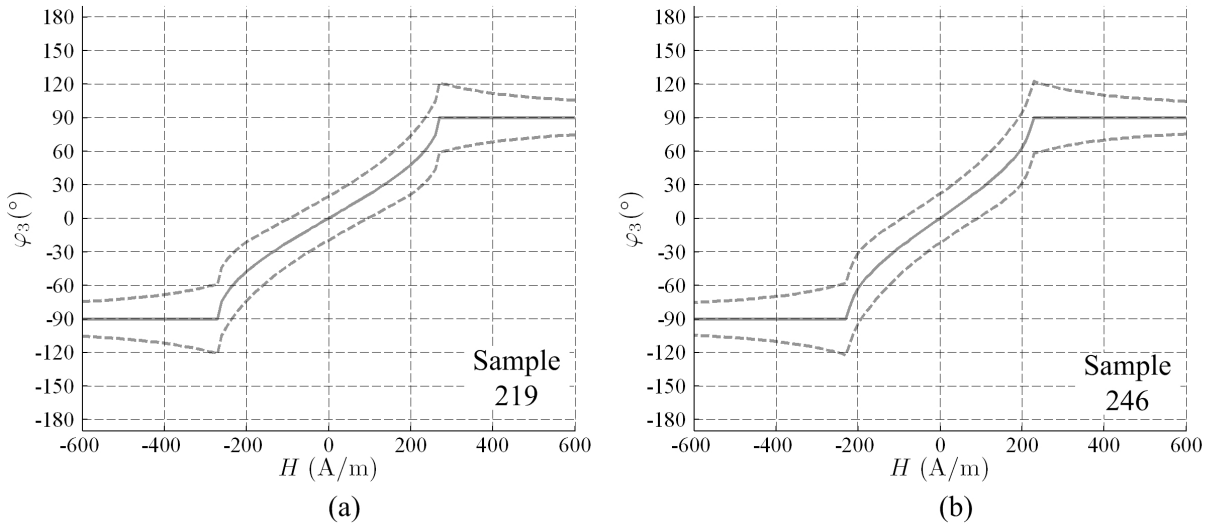

Figure 6.15: Angle $\bar{\varphi}_3$ and standard deviation $\bar{\varphi}_3 \pm \sigma_3$ (dotted line) for the upper branch of the hard axis magnetization curve of sample 219 (a) and 246 (b).

cooling phase of sample 246 leads to a smaller anisotropy field H_{Aniso}

$$\begin{array}{lllll} \text{Sample 219:} & I_{\text{F,Cooling}} = 4 \text{ A} & \Rightarrow & H_{\text{Aniso}} = 270 \text{ A} & K_1 = 135 \text{ J/m}^3 \\ \text{Sample 246:} & I_{\text{F,Cooling}} = 2 \text{ A} & \Rightarrow & H_{\text{Aniso}} = 224 \text{ A} & K_1 = 112 \text{ J/m}^3 \end{array} \quad .$$

For AMR sensor applications, a small anisotropy field is desirable, because it increases the sensitivity of the sensor.

Change in the Target-Substrate Distance

The distance from target to substrate d_{TS} is the way that the Permalloy particles have to pass through the Ar plasma. Together with the Ar pressure this distance determines the probability of collision between the Permalloy particles and the Ar ions and therefore the energy with which the target atoms arrive at the substrate. For small d_{TS} the kinetic energy of the arriving atoms can be too high, so that layers which have already been sputtered become destructed. For large d_{TS} the energy and thus the mobility of the arriving atoms can be so small, that impurities or irregularities in the layer stacking may result.

For sample 246, the increase in the target-substrate distance together with the reduced magnetic field in the cooling phase may reason the formation of a magnetic ripple structure, because of the reduced mobility of the arriving atoms and the lower aligning force due to the lower field.

$$\begin{array}{lllll} \text{Sample 219:} & I_{\text{F,Cooling}} = 4 \text{ A} \quad d_{\text{TS}} = 40 \text{ mm} & \Rightarrow & v_{0,34} = 0.01 \\ \text{Sample 246:} & I_{\text{F,Cooling}} = 2 \text{ A} \quad d_{\text{TS}} = 42 \text{ mm} & \Rightarrow & v_{0,34} = 0.10 \end{array} \quad .$$

Change in the Target Voltage

The DC target voltage U_{T} is related to the kinetic energy of the Ar-ions shooting particles out of the target material. Generally, a lower absolute value of the target voltage decreases the size of the Permalloy particles and increases homogeneity.

This homogeneity is reflected in a nearly non-hysteretic behavior of the magnetization curve and is incorporated in the model by a lower value of the dispersion change coefficient $k_{\mathrm{RevIrrDisp}}$.

$$\begin{aligned} &\text{Sample 219:} && U_{\mathrm{T}} = \text{-900 V} && \Rightarrow && k_{\mathrm{RevIrrDisp}} = 18 \\ &\text{Sample 246:} && U_{\mathrm{T}} = \text{-600 V} && \Rightarrow && k_{\mathrm{RevIrrDisp}} = 12 \quad . \end{aligned}$$

Resistivity and AMR Coefficient

In Tab. 6.6 the measured values [45] for the electrical resistivity and the AMR coefficient for the investigated samples are shown.

Parameter	**Symbol**	**Sample 219**	**Sample 246**
Resistivity	ρ	$48{\cdot}10^{-9}$ Ωm	$112{\cdot}10^{-9}$ Ωm
AMR coefficient	$\Delta\rho/\rho$	3.72 %	2.96 %

Table 6.6: Electrical resistivity and AMR coefficient for thin film samples 219 and 246.

Besides many other factors, the electrical resistance depends on the grain size of the thin film and on the density of non-resistive (gas) inclusions. The lower target voltage of sample 246 may cause a decreasing grain size, therefore an increasing number of grain boundaries, and so result in a higher resistivity.

Basically, the magnetization dispersion lowers the change in resistance depending on the magnetic field and reduces the AMR coefficient. The increase in magnetization dispersion is reflected in the EM by higher initial volume fractions $v_{0,34}$ of the incoherent rotating domain classes.

$$\begin{aligned} &\text{Sample 219} \;: && v_{0,34} = 0.01 && \Leftrightarrow && \Delta\rho/\rho = 3.72\ \% \\ &\text{Sample 246} \;: && v_{0,34} = 0.10 && \Leftrightarrow && \Delta\rho/\rho = 2.96\ \% \quad . \end{aligned}$$

More details about the influence of anisotropy dispersion on the AMR effect are summarized in [80].

6.5 Temperature Dependence of Spontaneous Magnetization

So far, the variance of the angular distribution of magnetic entities within a statistical domain class has been used to model magnetization dispersion in thin Permalloy films. Within this section the variance and the corresponding entropy represent the thermal excitations of the magnetic dipole moments. So it is possible to describe the temperature dependence of the spontaneous magnetization by the generalized EM as published in [32].

6.5.1 Model Setup

When analyzing the thermal excitations of the magnetic dipole moments, these atomic magnetic dipoles are treated as magnetic entities. The number of magnetic entities per volume η can be estimated from the atomic magnetic moment $\mathfrak{m}_{J,z}$ and the saturation magnetization (at 0 K) $M_{\mathrm{s},0}$ as (see Tab. 6.2)

$$\eta = \frac{M_{\mathrm{s},0}}{\mathfrak{m}_{J,z}} = \frac{8.28 \cdot 10^5 \text{ A/m}}{1.02\ 9.27 \cdot 10^{-24} \text{ Am}^2} = 8.76 \cdot 10^{28} \text{ 1/m}^3 \quad . \tag{6.18}$$

Combined with the thermal energy at the Curie temperature

$$k_{\mathrm{B}} T_{\mathrm{C}} = 1.38 \cdot 10^{-23} \text{ J/K } 843 \text{ K} = 1.16 \cdot 10^{-20} \text{ J} \tag{6.19}$$

the corresponding energy coefficient

$$\eta\, k_{\mathrm{B}} T_{\mathrm{C}} = 1.02 \cdot 10^9 \text{ J/m}^3 \tag{6.20}$$

is far beyond the applied field energy, the anisotropy energy, and the stray field energy.

So it is sufficient to restrict the investigation to only one representative domain class $\mathcal{D}_i$ and consider only the thermal excitations energy contribution $w_{\mathrm{T},i}$ and the exchange energy $w_{\mathrm{Ex},i}$ within this domain class. Minimizing these energy terms

$$\sigma_i^2(T): \quad \min_{\sigma_i^2} \left\{ w_{\mathrm{T},i}(\sigma_i^2, T) + w_{\mathrm{Ex},i}(\sigma_i^2) \right\} \tag{6.21}$$

with

$$\begin{aligned} &(5.49): \quad w_{\mathrm{T},i}(\sigma_i^2, T) = -\eta\, T\, k_{\mathrm{B}} \left(\ln(2\pi) - \tfrac{1}{2} \ln\left(\exp(2) + \tfrac{2\pi}{\exp(1)} \tfrac{1}{\sigma_i^2} \right) \exp\left(-\sigma_i^2\right) \right) \\ &(5.54): \quad w_{\mathrm{Ex},i}(\sigma_i^2) = -\eta \nu_{\mathrm{NN}}\, J_{\mathrm{Ex}}\, \exp(-\sigma_i^2(1-\rho_i)) \end{aligned}$$

gives the variance σ_i^2 of the magnetic dipole orientation and further the reduced magnetization (Tab. 5.1)

$$m_i(T) = |\vec{m}_i(T)| = \exp\left(-\frac{\sigma_i^2(T)}{2} \right) \quad . \tag{6.22}$$

For bulk material, the coefficient $\nu_{\mathrm{NN,Bulk}}$ proportional to the number of neighbors is determined by the Curie temperature T_{C} as

$$\nu_{\mathrm{NN,Bulk}} = \frac{k_{\mathrm{B}} T_{\mathrm{C}}}{1.02\, J_{\mathrm{Ex}}} = \frac{1.16 \cdot 10^{-20} \text{ J}}{1.02\ 1.60 \cdot 10^{-19} \text{ J}} = 0.07 \quad . \tag{6.23}$$

The individual magnetic moment are only correlated by the exchange energy, so no further intrinsic correlations are assumed $\rho_i = 0$.

6.5.2 Comparison with Classical Mean Field Models

When thermal excitations are treated by classical thermodynamics, like in the *Weiss molecular field model*, the reduced spontaneous magnetization is described by the Brillouin function $\mathcal{B}_J(x)$ [62]

$$m = \mathcal{B}_J(\frac{3\mathtt{J}}{\mathtt{J}+1} m \frac{T_\mathrm{C}}{T}) \quad . \tag{6.24}$$

If only two states of the magnetic moment (e.g. spin-up and spin-down) are allowed, the quantum number for the total angular momentum $\mathtt{J} = 1/2$ and

$$m = \mathcal{B}_{1/2}(m \frac{T_\mathrm{C}}{T}) \quad . \tag{6.25}$$

In the classical limit, where all orientations of the magnetic moments are allowed ($\mathtt{J} \to \infty$), the Brillouin function degenerates to the Langevin function

$$m = \mathcal{B}_\infty(m \frac{T_\mathrm{C}}{T}) \quad . \tag{6.26}$$

Since the magnetic moment has more degree of freedom in the classical point of view, where all orientations are allowed, the spontaneous magnetization is always below the two-state case.

Model Prediction

Based on the described setup of the generalized EM, the reduced magnetization $m_i(T)$ is calculated in dependence of the temperature. The simulation results together with the classical Langevin function and the Brillouin function (for J=1/2) are shown in Fig. 6.16.

Discussion

The generalized EM prediction is between the two-state Brillouin function and the continuos Langevin function, except for temperatures near the Curie point. Basically, the reason for this behavior is that the magnetic dipoles are restricted to the 2D directions, whereas in the classical point of view all directions in the 3D space are possible. But, compared to the two-state (spin-up and spin-down) solution the degree of freedom is higher.

In principle, the Weiss model is based on the classical Boltzmann distribution, which has a higher probability in the tails compared to the wrapped normal distribution used in the EM as shown in Fig. 5.6. This difference can reason the difference near the Curie point.

So, the EM does not predict a second order phase transition from the ordered ferromagnetic to the paramagnetic state. In practice, thermal fluctuations in the critical region can distort the energy bands by a modification in the density of states and therefore smear out a sharp phase transition. Furthermore, in thin films interactions at the surface or in the volume can influence the magnetic order in the critical region, too.

If the magnetic entities in the generalized EM be discrete distributed such that p is the probability to find the magnetic entity aligned in a certain direction and $(1 - p)$ is the

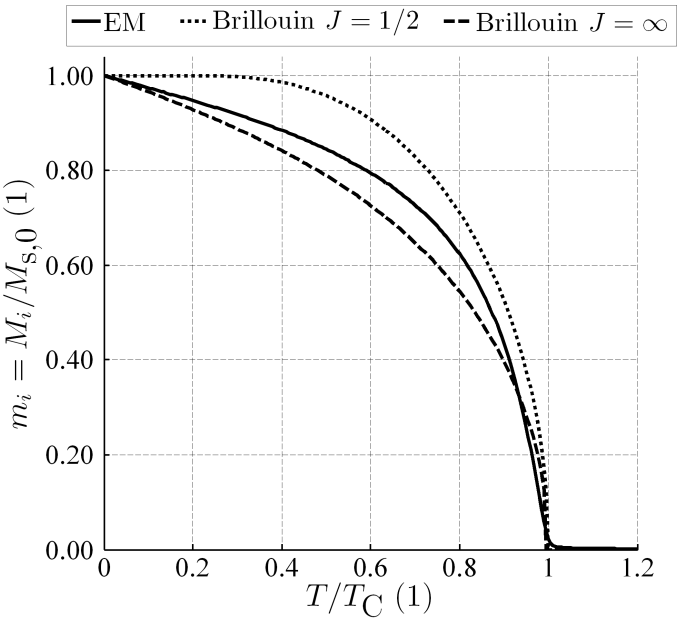

Figure 6.16: Temperature dependence of the spontaneous magnetization predicted by different models.

probability to find it in antiparallel orientation, the EM prediction would be exactly reflect the $\mathcal{B}_{1/2}$ temperature dependence of the spontaneous magnetization.

As stated above, no intrinsic correlations between the magnetic dipoles are considered ($\rho_i = 0$). Thus, the assumption of statistically independent magnetic entities is comparable to *single particle excitations*, as assumed in the Weiss model. For future research, it can be investigated how the incorporation of intrinsic correlations in the EM can lead to *collective excitations* as described by the Heisenberg model, for example.

6.5.3 Ultrathin Permalloy Films

In the generalized EM the parameter ν_{NN} is assumed to be proportional to the number of neighboring magnetic dipoles that are relevant for exchange interactions. Based on the measurement results published by Mauri [60], it can be studied how this parameter ν_{NN} changes when film thickness is in the range of several monolayers. In his work, Mauri published the temperature dependence of the spontaneous magnetic polarization for polycrystalline monolayers of Permalloy on Ta, where the film thickness is about 2.6 and 1.6 monolayers.

Model Prediction

Here, the model parameter ν_{NN} is chosen such that the simulated temperature curve meets the measurement results

$$\begin{aligned} &\text{2.6 monolayer film:} \quad \nu_{\mathrm{NN}}/\nu_{\mathrm{NN,Bulk}} = 0.585 \\ &\text{1.6 monolayer film:} \quad \nu_{\mathrm{NN}}/\nu_{\mathrm{NN,Bulk}} = 0.405 \end{aligned} \quad ,$$

as shown in Fig. 6.17.

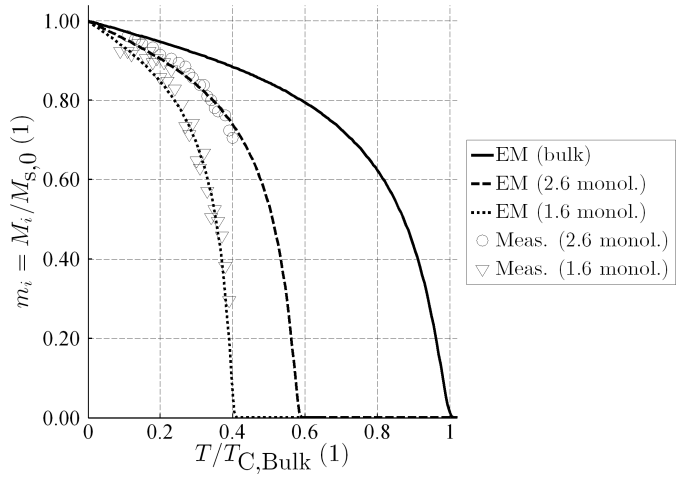

Figure 6.17: EM prediction of the temperature dependence of the spontaneous magnetization for bulk material and ultrathin films compared to measurement data from [60].

Discussion

Generally, it becomes clear that the number of neighbors decreases with the film thickness, particularly in the ultrathin film region. As a rough estimation, it can be assumed that number of neighbors in the surface layers is half of the value inside the film. Then, the coefficient ν_{NN} is

$$\nu_{\mathrm{NN}} = \frac{1}{n_{\mathrm{Layer}}} \left(\underbrace{(n_{\mathrm{Layer}} - 2)\nu_{\mathrm{NN,Bulk}}}_{\text{inner layer}} + \underbrace{2\frac{\nu_{\mathrm{NN,Bulk}}}{2}}_{\text{surface layer}} \right) = \nu_{\mathrm{NN,Bulk}} \left(1 - \frac{1}{n_{\mathrm{Layer}}} \right) \quad , \tag{6.27}$$

where n_{Layer} is the number of atomic monolayers of the film. The comparison of the values for $\nu_{\mathrm{NN}}/\nu_{\mathrm{NN,Bulk}}$ between the identification from measurement data and the simplified estimation by (6.27) is provided in Tab. 6.7, which approves the trend qualitatively.

$\nu_{\mathrm{NN}}/\nu_{\mathrm{NN,Bulk}}$	**Measurement**	**Estimation**
2.6 monolayer film	0.585	0.615
1.6 monolayer film	0.405	0.375

Table 6.7: Nearest neighbor coefficient for ultrathin Permalloy films.

Particularly, when the film thickness is in the range of some monolayers, there interactions between the thin film layers and the substrate become important. Together with other mechanisms that influence the magnetic behavior in such ultrathin films significantly, a treatment within a macroscopic model is restricted to some basic considerations. Hence, the EM predictions of the temperature dependence of the spontaneous magnetization is sufficiently accurate for the problems that this type of model is able to cover.

6.6 Summary

In this chapter the generalized energetic model is used for the simulation and prediction of magnetization curves in Permalloy thin films. In the polycrystalline films local anisotropy variations of the individual grains cause a magnetic ripple structure, which influences the hard-axis magnetization curve. In the stochastic 2D approach of the EM, such an anisotropy dispersion can be considered via additional domain classes in a self-consistent way. The identification of the phenomenological EM parameters is done by easy axis and hard axis magnetization curves measured with a magneto-optical Kerr system.

For the first investigations, the parametrized EM is used to predict the magnetization curves when the applied field is orientated a few degrees different from the hard axis. It can be seen that the magnetization curve is widening up for fields below the anisotropy field. But this phenomenon must not be interpreted as coercive field due to irreversible losses, because it results entirely from the coherent magnetization rotation, if the field is not exactly applied in the hard axis direction. However, the EM predictions are confirmed by corresponding measurement data.

Second, two films differing in the technological parameters of the sputter process are used to identify the EM. It can be shown that the EM parameters can be qualitatively related to the sputter process parameters and the resulting AMR characteristics. The undesired anisotropy dispersion, which reduces the AMR coefficient can be quantified by the initial volume fractions of the corresponding domain classes. Even if no elaborate analyses of the magnetic and crystalline microstructure have been presented, the inference from the magnetization curves on this local anisotropy dispersion is justified. The physical reasoning of the influence of the technological parameters and the resulting AMR characteristics confirm the modeled behavior.

Finally, the variance of the orientation of the magnetic entities in a domain class can be also related to thermal excitations of magnetic dipole moments. Under this assumption, the temperature dependence of the spontaneous magnetization can be predicted from the first principles within the generalized EM. Due to the two-dimensional geometry, the resulting magnetization is between the classical Langevin function, where all orientations of the magnetic moments are allowed and the two-state (spin-up and spin-down) Brillouin function. The EM model predictions are compared to measurement data of ultrathin Permalloy films from literature. The influence of the EM coefficient that represents the number of nearest neighbors in the exchange energy term is in good accordance with the measured behavior in the films of several monolayer thickness.

Chapter 7

Conclusion and Outlook

7.1 Conclusion

7.1.1 Limits of the Classical Energetic Model

In principle, the classical Energetic Model of ferromagnetic hysteresis developed by H. HAUSER is a well-proven tool for the description of the magnetization process based on small set of parameters. It can explain a variety of magnetic phenomena by a manageable set of analytical model equations that ensure short calculation time. Even though this classical EM can be applied for material with cubic crystal structure, the component of magnetization parallel to the applied magnetic field is estimated by a scalar model setup with different parameters depending on the field direction. The model predictions are in conformity with the measured magnetization curves as long as domain wall motion dominates the magnetization process. But if magnetization rotation and switching processes become important, the classical EM is not able to describe this phenomena satisfactorily.

For this reason it became necessary to extend the classical EM to a fully two-dimensional formulation. Additionally, the orientation of the elemetary magnetic dipoles in a statistical domain class are allowed to disperse with respect to an average direction, according to a circular statistical distribution function. Further, the formulation of all energy contributions is adapted such that more than two statistical domain classes can be handled. Based on the idea of the classical EM, the two-dimensional formulation, the statistical distribution of the magnetic moments' orientations within a domain class, and adaption for more than two domain classes lead to the *generalized Energetic Model*, which is described within this thesis.

7.1.2 Development of the Generalized Energetic Model

The generalized EM presented in this work is the result of several scientific studies that are published in scientific journals and presented on international conferences.

In 2004 [33], an EM based on four domain classes has been applied to describe the hard axis magnetization curves of Permalloy thin films with non-negligible coercivity due to irreversible losses. This setup allowed to distinguish between domain wall motion and magnetization rotation as the basic mechanisms of the magnetization process and to quantify the proportion of these contributions.

In 2005 [30], the statistical distribution of the magnetic moments in a domain class has been introduced. Here, the reversible anhysteretic energy was related to the differential entropy of a Dirichlet distribution. But this approach allows to estimate only a limited range of magnetization curves, so it is no longer present in the generalized EM described in this thesis.

In 2008 [32], the entropy of the distribution of the magnetic moments has been related to thermal excitations. Together with an expression for the exchange energy it is possible to calculate the temperature dependence of the spontaneous magnetization directly within the generalized EM. The model predictions are confirmed by measurement of ultrathin films from literature. Besides, the elementary magnetic entities have been introduced at that time.

In 2010 [31], the variance of the statistical distribution of the magnetic entities has been used as a measure for inhomogeneities within Permalloy thin films. It has been shown, how the EM parameters can be related to the technological parameters of the thin film production process.

7.1.3 Current State of the Generalized Energetic Model

Within this thesis, the current state of the generalized EM is presented. In addition to prior publications, the phenomenological energy contributions such as the reversible anhysteretic energy, the reversible and irreversible work due to domain wall motion, and the internal entropy representing magnetization dispersion are revised in order to get a consistent model formulation.

Hence, the generalized EM can be used to describe the two-dimensional magnetization process, including domain wall motion, magnetization rotation, and irreversible switching. In order to demonstrate these characteristics of the EM, the model is evaluated on Permalloy thin films with dominant coherent magnetization rotation as it is desired for the use in AMR sensor applications. Basically, the predictions of the model are in good agreement with practical magnetization curves obtained from a magneto-optical Kerr measurement setup. Further, the EM parameters can be used to quantify microstructural properties such as anisotropy dispersion and relate the measured magnetization curve to technological parameters of the production process. All together, the generalized EM is a useful tool for predicting and analyzing of magnetization curves of thin film materials with in-plane magnetization.

7.1.4 Limits of the Generalized Energetic Model

Due to the fact, that the energy surface depending on the volume fractions of the domain classes is complex in nature and consists of many local minima, the calculation process is intricate and time consuming with an increasing number of domain classes. So, if fast model predictions are needed as in finite element simulations for example, other models that are based on analytical formulas must be preferred.

In principle, the generalized EM is flexible in its structure regarding the setup of domain classes with different properties and the extension with further energy terms. But for a proper setup of the EM, some a-priori information about the magnetization process to be modeled is needed.

7.2 Outlook

7.2.1 Comprehensive Evaluation of the Model Characteristics

Although the formulation of the generalized Energetic Model is derived in a consistent way, there are still some open issues. So some general properties of the EM need to be analyzed, such as the characteristics of minor loops, the influence of external stress, or the predictability of dynamic magnetization curves. In addition, a comparison between the generalized formulation and the scalar setup of the energetic model has to be performed. As far as practicable, the identification of the model parameters and their influence on the resulting magnetization curves should be described, in general.

Particularly for Permalloy thin films, an extensive evaluation of the magnetization curves for a variety of samples combined with detailed microstructural analysis and magnetic domain imaging would be helpful to get a better understanding of the relation between the intrinsic factors governing the magnetization process.

7.2.2 Improvements in Model Formulation and Calculation

Further, there may exist other formulations for the reversible anhysteretic energy that allow to reproduce and predict a greater variety of hysteresis phenomena. This is one of the major topics for future investigations.

In order to reduce the calculation time, a solver with an optimization algorithm of higher performance would be helpful. Thus, the search for a proper solver or the improvement of the proprietary developed algorithm that is used for the simulations presented within this thesis is a matter for future work.

7.2.3 Further Applications

In principle, the generalized EM can also be applied to other than Permalloy thin film materials, if the magnetization process can be described in a two-dimensional framework. So, magnetic steel sheets, magnetic tapes, or nanocrystalline films would be promising candidates for future investigations. Especially the transition from the magnetic ordered state to superparamagnetism for nano-particulated media would be of scientific interest.

Furthermore, the magnetic behavior of multilayer thin films, where the interaction between the different layers governs the magnetization process is a challenging issue for future studies.

Concluding, it can be stated that the work presented within this thesis provides a generic basis for two-dimensional Energetic Modeling. Although the generalized EM is successfully applied to predict and interpret the magnetization curves in Permalloy thin films with dominant magnetization rotation, there is still a wide field of magnetic phenomena that can be described with this model approach, even if the need for modifications becomes evident. But it is precisely this general model setup based on statistical domain classes and the distinction of local, reversible and irreversible energy contributions, which allows the EM a prediction of rather complex microscopic behavior with a small set of physical and phenomenological parameters.

Appendix

Appendix A

Detailed Derivations to the Generalized Energetic Model

This appendix contains some formal derivations for the "Generalized Two-Dimensional Energetic Model" (EM) presented in chapter 5.

As a technical appendix, the focus is set on a mathematical point of view, rather on modeling issues, which are described in the main part of this work.

A.1 Expectation Value of Wrapped Circular Distributions

For a system with statistically distributed orientations related to a specified axis, the stochastic (continuous) random variable[1] Φ_i is represented by a circular probability density function $\Phi_i \sim f_i(\varphi)$, where the angle φ is bounded to the interval $(-\pi, \pi]$. The circular probability density function has to fulfill the standardization condition

$$\int_{-\pi}^{\pi} f_i(\varphi)\, \mathrm{d}\varphi = 1 \quad . \tag{A.1}$$

Circular distributions can be obtained by wrapping a linear distribution $f_i^{\phi}(\phi)$ defined on the real line $\phi \in (-\infty, \infty]$ around the unit circle. The probability density function of the so called *wrapped distribution* is gained by summarizing the density values of the linear distribution over all equivalent directions $\phi = \varphi \pm 2\pi k$ with $k = 0, 1, 2, ...$ as

$$f_i(\varphi) = \sum_{k \in \mathbb{Z}} f_i^{\phi}(\phi = \varphi + 2\pi k) \quad . \tag{A.2}$$

For more detailed information on circular statistics, the textbook [44] can be used as reference, for example.

[1] In general, a stochastic random variable X represents the results of a random experiment, which are not a deterministic numbers, but a set of possible values within a defined sample space. Each random variable has an associated probability measure (e.g. probability density function) that characterizes the stochastic system. Based on this probability measure, statistical operators, such as expectation Value $\mathbb{E}[X]$, variance $\mathrm{Var}[X]$, or probability $\mathbb{P}[X < x]$ can be applied, for example.

A.1.1 Expectation Value for 2π-Periodic Functions

For a 2π-periodic function

$$g(\varphi) = g(\varphi + 2\pi k) \quad k \in \mathbb{Z} \tag{A.3}$$

the expectation value can be calculated as

$$\begin{aligned}
\mathbb{E}\left[g(\Phi_i)\right] &= \int_{-\pi}^{\pi} g(\varphi)\, f_i(\varphi)\, \mathrm{d}\varphi \\
&= \int_{-\pi}^{\pi} g(\varphi) \sum_{k\in\mathbb{Z}} f_i^{\phi}(\varphi + 2\pi k)\, \mathrm{d}\varphi \\
&= \sum_{k\in\mathbb{Z}} \int_{-\pi}^{\pi} g(\varphi + 2\pi k)\; f_i^{\phi}(\varphi + 2\pi k)\, \mathrm{d}\varphi \\
&= \sum_{k\in\mathbb{Z}} \int_{2\pi k-\pi}^{2\pi k+\pi} g(\phi)\; f_i^{\phi}(\phi)\, \mathrm{d}\phi \\
&= \int_{-\infty}^{\infty} g(\phi)\; f_i^{\phi}(\phi)\, \mathrm{d}\phi \quad .
\end{aligned} \tag{A.4}$$

Thus, the expectation value of a 2π-periodic function can either be calculated based on the wrapped circular distribution $f_i(\varphi)$ or equivalently on the corresponding linear distribution $f_i^{\phi}(\phi)$.

A.1.2 Analytical Results for the Wrapped Normal Distribution

The *wrapped normal distribution* $\mathrm{WN}(\bar{\varphi}_i, \sigma_i^2)$ is based on the *linear normal distribution* $\mathrm{N}(\bar{\varphi}_i, \sigma_i^2)$ with the probability density function

$$f_i^{\phi}(\phi) = \frac{1}{\sqrt{2\pi}\sigma_i} \exp\left(-\frac{1}{2}\frac{(\phi - \bar{\varphi}_i)^2}{\sigma_i^2}\right) \tag{A.5}$$

that is described by two parameters, the mean direction $\bar{\varphi}_i$ and the variance σ_i^2.

In the following paragraphs, the expectation value for typical 2π-periodic functions is calculated on the basis of this wrapped normal distribution $\mathrm{WN}(\bar{\varphi}_i, \sigma_i^2)$.

Sine and Cosine

For $g(\varphi) = \cos(a\varphi + b)$ ($a \in \mathbb{Z}$ to ensure 2π-periodicity, $b \in \mathbb{R}$) the expectation value based on a wrapped normal distribution (A.5) is derived by employing (A.4)

$$\begin{aligned}
\mathbb{E}\left[\cos(a\Phi_i + b)\right] &= \int_{-\infty}^{\infty} \cos(a\phi + b)\, \frac{1}{\sqrt{2\pi}\sigma_i} \exp\left(-\frac{1}{2}\frac{(\phi - \bar{\varphi}_i)^2}{\sigma_i^2}\right)\, \mathrm{d}\phi \\
&= \frac{1}{\sqrt{2\pi}} \int_{-\infty}^{\infty} \cos(a(z\sigma_i + \bar{\varphi}_i) + b)\, \exp\left(-\frac{1}{2}z^2\right)\, \mathrm{d}z \\
&= \frac{1}{\sqrt{2\pi}}\frac{1}{2}\left(\int_{-\infty}^{\infty} \exp(j(a\sigma_i z + a\bar{\varphi}_i + b) - \frac{z^2}{2})\, \mathrm{d}z + \right. \\
&\qquad \left. + \int_{-\infty}^{\infty} \exp(-j(a\sigma_i z + a\bar{\varphi}_i + b) - \frac{z^2}{2})\, \mathrm{d}z\right) \\
&= \frac{1}{\sqrt{2\pi}}\frac{1}{2}\left(\exp(j(a\bar{\varphi}_i + b)) \int_{-\infty}^{\infty} \exp(ja\sigma_i z - \frac{z^2}{2})\, \mathrm{d}z + \right. \\
&\qquad \left. + \exp(-j(a\bar{\varphi}_i + b)) \int_{-\infty}^{\infty} \exp(-ja\sigma_i z - \frac{z^2}{2})\, \mathrm{d}z\right) \\
&= \frac{1}{\sqrt{2\pi}}\frac{1}{2}\left(\exp(j(a\bar{\varphi}_i + b))\sqrt{2\pi}\exp(-\frac{a^2\sigma_i^2}{2}) + \right. \\
&\qquad \left. + \exp(-j(a\bar{\varphi}_i + b))\sqrt{2\pi}\exp(-\frac{a^2\sigma_i^2}{2})\right) \\
&= \exp(-\frac{a^2\sigma_i^2}{2})\frac{1}{2}\left(\exp(j(a\bar{\varphi}_i + b)) + \exp(-j(a\bar{\varphi}_i + b))\right) \\
&= \exp(-\frac{a^2\sigma_i^2}{2})\, \cos(a\bar{\varphi}_i + b) \qquad \text{(A.6)}
\end{aligned}$$

Thereby, the integral is calculated as

$$\begin{aligned}
\int_{-\infty}^{\infty} \exp(\pm ja\sigma_i z - \frac{z^2}{2})\, \mathrm{d}z &= \exp(-\frac{a^2\sigma_i^2}{2}) \int_{-\infty}^{\infty} \exp(\frac{a^2\sigma_i^2}{2} \pm ja\sigma_i z - \frac{z^2}{2})\, \mathrm{d}z \\
&= \exp(-\frac{a^2\sigma_i^2}{2}) \int_{-\infty}^{\infty} \exp(-\frac{1}{2}(z \mp ja\sigma_i)^2)\, \mathrm{d}z \\
&= \sqrt{2\pi}\exp(-\frac{a^2\sigma_i^2}{2}) \underbrace{\int_{-\infty}^{\infty} \frac{1}{\sqrt{2\pi}} \exp(-\frac{1}{2}(z \mp ja\sigma_i)^2)\, \mathrm{d}z}_{1} . \qquad \text{(A.7)}
\end{aligned}$$

Because of $g(\varphi) = \sin(a\varphi + b) = \cos(a\varphi + b - \pi/2)$

$$\mathbb{E}\left[\sin(a\Phi_i + b)\right] = \exp(-\frac{a^2\sigma_i^2}{2})\ \sin(a\bar{\varphi}_i + b) \tag{A.8}$$

follows immediately.

Sine and Cosine Squared

Using the trigonometric relation $g(\varphi) = \sin^2(a\varphi+b) = 1/2(1-\cos(2(a\varphi+b)))$ and the result from (A.6) yields

$$\begin{aligned}
\mathbb{E}\left[\sin^2(a\Phi_i + b)\right] &= \frac{1}{2}\left(1 - \mathbb{E}\left[\cos(2a\Phi_i + 2b)\right]\right) \\
&= \frac{1}{2}\left(1 - \exp(-\frac{(2a)^2\,\sigma_i^2}{2})\ \cos(2a\bar{\varphi}_i + 2b)\right) \\
&= \frac{1}{2}\left(1 - \exp(-2a^2\sigma_i^2)\ \left(1 - 2\sin^2(a\bar{\varphi}_i + b)\right)\right) \\
&= \frac{1 - \exp(-2a^2\sigma_i^2)}{2} + \exp(-2a^2\sigma_i^2)\sin^2(a\bar{\varphi}_i + b) \quad ,
\end{aligned} \tag{A.9}$$

and for $g(\varphi) = \cos^2(a\varphi + b) = 1 - \sin^2(a\varphi + b)$ we get

$$\begin{aligned}
\mathbb{E}\left[\cos^2(a\Phi_i + b)\right] &= 1 - \mathbb{E}\left[\sin^2(a\Phi_i + b)\right] \\
&= \frac{1 - \exp(-2a^2\sigma_i^2)}{2} + \exp(-2a^2\sigma_i^2)\cos^2(a\bar{\varphi}_i + b) \quad .
\end{aligned} \tag{A.10}$$

A.1.3 Application to Domain Class Magnetization

The x-component of the reduced magnetization vector $\vec{m}_i = \vec{M}_i/M_\mathrm{s}$ of domain class $\mathcal{D}_i$ can be calculated for the wrapped normal distribution by using (A.6) with $a = 1$ and $b = 0$ as

$$\begin{aligned}
m_{i,x} &= \int_{-\pi}^{\pi} \cos(\varphi)\ f_i(\varphi)\,\mathrm{d}\varphi \\
&= \mathbb{E}\left[\cos(\Phi_i)\right] \\
&= \exp(-\frac{\sigma_i^2}{2})\ \cos(\bar{\varphi}_i) \quad .
\end{aligned} \tag{A.11}$$

Similarly, the y-component results according to (A.8) as

$$\begin{aligned}
m_{i,y} &= \int_{-\pi}^{\pi} \sin(\varphi)\ f_i(\varphi)\,\mathrm{d}\varphi \\
&= \mathbb{E}\left[\sin(\Phi_i)\right] \\
&= \exp(-\frac{\sigma_i^2}{2})\ \sin(\bar{\varphi}_i) \quad .
\end{aligned} \tag{A.12}$$

A.1.4 Application to Local Energy Contributions

Applied Field Energy

Assuming a wrapped normal distribution and using (A.6) with $a = 1$ and $b = \varphi_{\mathrm{H}}$, the applied field energy yields

$$\begin{aligned} w_{\mathrm{H},i} &= \mathbb{E}\left[-\mu_0 M_{\mathrm{s}}\, H\, \cos(\Phi_i - \varphi_{\mathrm{H}})\right] \\ &= -\mu_0 M_{\mathrm{s}}\, H\, \mathbb{E}\left[\cos(\Phi_i - \varphi_{\mathrm{H}})\right] \\ &= -\mu_0 M_{\mathrm{s}}\, H\, \exp(-\frac{\sigma_i^2}{2})\, \cos(\bar{\varphi}_i - \varphi_{\mathrm{H}}) \quad . \end{aligned} \tag{A.13}$$

Anisotropy Energy

Applying (A.9) to the anisotropy energy, it can be expressed as

$$\begin{aligned} w_{\mathrm{Aniso},i} &= \mathbb{E}\left[K_1 \sin^2(\Phi_i - \varphi_{\mathrm{Aniso}})\right] \\ &= K_1\, \mathbb{E}\left[\sin^2(\Phi_i - \varphi_{\mathrm{Aniso}})\right] \\ &= K_1 \left(\frac{1 - \exp(-2\sigma_i^2)}{2} + \exp(-2\sigma_i^2) \sin^2(\bar{\varphi}_i - \varphi_{\mathrm{Aniso}})\right) \quad . \end{aligned} \tag{A.14}$$

A.2 Expectation Value of Bivariate Wrapped Circular Distributions

Basically, it is assumed that two random variables Φ_{i1} and Φ_{i2} are represented by the bivariate circular probability density function $(\Phi_{i1}, \Phi_{i2}) \sim f_i(\varphi_1, \varphi_2)$, fulfilling the standardization condition

$$\int_{-\pi}^{\pi} \int_{-\pi}^{\pi} f_i(\varphi_1, \varphi_2)\, \mathrm{d}\varphi_2\, \mathrm{d}\varphi_1 = 1 \quad . \tag{A.15}$$

Similarly to the univariate case, the wrapped circular distribution can be gained by wrapping of a linear distribution

$$f_i(\varphi_1, \varphi_2) = \sum_{k \in \mathbb{Z}} \sum_{l \in \mathbb{Z}} f_i^{\phi}(\phi_1 = \varphi_1 + 2\pi k, \phi_2 = \varphi_2 + 2\pi l) \quad . \tag{A.16}$$

A.2.1 Expectation Value for 2π-Periodic Functions

For a 2π-periodic function in two variables φ_1 and φ_2

$$g(\varphi_1, \varphi_2) = g(\varphi_1 + 2\pi k, \varphi_2 + 2\pi l) \quad k, l \in \mathbb{Z} \tag{A.17}$$

the expectation value can be calculated as

$$\begin{aligned}
\mathbb{E}\left[g(\Phi_{i1},\Phi_{i2})\right] &= \int_{-\pi}^{\pi}\int_{-\pi}^{\pi} g(\varphi_1,\varphi_2)\; f_i(\varphi_1,\varphi_2)\,\mathrm{d}\varphi_2\,\mathrm{d}\varphi_1 \\
&= \int_{-\pi}^{\pi}\int_{-\pi}^{\pi} g(\varphi_1,\varphi_2)\; \sum_{k\in\mathbb{Z}}\sum_{l\in\mathbb{Z}} f_i^{\phi}(\varphi_1+2\pi k,\varphi_2+2\pi l)\,\mathrm{d}\varphi_2\,\mathrm{d}\varphi_1 \\
&= \sum_{k\in\mathbb{Z}}\sum_{l\in\mathbb{Z}}\int_{-\pi}^{\pi}\int_{-\pi}^{\pi} g(\varphi_1+2\pi k,\varphi_2+2\pi l)\; f_i^{\phi}(\varphi_1+2\pi k,\varphi_2+2\pi l)\,\mathrm{d}\varphi \\
&= \sum_{k\in\mathbb{Z}}\int_{2\pi k-\pi}^{2\pi k+\pi}\sum_{l\in\mathbb{Z}}\int_{2\pi l-\pi}^{2\pi l+\pi} g(\phi_1,\phi_2)\; f_i^{\phi}(\phi_1,\phi_2)\,\mathrm{d}\phi_2\,\mathrm{d}\phi_1 \\
&= \int_{-\infty}^{\infty}\int_{-\infty}^{\infty} g(\phi_1,\phi_2)\; f_i^{\phi}(\phi_1,\phi_2)\,\mathrm{d}\phi_2\,\mathrm{d}\phi_1 \quad . \qquad \text{(A.18)}
\end{aligned}$$

As for the univariate distribution, the expectation value of a 2π-periodic function can either be calculated based on the bivariate wrapped circular distribution or equivalently on the corresponding linear distribution.

A.2.2 Analytical Results for the Wrapped Normal Distribution

The *bivariate wrapped normal distribution* $\mathrm{WN}_2(\bar{\varphi}_{i1},\bar{\varphi}_{i2},\sigma_{i1}^2,\sigma_{i2}^2,\rho_i)$ is based on the *linear bivariate normal distribution* $\mathrm{N}_2(\bar{\varphi}_{i1},\bar{\varphi}_{i2},\sigma_{i1}^2,\sigma_{i2}^2,\rho_i)$

$$\begin{aligned}
f_i^{\phi}(\phi_1,\phi_2) &= \frac{1}{2\pi\sqrt{\sigma_{i1}^2\sigma_{i2}^2}\sqrt{1-\rho_i^2}}\cdot \\
&\quad \cdot\exp\left(-\frac{1}{2\left(1-\rho_i^2\right)}\left(\frac{\left(\phi_1-\bar{\varphi}_{i1}\right)^2}{\sigma_{i1}^2}+\frac{\left(\phi_2-\bar{\varphi}_{i2}\right)^2}{\sigma_{i2}^2}-\frac{2\rho_i\left(\phi_1-\bar{\varphi}_{i1}\right)\left(\phi_2-\bar{\varphi}_{i2}\right)}{\sqrt{\sigma_{i1}^2\sigma_{i2}^2}}\right)\right)
\end{aligned} \qquad \text{(A.19)}$$

with mean directions $\bar{\varphi}_{i1}$ and $\bar{\varphi}_{i2}$, the variances $\sigma_{i1}^2$and σ_{i2}^2, and the correlation coefficient ρ_i.

Cosine of the Difference

The function $g(\varphi_1,\varphi_2)=\cos(\varphi_1-\varphi_2)$ is 2π-periodic, since

$$\begin{aligned}
g(\varphi_1+2\pi k,\varphi_2+2\pi l) &= \cos(\varphi_1-\varphi_2+2\pi(k-l)) \\
&= \cos(\varphi_1-\varphi_2)\cos(2\pi(k-l))-\sin(\varphi_1-\varphi_2)\sin(2\pi(k-l)) \\
&= \cos(\varphi_1-\varphi_2) \quad .
\end{aligned}$$

So, the expectation value based on a bivariate wrapped normal distribution (A.19) is derived by employing (A.18)

$$
\begin{aligned}
\mathbb{E}\left[\cos(\Phi_{i1}-\Phi_{i2})\right] &= \int_{-\infty}^{\infty}\int_{-\infty}^{\infty} \cos(\phi_1-\phi_2)\; f_i^{\phi}(\phi_1,\phi_2)\;\; \mathrm{d}\phi_2\,\mathrm{d}\phi_1 \\
&= \int_{-\infty}^{\infty}\int_{-\infty}^{\infty} \left(\cos(\phi_1)\cos(\phi_2)+\sin(\phi_1)\sin(\phi_2)\right)\; f_i^{\phi}(\phi_1,\phi_2)\;\; \mathrm{d}\phi_2\,\mathrm{d}\phi_1 \\
&= \int_{-\infty}^{\infty} \cos(\phi_1) \underbrace{\int_{-\infty}^{\infty} \cos(\phi_2)\, f_i^{\phi}(\phi_1,\phi_2)\;\; \mathrm{d}\phi_2}_{C(\phi_1)}\,\mathrm{d}\phi_1 + \\
&\quad + \int_{-\infty}^{\infty} \sin(\phi_1) \underbrace{\int_{-\infty}^{\infty} \sin(\phi_2)\, f_i^{\phi}(\phi_1,\phi_2)\;\; \mathrm{d}\phi_2}_{S(\phi_1)}\,\mathrm{d}\phi_1
\end{aligned} \tag{A.20}
$$

Next, the following substitution of variables is applied

$$
z_1 := \frac{\phi_1-\bar{\varphi}_{i1}}{\sigma_{i1}} \quad \text{and} \quad z_2 := \frac{\phi_2-\bar{\varphi}_{i2}}{\sigma_{i2}} \quad . \tag{A.21}
$$

Hence, the integrals of (A.20) result as

$$
\begin{aligned}
C(\phi_1) &= \int_{-\infty}^{\infty} \cos(\phi_2)\, f_i^{\phi}(\phi_1,\phi_2)\;\; \mathrm{d}\phi_2 \\
C(z_1) &= \int_{-\infty}^{\infty} \cos(z_2\sigma_{i2}+\bar{\varphi}_{i2}) \tfrac{1}{2\pi\sigma_{i1}\sigma_{i2}\sqrt{1-\rho_i^2}} \exp\left(-\tfrac{1}{2\left(1-\rho_i^2\right)}\left(z_1^2+z_2^2-2\rho_i z_1 z_2\right)\right)\;\; \sigma_{i2}\mathrm{d}z_2 \\
&= \tfrac{1}{2\pi\sigma_{i1}\sqrt{1-\rho_i^2}} \exp\left(-\tfrac{1}{2}z_1^2\right) \int_{-\infty}^{\infty} \cos(z_2\sigma_{i2}+\bar{\varphi}_{i2}) \exp\left(-\tfrac{1}{2}\left(\frac{z_1^2-2\rho_i z_1 z_2+z_2^2}{1-\rho_i^2}-z_1^2\right)\right)\;\; \mathrm{d}z_2 \\
&= \tfrac{1}{2\pi\sigma_{i1}\sqrt{1-\rho_i^2}} \exp\left(-\tfrac{1}{2}z_1^2\right) \int_{-\infty}^{\infty} \cos(z_2\sigma_{i2}+\bar{\varphi}_{i2}) \exp\left(-\tfrac{1}{2}\left(\frac{\rho_i^2 z_1^2-2\rho_i z_1 z_2+z_2^2}{1-\rho_i^2}\right)\right)\;\; \mathrm{d}z_2 \\
&= \tfrac{1}{\sqrt{2\pi}\sigma_{i1}} \exp\left(-\tfrac{1}{2}z_1^2\right) \int_{-\infty}^{\infty} \cos(z_2\underbrace{\sigma_{i2}}_{a}+\underbrace{\bar{\varphi}_{i2}}_{b}) \underbrace{\tfrac{1}{\sqrt{2\pi}\sqrt{1-\rho_i^2}} \exp\left(-\tfrac{1}{2}\left(\frac{z_2-\rho_i z_1}{\sqrt{1-\rho_i^2}}\right)^2\right)}_{f(\rho_i z_1, 1-\rho_i^2)}\;\; \mathrm{d}z_2 \\
&= \tfrac{1}{\sqrt{2\pi}\sigma_{i1}} \exp\left(-\tfrac{1}{2}z_1^2\right)\; \exp\left(-\frac{\sigma_{i2}^2(1-\rho_i^2)}{2}\right) \cos\left(\sigma_{i2}\rho_i z_1+\bar{\varphi}_{i2}\right)
\end{aligned} \tag{A.22}
$$

and

$$
\begin{aligned}
S(\phi_1) &= \int_{-\infty}^{\infty} \sin(\phi_2)\, f_i^{\phi}(\phi_1,\phi_2)\ \mathrm{d}\phi_2 \\
S(z_1) &= \int_{-\infty}^{\infty} \sin(z_2\sigma_{i2}+\bar{\varphi}_{i2}) \tfrac{1}{2\pi\sigma_{i1}\sigma_{i2}\sqrt{1-\rho_i^2}} \exp\left(-\tfrac{1}{2\left(1-\rho_i^2\right)}\left(z_1^2+z_2^2-2\rho_i z_1 z_2\right)\right)\ \sigma_{i2}\mathrm{d}z_2 \\
&= \tfrac{1}{2\pi\sigma_{i1}\sqrt{1-\rho_i^2}} \exp\left(-\tfrac{1}{2}z_1^2\right) \int_{-\infty}^{\infty} \sin(z_2\sigma_{i2}+\bar{\varphi}_{i2}) \exp\left(-\tfrac{1}{2}\left(\frac{z_1^2-2\rho_i z_1 z_2+z_2^2}{1-\rho_i^2}-z_1^2\right)\right)\ \mathrm{d}z_2 \\
&= \tfrac{1}{2\pi\sigma_{i1}\sqrt{1-\rho_i^2}} \exp\left(-\tfrac{1}{2}z_1^2\right) \int_{-\infty}^{\infty} \sin(z_2\sigma_{i2}+\bar{\varphi}_{i2}) \exp\left(-\tfrac{1}{2}\left(\frac{\rho_i^2 z_1^2-2\rho_i z_1 z_2+z_2^2}{1-\rho_i^2}\right)\right)\ \mathrm{d}z_2 \\
&= \tfrac{1}{\sqrt{2\pi}\sigma_{i1}} \exp\left(-\tfrac{1}{2}z_1^2\right) \int_{-\infty}^{\infty} \sin(z_2\underbrace{\sigma_{i2}}_{a}+\underbrace{\bar{\varphi}_{i2}}_{b}) \underbrace{\tfrac{1}{\sqrt{2\pi}\sqrt{1-\rho_i^2}} \exp\left(-\tfrac{1}{2}\left(\frac{z_2-\rho_i z_1}{\sqrt{1-\rho_i^2}}\right)^2\right)}_{f(\rho_i z_1,1-\rho_i^2)}\ \mathrm{d}z_2 \\
&= \tfrac{1}{\sqrt{2\pi}\sigma_{i1}} \exp\left(-\tfrac{1}{2}z_1^2\right) \exp\left(-\frac{\sigma_{i2}^2(1-\rho_i^2)}{2}\right) \sin\left(\sigma_{i2}\rho_i z_1+\bar{\varphi}_{i2}\right) \quad . \qquad \text{(A.23)}
\end{aligned}
$$

Thereby, the integrals are calculated by using (A.6) and (A.8).

Proceeding with (A.20), the expectation value results as

$$
\begin{aligned}
\mathbb{E}\left[\cos(\Phi_{i1}-\Phi_{i2})\right] &= \int_{-\infty}^{\infty} \cos(\phi_1)C(\phi_1)\ \mathrm{d}\phi_1 + \int_{-\infty}^{\infty} \sin(\phi_1)S(\phi_1)\ \mathrm{d}\phi_1 \\
&= \int_{-\infty}^{\infty} \cos(z_1\sigma_{i1}+\bar{\varphi}_{i1})C(z_1) + \sin(z_1\sigma_{i1}+\bar{\varphi}_{i1})S(z_1)\ \sigma_{i1}\mathrm{d}z_1 \\
&= \tfrac{1}{\sqrt{2\pi}} \exp\left(-\tfrac{\sigma_{i2}^2(1-\rho_i^2)}{2}\right) \int_{-\infty}^{\infty} \left(\cos(z_1\sigma_{i1}+\bar{\varphi}_{i1})\cos\left(\sigma_{i2}\rho_i z_1+\bar{\varphi}_{i2}\right)+\right. \\
&\qquad \left. +\sin(z_1\sigma_{i1}+\bar{\varphi}_{i1})\sin\left(\sigma_{i2}\rho_i z_1+\bar{\varphi}_{i2}\right)\right) \exp\left(-\tfrac{1}{2}z_1^2\right)\ \mathrm{d}z_1 \\
&= \tfrac{1}{\sqrt{2\pi}} \exp\left(-\tfrac{\sigma_{i2}^2(1-\rho_i^2)}{2}\right) \int_{-\infty}^{\infty} \cos(z_1\sigma_{i1}+\bar{\varphi}_{i1}-\sigma_{i2}\rho_i z_1-\bar{\varphi}_{i2}) \exp\left(-\tfrac{1}{2}z_1^2\right)\ \mathrm{d}z_1 \\
&= \exp\left(-\tfrac{\sigma_{i2}^2(1-\rho_i^2)}{2}\right) \int_{-\infty}^{\infty} \cos(\underbrace{(\sigma_{i1}-\sigma_{i2}\rho_i)}_{a}z_1+\underbrace{(\bar{\varphi}_{i1}-\bar{\varphi}_{i2})}_{b}) \underbrace{\tfrac{1}{\sqrt{2\pi}} \exp\left(-\tfrac{1}{2}z_1^2\right)}_{f(0,1)}\ \mathrm{d}z_1 \\
&= \exp\left(-\tfrac{\sigma_{i2}^2(1-\rho_i^2)}{2}\right) \exp\left(-\tfrac{(\sigma_{i1}-\sigma_{i2}\rho_i)^2}{2}\right) \cos\left((\sigma_{i1}-\sigma_{i2}\rho_i)\cdot 0+(\bar{\varphi}_{i1}-\bar{\varphi}_{i2})\right) \\
&= \exp\left(-\tfrac{\sigma_{i1}^2-2\rho_i\sigma_{i1}\sigma_{i2}+\sigma_{i2}^2}{2}\right) \cos\left(\bar{\varphi}_{i1}-\bar{\varphi}_{i2}\right) \quad . \qquad \text{(A.24)}
\end{aligned}
$$

In case of identical mean values $\bar{\varphi}_i = \bar{\varphi}_{i1} = \bar{\varphi}_{i2}$ and identical variances $\sigma_i^2 = \sigma_{i1}^2 = \sigma_{i2}^2$, (A.24) simplifies to

$$\mathbb{E}\left[\cos(\Phi_{i1} - \Phi_{i2})\right] = \exp\left(-\sigma_i^2(1-\rho_i)\right) \quad . \tag{A.25}$$

A.3 Reversible Anhysteretic Energy

A.3.1 Fermi Statistics and Stirling's Approximation

For a large number of indistinguishable particles, Stirling's approximation

$$n! \approx \frac{n^n}{\mathrm{e}^n} \tag{A.26}$$

can be applied to Fermi statistics

$$\begin{aligned}
P &= \prod_{i=1}^{N_\mathcal{D}} \binom{a_{\mathcal{D}_i}}{n_{\mathcal{D}_i}} \\
&= \prod_{i=1}^{N_\mathcal{D}} \frac{a_{\mathcal{D}_i}!}{n_{\mathcal{D}_i}!\,(a_{\mathcal{D}_i} - n_{\mathcal{D}_i})!} \\
&= \prod_{i=1}^{N_\mathcal{D}} \frac{(a_{\mathcal{D}_i})^{a_{\mathcal{D}_i}}\,\mathrm{e}^{n_{\mathcal{D}_i}}\,\mathrm{e}^{a_{\mathcal{D}_i}-n_{\mathcal{D}_i}}}{\mathrm{e}^{a_{\mathcal{D}_i}}(n_{\mathcal{D}_i})^{n_{\mathcal{D}_i}}\,(a_{\mathcal{D}_i} - n_{\mathcal{D}_i})^{a_{\mathcal{D}_i}-n_{\mathcal{D}_i}}} \\
&= \prod_{i=1}^{N_\mathcal{D}} \frac{(a_{\mathcal{D}_i})^{a_{\mathcal{D}_i}}}{(n_{\mathcal{D}_i})^{n_{\mathcal{D}_i}}\,(a_{\mathcal{D}_i} - n_{\mathcal{D}_i})^{a_{\mathcal{D}_i}-n_{\mathcal{D}_i}}} \\
&= \prod_{i=1}^{N_\mathcal{D}} \frac{\left(\frac{a_{\mathcal{D}_i}}{n_\mathcal{V}}\right)^{a_{\mathcal{D}_i}}}{\left(\frac{n_{\mathcal{D}_i}}{n_\mathcal{V}}\right)^{n_{\mathcal{D}_i}}\left(\frac{a_{\mathcal{D}_i}-n_{\mathcal{D}_i}}{n_\mathcal{V}}\right)^{a_{\mathcal{D}_i}-n_{\mathcal{D}_i}}} \\
&= \prod_{i=1}^{N_\mathcal{D}} \left(\frac{\left(\frac{a_{\mathcal{D}_i}}{n_\mathcal{V}}\right)^{\frac{a_{\mathcal{D}_i}}{n_\mathcal{V}}}}{\left(\frac{n_{\mathcal{D}_i}}{n_\mathcal{V}}\right)^{\frac{n_{\mathcal{D}_i}}{n_\mathcal{V}}}\left(\frac{a_{\mathcal{D}_i}-n_{\mathcal{D}_i}}{n_\mathcal{V}}\right)^{\frac{a_{\mathcal{D}_i}-n_{\mathcal{D}_i}}{n_\mathcal{V}}}} \right)^{n_\mathcal{V}} \quad .
\end{aligned} \tag{A.27}$$

When using volume fractions instead of particles

$$v_i = \frac{n_{\mathcal{D}_i}}{n_\mathcal{V}} \quad \text{and} \quad v_{\max,i} = \frac{a_{\mathcal{D}_i}}{n_\mathcal{V}} \quad , \tag{A.28}$$

the number of states is

$$P(v_1, ..., v_{N_\mathcal{D}}) = \left(\prod_{i=1}^{N_\mathcal{D}} \frac{v_{\max,i}^{v_{\max,i}}}{v_i^{v_i}\,(v_{\max,i} - v_i)^{v_{\max,i}-v_i}} \right)^{n_\mathcal{V}} \quad . \tag{A.29}$$

A.3.2 Reversible Anhysteretic Energy

Let

$$\begin{aligned} w_{\mathrm{REVANH}} &= -k_{\mathrm{RevAnh}} \frac{1}{n\mathcal{V}} \ln(P(v_1, ..., v_{N_\mathcal{D}})) && \text{(A.30a)} \\ &= -k_{\mathrm{RevAnh}} \sum_{i=1}^{N_\mathcal{D}} \ln\left(\frac{v_{\mathrm{max},i}^{v_{\mathrm{max},i}}}{v_i^{v_i} \ (v_{\mathrm{max},i} - v_i)^{v_{\mathrm{max},i} - v_i}} \right) && \text{(A.30b)} \\ &= -k_{\mathrm{RevAnh}} \sum_{i=1}^{N_\mathcal{D}} \left(v_{\mathrm{max},i} \ln(v_{\mathrm{max},i}) - v_i \ln(v_i) - (v_{\mathrm{max},i} - v_i) \ln\left(v_{\mathrm{max},i} - v_i\right) \right) \end{aligned}$$

be the (global) part of the reversible anhysteretic energy that phenomenologically describes the intrinsic order of the domain classes by means of statistics. Then, the derivation with respect to a certain volume fraction v_k is

$$\begin{aligned} \frac{\partial w_{\mathrm{REVANH}}}{\partial v_k} &= k_{\mathrm{RevAnh}} \left((1 + \ln(v_i)) - (1 + \ln(v_{\mathrm{max},i} - v_i)) \right) \\ &= k_{\mathrm{RevAnh}} \ln\left(\frac{v_i}{v_{\mathrm{max},i} - v_i} \right) \quad . && \text{(A.31)} \end{aligned}$$

Minimization

In order to calculate the equilibrium state, the free energy has to be minimized according to

$$\min_v \left\{ w_{\mathrm{Loc}} + w_{\mathrm{d}} + w_{\mathrm{RevAnh}} \right\} \qquad \text{s.t.} \quad \sum_{i=1}^{N_\mathcal{D}} v_i = 1 \quad . \tag{A.32}$$

The optimization problem with constraints can be solved by means of Lagrangian multipliers λ, so the Lagrange function is

$$\mathcal{L}(v_1, ..., v_{N_\mathcal{D}}, \lambda) = w_{\mathrm{Loc}} + w_{\mathrm{d}} + w_{\mathrm{RevAnh}} + \lambda \left(1 - \sum_{i=1}^{N_\mathcal{D}} v_i \right) \quad , \tag{A.33}$$

and the derivations with respect to v_k give the conditions for the optimum

$$\frac{\partial \mathcal{L}(v_1, ..., v_{N_\mathcal{D}}, \lambda)}{\partial v_k} = \frac{\partial w_{\mathrm{Loc}}}{\partial v_k} + \frac{\partial w_{\mathrm{d}}}{\partial v_k} + \frac{\partial w_{\mathrm{RevAnh}}}{\partial v_k} + \lambda \stackrel{!}{=} 0 \quad . \tag{A.34}$$

For the demagnetized state, the specified initial volume fractions $v_{0,i}$ must correspond to the energy minimum determined by (A.34). Thus, the reversible anhysteretic energy is defined as

$$w_{\mathrm{RevAnh}} = w_{\mathrm{REVANH}} + \sum_{i=1}^{N_\mathcal{D}} v_i w_{\mathrm{RevAnh0},i} \quad , \tag{A.35}$$

where the local contribution $w_{\mathrm{RevAnh0},i}$ is determined from the demagnetized state. Using condition (A.34) for the energy minimum in the demagnetized state

$$\begin{aligned}
&\frac{\partial w_{\mathrm{Loc}}}{\partial v_k} + \frac{\partial w_{\mathrm{d}}}{\partial v_k} + \frac{\partial w_{\mathrm{RevAnh}}}{\partial v_k} + \lambda \stackrel{!}{=} 0 \\
&w_{\mathrm{Loc0},k} + \left.\frac{\partial w_{\mathrm{d}}}{\partial v_k}\right|_{v_{0,k}} + \left.\frac{\partial w_{\mathrm{REVANH}}}{\partial v_k}\right|_{v_{0,k}} + w_{\mathrm{RevAnh0},k} + \lambda \stackrel{!}{=} 0 \quad ,
\end{aligned} \tag{A.36}$$

the local part of the reversible anhysteretic energy results as

$$\begin{aligned}
w_{\mathrm{RevAnh0},k} &= -k_{\mathrm{RevAnh}} \ln\left(\frac{v_{0,k}}{v_{\mathrm{max},k} - v_{0,k}}\right) - w_{\mathrm{Loc0},k} - \lambda \\
&= k_{\mathrm{RevAnh}} \ln\left(\frac{v_{\mathrm{max},k} - v_{0,k}}{v_{0,k}}\right) - w_{\mathrm{Loc0},k} - \lambda \quad .
\end{aligned} \tag{A.37}$$

Since the local energy contributions $w_{\mathrm{Loc0},k}$ should not affect the value of the reversible anhysteretic energy in the demagnetized state

$$w_{\mathrm{RevAnh0},k} = k_{\mathrm{RevAnh}} \ln\left(\frac{v_{\mathrm{max},k} - v_{0,k}}{v_{0,k}}\right) - (w_{\mathrm{Loc0},k} - w_{\mathrm{Loc0}}) \quad , \tag{A.38}$$

so that

$$\begin{aligned}
w_{\mathrm{RevAnh}}|_{v_0} &= w_{\mathrm{REVANH}}|_{v_0} + \sum_{i=1}^{N_{\mathcal{D}}} v_{0,i} \left(k_{\mathrm{RevAnh}} \ln\left(\frac{v_{\mathrm{max},i}}{v_{0,i}} - 1\right) - (w_{\mathrm{Loc0},i} - w_{\mathrm{Loc0}})\right) \\
&= w_{\mathrm{REVANH}}|_{v_0} + k_{\mathrm{RevAnh}} \sum_{i=1}^{N_{\mathcal{D}}} v_{0,i} \ln\left(\frac{v_{\mathrm{max},i}}{v_{0,i}} - 1\right) - \underbrace{\sum_{i=1}^{N_{\mathcal{D}}} v_{0,i} w_{\mathrm{Loc0},i}}_{w_{\mathrm{Loc0}}} + w_{\mathrm{Loc0}} \underbrace{\sum_{i=1}^{N_{\mathcal{D}}} v_{0,i}}_{1} \\
&= w_{\mathrm{REVANH}}|_{v_0} + k_{\mathrm{RevAnh}} \sum_{i=1}^{N_{\mathcal{D}}} v_{0,i} \ln\left(\frac{v_{\mathrm{max},i}}{v_{0,i}} - 1\right) \quad .
\end{aligned} \tag{A.39}$$

As a remark, the derivation of the demagnetizing energy w_{d} in the demagnetized state is zero, because of

$$\begin{aligned}
\frac{\partial w_{\mathrm{d}}}{\partial v_k} &= \frac{1}{2}\mu_0 M_{\mathrm{s}}^2 \frac{\partial}{\partial v_k}\left(m_x^2 N_{xx} + 2 m_x m_y N_{xy} + m_y^2 N_{yy}\right) \\
&= \frac{1}{2}\mu_0 M_{\mathrm{s}}^2 \left(2 m_x \frac{\partial m_x}{\partial v_k} N_{xx} + 2\left(\frac{\partial m_x}{\partial v_k} m_y + m_x \frac{\partial m_y}{\partial v_k}\right) N_{xy} + 2 m_y \frac{\partial m_y}{\partial v_k} N_{yy}\right) \\
&= \mu_0 M_{\mathrm{s}}^2 \left(m_x m_{xk} N_{xx} + (m_{xk} m_y + m_x m_{yk}) N_{xy} + m_y m_{yk} N_{yy}\right) \quad ,
\end{aligned} \tag{A.40}$$

and the fact that for the demagnetized state the sample magnetization $\vec{m} = \vec{0}$, and hence the orthogonal projections $m_x = 0$ and $m_y = 0$, yielding

$$\left.\frac{\partial w_{\mathrm{d}}}{\partial v_k}\right|_{v_{0,k}} = 0 \quad . \tag{A.41}$$

A.4 Volume Change due to Domain Wall Motion

In the following section it is demonstrated how to estimate the transition matrix $\{\Delta v_{ij}\}$ from given volume changes (Δv_i), based on

$$\Delta v_i = v_i(t+\Delta t) - v_i(t) = -\sum_{j=1}^{N_\mathcal{D}} \Delta v_{ij} \tag{A.42a}$$

$$\Delta v_j = v_j(t+\Delta t) - v_j(t) = \sum_{i=1}^{N_\mathcal{D}} \Delta v_{ij} \quad . \tag{A.42b}$$

As a general rule, it is assumed that the resulting domain wall motion is minimal for a given change in volume. Hence, it is stated that there is no significant domain wall motion between two increasing or decreasing domain classes.

$$\text{For } \Delta v_i > 0 \ \wedge \ \Delta v_j > 0 \quad \Rightarrow \Delta v_{ij} = 0 \tag{A.43a}$$

$$\text{or } \Delta v_i < 0 \ \wedge \ \Delta v_j < 0 \quad \Rightarrow \Delta v_{ij} = 0 \quad . \tag{A.43b}$$

Within the subsections below, analytical expressions are derived for the estimation of the transition matrix in case of 2, 3, and 4 domain classes.

A.4.1 Estimation of the Transition Matrix for 2 Domain Classes

For 2 domain classes, the transition matrix is

$$\begin{matrix} \\ \text{from} \end{matrix} \begin{matrix} \overbrace{\begin{matrix} \mathcal{D}_1 & \mathcal{D}_2 \end{matrix}}^{\text{to domain class}} \\ \begin{matrix} \mathcal{D}_1 \\ \mathcal{D}_2 \end{matrix} \end{matrix} \begin{pmatrix} 0 & \Delta v_{12} \\ -\Delta v_{12} & 0 \end{pmatrix} \quad . \tag{A.44}$$

Here, the volume transition is simply given by

$$\Delta v_{12} = -\Delta v_1 \quad . \tag{A.45}$$

A.4.2 Estimation of the Transition Matrix for 3 Domain Classes

In case of 3 domain classes, the transition matrix is

$$\begin{matrix} \\ \text{from} \end{matrix} \begin{matrix} \overbrace{\begin{matrix} \mathcal{D}_1 & \mathcal{D}_2 & \mathcal{D}_3 \end{matrix}}^{\text{to domain class}} \\ \begin{matrix} \mathcal{D}_1 \\ \mathcal{D}_2 \\ \mathcal{D}_3 \end{matrix} \end{matrix} \begin{pmatrix} 0 & \Delta v_{12} & \Delta v_{13} \\ -\Delta v_{12} & 0 & \Delta v_{23} \\ -\Delta v_{13} & -\Delta v_{23} & 0 \end{pmatrix} \quad . \tag{A.46}$$

Case 1: Only One Increasing Domain Class

If only one domain class has increasing volume fraction, re-indexing according to

$$\begin{aligned} \text{Increasing domain class:} \quad & \Delta v_a > 0 \\ \text{Decreasing domain classes:} \quad & 0 \geq \Delta v_y \geq \Delta v_z \quad , \end{aligned}$$

yields the corresponding transition matrix

$$\begin{array}{c} \\ \mathcal{D}_z \\ \mathcal{D}_y \\ \mathcal{D}_a \end{array} \begin{array}{c} \begin{array}{ccc} \mathcal{D}_z & \mathcal{D}_y & \mathcal{D}_a \end{array} \\ \begin{pmatrix} 0 & 0 & \Delta v_{za} \\ 0 & 0 & \Delta v_{ya} \\ -\Delta v_{za} & -\Delta v_{ya} & 0 \end{pmatrix} \end{array} \quad , \tag{A.47}$$

when (A.43) is considered. Hence, the volume transitions are

$$\Delta v_{ya} = -\Delta v_y \tag{A.48a}$$

$$\Delta v_{za} = -\Delta v_z \quad . \tag{A.48b}$$

Case 2: Only One Decreasing Domain Class

Similar to case 1, a re-indexing is done with respect to the decreasing domain class

$$\begin{aligned} \text{Increasing domain classes:} \quad & \Delta v_a \geq \Delta v_b \geq 0 \\ \text{Decreasing domain class:} \quad & 0 > \Delta v_z \quad , \end{aligned}$$

that yields the corresponding transition matrix

$$\begin{array}{c} \\ \mathcal{D}_z \\ \mathcal{D}_b \\ \mathcal{D}_a \end{array} \begin{array}{c} \begin{array}{ccc} \mathcal{D}_z & \mathcal{D}_b & \mathcal{D}_a \end{array} \\ \begin{pmatrix} 0 & \Delta v_{zb} & \Delta v_{za} \\ -\Delta v_{zb} & 0 & 0 \\ -\Delta v_{za} & 0 & 0 \end{pmatrix} \end{array} \quad , \tag{A.49}$$

when (A.43) is considered. Hence, the volume transitions are

$$\Delta v_{zb} = \Delta v_b \tag{A.50a}$$

$$\Delta v_{za} = \Delta v_a \quad . \tag{A.50b}$$

A.4.3 Estimation of the Transition Matrix for 4 Domain Classes

In case of 4 domain classes, the transition matrix is

$$\begin{array}{c} \\ \text{from} \\ \\ \\ \\ \end{array} \begin{array}{c} \overbrace{\begin{array}{cccc} \mathcal{D}_1 & \mathcal{D}_2 & \mathcal{D}_3 & \mathcal{D}_4 \end{array}}^{\text{to domain class}} \\ \begin{pmatrix} 0 & \Delta v_{12} & \Delta v_{13} & \Delta v_{14} \\ -\Delta v_{12} & 0 & \Delta v_{23} & \Delta v_{24} \\ -\Delta v_{13} & -\Delta v_{23} & 0 & \Delta v_{34} \\ -\Delta v_{14} & -\Delta v_{24} & -\Delta v_{34} & 0 \end{pmatrix} \end{array} \begin{array}{l} \\ \mathcal{D}_1 \\ \mathcal{D}_2 \\ \mathcal{D}_3 \\ \mathcal{D}_4 \end{array} \quad . \tag{A.51}$$

Case 1: Only One Increasing Domain Class

First, the re-indexing is done as follows

$$\begin{aligned} \text{Increasing domain class} &: \quad \Delta v_a > 0 \\ \text{Decreasing domain classes} &: \quad 0 \geq \Delta v_x \geq \Delta v_y \geq \Delta v_z \quad , \end{aligned}$$

and gives the transition matrix

$$\begin{array}{c} \\ \mathcal{D}_z \\ \mathcal{D}_y \\ \mathcal{D}_x \\ \mathcal{D}_a \end{array} \begin{array}{c} \begin{array}{cccc} \mathcal{D}_z & \mathcal{D}_y & \mathcal{D}_x & \mathcal{D}_a \end{array} \\ \begin{pmatrix} 0 & 0 & 0 & \Delta v_{za} \\ 0 & 0 & 0 & \Delta v_{ya} \\ 0 & 0 & 0 & \Delta v_{xa} \\ -\Delta v_{za} & -\Delta v_{ya} & -\Delta v_{xa} & 0 \end{pmatrix} \end{array} \quad . \tag{A.52}$$

In this case, it is clear that the transition of volumes is from each of the decreasing domain classes to the increasing domain class

$$\Delta v_{xa} = -\Delta v_x \tag{A.53a}$$
$$\Delta v_{ya} = -\Delta v_y \tag{A.53b}$$
$$\Delta v_{za} = -\Delta v_z \quad . \tag{A.53c}$$

Case 2: Only One Decreasing Domain Class

Re-indexing gives

$$\begin{aligned} \text{Increasing domain classes:} &\quad \Delta v_a \geq \Delta v_b \geq \Delta v_c \geq 0 \\ \text{Decreasing domain class:} &\quad 0 > \Delta v_z \quad , \end{aligned}$$

so that the transition matrix is

$$\begin{array}{c} \\ \mathcal{D}_z \\ \mathcal{D}_c \\ \mathcal{D}_b \\ \mathcal{D}_a \end{array} \begin{array}{c} \begin{array}{cccc} \mathcal{D}_z & \mathcal{D}_c & \mathcal{D}_b & \mathcal{D}_a \end{array} \\ \begin{pmatrix} 0 & \Delta v_{zc} & \Delta v_{zb} & \Delta v_{za} \\ -\Delta v_{zc} & 0 & 0 & 0 \\ -\Delta v_{zb} & 0 & 0 & 0 \\ -\Delta v_{za} & 0 & 0 & 0 \end{pmatrix} \end{array} \quad . \tag{A.54}$$

In this case, it is clear that the transition of volumes is from each of the decreasing domain class to every of the increasing domain classes

$$\Delta v_{zc} = \Delta v_c \tag{A.55a}$$
$$\Delta v_{zb} = \Delta v_b \tag{A.55b}$$
$$\Delta v_{za} = \Delta v_a \quad . \tag{A.55c}$$

Case 3: Two Increasing Domain Classes

The re-indexing is done as follows

$$\begin{aligned} \text{Increasing domain classes:} &\quad \Delta v_a \geq \Delta v_b \geq 0 \\ \text{Decreasing domain classes:} &\quad 0 \geq \Delta v_y \geq \Delta v_z \quad , \end{aligned}$$

and gives the transition matrix

$$\begin{array}{c} \\ \mathcal{D}_z \\ \mathcal{D}_y \\ \mathcal{D}_b \\ \mathcal{D}_a \end{array} \begin{array}{c} \begin{array}{cccc} \mathcal{D}_z & \mathcal{D}_y & \mathcal{D}_b & \mathcal{D}_a \end{array} \\ \begin{pmatrix} 0 & 0 & \Delta v_{zb} & \Delta v_{za} \\ 0 & 0 & \Delta v_{yb} & \Delta v_{ya} \\ -\Delta v_{zb} & -\Delta v_{yb} & 0 & 0 \\ -\Delta v_{za} & -\Delta v_{ya} & 0 & 0 \end{pmatrix} \end{array} \quad . \tag{A.56}$$

Here we have 4 unknown variables, which have to be calculated from 3 independent variables, leading to 3 independent equations

$$\begin{aligned} \Delta v_{zb} + \Delta v_{za} &= -\Delta v_z && \text{(A.57a)} \\ \Delta v_{yb} + \Delta v_{ya} &= -\Delta v_y && \text{(A.57b)} \\ -\Delta v_{zb} - \Delta v_{yb} &= -\Delta v_b \quad . && \text{(A.57c)} \end{aligned}$$

In order to solve the problem, an additional criterion has to be stated

$$\Lambda = \sum_{i=1}^{N_\mathcal{D}} \sum_{j=1}^{N_\mathcal{D}} (\Delta v_{ij})^2 \longrightarrow MIN \quad . \tag{A.58}$$

From (A.57) all the volume transitions can be expressed in terms of Δv_{zb}

$$\begin{aligned} \Delta v_{za} &= -\Delta v_z - \Delta v_{zb} && \text{(A.59a)} \\ \Delta v_{yb} &= \Delta v_b - \Delta v_{zb} && \text{(A.59b)} \\ \Delta v_{ya} &= -\Delta v_y - \Delta v_b + \Delta v_{zb} && \text{(A.59c)} \end{aligned}$$

so that sum of squares is

$$\begin{aligned} \Lambda &= (\Delta v_{zb})^2 + (\Delta v_{za})^2 + (\Delta v_{yb})^2 + (\Delta v_{ya})^2 \\ &= (\Delta v_{zb})^2 + (-\Delta v_z - \Delta v_{zb})^2 + (-\Delta v_b + \Delta v_{zb})^2 + (-\Delta v_y - \Delta v_b + \Delta v_{zb})^2 \\ &= 4(\Delta v_{zb})^2 + 2\Delta v_{zb}\,(-\Delta v_y + \Delta v_z - 2\Delta v_b) + (\Delta v_z)^2 + (\Delta v_b)^2 + (\Delta v_b + \Delta v_y)^2 \quad . \end{aligned} \tag{A.60}$$

Now the minimum can be calculated on the unknown variable Δv_{zb} by setting the first derivative to zero

$$\frac{\mathrm{d}\Lambda}{\mathrm{d}\Delta v_{zb}} = 8\Delta v_{zb} + 2\,(-\Delta v_y + \Delta v_z - 2\Delta v_b) \stackrel{!}{=} 0 \quad , \tag{A.61}$$

and the transition volumes can be estimated from the volume changes as

$$\begin{aligned} \Delta v_{zb} &= \tfrac{1}{4}\,(2\Delta v_b + \Delta v_y - \Delta v_z) && \text{(A.62a)} \\ \Delta v_{za} &= \tfrac{1}{4}\,(-2\Delta v_b - \Delta v_y - 3\Delta v_z) && \text{(A.62b)} \\ \Delta v_{yb} &= \tfrac{1}{4}\,(2\Delta v_b - \Delta v_y + \Delta v_z) && \text{(A.62c)} \\ \Delta v_{ya} &= \tfrac{1}{4}\,(-2\Delta v_b - 3\Delta v_y - \Delta v_z) \quad . && \text{(A.62d)} \end{aligned}$$

Finally, the constraints that volume transitions are still directed from decreasing to increasing domain classes, have to be checked

$$\begin{aligned}
\Delta v_{zb} &= \tfrac{1}{4}\left(2\Delta v_b + \Delta v_y - \Delta v_z\right) \geq 0 && \text{(A.63)}\\
&\Rightarrow \underbrace{\Delta v_b}_{\geq 0} \geq \tfrac{1}{2}(\underbrace{-\Delta v_y + \Delta v_z}_{\Delta v_z \leq \Delta v_y})
\end{aligned}$$

$$\begin{aligned}
\Delta v_{za} &= \tfrac{1}{4}\left(-2\Delta v_b - \Delta v_y - 3\Delta v_z\right) \geq 0 && \text{(A.64)}\\
&\Rightarrow \Delta v_b \leq \tfrac{1}{2}(-\Delta v_y - 3\Delta v_z)\\
&\Rightarrow \Delta v_b \leq -\tfrac{1}{2}(\Delta v_y + \Delta v_z) - \Delta v_z\\
&\Rightarrow \Delta v_b \leq \tfrac{1}{2}(\Delta v_a + \Delta v_b) - \Delta v_z\\
&\Rightarrow \underbrace{\Delta v_z}_{\leq 0} \leq \tfrac{1}{2}(\underbrace{\Delta v_a - \Delta v_b}_{\Delta v_a \geq \Delta v_b})
\end{aligned}$$

$$\begin{aligned}
\Delta v_{yb} &= \tfrac{1}{4}\left(2\Delta v_b - \Delta v_y + \Delta v_z\right) \geq 0 && \text{(A.65)}\\
&\Rightarrow \underbrace{\Delta v_b}_{\geq 0} \geq \tfrac{1}{2}(\underbrace{\Delta v_y - \Delta v_z}_{\Delta v_z \leq \Delta v_y})\\
&\Rightarrow \text{ Not fulfilled, in general}
\end{aligned}$$

$$\begin{aligned}
\Delta v_{ya} &= \tfrac{1}{4}\left(-2\Delta v_b - 3\Delta v_y - \Delta v_z\right) \geq 0 && \text{(A.66)}\\
&\Rightarrow \Delta v_b \leq \tfrac{1}{2}(-3\Delta v_y - \Delta v_z)\\
&\Rightarrow \Delta v_b \leq -\tfrac{1}{2}(\Delta v_y + \Delta v_z) - \Delta v_y\\
&\Rightarrow \Delta v_b \leq \tfrac{1}{2}(\Delta v_a + \Delta v_b) - \Delta v_y\\
&\Rightarrow \underbrace{\Delta v_y}_{\leq 0} \leq \tfrac{1}{2}(\underbrace{\Delta v_a - \Delta v_b}_{\Delta v_a \geq \Delta v_b})
\end{aligned}$$

Because of (A.66), the solution (A.62) is only valid, if

$$\Delta v_b \geq \tfrac{1}{2}(\Delta v_y - \Delta v_z) \quad . \tag{A.67}$$

Otherwise, $\Delta v_{yb} = 0$ resulting in the boundary solution

$$\begin{aligned}
\Delta v_{zb} &= \Delta v_b && \text{(A.68a)}\\
\Delta v_{za} &= -\Delta v_b - \Delta v_z && \text{(A.68b)}\\
\Delta v_{yb} &= 0 && \text{(A.68c)}\\
\Delta v_{ya} &= -\Delta v_y \quad . && \text{(A.68d)}
\end{aligned}$$

A.5 Probability of Reversible Domain Wall Motion

Basically, the probability for a reversible domain wall motion $P_{\mathrm{Rev}}(\Delta\xi)$ is given by the function

$$P_{\mathrm{Rev}}(\Delta\xi) = \begin{cases} 1 & \text{for } \Delta\xi = 0 \\ \exp\left(-\frac{q_{\mathrm{p}}}{\kappa_{\mathrm{J}}}(|\Delta\xi| - x_{\mathrm{J}})\right) & \text{for } 0 < |\Delta\xi| \leq |\Delta\xi_{\mathrm{NJ}}| \\ \exp\left(-\frac{q_{\mathrm{p}}}{\kappa_{\mathrm{NJ}}}(|\Delta\xi| - x_{\mathrm{NJ}})\right) & \text{for } |\Delta\xi| > |\Delta\xi_{\mathrm{NJ}}| \end{cases} , \tag{A.69}$$

and typical probability curves are depicted in Fig. A.1.

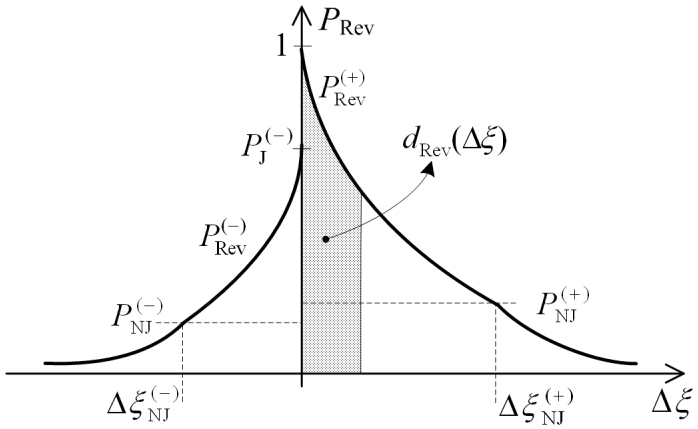

Figure A.1: Probability curves for reversible domain wall motion.

A.5.1 Properties of the Probability Function

Condition of Continuity

The parameters have to be chosen such that the probability curve is smooth at the point $(\Delta\xi_{\mathrm{NJ}}, P_{\mathrm{NJ}})$, i.e.

$$P_{\mathrm{NJ}} = P_{\mathrm{Rev}}(\Delta\xi_{\mathrm{NJ}}) \tag{A.70a}$$

$$= \exp\left(-\frac{q_{\mathrm{p}}}{\kappa_{\mathrm{J}}}(|\Delta\xi_{\mathrm{NJ}}| - x_{\mathrm{J}})\right) = \exp\left(-\frac{q_{\mathrm{p}}}{\kappa_{\mathrm{NJ}}}(|\Delta\xi_{\mathrm{NJ}}| - x_{\mathrm{NJ}})\right) \tag{A.70b}$$

$$\Rightarrow \Delta\xi_{\mathrm{NJ}}\left(\frac{1}{\kappa_{\mathrm{J}}} - \frac{1}{\kappa_{\mathrm{NJ}}}\right) = \frac{x_{\mathrm{J}}}{\kappa_{\mathrm{J}}} - \frac{x_{\mathrm{NJ}}}{\kappa_{\mathrm{NJ}}} \quad . \tag{A.70c}$$

A.5.2 Distance of Reversible Movement

If the domain wall has been moving over a certain distance $\Delta\xi$, the reversible part of movement d_{Rev} corresponds to the area under the probability curve

$$d_{\mathrm{Rev}}(\Delta\xi) = \int_0^{\Delta\xi} P_{\mathrm{Rev}}(x)\,\mathrm{d}x \quad . \tag{A.71}$$

For further calculations, the following derivations are required:

- Parameter $\Delta\xi_{\mathrm{NJ}}$ from (A.70b)

$$\begin{aligned} \Delta\xi_{\mathrm{NJ}} &= x_{\mathrm{J}} - \frac{\kappa_{\mathrm{J}}}{q_{\mathrm{p}}} \ln(P_{\mathrm{NJ}}) && \text{(A.72a)} \\ &= x_{\mathrm{NJ}} - \frac{\kappa_{\mathrm{NJ}}}{q_{\mathrm{p}}} \ln(P_{\mathrm{NJ}}) && \text{(A.72b)} \end{aligned}$$

- Area between $\Delta\xi \geq \Delta\xi_{\mathrm{NJ}}$ and infinity

$$\begin{aligned} \int_{\Delta\xi}^{\infty} P_{\mathrm{Rev}}(x)\,\mathrm{d}x &= \int_{\Delta\xi}^{\infty} \exp\left(-\frac{q_{\mathrm{p}}}{\kappa_{\mathrm{NJ}}}(|x| - x_{\mathrm{NJ}})\right)\,\mathrm{d}x \\ &= \frac{\kappa_{\mathrm{NJ}}}{q_{\mathrm{p}}} \exp\left(-\frac{q_{\mathrm{p}}}{\kappa_{\mathrm{NJ}}}(|\Delta\xi| - x_{\mathrm{NJ}})\right) \\ &= \frac{\kappa_{\mathrm{NJ}}}{q_{\mathrm{p}}} P_{\mathrm{Rev}}(\Delta\xi) && \text{(A.73)} \end{aligned}$$

and for the special case $\Delta\xi = \Delta\xi_{\mathrm{NJ}}$

$$\int_{\Delta\xi_{\mathrm{NJ}}}^{\infty} P_{\mathrm{Rev}}(x)\,\mathrm{d}x = \frac{\kappa_{\mathrm{NJ}}}{q_{\mathrm{p}}} P_{\mathrm{NJ}} \qquad \text{(A.74)}$$

- Area between $\Delta\xi \leq \Delta\xi_{\mathrm{NJ}}$ and $\Delta\xi_{\mathrm{NJ}}$

$$\begin{aligned} \int_{\Delta\xi}^{\Delta\xi_{\mathrm{NJ}}} P_{\mathrm{Rev}}(x)\,\mathrm{d}x &= \int_{\Delta\xi}^{\Delta\xi_{\mathrm{NJ}}} \exp\left(-\frac{q_{\mathrm{p}}}{\kappa_{\mathrm{J}}}(|x| - x_{\mathrm{J}})\right)\,\mathrm{d}x \\ &= \frac{\kappa_{\mathrm{J}}}{q_{\mathrm{p}}} \left(\exp\left(-\frac{q_{\mathrm{p}}}{\kappa_{\mathrm{J}}}(|\Delta\xi| - x_{\mathrm{J}})\right) - \exp\left(-\frac{q_{\mathrm{p}}}{\kappa_{\mathrm{J}}}(|\Delta\xi_{\mathrm{NJ}}| - x_{\mathrm{J}})\right)\right) \\ &= \frac{\kappa_{\mathrm{J}}}{q_{\mathrm{p}}} \left(P_{\mathrm{Rev}}(\Delta\xi) - P_{\mathrm{NJ}}\right) && \text{(A.75)} \end{aligned}$$

and for $\Delta\xi = 0$

$$\int_{0}^{\Delta\xi_{\mathrm{NJ}}} P_{\mathrm{Rev}}(x)\,\mathrm{d}x = \frac{\kappa_{\mathrm{J}}}{q_{\mathrm{p}}} \left(P_{\mathrm{J}} - P_{\mathrm{NJ}}\right) \qquad \text{(A.76)}$$

Maximum Distance of Reversible Movement

The maximum distance of reversible movement corresponds to the total area under the probability curve

$$\begin{aligned} d_{\mathrm{Rev,Max}} &= \int_0^{\infty} P_{\mathrm{Rev}}(x)\,dx \\ &= \int_0^{\Delta\xi_{\mathrm{NJ}}} P_{\mathrm{Rev}}(x)\,\mathrm{d}x + \int_{\Delta\xi_{\mathrm{NJ}}}^{\infty} P_{\mathrm{Rev}}(x)\,\mathrm{d}x \\ &= \frac{\kappa_{\mathrm{J}}}{q_{\mathrm{p}}}\left(P_{\mathrm{J}} - P_{\mathrm{NJ}}\right) + \frac{\kappa_{\mathrm{NJ}}}{q_{\mathrm{p}}} P_{\mathrm{NJ}} \\ &= \frac{1}{q_{\mathrm{p}}}\left(\kappa_{\mathrm{J}} P_{\mathrm{J}} - (\kappa_{\mathrm{J}} - \kappa_{\mathrm{NJ}}) P_{\mathrm{NJ}}\right) \quad . \end{aligned} \tag{A.77}$$

Hence, the total area under both parts of the probability curve is constant

$$d_{\mathrm{Rev,MAX}} = d^{(-)}_{\mathrm{Rev,Max}} + d^{(+)}_{\mathrm{Rev,Max}} = \frac{2}{q_{\mathrm{p}}} \quad , \tag{A.78}$$

independent of the domain wall motion reversal.

A.5.3 Reversal Point of Domain Wall Motion

For all further considerations, it is assumed that the (potential) reversal point of domain wall motion is reached coming from the positive $\Delta\xi$-direction, marked as $(+)$. After the reversal, the domain wall moves in the negative $\Delta\xi$-direction, marked as $(-)$.

Hence, at a (potential) reversal point $\Delta\xi_{\mathrm{R}}$ the corresponding probability P_{R} is

$$P_{\mathrm{R}} = P^{(+)}_{\mathrm{Rev}}(\Delta\xi_{\mathrm{R}}) \quad . \tag{A.79}$$

Whenever the term "New" is used, it indicates that the corresponding parameters are related to the updated probability curves after the reversal.

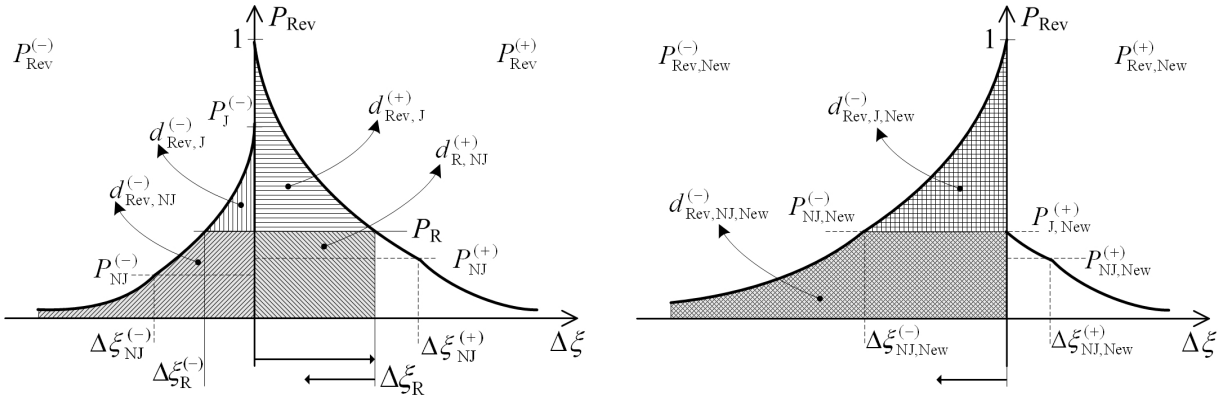

Figure A.2: Update of probability curves at a reversal point of domain wall motion.

Residual Distance of Reversible Movement at the Reversal Point

The maximum distance of reversible movement in the new $\Delta\xi$-direction, after having reached the equilibrium point is

$$d^{(-)}_{\mathrm{Rev,New}} = d^{(-)}_{\mathrm{Rev,NJ,New}} + d^{(-)}_{\mathrm{Rev,J,New}} \quad . \tag{A.80}$$

NJ-Part:

$$d^{(-)}_{\mathrm{Rev,NJ}} = \int_0^{\infty} \min\left(P_{\mathrm{R}}, P^{(-)}_{\mathrm{Rev}}(x)\right) \mathrm{d}x \quad . \tag{A.81}$$

If $P_{\mathrm{R}} \leq P^{(-)}_{\mathrm{NJ}}$ then

$$\begin{aligned} d^{(-)}_{\mathrm{Rev,NJ}} &= \Delta\xi^{(-)}_{\mathrm{R}} \cdot P_{\mathrm{R}} + \int_{\Delta\xi^{(-)}_{\mathrm{R}}}^{\infty} P^{(-)}_{\mathrm{Rev}}(x)\,\mathrm{d}x \\ &= \left(x^{(-)}_{\mathrm{NJ}} - \frac{\kappa^{(-)}_{\mathrm{NJ}}}{q_{\mathrm{p}}}\ln(P_{\mathrm{R}})\right) P_{\mathrm{R}} + \frac{\kappa^{(-)}_{\mathrm{NJ}}}{q_{\mathrm{p}}} P_{\mathrm{R}} \\ &= \frac{1}{q_{\mathrm{p}}} P_{\mathrm{R}} \left(q_{\mathrm{p}} x^{(-)}_{\mathrm{NJ}} + \kappa^{(-)}_{\mathrm{NJ}}(1 - \ln(P_{\mathrm{R}}))\right) \quad . \end{aligned} \tag{A.82}$$

Otherwise, for $P_{\mathrm{R}} > P^{(-)}_{\mathrm{NJ}}$

$$\begin{aligned} d^{(-)}_{\mathrm{Rev,NJ}} &= \Delta\xi^{(-)}_{\mathrm{R}} \cdot P_{\mathrm{R}} + \int_{\Delta\xi^{(-)}_{\mathrm{R}}}^{\Delta\xi_{\mathrm{NJ}}} P^{(-)}_{\mathrm{Rev}}(x)\,\mathrm{d}x + \int_{\Delta\xi_{\mathrm{NJ}}}^{\infty} P^{(-)}_{\mathrm{Rev}}(x)\,\mathrm{d}x \\ &= \left(x^{(-)}_{\mathrm{J}} - \frac{\kappa^{(-)}_{\mathrm{J}}}{q_{\mathrm{p}}}\ln(P_{\mathrm{R}})\right) P_{\mathrm{R}} + \frac{\kappa^{(-)}_{\mathrm{J}}}{q_{\mathrm{p}}}\left(P_{\mathrm{R}} - P_{\mathrm{NJ}}\right) + \frac{\kappa^{(-)}_{\mathrm{NJ}}}{q_{\mathrm{p}}} P_{\mathrm{NJ}} \\ &= \frac{1}{q_{\mathrm{p}}} P_{\mathrm{R}} \left(q_{\mathrm{p}} x^{(-)}_{\mathrm{J}} + \kappa^{(-)}_{\mathrm{J}}(1 - \ln(P_{\mathrm{R}}))\right) - \frac{1}{q_{\mathrm{p}}} P_{\mathrm{NJ}} \left(\kappa^{(-)}_{\mathrm{J}} - \kappa^{(-)}_{\mathrm{NJ}}\right) \quad . \end{aligned} \tag{A.83}$$

The NJ-part of the reversible distance before the domain wall motion is

$$d^{(+)}_{\mathrm{R,NJ}} = \Delta\xi_{\mathrm{R}} \cdot P_{\mathrm{R}} \tag{A.84}$$

$$= \begin{cases} \frac{1}{q_{\mathrm{p}}} P_{\mathrm{R}} \left(q_{\mathrm{p}} x^{(+)}_{\mathrm{NJ}} - \kappa^{(+)}_{\mathrm{NJ}} \ln(P_{\mathrm{R}})\right) & \text{for } P_{\mathrm{R}} \leq P^{(+)}_{\mathrm{NJ}} \\ \frac{1}{q_{\mathrm{p}}} P_{\mathrm{R}} \left(q_{\mathrm{p}} x^{(+)}_{\mathrm{J}} - \kappa^{(+)}_{\mathrm{J}} \ln(P_{\mathrm{R}})\right) & \text{for } P_{\mathrm{R}} > P^{(+)}_{\mathrm{NJ}} \end{cases} \quad . \tag{A.85}$$

Finally, the total reversible NJ-distance after the domain wall motion reversal is :

- in direction of the domain wall motion after the reversal $(-)$

$$d^{(-)}_{\mathrm{Rev,NJ,New}} = d^{(+)}_{\mathrm{R,NJ}} + d^{(-)}_{\mathrm{Rev,NJ}} \quad , \tag{A.86}$$

- in direction of the domain wall motion before the reversal $(+)$

$$d^{(+)}_{\mathrm{Rev,NJ,New}} = d^{(+)}_{\mathrm{Rev,NJ}} - d^{(+)}_{\mathrm{R,NJ}} \quad . \tag{A.87}$$

J-Part: The J-part can be calculated as different between the total area (A.77) and the NJ-part as

$$\begin{aligned} d^{(-)}_{\mathrm{Rev,J}} &= d^{(-)}_{\mathrm{Rev,Max}} - d^{(-)}_{\mathrm{Rev,NJ}} \\ &= \frac{1}{q_{\mathrm{p}}}\left(\kappa^{(-)}_{\mathrm{J}} P^{(-)}_{\mathrm{J}} - (\kappa^{(-)}_{\mathrm{J}} - \kappa^{(-)}_{\mathrm{NJ}}) P^{(-)}_{\mathrm{NJ}}\right) - d^{(-)}_{\mathrm{Rev,NJ}} \quad , \end{aligned} \tag{A.88}$$

and

$$\begin{aligned} d^{(+)}_{\mathrm{Rev,J}} &= d^{(+)}_{\mathrm{Rev,Max}} - d^{(+)}_{\mathrm{Rev,NJ}} \\ &= \frac{1}{q_{\mathrm{p}}}\left(\kappa^{(+)}_{\mathrm{J}} P^{(+)}_{\mathrm{J}} - (\kappa^{(+)}_{\mathrm{J}} - \kappa^{(+)}_{\mathrm{NJ}}) P^{(+)}_{\mathrm{NJ}}\right) - d^{(+)}_{\mathrm{Rev,NJ}} \quad . \end{aligned} \tag{A.89}$$

Finally, the total reversible J-distance after the domain wall motion reversal is :

- in direction of the domain wall motion after the reversal $(-)$

$$d^{(-)}_{\mathrm{Rev,J,New}} = d^{(+)}_{\mathrm{Rev,J}} + d^{(-)}_{\mathrm{Rev,J}} \quad , \tag{A.90}$$

- in direction of the domain wall motion before the reversal $(+)$

$$d^{(+)}_{\mathrm{Rev,J,New}} = 0 \quad . \tag{A.91}$$

Update of Parameters at the Reversal Point

Demagnetized State: For the demagnetized state, as starting point of the EM calculations, it is assumed that all domain walls are in equilibrium position and the probability of reversal motion is exponentially distributed according to the Poisson process. In this case, the parameters of the probability curves are

$$\kappa^{(+)}_{\mathrm{J,New}} = \kappa^{(-)}_{\mathrm{J,New}} = 2.0 \tag{A.92a}$$
$$x^{(+)}_{\mathrm{J,New}} = x^{(-)}_{\mathrm{J,New}} = 0.0 \tag{A.92b}$$
$$\kappa^{(+)}_{\mathrm{NJ,New}} = \kappa^{(-)}_{\mathrm{NJ,New}} = 1.0 \tag{A.92c}$$
$$x^{(+)}_{\mathrm{NJ,New}} = x^{(-)}_{\mathrm{NJ,New}} = 0.0 \tag{A.92d}$$
$$P^{(+)}_{\mathrm{J,New}} = P^{(-)}_{\mathrm{J,New}} = 1 \tag{A.92e}$$
$$P^{(+)}_{\mathrm{NJ,New}} = P^{(-)}_{\mathrm{NJ,New}} = 1 \tag{A.92f}$$
$$\Delta\xi^{(+)}_{\mathrm{NJ,New}} = \Delta\xi^{(-)}_{\mathrm{NJ,New}} = 0 \quad . \tag{A.92g}$$

Probability Curve in the New Direction of Movement: After the domain wall motion reversal, the parameters

$$\kappa^{(-)}_{\mathrm{J,New}}, x^{(-)}_{\mathrm{J,New}}, \kappa^{(-)}_{\mathrm{NJ,New}}, x^{(-)}_{\mathrm{NJ,New}}$$
$$P^{(-)}_{\mathrm{J,New}}, P^{(-)}_{\mathrm{NJ,New}}, \Delta\xi^{(-)}_{\mathrm{NJ,New}}$$

for the probability function $P^{(-)}_{\mathrm{Rev}}(.)$ of reversible movement have to be updated based on

$$P_{\mathrm{R}}, d^{(-)}_{\mathrm{Rev,J,New}}, d^{(-)}_{\mathrm{Rev,NJ,New}} \quad .$$

First, an incremental movement in the new direction is entirely reversible, so that

$$P^{(-)}_{\mathrm{J,New}} = 1 \tag{A.93}$$

$$\Rightarrow \quad x^{(-)}_{\mathrm{J,New}} = 0 \tag{A.94}$$

and the separation between J-part and NJ-part is given by

$$P^{(-)}_{\mathrm{NJ,New}} = P_{\mathrm{R}} \quad . \tag{A.95}$$

From the given reversible J-distance $d^{(-)}_{\mathrm{Rev,J,New}}$ with (A.76) and (A.72a)

$$\begin{aligned} d^{(-)}_{\mathrm{Rev,J,New}} &= \int_0^{\Delta\xi^{(-)}_{\mathrm{NJ}}} P^{(-)}_{\mathrm{Rev}}(x)\,\mathrm{d}x - P^{(-)}_{\mathrm{NJ,New}}\Delta\xi^{(-)}_{\mathrm{NJ,New}} \\ &= \frac{\kappa^{(-)}_{\mathrm{J,New}}}{q_{\mathrm{p}}}\left(P^{(-)}_{\mathrm{J,New}} - P^{(-)}_{\mathrm{NJ,New}}\right) - \frac{1}{q_{\mathrm{p}}}P^{(-)}_{\mathrm{NJ,New}}\left(q_{\mathrm{p}}x^{(-)}_{\mathrm{J,New}} - \kappa^{(-)}_{\mathrm{J,New}}\ln(P^{(-)}_{\mathrm{NJ,New}})\right) \\ &= \frac{\kappa^{(-)}_{\mathrm{J,New}}}{q_{\mathrm{p}}}\left(1 - P_{\mathrm{R}}\right) - \frac{1}{q_{\mathrm{p}}}P_{\mathrm{R}}\left(q_{\mathrm{p}}0 - \kappa^{(-)}_{\mathrm{J,New}}\ln(P_{\mathrm{R}})\right) \\ &= \frac{\kappa^{(-)}_{\mathrm{J,New}}}{q_{\mathrm{p}}}\left(1 - P_{\mathrm{R}}\left(1 - \ln(P_{\mathrm{R}})\right)\right) \end{aligned} \tag{A.96}$$

the parameter $\kappa^{(-)}_{\mathrm{J,New}}$ can be estimated as

$$\kappa^{(-)}_{\mathrm{J,New}} = \frac{q_{\mathrm{p}}d^{(-)}_{\mathrm{Rev,J,New}}}{1 - P_{\mathrm{R}}\left(1 - \ln(P_{\mathrm{R}})\right)} \leq 2 \quad . \tag{A.97}$$

From the given reversible NJ-distance $d^{(-)}_{\mathrm{Rev,NJ,New}}$ with (A.74) and (A.72a)

$$\begin{aligned} d^{(-)}_{\mathrm{Rev,NJ,New}} &= P^{(-)}_{\mathrm{NJ,New}}\Delta\xi^{(-)}_{\mathrm{NJ,New}} + \int_{\Delta\xi^{(-)}_{\mathrm{NJ}}}^{\infty} P^{(-)}_{\mathrm{Rev}}(x)\,\mathrm{d}x \\ &= \frac{1}{q_{\mathrm{p}}}P^{(-)}_{\mathrm{NJ,New}}\left(q_{\mathrm{p}}x^{(-)}_{\mathrm{J,New}} - \kappa^{(-)}_{\mathrm{J,New}}\ln(P^{(-)}_{\mathrm{NJ,New}})\right) + \frac{\kappa^{(-)}_{\mathrm{NJ,New}}}{q_{\mathrm{p}}}P^{(-)}_{\mathrm{NJ,New}} \\ &= \frac{1}{q_{\mathrm{p}}}P_{\mathrm{R}}\left(q_{\mathrm{p}}0 - \kappa^{(-)}_{\mathrm{J,New}}\ln(P_{\mathrm{R}})\right) + \frac{\kappa^{(-)}_{\mathrm{NJ,New}}}{q_{\mathrm{p}}}P_{\mathrm{R}} \\ &= \frac{1}{q_{\mathrm{p}}}P_{\mathrm{R}}\left(\kappa^{(-)}_{\mathrm{NJ,New}} - \kappa^{(-)}_{\mathrm{J,New}}\ln(P_{\mathrm{R}})\right) \end{aligned} \tag{A.98}$$

the parameter $\kappa^{(-)}_{\mathrm{NJ,New}}$ can be estimated as

$$\kappa^{(-)}_{\mathrm{NJ,New}} = \frac{q_{\mathrm{p}}d^{(-)}_{\mathrm{Rev,NJ,New}}}{P_{\mathrm{R}}} + \kappa^{(-)}_{\mathrm{J,New}}\ln(P_{\mathrm{R}}) \quad . \tag{A.99}$$

Using

$$\begin{aligned}\Delta\xi^{(-)}_{\mathrm{NJ,New}} &= \frac{1}{q_\mathrm{p}}\left(q_\mathrm{p}x^{(-)}_{\mathrm{J,New}} - \kappa^{(-)}_{\mathrm{J,New}}\ln(P^{(-)}_{\mathrm{NJ,New}})\right)\\ &= \frac{1}{q_\mathrm{p}}\left(q_\mathrm{p}0 - \kappa^{(-)}_{\mathrm{J,New}}\ln(P_\mathrm{R})\right)\\ &= \frac{\kappa^{(-)}_{\mathrm{J,New}}}{q_\mathrm{p}}\ln(P_\mathrm{R}) \qquad \text{(A.100)}\end{aligned}$$

together with (A.70c), the parameter $x^{(-)}_{\mathrm{NJ,New}}$ results as

$$x^{(-)}_{\mathrm{NJ,New}} = \frac{1}{q_\mathrm{p}}\ln(P_\mathrm{R})\left(\kappa^{(-)}_{\mathrm{NJ,New}} - \kappa^{(-)}_{\mathrm{J,New}}\right) \quad . \qquad \text{(A.101)}$$

In summary, the formulas for the parameter update are

$$\begin{aligned}\kappa^{(-)}_{\mathrm{J,New}} &= \frac{q_\mathrm{p}d^{(-)}_{\mathrm{Rev,J,New}}}{1-P_\mathrm{R}\left(1-\ln(P_\mathrm{R})\right)} && \text{(A.102a)}\\ x^{(-)}_{\mathrm{J,New}} &= 0 && \text{(A.102b)}\\ \kappa^{(-)}_{\mathrm{NJ,New}} &= \frac{q_\mathrm{p}d^{(-)}_{\mathrm{Rev,NJ,New}}}{P_\mathrm{R}} + \kappa^{(-)}_{\mathrm{J,New}}\ln(P_\mathrm{R}) && \text{(A.102c)}\\ x^{(-)}_{\mathrm{NJ,New}} &= \frac{1}{q_\mathrm{p}}\ln(P_\mathrm{R})\left(\kappa^{(-)}_{\mathrm{NJ,New}} - \kappa^{(-)}_{\mathrm{J,New}}\right) && \text{(A.102d)}\\ P^{(-)}_{\mathrm{J,New}} &= 1 && \text{(A.102e)}\\ P^{(-)}_{\mathrm{NJ,New}} &= P_\mathrm{R} && \text{(A.102f)}\\ \Delta\xi^{(-)}_{\mathrm{NJ,New}} &= \frac{1}{q_\mathrm{p}}\kappa^{(-)}_{\mathrm{J,New}}\ln(P_\mathrm{R}) \quad . && \text{(A.102g)}\end{aligned}$$

Probability Curve in the Current Direction of Movement: If there would be no domain wall motion reversal, the probability function $P^{(+)}_{\mathrm{Rev}}(.)$ of reversible movement is just shifted, so that the corresponding parameters are given by

$$\begin{aligned}\kappa^{(+)}_{\mathrm{J,New}} &= \kappa^{(+)}_{\mathrm{J}} && \text{(A.103a)}\\ x^{(+)}_{\mathrm{J,New}} &= x^{(+)}_{\mathrm{J}} - |\Delta\xi_\mathrm{R}| && \text{(A.103b)}\\ \kappa^{(+)}_{\mathrm{NJ,New}} &= \kappa^{(+)}_{\mathrm{NJ}} && \text{(A.103c)}\\ x^{(+)}_{\mathrm{NJ,New}} &= x^{(+)}_{\mathrm{NJ}} - |\Delta\xi_\mathrm{R}| && \text{(A.103d)}\\ P^{(+)}_{\mathrm{J,New}} &= P_\mathrm{R} && \text{(A.103e)}\\ P^{(+)}_{\mathrm{NJ,New}} &= \min\{P^{(+)}_{\mathrm{NJ}}, P_\mathrm{R}\} && \text{(A.103f)}\\ \Delta\xi^{(+)}_{\mathrm{NJ,New}} &= \max\{0, |\Delta\xi^{(+)}_{\mathrm{NJ}}| - |\Delta\xi_\mathrm{R}|\} \quad . && \text{(A.103g)}\end{aligned}$$

So in principle, the probabilities do not change, if the domain wall motion reversal is not performed, and the domain wall moves according to the previous direction. Due to this effect, the probability curves $P^{(+)}_{\mathrm{Rev}}(.)$ and $P^{(-)}_{\mathrm{Rev}}(.)$ can be updated in every calculation step of the model, independent if the domain wall motion reversal takes places or not.

Bibliography

[1] Aharoni A.: *Introduction to the Theory of Ferromagnetism*. Oxford University Press, Oxford (1996).

[2] Aigner P.: *Herstellung dünner Permalloy-Schichten für magnetoresistive Sensoren*. Diploma thesis, Vienna University of Technology, Vienna (1997).

[3] Andrei P., Stoleriu L., and Hauser H.: *Hysteresis Model Identification for Particulate Media*. J. Appl. Phys. **87**(9), 6555 (2000).

[4] Appino C. and Coisson M.: *Reversible and irreversible magnetization process in materials displaying two-dimensional hysteresis*. Physica B **372**, 133 (2006).

[5] Barkhausen H.: *Geräusche beim Ummagnetisieren von Eisen*. Phys. Z. **20**, 401 (1919).

[6] Bates L. and Sherry N.: *The Direct Separation of the Reversible and Irreversible Components of the Magnetothermal Effect*. Proc. Phys. Soc. B **68**, 642 (1955).

[7] Bergqvist A.J.: *A Simple Vector Generalization of the Jiles-Atherton Model of Hysteresis*. IEEE Trans. Magn. **32**, 4213 (1996).

[8] Bertotti G.: *Hysteresis in Magnetism*. Academic Press, San Diego (1998).

[9] Bloch F.: *Zur Theorie des Austauschproblems und der Remanenzerscheinung der Ferromagnetika*. Z. Phys **74**, 295 (1932).

[10] Blundell S.: *Magnetism in Condensed Matter*. Oxford University Press, Oxford, New York (2001).

[11] Brown W.F.: *Domain Theory of Ferromagnetics Under Stress: Part I*. Phys. Rev. **52**, 325 (1937).

[12] Brown W.F.: *Micromagnetics*. Wiley Interscience, New York (1963).

[13] Cacciamani G., Dinsdale A., Palumbo M., and Pasturel A.: *The Fe-Ni System: Thermodynamic Modelling Assisted by Atomistic Calculations*. Intermetallics **18**(6), 1148 (2010).

[14] Cammarano R., McCormick P., and Street R.: *The interrelation of reversible and irreversible magnetization*. J. Phys. D: Appl. Phys. **29**, 2327 (1996).

[15] Chikazumi S.: *Physics of Magnetism*. John Wiley and Sons, Inc., New York (1964).

[16] Coey J.M.D.: *Magnetism and Magnetic Materials*. Cambridge University Press, Cambridge, New York (2010).

[17] Constant F.W.: *The Distribution of the Heat Emission in the Magnetic Hysteresis Cycle*. Phys. Rev. **32**, 486 (1928).

[18] Dupré L.R., Keer R.V., and Melkebeek J.A.: *Identification of the Relation between the Material Parameters in the Preisach Model and in the Jiles-Atherton Hysteresis Model*. J. Appl. Phys. **85**, 4376 (1999).

[19] Elmen G.W. and Arnold H.D.: *Permalloy, A New Magnetic Material of Very High Permeability*. Bell System Technical Journal **2**, 101 (1923).

[20] Fasching G.M.: *Magnetisierung und Feldstaerke im kubischen Kristall*. Acta Phys. Austr. **21**(4), 316 (1964).

[21] Feynman R.P., Leighton R.B., and Sands M.: *The Feynman Lectures on Physics*. Pearson Addison Wesley, San Francisco, definitive edn. (2006).

[22] Fidler J. and Schrefl T.: *Micromagnetic Modelling - The Current State of the Art*. J. Phys. D **33**, R135 (2000).

[23] Fulmek P. and Hauser H.: *Magnetization Calculations of (110)[001] FeSi Sheets in Different Directions by Statistical Domain Behaviour*. J. Magn. Magn. Mater. **157/158**, 361 (1996).

[24] Fulmek P. and Hauser H.: *Magnetization Reversal in an Energetic Hysteresis Model*. J. Magn. Magn. Mater. **160**, 35 (1996).

[25] Fulmek P. and Hauser H.: *Magnetization Reversal and Statistical Domain Behaviour*. J. Magn. Magn. Mater. **183**, 75 (1998).

[26] Fulmek P. and Hauser H.: *Statistical Hysteresis Model for Anisotropic and Isotropic Magnetic Materials*. J. Phys. IV **8**, 335 (1998).

[27] Gardiner C.W.: *Handbook of Stochastic Methods*. Springer, Berlin (1985).

[28] Gilbert T.L.: *A Lagrangian Formulation of Gyromagnetic Equation of the Magnetic Field*. Phys. Rev. **100**, 1243 (1955).

[29] Groessinger R., Hauser H., Dahlgren M., and Fidler J.: *Hysteresis of Nanocrystalline R-Fe-B*. Physica B **275**, 248 (1995).

[30] Haumer P.: *Relation between Physical and Phenomenological Aspects in the Framework of an Energetic Hysteresis Model*. J. Appl. Phys. **97**(10E517), 1 (2005).

[31] Haumer P. and Fulmek P.: *Estimation of the Effects of Microscopic Misalignments on the Magnetization Process in Thin Films by Energetic Modeling*. IEEE Trans. Magn. **46**(2), 247 (2010).

[32] Haumer P. and Fulmek P.L.: *Energetic Framework for the Description of Temperature Dependent Magnetization in Ferromagnetic Thin Films*. In: *ISSE 2008: Conference Proceedings*, 627–632. IEEE, Hungary (2008).

[33] Haumer P., Hauser H., Fulmek P., and Bajalan D.: *Hysteresis Modeling of Thin Permalloy Films and Parameter Interpretation*. IEEE Trans. Magn. **40**(4), 2745 (2004).

[34] Hauser H.: *Energetic Model of Ferromagnetic Hysteresis*. J. Appl. Phys. **75**(5), 2584 (1994).

[35] Hauser H.: *Energetic Model of Ferromagnetic Hysteresis 2: Magnetization Calculations of (110)[001] FeSi Sheets by Statistic Domain Behavior*. J. Appl. Phys. **77**(6), 2625 (1995).

[36] Hauser H.: *Energetic Model of Ferromagnetic Hysteresis: Isotropic Magnetization*. J. Appl. Phys. **96**(5), 2753 (2004).

[37] Hauser H. and Fulmek P.: *Simulation of Magnetization Curves of Anisotropic Materials*. J. Magn. Magn. Mater. **133**, 32 (1994).

[38] Hauser H. and Fulmek P.: *Hysteresis Calculations by Statistical Behaviour of Particles of High Density*. J. Magn. Magn. Mater. **155**, 34 (1996).

[39] Hauser H. and Groessinger R.: *Isotropic Hysteresis Modeling of Fe-Co-B Alloys*. J. Appl. Phys. **85**(8), 5133 (1999).

[40] Heisenberg W.: *Zur Theorie der Magnetostriktion und der Magnetisierungskurve*. Z. Phys. **69**, 287 (1931).

[41] Hoffmann H.: *Wellenstruktur der Magnetisierung in dünnen Permalloyschichten*. Z. Phys. B Condens. Matter **2**(1), 32 (1964).

[42] Hubert A. and Schaefer R.: *Magnetic Domains*. Springer, Berlin (2000).

[43] Iyer R.V. and Krishnaprasad P.S.: *On a Low-Dimensional Model for Ferromagnetism*. Nonlinear Analysis **61(8)**, 1447 (2005).

[44] Jammalamadaka S.R. and Gupta A.S.: *Topics in Circular Statistics*. World Scientific Pubslishing, Singapore (2001).

[45] Janiba M.: *Optimierung der technologischen Schritte zur Herstellung eines magnetoresistiven Sensors*. Diploma thesis, Vienna University of Technology, Vienna (1999).

[46] Jiles D.C.: *Introduction to Magnetism and Magnetic Materials*. Chapman and Hall, London (1991).

[47] Jiles D.C.: *A Self-Consistent Generalized Model for the Calculation of Minor Loop Excursions in the Theory of Hysteresis*. IEEE Trans. Magn. **28**, 2602 (1992).

[48] Jiles D.C. and Atherton D.L.: *Theory of the Magnetisation Process in Ferromagnetics and its Application to the Magnetomechanical Effect*. J. Phys. D **17**, 1265 (1984).

[49] Jiles D.C. and Atherton D.L.: *Theory of Ferromagnetic Hysteresis*. J. Magn. Magn. Mater. **61**, 48 (1986).

[50] Jiles D.C., Thoelke J.B., and Devine M.K.: *Numerical Determination of Hysteresis Parameters for the Modeling of Magnetic Properties Using the Theory of Ferromagnetic Hysteresis*. IEEE Trans. Magn. **28**, 27 (1992).

[51] Kaya S.: *Die Überstrukturbildung in den Nickel-Eisen Legierungen und das Permalloy Problem*. Journal of the Faculty of Science Hokkaido Universtiy **2**, 29 (1938).

[52] Kloibhofer R.: *Materialwissenschaftliche Aspekte eines magnetoresistiven Sensors*. Diploma thesis, Vienna University of Technology, Vienna (1996).

[53] Krasnoselskii M.A. and Pokrovskii A.V.: *Systems with Hysteresis*. Nauka, Moscow (1983). Translated by M. Niezgódka, Springer-Verlag, Berlin (1989).

[54] Kronmueller H. and Faehnle M.: *Micromagnetism and the Microstructure of Ferromagnetic Solids*. Cambridge University Press, Cambridge (2003).

[55] Kwiczala J. and Kasperczyk B.: *Standardization of anhysteretic magnetization curves*. J. Appl. Phys. **97**, 10E504 (2005).

[56] du Tremolet de Lacheisserie E., Gignoux D., and Schlenker M.: *Magnetism - Fundamentals*. Springer, New York (2005).

[57] Landau L. and Lifshitz E.: *On the Theory of Magnetic Permeability in Ferromagnetic Bodies*. Physik. Z. Sowjetunion **8**, 135 (1935).

[58] Leite J.V.: *The Inverse Jiles-Atherton Model Parameters Identification*. IEEE Trans. Magn. **39**, 1397 (2003).

[59] Massalski T.B.: *Binary Alloy Phase Diagrams*. ASM International, Ohio, USA (1990).

[60] Mauri D., Scholl D., Siegmann H.C., and Kay E.: *Universal Thermal Stabilization of the Magnetization in Ultrathin Ferromagnetic Films*. Phys. Rev. Lett. **62**(16), 1900 (1989).

[61] Mayergoyz I.D.: *Mathematical Models of Hysteresis*. Springer-Verlag, New York (1991).

[62] Mohn P.: *Magnetism in the Solid State: An Introduction*. Springer, Berlin, Heidelberg (2003).

[63] Néel L.: *Théorie des lois d'aimantation de Lord Rayleigh 1: Les déplacements d'une paroi isolée*. Cah. Phys. **12**, 1 (1942). English translation in: Kurti N., ed., *Selected Works of Lois Néel*, Gordon and Breach Science Publishers, New York, (1988).

[64] Néel L.: *Les Lois de l'Aimantation et de la Subdivision en Domaines Élémentaires d'un Monocristal de Fer (I)*. J. de Phys. Rad. **5**, 241 (1944).

[65] Néel L.: *Bases d'une nouvelle théorie générale du champ coercitif*. Ann. Univ. Grenoble. **22**, 299 (1946). English translation in: Kurti N., ed., *Selected Works of Lois Néel*, Gordon and Breach Science Publishers, New York, (1988).

[66] Néel L.: *Propriétés magnétiques des ferrites: ferrimagnétisme et antiferromagnétisme*. Ann. Phys. Paris **3**, 137 (1948). English translation in: Kurti N., ed., *Selected Works of Lois Néel*, Gordon and Breach Science Publishers, New York, 63 (1988).

[67] Néel L.: *Énergie des parois de Bloch dans les couches minces*. C. R. Acad. Sci. Paris **241**, 533 (1955). English translation in: Kurti N., ed., *Selected Works of Lois Néel*, Gordon and Breach Science Publishers, New York, 234 (1988).

[68] Nourdine A., Kedous-Lebouc A., Meunier G., and Chevalier T.: *A Chemical Reaction Hysteresis Model for Magnetic Materials*. IEEE Trans. Magn. **36**, 1230 (2000).

[69] Nourdine A., Kedous-Lebouc A., Meunier G., and Chevalier T.: *A New Hysteresis Model Generation - Application to the Transverse Axis of GO SiFe Sheet*. IEEE Trans. Magn. **37**, 3340 (2001).

[70] Nourdine A., Meunier G., and Kedous-Lebouc A.: *Numerical Computation of a Vectorial Hysteresis H(B) Magnetization Law*. IEEE Trans. Magn. **39**, 1393 (2003).

[71] Pasquale M., Bertotti G., Jiles D.C., and Bi Y.: *Application of the Preisach and Jiles-Atherton Models to the Simulation of Hysteresis in Soft Magnetic Alloys*. J. Appl. Phys. **85**, 4373 (1999).

[72] Preisach F.: *Über die magnetische Nachwirkung*. Z. Phys. **94**, 277 (1935).

[73] Prutton M.: *Thin Ferromagnetic Films*. Butterworth & Co. Ltd., London (1964).

[74] Rave W. and Hubert A.: *Magnetic Ground State of a Thin-Film Element*. IEEE Trans. Magn. **36**(6), 3886 (2000).

[75] Slonczewski J.C.: *Theory of Magnetic Hysteresis in Films and its Application to Computers*. IBM Research Memorandum **RM 003.111.224** (1956).

[76] Smith R.C. and Hom C.L.: *Domain Wall Theory for Ferroelectric Hysteresis*. J. Intelligent Mater. Syst. Struct. **10**, 195 (1999).

[77] Stoner E.C. and Wohlfarth E.P.: *A Mechanism of Magnetic Hysteresis in Heterogeneous Alloys*. Phil. Trans. Roy. Soc. **A240**, 599 (1948).

[78] Torre E.D.: *Magnetic Hysteresis*. IEEE Press, New York (1999).

[79] Townsend A.: *The Change in Thermal Energy which Accompanies a Change in Magnetization of Nickel*. Phys. Rev. **47**, 306 (1935).

[80] Tumanski S.: *Thin Film Magnetoresistive Sensors*. IOP Publishing Ltd., London (2001).

[81] VERANT A.: *Magnetoresistive Sensoren für die Positionierung in Nanometerbereich*. Diploma thesis, Vienna University of Technology, Vienna (2002).

[82] VISINTIN A.: *Differential Models of Hysteresis*. Springer, Berlin (1994).

[83] VAN VLECK J.H.: *The Theory of Electric and Magnetic Susceptibilities*. Oxford University Press, London (1932).

[84] VAN VLECK J.H.: *Quantum Mechanics - The Key to Understanding Magnetism*. Rev. Mod. Phys. **2**, 181 (1978).

[85] WARBURG E.: *Magnetische Untersuchungen*. Ann. d. Physik **249(5)**, 141 (1881).

[86] WEISS P.: *L'Hypothese du Champ Moleculaire et la Propriete Ferromagnetique*. J. de Phys. **6**, 661 (1907).

[87] WHITE R.M.: *Quantum Theory of Magnetism*. Springer, Berlin, Heidelberg, third edn. (2007).

[88] WHITTENBURG S.L.: *Micromagnetics of Nanoparticles and Nanoshaped Magnetic Elements*. In: *Magnetic Nanostructures*, 425–440. American Scientific Publishers, California (2002).

[89] YANG C.W., WILLIAMS D.B., and GOLDSTEIN J.I.: *A Revision of the Fe-Ni Phase Diagram at Low Temperatures (<400 °C)*. J. Phase Equil. **17**(6), 522 (1996).

[90] ZHANG Y. and ATHERTON D.: *Levels of Demagnetized States*. IEEE Trans. Magn. **31**(3), 2233 (1995).

List of Publications

Publications in Scientific Journals

H. Hauser, P. Fulmek, P. Haumer, M. Vopálenský, P. Ripka:
"*Flipping field and stability in anisotropic magnetoresistive sensors*"
Sensors and Actuators A: Physical, **106** (2003), 121 - 125.

P. Haumer, H. Hauser, P. Fulmek, D. Bajalan:
"*Hysteresis Modeling of Thin Permalloy Films and Parameter Interpretation*"
IEEE Transactions on Magnetics, **40** (2004), 4; 2745 - 2747.

P. Haumer:
"*Relation between physical and phenomenological aspects in the framework of an energetic hysteresis model*"
Journal of Applied Physics, **97** (2005), 10E517; 1 - 3.

P. Fulmek, H. Hauser, G. Steiner, P. Haumer:
"*Magnetic Modelling of Continuously Variable Transformers*"
Physica B, **372** (2006), 124 - 127.

P. Haumer, P. Fulmek:
"*Estimation of the effects of microscopic misalignments on the magnetization process in thin films by energetic modeling*"
IEEE Transactions on Magnetics, **46** (2010), 2; 247 - 250.

P. Fulmek, G. Holler, H. Wegleiter, B. Schweighofer, P. Haumer:
"*Method for the Measurement of Transient Magnetic AC Properties of Soft Ferrites*"
IEEE Transactions on Magnetics, **46** (2010), 2; 463 - 466.

P. Fulmek, P. Haumer, H. Wegleiter, B. Schweighofer:
"*Energetic model of ferromagnetic hysteresis*"
COMPEL, **29** (2010), 6; 1504 - 1513.

P. Fulmek, H. Wegleiter, P. Haumer, B. Schweighofer:
"*Measurement Of Time-Dependence Of Complex Magnetic Permeability Of Soft-Ferrites*"
Journal of Electrical Engineering, **61** (2010), 7/s; 54 - 57.

P. Fulmek, P. Haumer, I. Atassi, B. Schweighofer, H. Wegleiter:
"*Magnetic DC-Properties of LTCC-Ferrite Material and Their Temperature Dependence*"
IEEE Transactions on Magnetics, **48** (2012), 4; 1541 - 1544.

Contributions to Books

D. Bajalan, I. Groiss, G. Stangl, H. Hauser, P. Fulmek, P. Haumer:
"*Co/Pt Multi-Layer Production for Magnetic Nanostructures*"
in: "Sensor & Packaging", ÖVE, Wien, Austria, 2003, ISBN: 3-85133-032-3, 193 - 199.

Presentations and Conference Proceedings

H. Hauser, P. Fulmek, P. Haumer, M. Vopálenský, P. Ripka:
"*Prediction of the Flipping fields in AMR Sensors*"
Poster: 4th European Conference on Magnetic Sensors and Actuators (EMSA 2002)
Athens, Greece; 03.07.2002 - 05.07.2002
in: "Book of Abstracts EMSA 2002", (2002), S3_P6.

P. Haumer, H. Hauser, P. Fulmek:
"*Relation between micromagnetic and phenomenological magnetic models*"
Poster: 49th Annual Conference on Magnetism & Magnetic Materials (MMM 04)
Jacksonville, Florida, USA; 07.11.2004 - 11.11.2004
in: "Book of Abstracts - MMM 04", (2004), FD-09.

D. Bajalan, H. Hauser, P. Haumer, P. Fulmek:
"*Hysteresis Calculation for Thin Film Multi-Layers Nanostructured by Ion Irradiation*"
Poster: International Spring Seminar on Electronics Technology (ISSE 2005)
Wr. Neustadt, Austria; 19.05.2005 - 22.05.2005
in: "Book of Abstract", (2005), ISBN: 3-85133-036-6; 104 - 105.

P. Fulmek, H. Hauser, G. Steiner, P. Haumer:
"*Magnetic Modelling of Continuously Variable Transformers*"
Oral P.: 5th International Symposium on Hysteresis Modeling & Micromagn. (HMM 2005)
Budapest, Hungary; 30.05.2005 - 01.06.2005
in: "Book of Abstracts", (2005), ISBN: 963-420834-7; 243 - 244.

P. Haumer, P. Fulmek:
"*Energetic Framework for the Description of Temperature Dependent Magnetization in Ferromagnetic Thin Films*"
Oral P.: 31st International Spring Seminar on Electronics Technology (ISSE 2008)
Budapest, Hungary; 07.05.2008 - 11.05.2008
in: "Conference Proceedings", (2008), ISBN: 978-1-4244-3973-7; 627 - 632.

P. Fulmek, P. Haumer, G. Holler:
"*Hysteresis Modelling of NiZn-Ferrites*"
Poster: 31st International Spring Seminar on Electronics Technology (ISSE 2008)
Budapest, Hungary; 07.05.2008 - 11.05.2008
in: "ConferenceProceedings", (2008), ISBN: 978-1-4244-3974-4; 670 - 675.

P. Fulmek, P. Haumer:
"*Energetic Model of Ferromagnetic Hysteresis*"
Oral P.: International Symposium on Electric and Magnetic Fields
Mondovi, Italy; 26.05.2009 - 29.05.2009
in: "EMF 2009 - Book of Summaries", (2009), ISSN: 2030-546x; 29 - 30.
in: "Proceedings of the 8th International Symposium on Electric and Magnetic Fields, EMF 2009 (CD-ROM)", (2009), ISSN: 2030-546x, 4 S.

P. Fulmek, G. Holler, H. Wegleiter, B. Schweighofer, P. Haumer:
"*Measurement of Magnetic Accommodation in NiZn-Ferrite*"
Poster: 8th International Symposium on Electric and Magnetic Fields (EMF 2009)
Mondovi, Italy; 26.05.2009 - 29.05.2009
in: " EMF 2009 - Book of Summaries ", (2009), ISSN: 2030-546x; 137 - 138.
in: " Proceedings of the 8th International Symposium on Electric and Magnetic Fields EMF 2009 (CD-ROM)", (2009), ISSN: 2030-546x, 4 S.

P. Haumer, P. Fulmek:
"*Estimation of the effects of microscopic misalignments on the magnetization process in thin films by energetic modeling*"
Poster: 19th Soft Magnetic Materials Conference (SMM 19)
Torino, Italy; 06.09.2009 - 09.09.2009
in: "Book of Abstracts", (2009), B2-12.

P. Fulmek, N. Mehboob, P. Haumer, M. Kriegisch, R. Grössinger:
"*Magnetic characterisation of industrial high strength steels*"
Poster: 19th Soft Magnetic Materials Conference (SMM 19)
Torino, Italy; 06.09.2009 - 09.09.2009
in: "Book of Abstracts", (2009), B1-16.

P. Fulmek, P. Haumer, M. Kriegisch, R. Grössinger:
"*Frequency dependent magnetic properties of industrial high strenght steels*"
Poster: 19th Soft Magnetic Materials Conference (SMM 19)
Torino, Italy; 06.09.2009 - 09.09.2009
in: "Book of Abstracts", (2009), B1-23.

P. Fulmek, B. Schweighofer, P. Haumer, H. Wegleiter, G. Holler:
"*Measurement of transient magnetic AC-properties of NiZn-ferrites*"
Poster: 19th Soft Magnetic Materials Conference (SMM 19)
Torino, Italy; 06.09.2009 - 09.09.2009
in: "Book of Abstracts", (2009), E3-06.

P. Fulmek, P. Haumer, M. Weilguni, J. Nicolics:
"*High-Resolution Thermography for High-Power LED Quality Contro*l"
34th International Spring Seminar on Electronics Technology (ISSE 2011)
Kosice, Slovakia; 11.05.2011 - 15.05.2011
in: "Abstracts Proceedings", (2011), ISBN: 978-80-553-0646-9, 222 - 223.

P. Fulmek, P. Haumer, I. Atassi, B. Schweighofer, H. Wegleiter:
"*Magnetic DC-Properties of LTCC-Ferrite Materia*l"
Oral P.: 20th Soft Magnetic Materials Conference (SMM 20)
Kos Island, Greece; 18.09.2011 - 22.09.2011
in: "Book of Abstracts", (2011), ISBN: 978-960-9534-14-7; 239.

P. Haumer, P. Fulmek:
"*Generalized two-dimensional energetic hysteresis model for the representation of magnetization curves of thin film materials*"
Poster: 20th Soft Magnetic Materials Conference (SMM 20)
Kos Island, Greece; 18.09.2011 - 22.09.2011
in: "Book of Abstracts", (2011), ISBN: 978-960-9534-14-7; 445.

P. Haumer, P. Fulmek:
"*Generalized two-dimensional energetic model of ferromagnetic hysteresis for thin film material*"
Poster: 10th European Conference on Magnetic Sensors and Actuators (EMSA 2014)
Vienna, Austria; 06.07.2014 - 09.07.2014
in: "Book of Abstracts", (2014), ISBN: 978-3-85465-021-8; 239.

P. Fulmek, P. Haumer:
"*Evaluation of BH-loops from inductive measurements by numerical simulation*"
Poster: 10th European Conference on Magnetic Sensors and Actuators (EMSA 2014)
Vienna, Austria; 06.07.2014 - 09.07.2014
in: "Book of Abstracts", (2014), ISBN: 978-3-85465-021-8; 263.

Acknowledgements

Even if he is no longer with us, I would like to express my grateful acknowledgement to Prof. Hans Hauser who introduced me to magnetic hysteresis modeling. Due to his ability to arouse enthusiasm for this subject, I decided to concentrate my scientific focus to magnetism. Beside his excellent knowledge, he encouraged me to visit international conferences and publish my work in scientific journals.

My special gratitude is dedicated to Prof. Johann Nicolics, who has agreed to supervise this thesis after the death of Prof. Hauser. He spent his valuable time for extensive discussions on topics and problems related to this work and supported me with his broad knowledge and wide experience in the field of material science over many years. Further, he enabled me to do my research within a perfect working environment at the Department of Applied Electronic Materials of the Institute of Sensor and Actuator Systems.

In addition, I want to thank Prof. David Jiles for acting as an external examiner for this thesis and his willingness to travel to Vienna for the final examination. It will be my pleasure to meet him as an internationally renowned expert in the field of magnetic hysteresis modeling.

Among all my colleagues, I am particularly grateful for the assistance and support given by Dr. Paul Fulmek whenever I was at my wits' end. For more than one decade I have been enjoying a lot of discussions in a pleasant atmosphere, from where several scientific publications emerged.

Last but by no means least, I would like to thank my parents and all my friends for their support and encouragement throughout the time of my PhD study, so that I am able to accomplish this thesis.